2004

The Wave Structure Function And Temporal Frequency Spread In Weak To Strong Optical Turbulence

Aaron J. Masino
University of Central Florida

THE WAVE STRUCTURE FUNCTION AND TEMPORAL FREQUENCY SPREAD IN WEAK TO STRONG OPTICAL TURBULENCE

by

AARON J. MASINO
B.A. Rutgers University, 1997
M.E. University of Colorado, 1998

A dissertation submitted in partial fulfillment of the requirements
for the degree of Doctor of Philosophy
in the Department of Mathematics
in the College of Arts and Sciences
at the University of Central Florida
Orlando, Florida

Summer Term
2004

Major Professor: Cynthia Y. Young

ABSTRACT

This paper presents analytic expressions for the wave structure function, frequency spread of the temporal frequency spectrum, and the temporal frequency spectrum of optical signals propagating through a random medium, specifically the Earth's atmosphere. The results are believed to be valid for *all* optical turbulence conditions. These expressions are developed using the Rytov approximation method. Generally, the validity of statistical quantities obtained via this method is restricted to conditions of weak optical turbulence. However, in this work, by using a modification of the *effective* atmospheric spectral model presented by Andrews *et al.* for scintillation index, wave structure function expressions have been derived that are valid in all turbulence conditions as evidenced by comparison to experimental data. Analytic wave structure function results are developed for plane, spherical, and Gaussian-beam waves for one-way propagation. For the special case of a spherical wave, comparisons are made with experimental data. The double pass case is also considered. Analytic expressions for the wave structure function are given that incorporate reflection from a smooth target for an incident spherical wave. Additionally, analytic expressions for the frequency spread of the temporal frequency spectrum and the temporal frequency spectrum itself, after one-way propagation for horizontal and slant paths, are derived for plane and spherical waves. These results are also based on the Rytov perturbation method . Expressions that are believed to be valid in all turbulence conditions are also developed by use of the effective atmospheric spectral model used in the wave structure function development. Finally, double pass frequency spread expressions are also presented. As in the case of the wave structure function, reflection from a smooth target with an incident spherical wave is considered.

To my wife,
whose love and unwaivering support
made this work possible.

ACKNOWLEDGMENTS

I would like to thank my fellow students Fred Thomas and Chris Subich who provided invaluable assistance to this research. Additionally, I would like to thank Dr. Ron Phillips and Dr. Ram Mohapatra for their support of my graduate education and serving on my committee. I would also like to express my sincere appreciation to Dr. Larry Andrews for his guidance and selfless endurance of countless hours of my questions and confusion. Furthermore, though I do not have the words to even remotely express my heartfelt gratitude, I wish to thank my advisor, mentor, and friend Dr. Cynthia Young for her guidance of this research and my graduate education and her counsel in general. Without her belief in my abilities, her sincere concern for my future, and her boundless assistance, this work and my continued scientific endeavors would not be possible. Finally, I would be remiss if I did not acknowledge my family who provided a strong foundation for all of my pursuits and who continue to support and believe in me.

Funding for this work has been provided by the Office of Naval Research under contract number N00014-01-1-0412.

TABLE OF CONTENTS

LIST OF TABLES

LIST OF FIGURES

LIST OF SYMBOLS

$\mathbf{R}$ . . . . . Position vector in three dimensions

$\delta(x)$ . . . . . Dirac delta function

L_0 . . . . . Outer scale of turbulence

l_0 . . . . . Inner scale of turbulence

$n(\mathbf{R})$ . . . . . Index of refraction

C_n^2 . . . . . Index of refraction structure parameter

$\Phi_n(\kappa)$ . . . . . Three dimensional spatial power spectrum of refractive index

κ . . . . . Scalar spatial wave number

$\mathbf{K}$ . . . . . Vector spatial wave number

κ_m . . . . . Inner scale wave number parameter ($=5.92/l_0$)

κ_0 . . . . . Outer scale wave number parameter ($=2\pi/L_0$)

κ_l . . . . . Inner scale wave number parameter ($=3.3/l_0$)

$U(\mathbf{R})$ . . . . . Complex amplitude of the optical field in random medium

k . . . . . Optical wave number ($=2\pi/\lambda$)

λ . . . . . Wavelength

σ_1^2 . . . . . Rytov variance for a plane wave

W . . . . . Beam radius at receiver in free space

$U_0(\mathbf{R})$ . . . . . Complex amplitude of the optical field in free space

Ψ_1 . . . . . First order complex phase perturbation of Rytov approximation

Ψ_2 . . . . . Second order complex phase perturbation of Rytov approximation

$\mathbf{E}_n(\mathbf{r}_1,\mathbf{r}_2)$ . . . . . Second order moments of the complex phase perturbations

$d\nu(\mathbf{K},z)$ . . . . . Random amplitude of index of refraction

$J_0(x)$ . . . . . Bessel function of order zero

γ . . . . . Propagation path amplitude parameter

$I(\mathbf{r},L)$ . . . . . Irradiance of beam in random medium

σ_I^2 . . . . . Scintillation index (normalized irradiance variance)

Λ . . . . . Fresnel ratio of beam at receiver

Θ ..... Curvature parameter of beam at receiver

Λ_0 ..... Fresnel ratio of beam at transmitter

Θ_0 ..... Curvature parameter of beam at transmitter

W_0 ..... Beam radius at transmitter

F_0 ..... Phase front radius of curvature at transmitter

$\mathbf{r}$ ..... Center of gravity vector

$I_0(x)$ ..... Modified Bessel function of order zero

ρ_0 ..... Spatial coherence radius

$G_x(\kappa)$ ..... Large scale filter function

$G_y(\kappa)$ ..... Small scale filter function

κ_x ..... Large scale frequency cutoff

κ_y ..... Small scale frequency cutoff

WSF ..... Wave structure function

$D(\mathbf{r}_1,\mathbf{r}_2)$ ..... Wave structure function

D_χ ..... Log-amplitude structure function

D_S ..... Phase structure function

ρ ..... Scalar separation distance between two observation points

$D(\rho)$ ..... Wave structure function

$\mathbf{p}$ ..... Difference vector

$D_x(\rho,L)$ ..... Large scale WSF component

$D_y(\rho,L)$ ..... Small scale WSF component

η_x ..... Large scale nondimensional frequency cutoff

η_y ..... Small scale nondimensional frequency cutoff

Q_l ..... Nondimensional inner scale parameter ($=L\kappa_l^2/k$)

$\Gamma(\mathbf{r}_1,\mathbf{r}_2)$ ..... Mutual coherence function

ω_c ..... Angular temporal frequency spread of frequency spectrum

$W(\omega)$ ..... Temporal frequency spectrum

ρ_{pl} ..... Plane wave coherence radius

τ_c ..... Temporal coherence time

ρ_0 ..... Coherence radius of beam wave

DOC ..... Modulus of the complex degree of coherence

σ_f ..... Temporal frequency spread of frequency spectrum

σ_f^2 ..... Temporal frequency variance

$\mathrm{B}_s(\tau)$ ..... Temporal phase covariance

$\mathrm{B}_s(\rho)$ ..... Spatial phase covariance

$\sigma_{f,x}^2$ ..... Large scale temporal frequency variance

$\sigma_{f,y}^2$ ..... Small scale temporal frequency variance

ρ_{sp} ..... Spherical wave coherence radius

Ω_R ..... Fresnel ratio characterizing reflector radius

$\Gamma(\mathrm{x})$ ..... Gamma function

1. INTRODUCTION

The invention of the LASER, or Light Amplification by Stimulated Emission of Radiation, in 1960 generated significant theoretical and experimental interest. Scientists immediately recognized some of the potential applications of laser systems and the development of new applications continues even today, some forty years later. These applications include fiber optic communication systems, medical systems, data storage and retrieval as in computer compact discs (CD) and digital video discs (DVD), just to name a few. Another area of particular interest is the study of *free space optics* (FSO). In an FSO system the optical wave is propagated through whatever medium is present, i.e. air, water, or space, unlike, say, a fiber optic communication system where the optical wave is propagated within a fiber optic cable. Potential applications of free space optics include point-to-point communication systems, laser radar (lidar), remote sensing, and laser weaponry.

Free space optical systems offer many advantages over their conventional microwave radio counterparts. For example, potential data rates are significantly higher in the case of optical communication systems and lidar systems are lighter and require less power, while at the same time providing a more secure channel. There are, however, significant challenges that hinder the development of FSO systems. The most severe problems occur when propagation occurs in the Earth's atmosphere, water, or any medium that is not free space. When propagation occurs in any of these environments, the optical wave is subject to many deleterious effects. These effects are caused by the fact that the propagation medium has an index of refraction that is random in space and time due mainly to random temperature and pressure distributions in the medium.

This random index of refraction results in random amplitude and phase fluctuations in the optical signal. These random fluctuations in phase and amplitude result in effects such as beam wander, irradiance fluctuations, beam spreading, angle of arrival fluctuations, frequency fluctuations, and loss of coherence.

In the period shortly after the invention of the laser there were numerous scientific investigations of the effects of atmospheric laser propagation and possible application development, particularly for free space optical communication systems. However, owing largely to the success of fiber optic communication systems and the many challenges associated with free space optical propagation, interest in such systems waned. Recently, though, there has been a resurgence of interest in free space optical systems. This interest is a result of practical necessity in the case of lidar, remote sensing, and laser weaponry and financial considerations in the case of optical communication systems. The high installation price of fiber optical cable, costing as much as 100 to 500 thousand dollars per mile in certain urban settings, has restricted direct access to the nation's fiber optic backbone. Indeed, it has been estimated that ninety percent of businesses with at least one hundred employees are located at least one mile from the nearest direct access to the fiber optic backbone.[1] As a result of this factor, it is also estimated that only two to five percent of the fiber optic backbone is currently utilized.[1] Free space optics is viewed by many as the most viable method to bridge this gap.

Because the optical field propagating in a random medium is subject to random amplitude and phase fluctuations, it cannot be studied deterministically. Only statistical averages can be considered. The equation describing the the optical field of a laser beam propagating in a random

medium is a stochastic differential equation. Many methods have been espoused to solve the governing equations and develop statistical quantities. Most approaches do not allow analytic solutions because of their inherent mathematical intractability. A perturbation method known as the Rytov approximation does allow considerable progress in the development of analytic solutions due to its relative mathematical ease. However, the validity of statistical quantities obtained via this method is generally restricted to conditions of weak irradiance fluctuations. There has also been significant progress in the development of analytic asymptotic results in the asymptotic regime of strong irradiance fluctuations. There are few analytic results that are valid in all conditions of optical turbulence, particularly in the moderate regime, between the weak and strong cases. This is a significant restriction in that most "real-world" systems are likely to operate in this moderate regime.

The most common statistic studied in atmospheric optics is the scintillation index, or normalized irradiance variance. Recently, significant progress has been made in modelling the scintillation index with analytic results in all irradiance fluctuation regimes by using the Rytov approximation method and applying an *effective* atmospheric spectrum. This method will be described in detail in the following chapters. In the work presented here, a modification of this effective atmospheric spectrum is used to derive analytic expressions for the wave structure function, the temporal frequency spectrum, and the frequency spread of the temporal frequency spectrum of an optical wave propagating in the Earth's atmosphere. It is believed that these expressions are valid under all optical turbulence conditions. Analytic wave structure function results are developed for plane, spherical, and Gaussian-beam waves for one-way propagation

along horizontal paths and double pass propagation along horizontal paths for reflection from a smooth target assuming a transmitted spherical wave. Analytic expressions for the temporal frequency spectrum and the frequency spread of the temporal frequency spectrum are developed for plane and spherical waves for one-way propagation along horizontal and slant paths. Expressions for the frequency spread of the frequency spectrum for double pass propagation along horizontal paths for reflection from a smooth target assuming a transmitted spherical wave are also presented.

2. RANDOM FIELDS

2.1 Introduction

An optical wave propagating through the Earth's atmosphere is subject to random fluctuations in amplitude and phase due to random fluctuations in the index of refraction along the propagation path. Thus, the optical field cannot be described deterministically. However, it is possible to study the optical field in statistical terms. Before we can proceed, we will need several concepts from the study of *random fields*, which are closely related to *random processes,* also known as *stochastic processes.* Note that the work in this chapter closely follows the presentation given by Andrews and Phillips in [2].

A random process is a set of functions, known as an *ensemble*, that are time dependent, each of which is associated with a probability description.[2] We can represent any given member of this set of functions by $x\,(t)$, which is known as a realization of the random process. Then, for any fixed value of t, say t_1, $x\,(t_1)$ can be interpreted as a random variable. In other words, the value of $x\,(t)$ is not deterministic at the time t_1, it is random even at this specific time value. So, $x\,(t)$ is a random function of time, and the random process is made up of a set of these random functions.

When the random process is a function of time, t, *and* of a vector spatial variable, $\mathbf{R} = (x, y, z)$, then it is known as a random field and can be denoted as $x\,(\mathbf{R}, t)$. In general, it is necessary to know the joint probability distributions of all orders of the random field to describe it completely. However, it is usually impossible to derive the complete family of probability distributions, and therefore one usually works with only the lower order field moments. In our applications, we shall assume that the atmosphere does not change appreciably in the time

it takes the optical wave to propagate through the medium and therefore we shall suppress the time dependency. That is, we shall consider the random field to be of the form $x(\mathbf{R})$.

2.2 Spatial covariance function

Assuming we have suppressed the time dependency of the random field, we shall define the *mean value*, $m(\mathbf{R})$, of the random field, $x(\mathbf{R})$, by[2]

$$\langle x(\mathbf{R})\rangle = m(\mathbf{R}), \tag{1}$$

where the brackets $\langle\rangle$ denote an ensemble average, i.e. mean value. We can now define the *spatial covariance function*, $B_x(\mathbf{R}_1, \mathbf{R}_2)$, of the random field, $x(\mathbf{R})$, as[2]

$$B_x(\mathbf{R}_1, \mathbf{R}_2) = \left\langle [x(\mathbf{R}_1) - m(\mathbf{R}_1)]\left[x^*(\mathbf{R}_2) - m^*(\mathbf{R}_2)\right]\right\rangle, \tag{2}$$

where the x^* denotes the complex conjugate of x. The question still remains as to how we shall determine these ensemble averages and will be addressed in the following section.

Notice that the mean value of the random field, $m(\mathbf{R})$, is dependent on the spatial position, $\mathbf{R}$. That is, we see that, analogous to a realization of a random process, the value of the field at any specific position can be thought of as a random variable. Furthermore, any two positions in the field, say $\mathbf{R}_1$ and $\mathbf{R}_2$, may have different mean values, i.e. they are random variables with different probability descriptions. If, however, the mean value of the field is independent of the spatial position, $\mathbf{R}$, then the field is said to be *statistically homogeneous* and its mean value is denoted

simply by[2] $m = \langle x(\mathbf{R}) \rangle$. For a statistically homogeneous field, the spatial covariance function reduces to[2]

$$B_x(\mathbf{R}) = \left\langle x(\mathbf{R}_1) x^*(\mathbf{R}_1 + \mathbf{R}) \right\rangle - |m|^2, \tag{3}$$

where $\mathbf{R} = \mathbf{R}_2 - \mathbf{R}_1$. We note that homogeneity is the spatial equivalent of a random process which is stationary in time.[2]

Finally, if, in addition to being statistically homogeneous, the random field is dependent only on the scalar distance, $R = |\mathbf{R}_2 - \mathbf{R}_1|$, of the specific positions, $\mathbf{R}_1$ and $\mathbf{R}_2$, and not the positions themselves, the field is said to be *statistically isotropic*. In this case, the spatial covariance function can be written as a function of the scalar distance R, that is $B_x(R)$.

2.3 One-dimensional spatial power spectrum

In order to make use of the spatial covariance function definitions given in the previous section, it is necessary to mathematically define the ensemble average of the random field. We begin by considering a statistically homogeneous and isotropic random field. Such a field can be represented by a *Riemann-Stieltjes integral* of the form[2]

$$x(R) = \int_{-\infty}^{\infty} e^{i\kappa R} d\nu(\kappa), \tag{4}$$

where $d\nu(\kappa)$ is a random complex amplitude. Furthermore, we shall assume that the mean value of the random field is zero, i.e. $m = 0$. We can now use (4) to define the spatial covariance

function as[2]

$$B_x(R) = \int_{-\infty}^{\infty} e^{i\kappa R} V_x(\kappa)\, d\kappa, \tag{5}$$

where κ denotes the spatial frequency and $V_x(\kappa)$ is the one-dimensional spectrum of the random field $x(R)$. By the inverse Fourier transform, it follows that the one-dimensional spectrum, $V_x(\kappa)$ is given by[2]

$$V_x(\kappa) = \frac{1}{2\pi} \int_{-\infty}^{\infty} e^{-i\kappa R} B_x(R)\, dR. \tag{6}$$

2.4 Three-dimensional spatial power spectrum

Although the one-dimensional spatial power spectrum is useful in making experimental measurements, we shall need the three-dimensional spatial power spectrum for our theoretical development. Here, we assume that the field is statistically homogeneous with a zero mean. In this case, the field is dependent on the vector $\mathbf{R} = \mathbf{R}_2 - \mathbf{R}_1$, and can be represented by the Riemann-Stieltjes integral given by[2]

$$x(\mathbf{R}) = \int_{-\infty}^{\infty} e^{i\mathbf{K}\cdot\mathbf{R}} dv(\mathbf{K}), \tag{7}$$

where $\mathbf{K} = (\kappa_x, \kappa_y, \kappa_z)$ is the vector wave number and $dv(\mathbf{K})$ denotes the random amplitude of the field, $x(\mathbf{R})$. Note, that so far we have *not* assumed that the field is statistically isotropic. Applying the definition given by (2) and equation (7), the spatial covariance function can now be

written as[2]

$$\begin{aligned} B_x(\mathbf{R}) &= \left\langle x(\mathbf{R}_1)\, x^*(\mathbf{R}_2)\right\rangle \\ &= \int\int\int\int\int\int_{-\infty}^{\infty} \exp\left[i\left(\mathbf{K}\cdot\mathbf{R}_1 - \mathbf{K}'\cdot\mathbf{R}_2\right)\right] \left\langle dv(\mathbf{K})\, dv^*\left(\mathbf{K}'\right)\right\rangle. \end{aligned} \tag{8}$$

In order to satisfy the statistical homogeneity conditions, we must have

$$\left\langle dv(\mathbf{K})\, dv\left(\mathbf{K}'\right)\right\rangle = \delta\left(\mathbf{K}-\mathbf{K}'\right)\Phi_x(\mathbf{K})\, d^3\kappa d^3\kappa', \tag{9}$$

where *δ(x)* is the *Dirac delta function* and $\Phi_x(\mathbf{K})$ is the three-dimensional *spatial power spectrum* of the random field, $x(\mathbf{R})$. Now (8) simplifies to

$$B_x(\mathbf{R}) = \int\int\int_{-\infty}^{\infty} e^{i\mathbf{K}\cdot\mathbf{R}}\Phi_x(\mathbf{K})\, d^3\kappa. \tag{10}$$

In a manner analogous to the one-dimensional spatial power spectrum, $V_x(\kappa)$, the three-dimensional spatial power spectrum, $\Phi_x(\mathbf{K})$, can be obtained from the inverse Fourier transform relation[2]

$$\Phi_x(\mathbf{K}) = \left(\frac{1}{2\pi}\right)^3 \int\int\int_{-\infty}^{\infty} e^{-i\mathbf{K}\cdot\mathbf{R}} B_x(\mathbf{R})\, d^3R. \tag{11}$$

If we now also assume the random field is statistically homogeneous and isotropic, the Fourier transform pair, (10) and (11), reduce to[2]

$$\Phi_x(\kappa) = \frac{1}{2\pi^2\kappa}\int_0^\infty B_x(R)\sin(\kappa R)\,R\,dR, \tag{12}$$

$$B_x(R) = \frac{4\pi}{R}\int_0^\infty \Phi_x(\kappa)\sin(\kappa R)\,\kappa\,d\kappa, \tag{13}$$

where $\kappa = |\mathbf{K}|$ is the magnitude of the vector wave number. Using the relations given by (6) and (13), the three-dimensional spatial power spectrum can be related to the one-dimensional spatial power spectrum by[2]

$$\Phi_x(\kappa) = -\frac{1}{2\pi\kappa}\frac{dV_x(\kappa)}{d\kappa}. \tag{14}$$

2.5 Structure function

One of the main implications of assuming a statistically homogeneous field is that the mean value of the field is constant over all space. However, in many applications of interest the random field does not have a constant mean over large spatial distances. In particular, velocity fields in a turbulent medium do not have a constant mean over large spatial separations. Thus, one cannot generally assume that the field is strictly homogeneous. However, the velocity difference at two points in the field usually behaves like a statistically homogeneous field.

Random fields that can be expressed as the sum of a varying mean and a statistically homogeneous fluctuation are called *locally homogeneous.* Thus a locally homogeneous random

field, $x\,(\mathbf{R})$, can be written in the form[2]

$$x\,(\mathbf{R}) = m\,(\mathbf{R}) + x_1\,(\mathbf{R})\,, \tag{15}$$

where $m\,(\mathbf{R})$ represents the varying mean and $x_1\,(\mathbf{R})$ represents the statistically homogeneous fluctuation with mean value $\langle x_1\,(\mathbf{R})\rangle = 0$ for all vector positions, $\mathbf{R}$.

It is customary to characterize a locally homogeneous random field by its structure function rather than its covariance function. The structure function for a locally homogeneous random field, $x\,(\mathbf{R})$, of the form (15) is defined by[2]

$$\begin{aligned} D_x\,(\mathbf{R}_1, \mathbf{R}_2) &= D_x\,(\mathbf{R}) = \left\langle [x\,(\mathbf{R}_1) - x\,(\mathbf{R}_1 + \mathbf{R})]^2 \right\rangle \\ &\approx \left\langle [x_1\,(\mathbf{R}_1) - x_1\,(\mathbf{R}_1 + \mathbf{R})]^2 \right\rangle, \end{aligned} \tag{16}$$

and the power spectrum is related to this structure function by

$$D_x\,(\mathbf{R}) = 2 \int \int \int_{-\infty}^{\infty} \Phi_n\,(\mathbf{K})\,[1 - \cos\,(\mathbf{K} \cdot \mathbf{R})]\,d^3\kappa. \tag{17}$$

If the random field is both locally homogeneous and isotropic, the structure function is a function of the scalar distance, $R = |\mathbf{R}_2 - \mathbf{R}_1|$, only and can be related to the power spectrum through the relation[2]

$$D_x\,(R) = 8\pi \int_0^{\infty} \kappa^2 \Phi_x\,(\kappa) \left(1 - \frac{\sin \kappa R}{\kappa R}\right) d\kappa. \tag{18}$$

Finally, the spatial power spectrum can be determined from the inverse Fourier relation in the locally homogeneous and isotropic case by the relation[2]

$$\Phi_x(\kappa) = \frac{1}{4\pi^2\kappa^2}\int_0^\infty \frac{\sin\kappa R}{\kappa R}\frac{d}{dR}\left[R^2\frac{d}{dR}D_x(R)\right]dR. \tag{19}$$

3. ATMOSPHERIC TURBULENCE

3.1 Introduction

Most early investigations of turbulence centered around the concepts of velocity fluctuations in a viscous fluid. These concepts are directly related to atmospheric studies. In particular, the atmospheric longitudinal wind velocity, which fluctuates randomly about its mean value, can be studied as a random field using the concepts from the previous chapter. Treating the atmosphere as a viscous fluid, it can be considered to have laminar and turbulent flow. In the case of laminar flow, the changes in the velocity field are uniform. However, when the flow is in a turbulent state the velocity field develops random subfields known as *turbulent eddies*. In this case, changes in the velocity field are no longer uniform and do not follow a predictable pattern. The concept of turbulent eddies can be used to qualitatively describe the turbulent atmosphere. Essentially, the atmosphere is thought of as being made up of turbulent eddies, each with their own velocity characteristics. These eddies exist in a continuum of spatial dimensions. In essence, the larger eddies break-up into continuously smaller eddies and energy is transferred between these eddies in the form of velocity. There exists a largest eddy size, L_0, known as the *outer scale* of turbulence, and a smallest eddy size, l_0, known as the *inner scale* of turbulence. Scale sizes between the inner and outer scale form what is known as the *inertial subrange.* Scale sizes smaller than the inner scale belong to the dissipation range where energy is dissipated in the form of heat.

The *Reynolds number*, $\mathrm{Re} = Vl/\nu$, where V is the characteristic velocity, l is the dimension of the flow, and ν is the kinematic viscosity, can be used to characterize the transition from laminar to turbulent flow. For Reynolds numbers greater than what is commonly called the *critical*

Reynolds number, the flow is considered turbulent. Typical Reynolds numbers for ground level wind velocity are on the order Re $\approx 10^5$, for which the flow is considered highly turbulent.[2]

In order to apply these concepts in a meaningful way to the study of optical wave propagation, it is necessary to relate the atmospheric wind velocity fluctuations to a physical phenomenon that affects a propagating electromagnetic wave. Random fluctuations in wind velocity in the presence of atmospheric moisture and temperature gradients manifest themselves as random index of refraction fluctuations. That is, the atmospheric index of refraction can be treated as a random field where the index of refraction at any spatial point in the atmosphere at any given time can be considered a random variable. The main factor causing the randomness in the index of refraction is small temperature fluctuations in the atmosphere caused by the randomly fluctuating wind velocity. Although other factors, such as small pressure and humidity changes, contribute to the refractive index fluctuations they are dominated by the impact of the temperature fluctuations and are generally ignored in most atmospheric optics studies.

Statistical descriptions of the atmospheric wind velocity field and the relation to the index of refraction fluctuations have been well formulated. Noting that the index of refraction has a direct physical effect on a propagating electromagnetic signal, it is now possible to describe the effects of atmospheric turbulence on a propagating electromagnetic wave in statistical terms. This chapter provides a brief description of the refractive index fluctuations and the associated index of refraction spectral models. A more comprehensive treatment, including the development of the relations between velocity, temperature and refractive index fluctuations is given by Andrews and Phillips.[2]

3.2 Index of refraction fluctuations

It has already been stated that the atmospheric index of refraction can be treated as a random field. Specifically, the index of refraction is a random function of both space and time. However, in optical studies the time dependency of the index of refraction is usually suppressed. Furthermore, we shall assume that the index of refraction field is locally homogeneous and can be expressed in the form of equation (15). Thus, we can write the index of refraction, $n(\mathbf{R})$, as a random function of space in the form[2]

$$n(\mathbf{R}) = n_0 + n_1(\mathbf{R}), \tag{20}$$

where n_0 is the mean value and $n_1(\mathbf{R})$ is the statistically homogeneous fluctuation, whose mean value is taken to be zero, i.e. $\langle n_1(\mathbf{R})\rangle = 0$. The mean value, n_0, is typically taken to be one, i.e. $n_0 = \langle n(\mathbf{R})\rangle \approx 1$, so that the index of refraction, (20), is now

$$n(\mathbf{R}) = 1 + n_1(\mathbf{R}). \tag{21}$$

Though not presented here, it can be shown that the index of refraction function, (21), can be directly related to the random atmospheric temperature and pressure functions.[2] In turn, this relation can be used to define the index of refraction structure function. Assuming the index of refraction field is statistically homogeneous and isotropic, the refractive index structure function is[2]

$$D_n(R) = \begin{cases} C_n^2 R^{2/3}, & l_0 \ll R \ll L_0 \\ C_n^2 l_0^{-4/3} R^2, & l_0 \ll R \ll L_0 \end{cases}, \tag{22}$$

where l_0 is the inner scale of turbulence and C_n^2 is the index of refraction structure parameter, which is essentially a measure of the strength of the refractive index fluctuations. Values of C_n^2 have been measured experimentally and typically range between $10^{-17}\ m^{-2/3}$ and $10^{-13}\ m^{-2/3}$. The value of C_n^2 varies strongly with time of day, season, and environment. However, it can be considered constant for short time periods for propagation paths that have a constant height above the ground layer, so called horizontal paths. When the propagation path is a slant path, that is when the height above the ground layer is changing along the propagation path, the value of C_n^2 can no longer be considered constant as it has an altitude dependency. Similar statements are true of the inner scale of turbulence, l_0. For horizontal paths the inner scale is usually taken to be between one and ten millimeters.

3.3 Refractive index spatial power spectrum

In order to facilitate the work in the remaining chapters it is necessary to present the refractive index spatial power spectrum. Recall from chapter 2, that for a statistically homogeneous and isotropic field the spatial power spectrum is a scalar function and can be related to the covariance function by the Fourier transform as given in equation (12). In this case, the refractive index spatial power spectrum, $\Phi_n(\kappa)$, is given by[2]

$$\Phi_n(\kappa) = \frac{1}{2\pi^2\kappa}\int_0^\infty B_n(R)\sin(\kappa R)\, R\, dR, \tag{23}$$

where $\kappa = |\mathbf{K}|$ is the spatial wave number of the a given turbulent eddy size, i.e. $\kappa = 1/l$, where l is the eddy size, and $B_n(R)$ is the corresponding refractive index covariance function. Kolmogorov

presented a model for the refractive index spectral model given by[2]

$$\Phi_n(\kappa) = 0.033 C_n^2 \kappa^{-11/3}. \tag{24}$$

Equation (24) is commonly referred to as the *Kolmogorov spectrum*. In the development of this spectrum, Kolmogorov argued that the functional form of the refractive index spatial power spectrum is the same as that for the temperature spatial power spectrum and that temperature fluctuations observe the same spectral laws as velocity fluctuations. The validity of these arguments has been generally accepted and, with some modification, the Kolmogorov spectral model serves as the foundation of much of the work in the field of atmospheric optics. Note that the Kolmogorov spectrum assumes and infinite outer scale, L_0, and a zero inner scale, l_0, which is not always physically appropriate or mathematically convenient. Thus, it is necessary to modify the Kolmogorov spectral model when considering the spectrum in the dissipation range, i.e. when $\kappa > 1/l_0$. To account for these issues, Tatarskii suggested the spectral model given by[2]

$$\Phi_n(\kappa) = 0.033 C_n^2 \kappa^{-11/3} \exp\left(-\frac{\kappa^2}{\kappa_m^2}\right), \tag{25}$$

where $\kappa_m = 5.92/l_0$. This spectral model, known as the *Tatarskii spectral model*, essentially truncates the spectrum at the finite inner scale of turbulence, l_0. However this spectral model still has a singularity at $\kappa = 0$, that is as in the limiting case of an infinite outer scale. A finite outer scale of turbulence can be incorporated to remove the singularity as is done in the *von Kármán*

spectrum given by

$$\Phi_n(\kappa) = 0.033 C_n^2 \kappa^{-11/3} \frac{\exp\left(-\frac{\kappa^2}{\kappa_m^2}\right)}{\left(\kappa^2 + \kappa_0^2\right)^{11/6}}, \tag{26}$$

where $\kappa_0 = 2\pi / L_0$. For horizontal path propagation, the outer scale is often assumed to be equal to one-half the height above the ground level. Although the spectral models, (24)-(26) are useful in theoretical studies they do not completely represent the actual atmospheric index of refraction spectrum. In particular, it has been shown[2] that there exists a "bump" in the spectrum at high wave numbers, which none of these models predicts. A numerical model that does predict this bump has been developed by Hill. Andrews presented an analytic approximation to this spectrum given by

$$\Phi_n(\kappa) = 0.033 C_n^2 \left[1 + 1.802\left(\frac{\kappa}{\kappa_l}\right) - 0.254\left(\frac{\kappa}{\kappa_l}\right)^{7/6}\right] \frac{\exp\left(-\frac{\kappa^2}{\kappa_l^2}\right)}{\left(\kappa^2 + \kappa_0^2\right)^{11/6}}, \tag{27}$$

where $\kappa_l = 3.3 / l_0$. The spectral model, (27), shall be referred to as the *Hill* spectrum in this work. Notice that the spectral models (25)-(27) reduce to the Kolmogorov model, (24), as the inner scale approaches zero, $l_0 \longrightarrow 0$, and the outer scale approaches infinity, $L_0 \to \infty$.

4. RYTOV APPROXIMATION METHOD

4.1 Introduction

The notion of a random field has been discussed to some extent. The mathematical concepts of a random field have been used to characterize the random atmosphere, specifically the random atmospheric refractive index. These concepts can also be directly applied to describe an optical wave propagating in the atmosphere. In general, optical waves, which are subsets of a broader class of waves known as *electromagnetic waves,* are described mathematically through the notion of an *electromagnetic field.* In the specific case of electromagnetic waves occupying visible, or optical, wavelengths, this field is commonly known as an *optical field*. In the absence of turbulence, that is in free space, the optical field can be described deterministically. However, in the presence of optical turbulence in the form of a randomly fluctuating refractive index, the optical field cannot be described deterministically. Instead, the optical field must be treated as a random field and is most often characterized in statistical terms. The *random optical field*, denoted $U(\mathbf{R}, t)$, is a random function of space and time. As was the case for the random atmospheric index of refraction function, the time dependency of the optical field is generally suppressed and only spatial fluctuations are considered, thus, the random optical field depends only on position and is denoted by $U(\mathbf{R})$.

If one assumes that the propagating electromagnetic wave is monochromatic and is propagating in a medium with a random refractive index, it can be shown that the equation governing the vector amplitude of the electromagnetic field, $\mathbf{E}(\mathbf{R})$, is given by the vector *stochastic*

partial differential equation[2]

$$\nabla^2 \mathbf{E} + k^2 n^2 (\mathbf{R})\, \mathbf{E} + 2\nabla \left[\mathbf{E} \cdot \nabla \log n (\mathbf{R}) \right] = 0, \tag{28}$$

where $\mathbf{R} = (x, y, z)$ represents a point in space, k is the optical wave number related to the wavelength, λ, by the relation $k = 2\pi/\lambda$, $n(\mathbf{R})$ is the random position dependent index of refraction, and $\nabla^2 = \partial^2/\partial x^2 + \partial^2/\partial y^2 + \partial^2/\partial z^2$ is the Laplacian operator. Depending on the application of interest, certain assumptions can be made to simplify (28). For electromagnetic waves in the optical band, the wavelength is significantly smaller than the inner scale of turbulence, $\lambda \ll l_0$. This results in scattering that is contained in a small cone in the forward direction of propagation, and as a consequence the last term of (28), which relates to polarization of the wave, is generally neglected.[2] Applying this simplification, one can decompose the resulting vector equation into three scalar equations each describing one component of the vector field. This leads to a scalar stochastic partial differential equation of the form

$$\nabla^2 U + k^2 n^2 (\mathbf{R})\, U = 0, \tag{29}$$

where $U(\mathbf{R})$ denotes one of the scalar components of the optical field that is transverse to the propagation direction.

Although the wave equation given in (29) is a significant simplification of that given in (28), it still has not been solved exactly in closed form. Several solution methods to (29) have been proposed, including the Rytov approximation method, the extended Huygens-Fresnel principle,

and the parabolic equation method. Each of these methods has its respective pros and cons and none has proved to be completely satisfactory. The parabolic equation method is theoretically applicable under all conditions of optical turbulence for all field moments. The drawback to the parabolic equation method is that, although it does sometimes allow for analytic solutions, it is often restricted to numerical analysis because of its inherent mathematical difficulty. Although numerical results are very useful, analytic results are valuable because they more readily reveal the dependency of a statistical quantity on given system parameters. The extended Huygens-Fresnel principle has been shown to agree with the parabolic equation method in all conditions of optical turbulence for first and second order field moments. However, it has not been shown to be agree for fourth order field moments. As fourth order field moments are required to describe many statistical quantities, such as irradiance fluctuations, this is an important restriction. The main advantage of the Rytov approximation method, as compared to the parabolic equation method, is that it allows for the development of analytic expressions for many statistical quantities involving first, second, and fourth order field moments. The downside to the Rytov approximation method is that, generally, when compared to experimental data the validity of statistical expressions derived from this method is restricted to weak optical turbulence conditions. This is a significant restriction in that most real world free space optical systems of practical value are likely to operate in the moderate to strong turbulence regimes. In the remaining chapters, however, we shall detail a modification of the Rytov method that is believed to extend the validity of these statistical quantities into all optical turbulence conditions. The remainder of this chapter provides a background on

the Rytov method that is intentionally brief as this method has been well documented by several authors.[2,4,5]

4.2 Quantifying optical turbulence strength

As stated in the preceding section, the validity of the Rytov method is generally restricted to the weak optical turbulence regime. It remains to mathematically quantify the notion of turbulence strength as it relates to atmospheric optics. This is generally done using the *Rytov variance*, denoted σ_1^2. The Rytov variance is a measure of the scintillation index, which is the irradiance variance normalized by the mean irradiance. The Rytov variance is the scintillation index for a plane wave as determined using the Rytov approximation method where the Kolmogorov spectrum, (24), is applied. The Rytov variance is given by

$$\sigma_1^2 = 1.23 C_n^2 k^{7/6} L^{11/6}, \tag{30}$$

where C_n^2 is the atmospheric index of refraction structure parameter, L is the propagation path length, and $k = \frac{2\pi}{\lambda}$ is the optical wave number. Optical turbulence is considered weak when $\sigma_1^2 \ll 1$, strong when $\sigma_1^2 \gg 1$, and moderate otherwise. The limiting case, $\sigma_1^2 \longrightarrow \infty$, defines the so called *saturation regime*.

The classification of optical turbulence using only the Rytov variance implies that the scintillation index is much less than unity through out the wave profile. This is sufficient in the case of infinite plane and spherical waves where edge effects are not usually considered. However, in

the case of a finite Gaussian-beam wave, edge effects are significant and optical turbulence cannot be classified solely based on the Rytov variance. Thus, for the Gaussian-beam wave case, to ensure that the scintillation index is much less than unity throughout the beam profile, the following two conditions must be satisfied[2]

$$\sigma_1^2 \ll 1 \quad \textit{and} \quad \sigma_1^2 \left(\frac{2L}{kW^2} \right) \ll 1, \tag{31}$$

where W is the free space, i.e. in the absence of turbulence, beam radius after propagating a distance L. The beam radius is defined as the point at which the field amplitude is e^{-1} of that observed on the optical axis, i.e. the beam center. If either of the conditions given by (31) is not satisfied, the optical turbulence is considered to be in the moderate to strong regime.

4.3 Rytov approximation

The *Rytov approximation* is a perturbation solution to the wave equation (29) where the optical field is written in the form[2]

$$U(r, L) = U_0(r, L) \exp\left[\Psi(r, L)\right], \tag{32}$$

where $U_0(\mathbf{R})$ is the optical field in free space and Ψ is a complex phase perturbation due to turbulence that can be written as

$$\Psi(r, L) = \Psi_1(r, L) + \Psi_2(r, L) + \ldots \tag{33}$$

The terms Ψ_1 and Ψ_2 are known as the first and second order complex *phase perturbations* respectively. Although the Rytov method can be applied directly to (29), it is easier to relate the phase perturbations to the optical field perturbations obtained in the *Born approximation*.

The Born approximation is also a perturbation solution to the wave equation, (29), but instead of assuming a multiplicative perturbation, as in the Rytov method, an additive perturbation is used. That is, in the Born approximation the optical field is written as a sum of terms given by[2]

$$U(\mathbf{R}) = U_0(\mathbf{R}) + U_1(\mathbf{R}) + U_2(\mathbf{R}) + \ldots, \tag{34}$$

where U_0 is the optical field in free space and U_1 and U_2 represent *field perturbations* due to the presence of optical turbulence. It is also assumed that the square of the index of refraction, $n^2(\mathbf{R})$, can be written as

$$n^2(\mathbf{R}) \approx 1 + 2n_1(\mathbf{R}), \tag{35}$$

where the relation given by (21) has been used and it has been assumed that $\left|n_1^2(\mathbf{R})\right| \ll 1$. Substitution of equations (34) and (35) into the wave equation, (29), yields the system of differential equations[2]

$$\nabla^2 U_0 + k^2 U_0 = 0 \tag{36}$$

$$\nabla^2 U_1 + k^2 U_1 = -2k^2 n_1(\mathbf{R})\, U_0(\mathbf{R}) \tag{37}$$

$$\nabla^2 U_2 + k^2 U_2 = -2k^2 n_1(\mathbf{R})\, U_1(\mathbf{R}). \tag{38}$$

This represents a system of nonhomogeneous equations with constant coefficients, where the random coefficients have been relegated to the forcing terms, and can be solved by the method of Green's function.[2] Solving the system up to second order yields the first and second order perturbations[2]

$$U_1(\mathbf{r}, L) = \frac{k^2}{2\pi}\int_0^L dz \int\int_{-\infty}^{\infty} d^2s \exp\left[ik(L-z) + \frac{ik|\mathbf{s}-\mathbf{r}|^2}{2(L-z)}\right] U_0(\mathbf{s}, z)\frac{n_1(\mathbf{s}, z)}{L-z}, \quad (39)$$

$$U_2(\mathbf{r}, L) = \frac{k^2}{2\pi}\int_0^L dz \int\int_{-\infty}^{\infty} d^2s \exp\left[ik(L-z) + \frac{ik|\mathbf{s}-\mathbf{r}|^2}{2(L-z)}\right] U_1(\mathbf{s}, z)\frac{n_1(\mathbf{s}, z)}{L-z}. \quad (40)$$

In order to develop the expressions for the phase perturbations of the Rytov method using the Born approximation field perturbations, it is necessary to introduce the *normalized Born approximations* defined by

$$\phi_m(\mathbf{r}, L) = \frac{U_m(\mathbf{r}, L)}{U_0(\mathbf{r}, L)}, \qquad m = 1, 2, 3, \ldots \quad (41)$$

where m denotes the order of the perturbation. The first and second order Rytov phase perturbations can now be related to the first and second order normalized Born approximations through the relations[2]

$$\Psi_1(\mathbf{r}, L) = \ln\left[1 + \phi_1(\mathbf{r}, L)\right] \approx \phi_1(\mathbf{r}, L) \quad (42)$$

$$\Psi_2(\mathbf{r}, L) \approx \phi_2(\mathbf{r}, L) - \frac{1}{2}\phi_1^2(\mathbf{r}, L), \quad (43)$$

where it is assumed that the magnitude of the phase perturbations is small, i.e. $\left|\phi_1(\mathbf{r}, L)\right| \ll 1$ and $\left|\phi_2(\mathbf{r}, L)\right| \ll 1$.

4.4 Statistical moments

The remaining chapters will focus on certain statistical descriptions of an optical wave propagating in the Earth's atmosphere. To aid in the derivation of the statistical quantities of interest, it is useful to define the following three second-order statistical moments, $\mathbf{E}_n(\mathbf{r}_1,\mathbf{r}_2)$, of the complex phase perturbations[2]

$$\begin{aligned} E_1(\mathbf{r}, \mathbf{r}) &\equiv \langle \Psi_2(\mathbf{r}, L)\rangle + \frac{1}{2}\left\langle \Psi_1^2(\mathbf{r}, L)\right\rangle \\ E_2(\mathbf{r}_1, \mathbf{r}_2) &\equiv \left\langle \Psi_1(\mathbf{r}_1, L)\, \Psi_1^*(\mathbf{r}_2, L)\right\rangle, \\ E_3(\mathbf{r}_1, \mathbf{r}_2) &\equiv \langle \Psi_1(\mathbf{r}_1, L)\, \Psi_1(\mathbf{r}_2, L)\rangle, \end{aligned} \tag{44}$$

where the asterisk * denotes the complex conjugate. Integral expressions for these statistical moments can be given using equations (39)-(43). However, in order to calculate values for these statistical moments it is necessary to develop spectral representations of the the complex phase perturbations, Ψ_1 and Ψ_2. This can be done by expressing the index of refraction fluctuation in the form of a Riemann-Stieltjes integral[2]

$$n_1(\mathbf{s}, z) = \int\int_{-\infty}^{\infty} \exp(i\mathbf{K}\cdot\mathbf{s})\, d\nu(\mathbf{K}, z), \tag{45}$$

where dν(**K**,z) is the random amplitude of the refractive index fluctuations. Substitution of this expression into the integral definitions of the normalized Born approximations yields integral expressions for the spectral representations of the Rytov phase perturbations and hence the second-order statistical moments, (44). Usable integral definitions of the second-order statistical moments of the phase perturbations can now be derived using further assumptions about the form of the ensemble average of the random amplitude of the refractive index fluctuations, $\langle d\nu\,(\mathbf{K}, z)\rangle$, the relation of the two dimensional spatial power spectrum and the three dimensional spatial power spectrum, assuming the atmospheric refractive index field is statistically homogeneous and isotropic, and applying the method of cumulants These steps are well documented by Andrews and Phillips[2] and are not repeated here. It suffices to state that the resulting statistical moments are given by[2]

$$\begin{aligned} E_1(\mathbf{r},\mathbf{r}) &= E_1(0,0) = \langle \Psi_2(\mathbf{r}, L)\rangle + \frac{1}{2}\left\langle \Psi_1^2(\mathbf{r}, L)\right\rangle \\ &= -2\pi^2 k^2 \int_0^L \int_0^\infty \kappa \Phi_n(\kappa, z)\, d\kappa dz, \end{aligned} \tag{46}$$

$$\begin{aligned} E_2(\mathbf{r}_1,\mathbf{r}_2) &= \left\langle \Psi_1(\mathbf{r}_1, L)\, \Psi_1^*(\mathbf{r}_2, L)\right\rangle \\ &= 4\pi^2 k^2 \int_0^L \int_0^\infty \kappa \Phi_n(\kappa, z)\, J_0\left\{\kappa \left|\gamma\, \mathbf{r}_1 - \gamma^*\mathbf{r}_2\right|\right\} \\ &\quad \times \exp\left[-\frac{i\kappa^2}{2k}\left(\gamma - \gamma^*\right)(L - z)\right] d\kappa dz, \end{aligned} \tag{47}$$

$$
\begin{aligned}
E_3(\mathbf{r}_1, \mathbf{r}_2) &\equiv \langle \Psi_1(\mathbf{r}_1, L)\, \Psi_1(\mathbf{r}_2, L) \rangle \\
&= -4\pi^2 k^2 \int_0^L \int_0^\infty \kappa \Phi_n(\kappa, z)\, J_0(\gamma\, \kappa\, |\mathbf{r}_1 - \mathbf{r}_2|) \\
&\quad \times \exp\left[-\frac{i\kappa^2 \gamma}{k} (L - z) \right] d\kappa dz,
\end{aligned}
\tag{48}
$$

where $i = \sqrt{-1}$, $\Phi_n(\kappa, z)$ is the refractive index spectral model, $\mathbf{r}_1$ and $\mathbf{r}_2$ are any two points in the plane transverse to the propagation direction at a distance, *L,* along the propagation path, $J_0(x)$ is the zeroth order Bessel function of the first kind, and γ is the path amplitude ratio for the path of interest. Given the path amplitude ratio and the refractive index spectral model, equations (46)-(48) can now be used to develop analytic expressions for various statistical quantities. Note that the magnitude bars, ||, in the Bessel functions of the second order statistical moments do not represent the standard usage. They apply only to the vectors and their usage is detailed in Appendix A.

5. MODIFIED RYTOV METHOD

5.1 Introduction

In the last chapter, it was noted that the Rytov perturbation solution to the stochastic wave equation, (29), can often be used to develop analytic expressions for various statistical quantities describing an optical field propagating in a turbulent medium. This is a major advantage over the parabolic equation method, which is often restricted to numerical evaluation. However, it was also stated that the validity of statistical quantities developed using the Rytov method is generally restricted to weak optical turbulence conditions when compared to experimental data. Because most free space optics applications of interest would likely operate in moderate to strong optical turbulence, it is desirable to develop a method that readily yields analytic results but is also valid in all optical turbulence regimes. Recently, Andrews *et al.*[6,7,8] were able to develop analytic expressions for scintillation index that are believed to be valid in all optical turbulence conditions. Their expressions were derived using a modification of the Rytov method presented in the previous chapter, which for clarity we shall now refer to as the *standard Rytov method*. The *modified Rytov method* follows the exact same development as the standard Rytov method of the preceding chapter, except that the atmospheric refractive index spectral model, $\Phi_n(\kappa, z)$, is replaced with an *effective* atmospheric refractive index spectral model. In this chapter, we present the background for the modified Rytov method. In the remaining chapters, this method is applied, with some modification, to develop wave structure function and temporal frequency spread expressions.

5.2 Scintillation Index

The scintillation index is the irradiance variance normalized by the mean irradiance. Denoting the received irradiance by *I(***r***,L)*, the scintillation index, σ_I^2, can be expressed as

$$\sigma_I^2 = \frac{\langle I^2 \rangle - \langle I \rangle^2}{\langle I \rangle^2}. \tag{49}$$

The statistical moments (46)-(48) can be used to develop an evaluatable integral definition of (49). For a one-way horizontal propagation path, the path amplitude ratio, γ , is given by[2]

$$\gamma = 1 - \left(\bar{\Theta} + i\Lambda\right)\left(1 - \frac{z}{L}\right), \tag{50}$$

where Λ and Θ are beam parameters characterizing the optical wave at the *receiver*. Beam parameters describing the optical wave at the *transmitter,* Λ_0 and Θ_0*,* are given by

$$\Lambda_0 = \frac{2z}{kW_0^2}, \ \Theta_0 = 1 - \frac{z}{F_0} \tag{51}$$

where W_0 is the beam radius at the transmitter, F_0 is the phase front radius of curvature at the transmitter, z is the propagation path length, and k is the optical wave number. These parameters can be used to define the beam parameters at the receiver as

$$\Lambda = \frac{\Lambda_0}{\Lambda_0^2 + \Theta_0^2}, \ \Theta = \frac{\Theta_0}{\Lambda_0^2 + \Theta_0^2}, \ \bar{\Theta} = 1 - \Theta. \tag{52}$$

Note, in the special case of an infinite plane wave $\Theta_0 = 1$ and $\Lambda_0 = 0$ and in the special case of a point source, i.e. a spherical wave, $\Theta_0 = 0$ and $\Lambda_0 = 0$. For a collimated Gaussian-beam wave, the phase front radius of curvature is infinite, so that $\Theta_0 = 1$.

Substituting the path amplitude ratio, γ , given by (50), into the statistical moments (46)-(48), the resulting integral definition for the scintillation index for horizontal path propagation is given by[2]

$$\sigma_I^2(\mathbf{r}, L) = 4\sigma_r^2(\mathbf{r}, L) + \sigma_{I,l}^2(L), \tag{53}$$

where $\mathbf{r}=\frac{1}{2}(\mathbf{r}_1 + \mathbf{r}_2)$ is a center of gravity vector. The quantity σ_r represents the radial, or off-axis, component of scintillation and $\sigma_{I,l}$ represents the longitudinal, or on-axis, component. In the Rytov approximation, σ_r is defined by[2]

$$\begin{aligned}\sigma_r^2 &= \frac{1}{2}\left[E_2(\mathbf{r}, \mathbf{r}) - E_2(0, 0)\right] \\ &= 2\pi^2 k^2 L \int_0^1 \int_0^\infty \kappa \Phi_n(\kappa) \exp\left(-\frac{\Lambda L \kappa^2 \xi^2}{k}\right)\left[I_0(2\Lambda r \xi \kappa) - 1\right] d\kappa d\xi,\end{aligned} \tag{54}$$

where ξ is the normalized path length argument given by $\xi = 1 - \frac{z}{L}$, $r = |\mathbf{r}|$ is the magnitude of the center of gravity vector, and *$I_0(x)$* is the zeroth order modified Bessel function of the first kind. Also note that the refractive index spectral model, $\Phi_n(\kappa)$, has been expressed independently of the path length argument, z. This is because in the horizontal path case it is assumed that the spectral model is independent of the position along the propagation path. When the slant path case is considered, it will be necessary to include an altitude dependency for the refractive index

spectrum. The longitudinal component, $\sigma_{I,l}$, is given by[2]

$$\begin{aligned}\sigma_{I,l}^2(L) &= 2\,\mathrm{Re}\left[E_2(0,0)+E_3(0,0)\right] \\ &= 8\pi^2 k^2 L\int_0^1\int_0^\infty \kappa\Phi_n(\kappa)\exp\left(-\frac{\Lambda L\kappa^2\xi^2}{k}\right) \\ &\quad\times\left\{1-\cos\left[\frac{L\kappa^2}{k}\xi\left(1-\bar{\Theta}\xi\right)\right]\right\}d\kappa d\xi. \end{aligned} \tag{55}$$

5.3 Effective atmospheric spectrum

In the limiting case of an infinite plane wave $\Lambda = 0$ and $\Theta = 1$, the integral definition of the scintillation index reduces to

$$\sigma_I^2(L) = 8\pi^2 k^2 L\int_0^1\int_0^\infty \kappa\Phi_n(\kappa)\left[1-\cos\left(\frac{L\kappa^2}{k}\xi\right)\right]d\kappa d\xi, \tag{56}$$

where we note that the radial component is zero, $\sigma_r^2 = 0$, because $I_0(0) = 1$. Substituting the Kolmogorov spectrum, (24), into (56) and evaluating yields the standard Rytov expression for the plane wave scintillation index, also known as the Rytov variance,

$$\sigma_I^2 = \sigma_1^2 = 1.23 C_n^2 k^{7/6} L^{11/6}. \tag{57}$$

Although (57) is valid in the weak optical turbulence regime, it fails to accurately model the scintillation index in the moderate to strong optical turbulence regimes. It is known from asymptotic and experimental results that the scintillation index increases with increasing values of

the Rytov variance until it reaches a maximum value greater than unity in the regime characterized by random focusing. With increasing path length, or inhomogeneity strength, multiple scattering weakens the focusing effect and the irradiance fluctuations slowly begin to decrease, saturating at a level for which the scintillation index approaches unity from above. Saturation occurs because multiple scattering causes the optical wave to become increasingly less coherent as it propagates. However, the scintillation index expression given by the standard Rytov method, (57), increases without bound as the turbulence strength increases, that is, as L or C_n^2 increases, indicating that the Rytov method is valid only in the weak turbulence regime. Similar limitations are found in the spherical and Gaussian-beam wave cases. Figure 1, taken from [7], presents the plane wave scintillation index behavior as predicted by the standard Rytov method, (57), and the asymptotic results. The solid curve approximately represents the actual behavior.

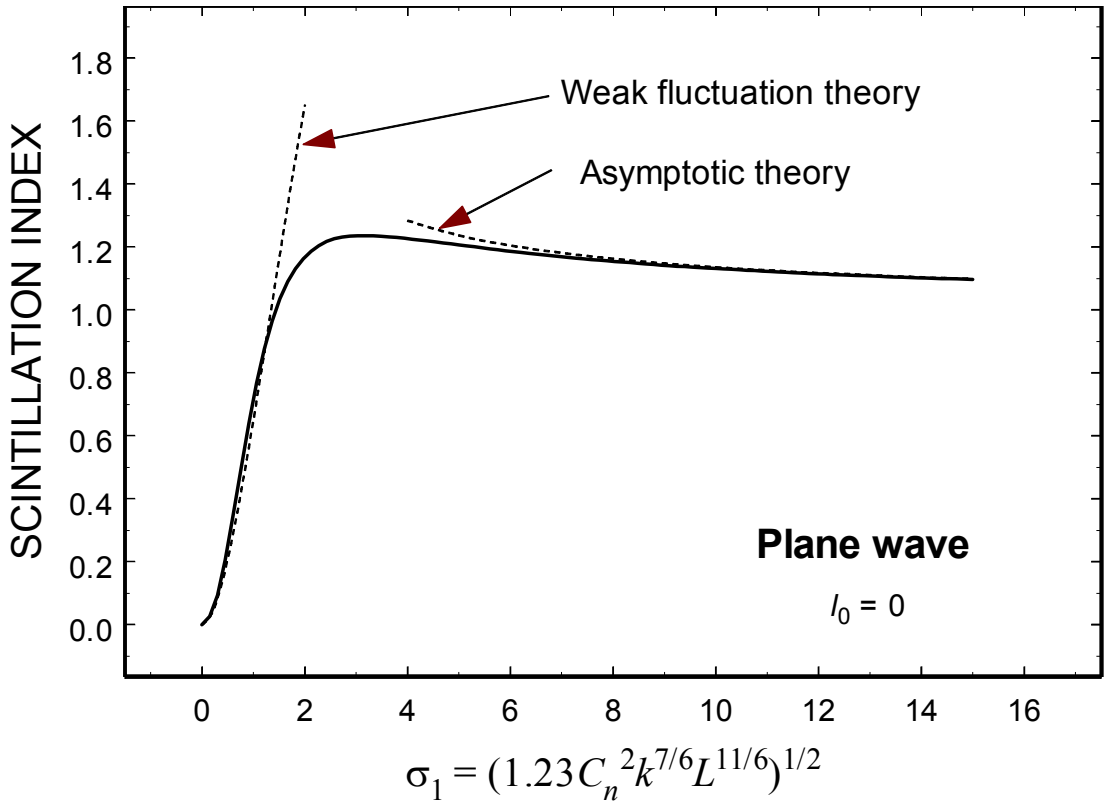

Figure 1 Scintillation index of a plane wave as a function of turbulence strength. The solid curve represents the actual behavior. The weak fluctuation theory is the curve obtained from (57).

In an effort to develop analytic expressions that accurately model the scintillation index in all turbulence regimes, Andrews *et al*.[6,7,8] argued that in the absence of both inner and outer scale effects, the irradiance is mainly affected by refractive index scale sizes described by the spatial coherence radius, ρ_0, the Fresnel zone size, $\sqrt{L/k}$, and the scattering disk, $\frac{L}{k\rho_0}$. They contend that only two sets of scale sizes contribute significantly to the scintillation index. The first set is a large scale component that includes only scale sizes larger than the maximum of the Fresnel zone and the scattering disk. The second set is a small scale component that includes only scale sizes smaller than the minimum of the Fresnel zone and the spatial coherence radius. Figure 2, taken from [7], presents curves for the Fresnel zone, the coherence radius, and the scattering disk as a function of increasing propagation path length, i.e. increasing turbulence strength. From figure 2, we see that the set of conditions for the scale sizes described above results in the inclusion of all scale sizes in the weak turbulence regime. However, as the propagation path length increases, the three curves intersect at roughly the onset of moderate to strong turbulence conditions and the set of conditions described above implies that the effects of intermediate scale sizes are not significant as the strength of turbulence increases. This leads to the notion that intermediate refractive index scale sizes, κ, effectively lose their ability to refract and diffract the optical wave as it propagates as a result of the continuing loss of transverse spatial coherence of the propagating wave. Thus, the failure of the standard Rytov approximation to accurately model the scintillation index in the moderate to strong turbulence regimes results because the standard method does not account for the decreasing effect of these intermediate scale sizes.

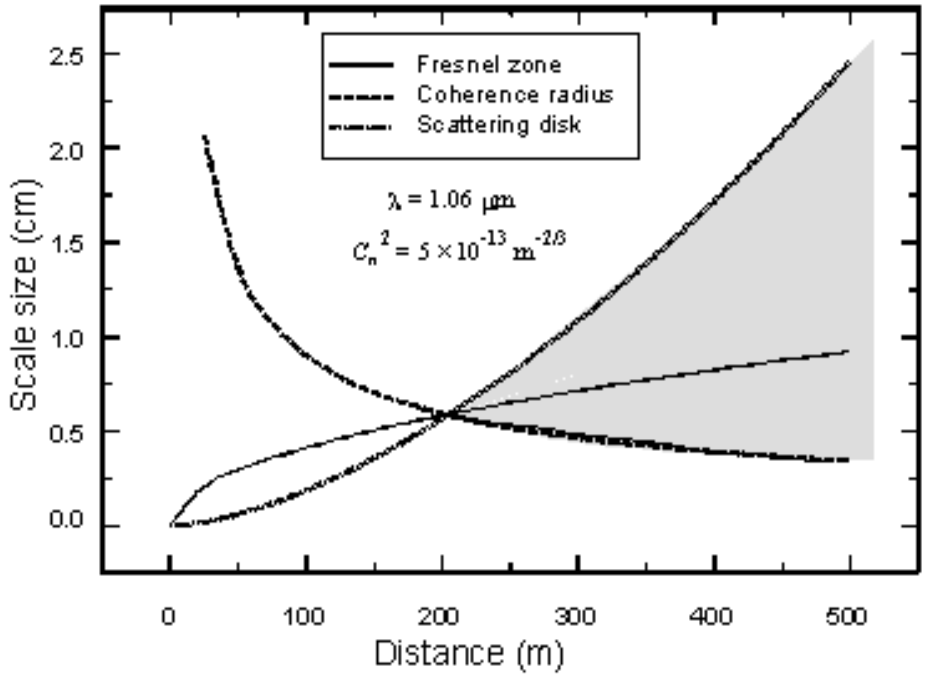

Figure 2 Relative scale sizes vs. propagation distance for an infinite plane wave. The point of intersection denotes the onset of strong fluctuations.[7]

In order to address this phenomenon mathematically, Andrews *et al.*[6,7,8] constructed an *effective* atmospheric spectral model by applying a filter function to the standard atmospheric spectral model. In effect, this filter function modifies the standard Kolmogorov spectrum by eliminating intermediate scale sizes that do not contribute to the refractive and diffractive effects on the optical wave. Specifically, they presented an *effective* atmospheric spectrum, given by[7]

$$\Phi_n(\kappa) = 0.033 C_n^2 \kappa^{-11/3} \left[f(\kappa l_0)\, g(\kappa L_0)\, G_x(\kappa) + G_y(\kappa) \right], \tag{58}$$

where κ is the refractive index spatial wave number and $G_x(\kappa)$ and $G_y(\kappa)$ represent the large and small scale filter functions, respectively. The filter functions are given by[7]

$$G_x(\kappa) = \exp\left[-\frac{\kappa^2}{\kappa_x^2} \right], \tag{59}$$

$$G_y(\kappa) = \frac{\kappa^{11/3}}{\left(\kappa^2 + \kappa_y^2 \right)^{11/6}}, \tag{60}$$

$$G_y(\kappa) = \frac{\kappa^{11/3}}{\left(\kappa^2 + \kappa_y^2 \right)^{11/6}} \exp\left[\frac{L \Lambda \kappa^2}{k} \left(1 - \frac{z}{L} \right)^2 \right], \tag{61}$$

where κ_x is the large scale frequency cutoff and κ_y is the small scale frequency cutoff. Equation (59) is applied to plane, spherical and Gaussian-beam waves, equation (60) is used for plane and spherical waves, and equation (61) is used for Gaussian-beam waves. The frequency filter functions, G_x and G_y, essentially allow only the effects of scale sizes, κ, satisfying $0 < \kappa < \kappa_x$ *or* $\kappa_y < \kappa < \infty$ to contribute to the scintillation index. In other words, the effects of the

refractive index scales sizes in the region $\kappa_x < \kappa < \kappa_y$ are eliminated. It is important to note that, unlike l_0 and L_0 which are assumed to be constant in most horizontal path cases, the values of κ_x and κ_y are not fixed. They are a function of the turbulence strength, σ_1^2, and of the wave type, i.e. plane, spherical, or Gaussian-beam wave. This makes sense given the set of curves in figure 2. In the figure, we see that the region of scale sizes that are significant changes as the propagation path length increases. Expressions describing the large and small scale frequency cutoffs, κ_x and κ_y, as a function of σ_1^2 for plane, spherical, and Gaussian-beam waves are given in [7] and are presented in the following chapters. The functions $f(\kappa l_0)$ and $g(\kappa L_0)$ are used to incorporate a finite inner and outer scale of turbulence. For example, setting both f and g equal to one is equivalent to having a zero inner scale and an infinite outer scale. In this case, the effective atmospheric spectrum, (58), represents an *effective Kolmogorov* spectrum. An *effective von Kármán spectrum* is obtained by setting

$$f_{vk}(\kappa l_0) = \exp\left[-\frac{\kappa^2}{\kappa_m^2}\right], \tag{62}$$

$$g(\kappa L_0) = 1 - \exp\left[-\frac{\kappa^2}{\kappa_0^2}\right], \tag{63}$$

where the *"vk"* subscript in $f_{vk}(\kappa l_0)$ indicates that this is for an effective von Kármán spectrum. Similarly, an *effective Hill spectrum* is obtained by taking the function g to be that given by (63) and setting

$$f_h(\kappa l_0) = \exp\left[-\frac{\kappa^2}{\kappa_l^2}\right]\left[1 + 1.802\left(\frac{\kappa}{\kappa_l}\right) - 0.254\left(\frac{\kappa}{\kappa_l}^{7/6}\right)\right], \tag{64}$$

where the *"h"* subscript in $f_h(\kappa l_0)$ indicates that this is for an effective Hill spectrum.

In the modified Rytov method, an expression for a given statistical quantity is obtained by substituting the effective atmospheric spectrum, (58), into the integral definition obtained from the standard Rytov method for that statistical quantity. For example, to develop scintillation index expressions, the effective atmospheric spectrum is substituted into the standard Rytov scintillation index integral definition, (53). Using this method, Andrews *et al*.[6,7,8] showed that the resulting scintillation index expressions agree with experimental and simulation data in all regimes of optical turbulence. Figure 3, taken from [7], presents experimental spherical wave scintillation index data as a function of increasing turbulence strength as given by Consortini *et al.*[9] with comparisons to the expressions developed using the modified Rytov method. It is seen in figure 3 that the theoretical curves developed from the modified Rytov method agree with the experimental data in all turbulence regimes. It should be noted that the model for scintillation index originally presented by Andrews *et al.*[6] did not include the effects of an outer scale, L_0. It was shown that the original expressions did not agree with the simulation results of Flatte and Gerber.[10] However, in a subsequent paper,[8] the effects of a finite outer scale were included, and the resulting scintillation index expressions were shown to be in good agreement with Flatte and Gerber's[10] simulation data and Consortini *et al's.*[9] experimental data.

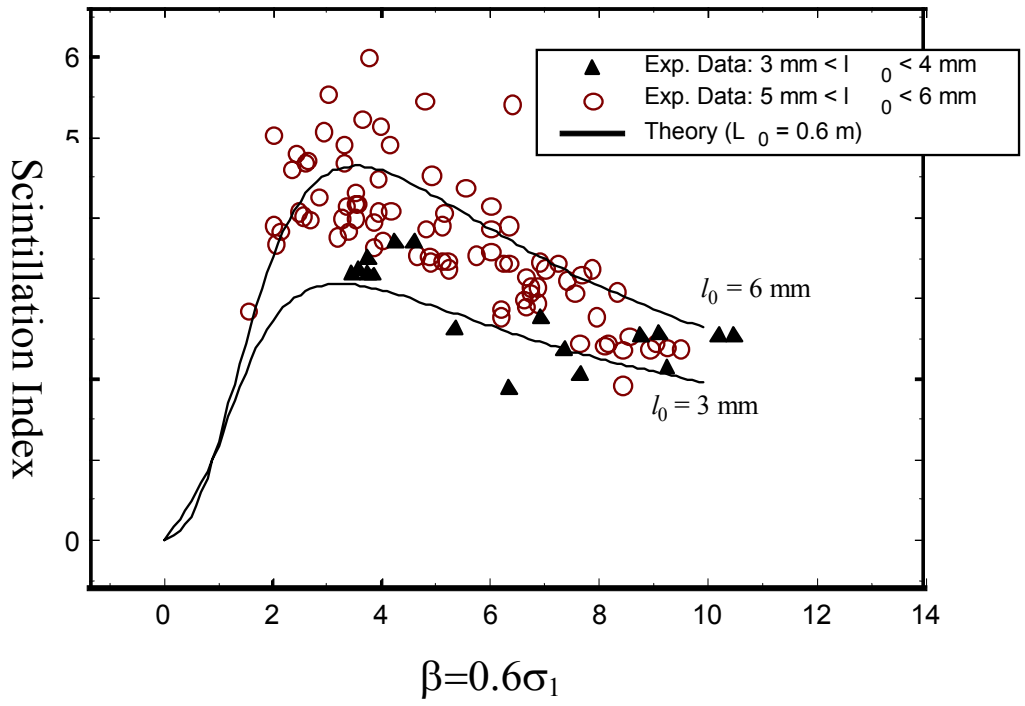

Figure 3 Comparison of modified Rytov method scintillation index results to experimental data for spherical waves. Open circles represent scintillation data for a fixed propagation distance of 1200 m taken from [9] and replotted here.

5.4 Modification of the effective atmospheric spectrum

Note that the effective atmospheric spectrum, (58), can be viewed as the sum of a large scale component, $\Phi_{n,x}$, given by

$$\Phi_{n,x}(\kappa) = 0.033 C_n^2 \kappa^{-11/3} f(\kappa l_0)\, g(\kappa L_0)\, G_x(\kappa), \tag{65}$$

and a small scale component, $\Phi_{n,y}$, given by

$$\Phi_{n,y}(\kappa) = 0.033 C_n^2 \kappa^{-11/3} G_y(\kappa). \tag{66}$$

The initial intent of this research was to use the effective spectral model, (58), to develop wave structure function and temporal frequency spread results that would be valid in all optical turbulence conditions. It was found, however, that when substituting the small scale portion of the effective spectral model, (66), into the standard Rytov method integrals defining the wave structure function that the integrals are divergent, even when including a finite inner and outer scale. This is a result of the fact that the inner scale effect is not included in the small scale component of the effective spectrum. Thus, to rectify this situation, the effective spectral model presented by Andrews *et al*.[6,7,8] has been modified in this work by multiplying both the large and small scale filter functions by the inner and outer scale functions, $f(\kappa l_0)$ and $g(\kappa L_0)$. Specifically, the following effective atmospheric spectral model is proposed[11]

$$\Phi_n(\kappa) = 0.033 C_n^2 \kappa^{-11/3} f(\kappa l_0)\, g(\kappa L_0) \left[G_x(\kappa) + G_y(\kappa) \right], \tag{67}$$

where G_x is given by (59) and

$$G_y(\kappa) = 1 - \exp\left[-\frac{\kappa^2}{\kappa_y^2}\right]. \tag{68}$$

The form of the small scale filter function, (68), was chosen for mathematical convenience. It is tentatively assumed that the same expressions for κ_x and κ_y given in [7] can be applied to (67). This modification allows for convergence of the integrals defining the wave structure function and temporal frequency spread as discussed in the remaining chapters. In the chapters that follow, references to the effective atmospheric spectrum or the modified Rytov method will assume the use of the effective spectral model given by (67).

Note, in the limit of weak optical turbulence, $\sigma_1^2 \ll 1$, that $\kappa_x \approx \kappa_y = \alpha$ for some constant α. Hence, in the limit of weak fluctuations

$$G_x(\kappa) - G_y(\kappa) \approx 1 + \exp\left[-\frac{\kappa^2}{\alpha^2}\right] - \exp\left[-\frac{\kappa^2}{\alpha^2}\right] = 1. \tag{69}$$

This implies that in the limit of weak irradiance fluctuations the spectral model given by (67) effectively reduces to the corresponding standard spectral model and that the modified Rytov method is equivalent to the standard Rytov method. For example, if $f(\kappa l_0) = 1$ and $g(\kappa L_0) = 1$ or $f(\kappa l_0) = \exp\left(-\frac{\kappa^2}{\kappa_m^2}\right)$ and $g(\kappa L_0) = \kappa^{11/3}\left(\kappa^2 + \kappa_0^2\right)^{-11/6}$, (67) reduces to the standard Kolmogorov or von Kármán spectral model, (24) and (26), respectively. This is significant because the standard Rytov method is believed to accurately describe the optical field in weak turbulence conditions.

It should be noted that the author does *not* argue that either (58) or (67) represents the actual shape of the atmospheric index of refraction spectrum. Indeed, the actual shape of the spectrum can be confirmed experimentally and is approximately modeled by the Kolmogorov spectrum, (24), and more accurately modeled by the Hill spectrum, (27), as described in [2]. It is believed, however, that these filter functions can be obtained in a manner physically consistent with the wave propagation problem by a consideration of the Green's function of the Rytov formulation where the angular spectrum of plane waves would be modified. However, this is a nontrivial problem and is the subject of current research by Andrews, Phillips, Young. Nonetheless, the modified Rytov method described above does seem to quite accurately capture the behavior of certain statistical quantities, albeit in a heuristic manner.

6. HORIZONTAL PATH WAVE STRUCTURE FUNCTION

6.1 Introduction

In this chapter we examine the wave structure function (WSF) when the modified Rytov method is applied. The wave structure function describes how closely related the optical field is at any two points in the observation plane. Consider the optical field propagating in a turbulent medium and assume that the optical field has a given amplitude and phase at the observation point, $\mathbf{r}_1$, at the receiver in the plane transverse to the propagation direction at some fixed point in time, t_0. Now assume that the optical field has a different amplitude and phase at another observation point at the receiver in the plane transverse to the propagation direction, $\mathbf{r}_2$, at the same time, t_0. If it is assumed that the mean value of the amplitude and phase are slowly varying, then the wave structure function is the sum of the average value of the square of the difference in the phase and the average value of the square of the difference in the log amplitude at the two observation points. In the absence of turbulence, the wave structure function would be zero. This is not the case when propagation is through a turbulent medium and indeed as the turbulence strength increases, it can be expected that the value of the wave structure function will increase.

In more precise mathematical terms, the wave structure function, $D(\mathbf{r}_1,\mathbf{r}_2)$, for an optical wave propagating in a turbulent atmosphere is defined by

$$D(\mathbf{r}_1, \mathbf{r}_2) = D_\chi + D_S \tag{70}$$

where D_χ is the *log-amplitude* structure function and D_S is the *phase* structure function. Usually, one does not develop analytic expressions for the wave structure function as a function of the two observation points, $\mathbf{r}_1$ and $\mathbf{r}_2$, but rather as a function of the scalar separation distance between the observation points, $\rho = |\mathbf{r}_2 - \mathbf{r}_1|$. Using the standard Rytov approximation, one can obtain analytic expressions for *D(ρ)* as a function of the propagation distance, L, and the atmospheric structure parameter, C_n^2.

Though most statistical quantities obtained via the standard Rytov method are considered valid only in the weak turbulence regime, it has been argued that no such restriction exists for the wave structure function. Tatarskii[5,12] indicated that although the validity of amplitude fluctuation statistics predicted by the standard Rytov method is restricted to the weak turbulence regime, phase fluctuation statistics should be valid for a wider range of parameters. In particular, for the special cases of plane and spherical waves, Tatarskii indicated that the phase structure function based on the standard Rytov method is in fact valid in all turbulence regimes under certain conditions. Specifically, Tatarskii postulated that if the value of the phase structure function is less than π, phase structure function results obtained using the standard Rytov method with the standard Kolmogorov or Tatarskii spectrums should be valid for all regimes of irradiance fluctuations.[12] It is commonly accepted that the effects of phase fluctuations dominate the wave structure function,[2] thus indicating that, by Tatarskii's argument, the wave structure function should be valid in all fluctuation regimes.

However, experimental data presented by Gurvich[13] does not support this conclusion. In [13], experimental results for the wave structure function are presented as a function of increasing

optical turbulence strength for a fixed value of scalar separation distance, ρ. The data, which is normalized (as discussed later), clearly does not follow a linear relation, as is predicted by the standard Rytov method, regardless of atmospheric spectral model. That is, when normalized in the manner presented in [13], the standard Rytov method analytic expression of the wave structure function follows a straight line (on a log-log plot). As will be shown, this is independent of the atmospheric spectral model used. Though use of the Kolmogorov, von Kármán, or Hill atmospheric spectrums result in different values for the wave structure function, they all result in a graph which, when normalized, is a straight line when the wave structure function is plotted as a function of turbulence strength for a fixed value of scalar separation distance, contradictory to the data presented in [13]. It will be shown that when applying the modified Rytov method, the resulting wave structure function does predict the behavior observed experimentally in [13].

Many other experimental measurements of the wave structure function have been published.[14−20] However, all of these works present wave structure function data as a function of ρ for a fixed value of turbulence strength. It will be shown that for a fixed value of turbulence strength, the behavior of the wave structure function expression obtained via the modified Rytov method has the same behavior as that obtained from the standard Rytov method when considered as a function of scalar separation distance. Thus, even though some of these experiments were conducted in strong turbulence conditions, the data is not useful when discussing the behavior of the wave structure function as a function of increasing fluctuation strength for a fixed value of ρ.

6.2 Integral definition

In the horizontal path case, the path amplitude ratio, γ, is given by equation (50) and the second order statistical moments, E_1, E_2, and E_3, given by equations (46)-(48), reduce to[2]

$$E_1(0,0) = -2\pi^2 k^2 L \int_0^\infty \kappa \Phi_n(\kappa)\, d\kappa, \tag{71}$$

$$\begin{aligned} E_2(\mathbf{r}_1, \mathbf{r}_2) &= 4\pi^2 k^2 L \int_0^1 \int_0^\infty \kappa \Phi_n(\kappa) \\ &\quad \times J_0\left[\kappa \left|\left(1-\bar{\Theta}\xi\right)\mathbf{p} - 2i\Lambda\xi\mathbf{r}\right|\right] \exp\left(-\frac{\Lambda L \kappa^2 \xi^2}{k}\right) d\kappa d\xi, \end{aligned} \tag{72}$$

$$\begin{aligned} E_3(\mathbf{r}_1, \mathbf{r}_2) &= -4\pi^2 k^2 L \int_0^1 \int_0^\infty \kappa \Phi_n(\kappa)\, J_0\left[\left(1-\bar{\Theta}\xi - i\Lambda\xi\right)\kappa\rho\right] \\ &\quad \times \exp\left(-\frac{\Lambda L \kappa^2 \xi^2}{k}\right) \exp\left[-\frac{iL\kappa^2}{k}\xi\left(1-\bar{\Theta}\xi\right)\right] d\kappa d\xi, \end{aligned} \tag{73}$$

where $\mathbf{r}_1$ and $\mathbf{r}_2$ are any to points in the plane transverse to the propagation direction at the distance L from the transmitter, $\mathbf{r}$ is the center of gravity vector given by

$$\mathbf{r} = \frac{1}{2}\left(\mathbf{r}_1 + \mathbf{r}_2\right), \tag{74}$$

$\mathbf{p}$ is the difference vector given by

$$\mathbf{p} = \mathbf{r}_1 - \mathbf{r}_2, \tag{75}$$

and Λ and Θ are the beam parameters given by (52).

Applying the standard Rytov method, it can be shown that for the case of a one-way horizontal path, the wave structure function can be expressed in terms of the second order moments as[2]

$$D(\mathbf{r}_1, \mathbf{r}_2) = \mathrm{Re}\left[\Delta(\mathbf{r}_1, \mathbf{r}_2, L)\right], \tag{76}$$

where $\mathrm{Re}(x)$ denotes the real part of x and

$$\begin{aligned}\Delta(\mathbf{r}_1, \mathbf{r}_2, L) &= E_2(\mathbf{r}_1, \mathbf{r}_1) + E_2(\mathbf{r}_2, \mathbf{r}_2) - 2E_2(\mathbf{r}_1, \mathbf{r}_2) \\ &= 4\pi^2 k^2 L \int_0^1 \int_0^\infty \kappa \Phi_n(\kappa) \exp\left(-\frac{\Lambda L \kappa^2 \xi^2}{k}\right) \{I_0(2\Lambda r_1 \xi \kappa) \\ &\quad + I_0(2\Lambda r_2 \xi \kappa) - 2J_0\left[\left|\left(1 - \bar{\Theta}\xi\right)\mathbf{p} - 2i\Lambda\xi\mathbf{r}\right|\kappa\right]\} d\kappa d\xi, \end{aligned} \tag{77}$$

where $r_1 = |\mathbf{r}_1|$ and $r_2 = |\mathbf{r}_2|$.

6.3 Plane wave

In the special case of a transmitted plane wave, the phase front radius of curvature and the beam radius at the transmitter are infinite, i.e. $F_0 = W_0 = \infty$, so that $\Lambda = 0$ and $\Theta = 1$. Thus, substituting $\Lambda = 0$ and $\Theta = 1$ into (77) yields the standard Rytov integral definition of the plane wave structure function[2]

$$D(\rho, L) = 8\pi^2 k^2 L \int_0^\infty \kappa \Phi_n(\kappa) \left[1 - J_0(\kappa\rho)\right] d\kappa \tag{78}$$

where $\rho = |\mathbf{p}|$ is the scalar separation distance of $\mathbf{r}_1$ and $\mathbf{r}_2$.

6.3.1 Standard Rytov plane wave structure function

Plane wave structure function results using the standard Rytov method can now be developed using the integral definition, (78). Substituting the von Kármán spectrum, (26), into (78), evaluating, and then restricting $l_0 \ll \rho \ll L_0$, we find that the plane wave structure function is approximately given by[2]

$$D(\rho, L) \approx 2.914 C_n^2 k^2 L \rho^{5/3} \qquad l_0 \ll \rho \ll L_0. \tag{79}$$

The expression given in (79) is commonly referred to as the five-thirds power law. Substituting the analytic approximation to the Hill spectrum, (27), into equation (78) yields a plane wave structure function that incorporates a finite inner scale, l_0, and a finite outer scale, L_0, given by[2]

$$\begin{aligned} D(\rho, L) &= 2.7 C_n^2 k^2 L l_0^{-1/3} \rho^2 \left[\frac{1}{\left(1 + 0.632 \frac{\rho^2}{l_0^2}\right)^{1/6}} + \frac{0.438}{\left(1 + 0.442 \frac{\rho^2}{l_0^2}\right)^{2/3}} \right. \\ &\quad \left. - \frac{0.056}{\left(1 + 0.376 \frac{\rho^2}{l_0^2}\right)^{3/4}} - 0.868 (\kappa_0 l_0)^{1/3} \right], \end{aligned} \tag{80}$$

where $\kappa_0 = \frac{2\pi}{L_0}$.

6.3.2 *Modified Rytov plane wave structure function*

The modified Rytov method described previously can now be applied to develop the plane wave structure function by substituting the effective atmospheric spectrum, (67), into the standard Rytov integral definition, (78). We are seeking only the basic behavior of the wave structure function in the inertial subrange, which implies that we should use an effective Kolmogorov spectrum. However, substituting the effective Kolmogorov spectrum into (78) results in a divergent integral. Thus it is necessary to use an effective von Kármán spectrum, where we let $f(\kappa l_0) = \exp\left(-\frac{\kappa^2}{\kappa_m^2}\right)$ and $g(\kappa L_0) = \kappa^{11/3}\left(\kappa^2 + \kappa_0^2\right)^{-11/6}$. As in the case of the standard Rytov wave structure function, (79), we shall make the restriction $l_0 \ll \rho \ll L_0$ after completion of the integration to obtain a wave structure function that is independent of inner and outer scale effects. Substituting the effective von Kármán spectrum into (78) and evaluating (see Appendix B) yields the modified Rytov method plane wave structure function[11,21]

$$D(\rho, L) = D_x(\rho, L) + D_y(\rho, L), \tag{81}$$

where $D_x(\rho,L)$ and $D_y(\rho,L)$ are the large and small scale components of the wave structure function, respectively. They are given by

$$D_x(\rho, L) = 8.7 C_n^2 k^2 L \kappa_{xm(pl)}^{-5/3}\left[{}_1F_1\left(-\tfrac{5}{6}; 1; -\tfrac{\rho^2\kappa_{xm(pl)}^2}{4}\right) - 1\right], \tag{82}$$

$$D_y(\rho, L) = 8.7C_n^2 k^2 L \left\{ \kappa_m^{-5/3} \left[{}_1F_1\left(-\tfrac{5}{6}; 1; -\tfrac{\rho^2\kappa_m^2}{4}\right) - 1 \right] - \kappa_{ym(pl)}^{-5/3} \left[{}_1F_1\left(-\tfrac{5}{6}; 1; -\tfrac{\rho^2\kappa_{ym(pl)}^2}{4}\right) - 1 \right] \right\}, \quad (83)$$

where ${}_1F_1(a; b; x)$ denotes the confluent hypergeometric function[22] and

$$\kappa_{xm(pl)}^2 = \frac{\kappa_{x(pl)}^2 \kappa_m^2}{\kappa_{x(pl)}^2 + \kappa_m^2}, \qquad \kappa_{ym(pl)}^2 = \frac{\kappa_{y(pl)}^2 \kappa_m^2}{\kappa_{y(pl)}^2 + \kappa_m^2}, \quad (84)$$

incorporate the inner scale wave number parameter $\kappa_m = \frac{5.92}{l_0}$ and the large and small scale plane wave refractive index spatial frequency cutoffs, $\kappa_{x(pl)}$ and $\kappa_{y(pl)}$. The *"pl"* subscript in the large and small scale frequency cutoffs, $\kappa_{x(pl)}$ and $\kappa_{y(pl)}$, is used to denote that these are for a plane wave. Note that this expression assumes the limit of an infinite outer scale. Restricting $l_0 \ll \rho \ll L_0$, taking the limit as the inner scale goes to zero, $l_0 \to 0$, so that $\kappa_{xm(pl)}^2 \to \kappa_{x(pl)}^2$ and $\kappa_{ym(pl)}^2 \to \kappa_{y(pl)}^2$, and making the approximation[2]

$${}_1F_1\left(-\tfrac{5}{6}; 1; -x\right) - 1 \approx \frac{5x}{6}(1 + 0.232x)^{-1/6}, \quad (85)$$

we find that the large and small scale components of the wave structure function can be written as the simpler algebraic expressions

$$D_x(\rho, L) = 1.47\sigma_1^2 \left(\frac{k\rho^2 \eta_{x(pl)}^{1/6}}{L}\right)\left(1 + 0.058\frac{k\rho^2\eta_{x(pl)}}{L}\right)^{-1/6}, \quad (86)$$

$$D_y(\rho, L) = 2.37\sigma_1^2 \left(\frac{k\rho^2}{L}\right)^{5/6} - 1.47\sigma_1^2 \left(\frac{k\rho^2 \eta_{y(pl)}^{1/6}}{L}\right)\left(1 + 0.058\frac{k\rho^2 \eta_{y(pl)}}{L}\right)^{-1/6}. \quad (87)$$

The nondimensional parameters, η_x and η_y are used to incorporate the refractive index spatial frequency cutoffs, κ_x and κ_y. In the specific case of a plane wave, $\eta_{x(pl)}$ and $\eta_{y(pl)}$, which incorporate the plane wave large scale and small scale frequency cutoffs, $\kappa_{x(pl)}$ and $\kappa_{y(pl)}$, are given by[7]

$$\eta_{x(pl)} = \frac{L\kappa_{x(pl)}^2}{k} = \frac{2.61}{1 + 1.11\left(\sigma_1^2\right)^{6/5}}, \quad (88)$$

$$\eta_{y(pl)} = \frac{L\kappa_{y(pl)}^2}{k} = 3\left[1 + 0.69\left(\sigma_1^2\right)^{6/5}\right]. \quad (89)$$

6.3.3 Comparisons

In figure 4 the full wave structure function, (81), and the large scale portion of the wave structure function, (86), are plotted as a function of increasing turbulence strength. It can be seen in figure 4, that the large scale component dominates the wave structure function. This is expected, as it is believed that the wave structure function is dominated by the phase structure function and phase fluctuations are generally considered to be a large scale phenomenon.

It was stated previously that when considered as a function of scalar separation distance, ρ, that the wave structure function obtained from the modified Rytov method has identical behavior as that predicted by the standard Rytov method. In figure 5, the standard Rytov plane WSF, (79), and the modified Rytov plane WSF, (81), are plotted as a function of increasing scalar distance, ρ, in the weak turbulence regime, $\sigma_1^2 = 0.1$, where it is expected that the standard Rytov method

is valid. The figure indicates that when considered in this manner, the two methods predict an identical behavior.

Despite the fact that the standard and modified Rytov method wave structure functions predict identical behavior when considered as a function of ρ, they have very different behavior when considered as a function of increasing turbulence strength for a fixed value of ρ. We see in figure 6 that in the weak turbulence regime, $\sigma_1^2 \ll 1$, the new model, (81), agrees with the traditional five-thirds power law given by (79). However, the two expressions begin to separate from each other in moderate fluctuations, $\sigma_1^2 \approx 1$. The separation between the two expressions increases significantly as the fluctuations move into the strong fluctuation regime, $\sigma_1^2 \gg 1$. The most important information contained in figure 6 is that the standard Rytov method models for the wave structure function, (79) and (80), predict a linear increase of the wave structure function (on a log-log graph) as a function of increasing turbulence strength, regardless of the spectral model used. The two lines also have the same slope. This indicates that the ratio of the wave structure function expression developed with the Kolmogorov spectral model to that developed with Hill spectral model is constant as a function of increasing turbulence strength for a fixed value of separation distance, ρ. However, the expression developed using the modified Rytov method, (81), predicts a non-linear increase, indicating that the ratio between the new model and any of the standard expressions is not constant as a function of increasing turbulence strength. The significance of these points is discussed in the comparison to experimental data.

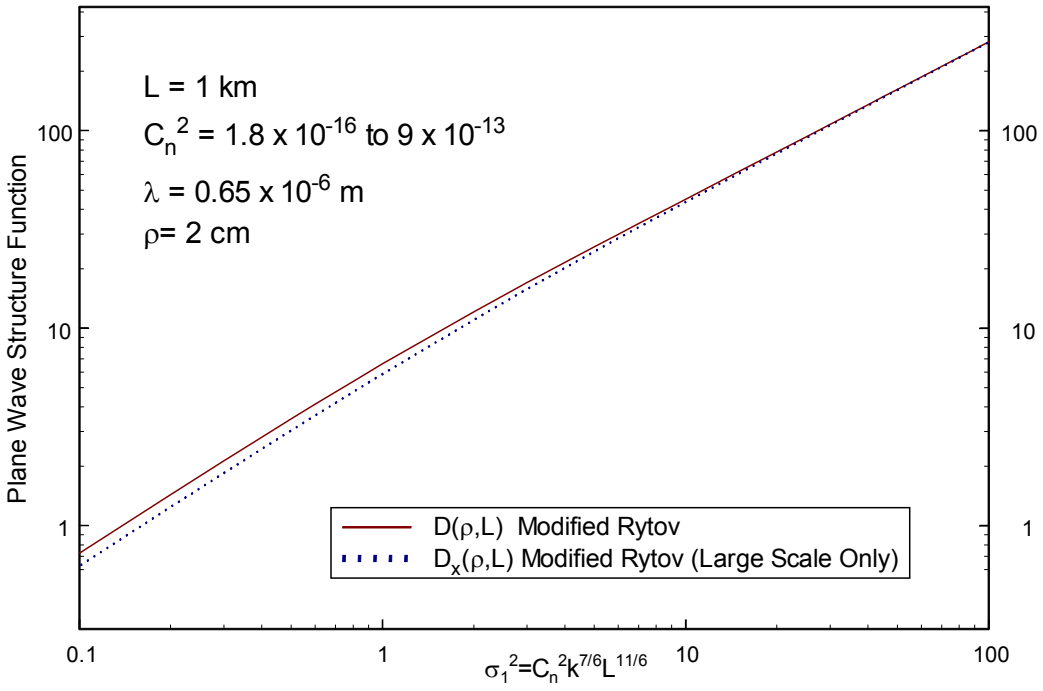

Figure 4 Modified Rytov method plane wave structure function as a function of turbulence strength. The solid curve is equation (81) using equations (86) and (87). The dashed curve is the large scale portion only, equation (86).

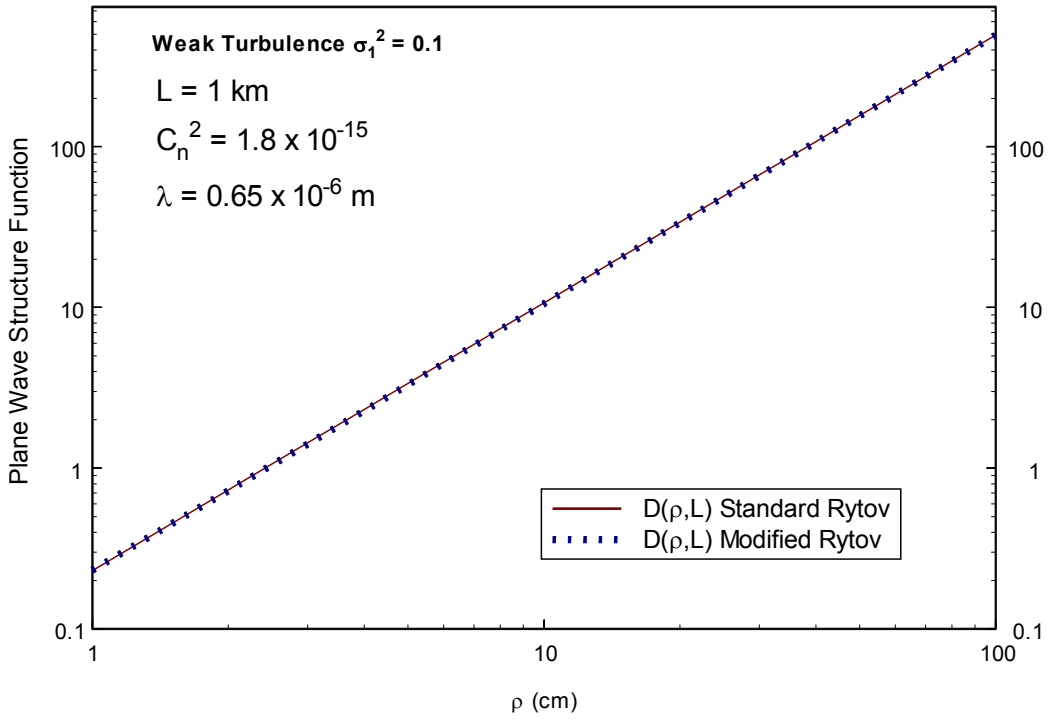

Figure 5 Plane wave structure function as a function of ρ. The solid curve is the standard Rytov equation, (79). The dashed curve is the modified Rytov equation, (81).

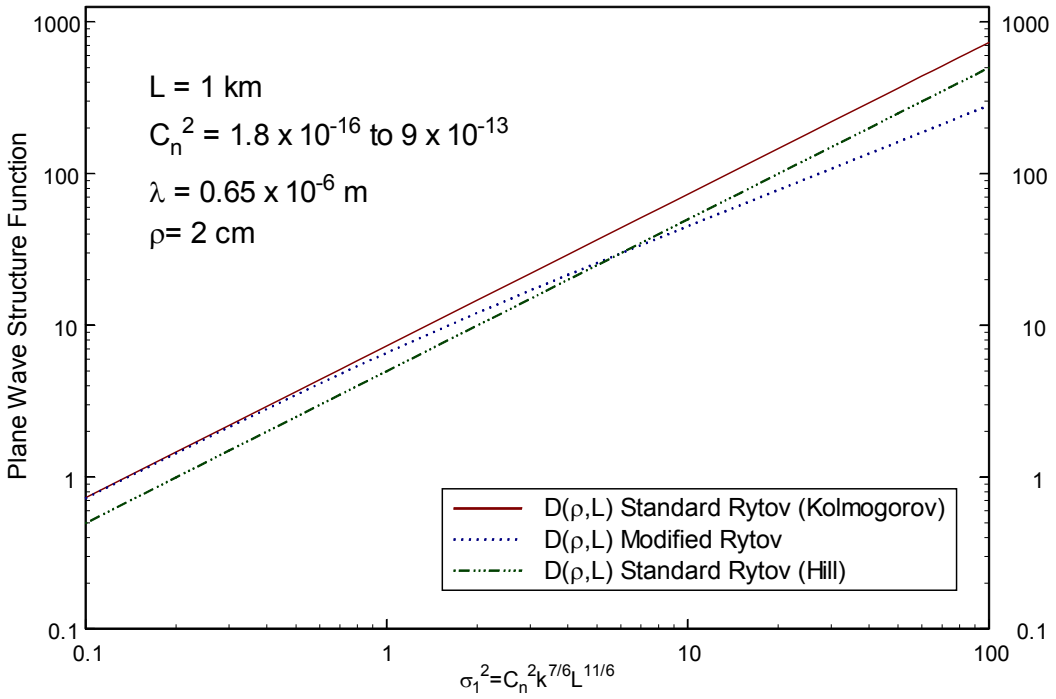

Figure 6 Plane WSF as a function of increasing turbulence strength. The Kolmogorov curve represents equation (79), the Hill curve represents equation (80), and the modified Rytov curve represents equation (81).

6.4 Spherical wave

In the special case of a transmitted spherical wave, the phase front radius of curvature is equal to the propagation path length, i.e. $F_0 = L$, and the beam radius approaches zero at the transmitter, i.e. $W_0 \to 0$ as $L \to 0$, so that $\Lambda_0 \to \infty$ and $\Theta_0 = 0$. Thus, for a spherical wave $\Lambda \to 0$ and $\Theta = 0$. Substituting $\Lambda = 0$ and $\Theta = 0$ into (77) yields the standard Rytov integral definition of the spherical wave structure function[2]

$$D(\rho, L) = 8\pi^2 k^2 L \int_0^1 \int_0^\infty \kappa \Phi_n(\kappa) [1 - J_0(\kappa \xi \rho)] \, d\kappa d\xi. \tag{90}$$

6.4.1 Standard Rytov spherical wave structure function

Spherical wave structure function results using the standard Rytov method can now be developed using the integral definition, (90). Substituting the von Kármán spectrum, (26), into (90), evaluating, and then restricting $l_0 \ll \rho \ll L_0$, we find that the spherical wave structure function is approximately given by[2]

$$D(\rho, L) \approx 1.093 C_n^2 k^2 L \rho^{5/3} \qquad l_0 \ll \rho \ll L_0. \tag{91}$$

Substituting the analytic approximation to the Hill spectrum, (27), into equation (90) yields a spherical wave structure function that incorporates a finite inner scale, l_0, and a finite outer scale,

L_0, given by[2]

$$D(\rho, L) = 0.9C_n^2 k^2 L l_0^{-1/3} \rho^2 \left[\frac{1}{\left(1 + 0.311\frac{\rho^2}{l_0^2}\right)^{1/6}} + \frac{0.438}{\left(1 + 0.183\frac{\rho^2}{l_0^2}\right)^{2/3}} - \frac{0.056}{\left(1 + 0.149\frac{\rho^2}{l_0^2}\right)^{3/4}} - 0.868\,(\kappa_0 l_0)^{1/3} \right]. \quad (92)$$

6.4.2 Modified Rytov spherical wave structure function

A spherical WSF function can be developed using the modified Rytov method in the same manner as for the plane wave case by substituting the effective von Kármán spectrum, equation (67) with $f(\kappa l_0) = \exp\left(-\frac{\kappa^2}{\kappa_m^2}\right)$ and $g(\kappa L_0) = \kappa^{11/3}\left(\kappa^2 + \kappa_0^2\right)^{-11/6}$, into (90). As in the plane wave case, we shall make the restriction $l_0 \ll \rho \ll L_0$ after completion of the integration to obtain a wave structure function that is independent of inner and outer scale effects. Substituting the effective von Kármán spectrum into (90) and evaluating (see Appendix C) yields the modified Rytov method spherical wave structure function which is again the sum of a large and small component, that is[11,21]

$$D(\rho, L) = D_x(\rho, L) + D_y(\rho, L), \quad (93)$$

where

$$D_x(\rho, L) = 8.7C_n^2 k^2 L \kappa_{xm(sp)}^{-5/3} \left[{}_2F_2\left(-\tfrac{5}{6}, \tfrac{1}{2}; 1, \tfrac{3}{2}; -\tfrac{\rho^2 \kappa_{xm(sp)}^2}{4}\right) - 1 \right], \quad (94)$$

$$D_y(\rho, L) = 8.7C_n^2 k^2 L \left\{ \kappa_m^{-5/3} \left[{}_2F_2\left(-\tfrac{5}{6}, \tfrac{1}{2}; 1, \tfrac{3}{2}; -\tfrac{\rho^2\kappa_m^2}{4}\right) - 1 \right] - \kappa_{ym(sp)}^{-5/3} \left[{}_2F_2\left(-\tfrac{5}{6}, \tfrac{1}{2}; 1, \tfrac{3}{2}; -\tfrac{\rho^2\kappa_{ym(sp)}^2}{4}\right) - 1 \right] \right\}. \quad (95)$$

The function ${}_2F_2(a, b; c, d; x)$ denotes a generalized hypergeometric function[22] and

$$\kappa_{xm(sp)}^2 = \frac{\kappa_{x(sp)}^2 \kappa_m^2}{\kappa_{x(sp)}^2 + \kappa_m^2}, \qquad \kappa_{ym(sp)}^2 = \frac{\kappa_{y(sp)}^2 \kappa_m^2}{\kappa_{y(sp)}^2 + \kappa_m^2} \quad (96)$$

are used to incorporate the large and small scale spherical wave refractive index spatial frequency cutoffs, $\kappa_{x(sp)}$ and $\kappa_{y(sp)}$. The *"sp"* subscript in the large and small scale frequency cutoffs is used to denote that these are for a spherical wave. Similar to the plane wave case, this expression assumes the limit of an infinite outer scale. We again restrict $l_0 \ll \rho \ll L_0$, take the limit as the inner scale goes to zero, $l_0 \to 0$, so that $\kappa_{xm(sp)}^2 \to \kappa_{x(sp)}^2$ and $\kappa_{ym(sp)}^2 \to \kappa_{y(sp)}^2$, and make the approximation[2]

$${}_2F_2\left(-\tfrac{5}{6}, \tfrac{1}{2}; 1, \tfrac{3}{2}; -x\right) - 1 \approx \frac{5x}{18}(1 + 0.132x)^{-1/6}, \quad (97)$$

so that the large and small scale components of the wave structure function can be written as the simpler algebraic expressions

$$D_x(\rho, L) = 0.49\sigma_1^2 \left(\frac{k\rho^2 \eta_{x(sp)}^{1/6}}{L}\right)\left(1 + 0.033\frac{k\rho^2\eta_{x(sp)}}{L}\right)^{-1/6}, \quad (98)$$

$$D_y(\rho, L) = 0.89\sigma_1^2 \left(\frac{k\rho^2}{L}\right)^{5/6} - 0.49\sigma_1^2 \left(\frac{k\rho^2 \eta_{y(sp)}^{1/6}}{L}\right)\left(1 + 0.033\frac{k\rho^2\eta_{y(sp)}}{L}\right)^{-1/6}. \quad (99)$$

The spherical wave nondimensional parameters $\eta_{x(sp)}$ and $\eta_{y(sp)}$ are given by[7]

$$\eta_{x(sp)} = \frac{L\kappa_{x(sp)}^2}{k} = \frac{8.56}{1 + 0.19\left(\sigma_1^2\right)^{6/5}}, \tag{100}$$

$$\eta_{y(sp)} = \frac{L\kappa_{y(sp)}^2}{k} = 9\left[1 + 0.23\left(\sigma_1^2\right)^{6/5}\right]. \tag{101}$$

6.4.3 Comparisons

Comparing the spherical wave structure function obtained via the modified Rytov method, (93), with the standard Rytov method results, (91) and (92), as a function of increasing turbulence strength for a fixed valued of scalar separation distance, we find results that are similar to the plane wave. The new model agrees with the standard Rytov theory models in the limit of weak turbulence but predicts smaller values in moderate to strong turbulence. These results are presented in figure 7. As in the case of a plane wave, the key observation for figure 7, is the qualitative behavior of the three wave structure function models as a function of turbulence strength for a fixed value of separation distance. On the log-log graph of figure 7, it is seen that the wave structure functions obtained via the standard Rytov approximation follow a linear behavior with the same slope, whereas the new model presented here follows a non-linear trend. That is, the new model has a decreasing slope as irradiance fluctuation strength increases. The significance of this trend will be discussed further when comparisons are made to experimental data. Though not depicted graphically, we also find that the spherical wave structure function is dominated by the large scale

component, $D_x(\rho, L)$. Additionally, we find that the two methods yield identical behavior when considered as a function of ρ for a fixed value of σ_1^2.

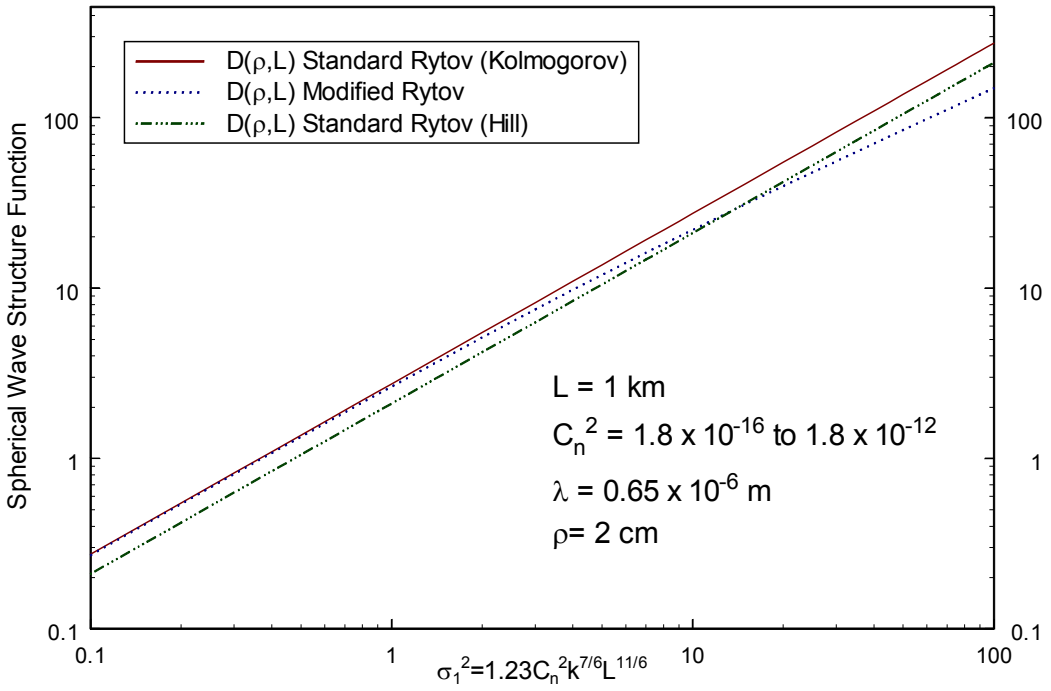

Figure 7 Spherical WSF as a function of increasing turbulence strength. The Kolmogorov curve represents equation (91), the Hill curve represents equation (92), and the modified Rytov curve represents equation (93).

6.5 Gaussian-beam wave

We now consider the general case of a Gaussian-beam wave where no assumptions can be made on the beam parameters Λ and Θ. In this case, the wave structure function is described by the full Rytov integral definition, (76). Notice that when no simplifications are made the wave structure function, (76), is statistically inhomogeneous in that it depends implicitly on the position of the two observation points $\mathbf{r}_1$ and $\mathbf{r}_2$. However, if we consider the special case where the observation points are symmetrically located about the optical axis, i.e. $\mathbf{r}_1 = -\mathbf{r}_2$, so that $\mathbf{r} = 0$, we find the wave structure function can be considered statistically homogeneous. Considering this special case, we find that the Gaussian-beam wave structure function as obtained from the standard Rytov method is given by[2]

$$D(\rho, L) = d(\rho, L) + 4\sigma_r^2(\rho, L), \tag{102}$$

where $d(\rho, L)$ describes the on-axis, or longitudinal, component and $\sigma_r^2(\rho, L)$ describes the transverse, or radial, component of the wave structure function. They are given by

$$d(\rho, L) = 8\pi^2 k^2 L \int_0^1 \int_0^\infty \kappa \Phi_n(\kappa) \exp\left(-\frac{\Lambda L \kappa^2 \xi^2}{k}\right) \left\{1 - J_0\left[\left(1 - \bar{\Theta}\xi\right)\rho\kappa\right]\right\} d\kappa d\xi, \tag{103}$$

$$\sigma_r^2(\rho, L) = 2\pi^2 k^2 L \int_0^1 \int_0^\infty \kappa \Phi_n(\kappa) \exp\left(-\frac{\Lambda L \kappa^2 \xi^2}{k}\right) \left[I_0(\Lambda \rho \xi \kappa) - 1\right] d\kappa d\xi. \tag{104}$$

6.5.1 *Standard Rytov Gaussian-beam wave structure function*

Substituting the Kolmogorov spectrum, (24), into (103) and (104) yields the standard Rytov method wave structure function for a Gaussian beam wave, approximately given by[2]

$$D(\rho, L) = 0.889\sigma_1^2 \left[A \left(\frac{k\rho^2}{L} \right)^{5/6} + 0.618\Lambda^{11/6} \left(\frac{k\rho^2}{L} \right) \right] \qquad l_0 \ll \rho \ll L_0, \tag{105}$$

where

$$A = \begin{cases} \dfrac{1-\Theta^{8/3}}{1-\Theta}, & \Theta \geq 0, \\ \dfrac{1+|\Theta|^{8/3}}{1-\Theta}, & \Theta < 0. \end{cases} \tag{106}$$

Notice that for the Gaussian-beam wave it is mathematically sufficient to use the Kolmogorov spectrum and still have convergence of the integrals, unlike the situation for plane and spherical waves where it was necessary to use the von Kármán spectrum. The reason for this is the exponential function in equations (103) and (104) allows for convergence of the integrals.

Substituting the analytic approximation to the Hill spectrum, (27), into (103) and (104), yields a Gaussian-beam wave structure function that includes inner and outer scale effects given

by[2]

$$
\begin{aligned}
D(\rho, L) \;=\; & 0.9 C_n^2 k^2 L l_0^{-1/3} \rho^2 \left\{ \frac{\Lambda^2}{(1+0.52\Lambda Q_l)^{1/6}} + \frac{0.438(\Lambda Q_l)^{1/6}}{(1+0.7\Lambda Q_l)^{2/3}} - \frac{0.056(\Lambda Q_l)^{1/6}}{(1+0.7\Lambda Q_l)^{3/4}} \right. \\
& -0.868\left(1+\Theta+\Theta^2+\Lambda^2\right)(\kappa_0 l_0)^{1/3} \\
& +\frac{1}{1-\Theta}\left[\frac{1}{\left(1+0.11\Lambda Q_l+0.311\rho^2/l_0^2\right)^{1/6}}\right. \\
& \left.-\frac{\Theta^3}{\left(1+0.11\Lambda Q_l+0.311\Theta^2\rho^2/l_0^2\right)^{1/6}}\right] \\
& +\frac{0.438}{1-\Theta}\left[\frac{1}{\left(1+0.21\Lambda Q_l+0.183\rho^2/l_0^2\right)^{2/3}}\right. \\
& \left.-\frac{\Theta^3}{\left(1+0.21\Lambda Q_l+0.183\Theta^2\rho^2/l_0^2\right)^{2/3}}\right] \\
& -\frac{0.056}{1-\Theta}\left[\frac{1}{\left(1+0.38\Lambda Q_l+0.149\rho^2/l_0^2\right)^{3/4}}\right. \\
& \left.\left.-\frac{\Theta^3}{\left(1+0.38\Lambda Q_l+0.149\Theta^2\rho^2/l_0^2\right)^{3/4}}\right]\right\},
\end{aligned}
\tag{107}
$$

where $Q_l = \frac{L\kappa_l^2}{k}$ is the nondimensional inner scale parameter related to $\kappa_l = 3.3/l_0$.

6.5.2 Modified Rytov Gaussian-beam wave structure function

An expression for the Gaussian-beam wave structure function can be now be developed using the modified Rytov method by again considering the special case $\mathbf{r}_1 = -\mathbf{r}_2$ and substituting the effective Kolmogorov spectrum, equation (67) with $f(\kappa l_0) = 1$ and $g(\kappa L_0) = 1$, into (103) and (104). Let us first consider the longitudinal component, (103), which will now be the sum of a large scale component, $d_x(\rho, L)$, and a small scale component, $d_y(\rho, L)$, i.e. $d(\rho, L) =$

$d_x(\rho, L) + d_y(\rho, L)$, where[11]

$$d_x(\rho, L) \approx 2.606 C_n^2 k^2 L \int_0^1 \int_0^\infty \kappa^{-8/3} \exp\left(-\frac{\kappa^2}{\kappa_{x(gb)}^2}\right) \exp\left(-\frac{\Lambda L \kappa^2 \xi^2}{k}\right) \times \left\{1 - J_0\left[\left(1 - \bar{\Theta}\xi\right)\rho\kappa\right]\right\} d\kappa d\xi, \tag{108}$$

$$d_y(\rho, L) \approx 0.889 \sigma_1^2 \left[A\left(\frac{k\rho^2}{L}\right)^{5/6}\right] - 2.606 C_n^2 k^2 L \int_0^1 \int_0^\infty \kappa^{-8/3} \exp\left(-\frac{\kappa^2}{\kappa_{y(gb)}^2}\right) \times \exp\left(-\frac{\Lambda L \kappa^2 \xi^2}{k}\right) \left\{1 - J_0\left[\left(1 - \bar{\Theta}\xi\right)\rho\kappa\right]\right\} d\kappa d\xi, \tag{109}$$

where $\kappa_{x(gb)}$ and $\kappa_{y(gb)}$ are the Gaussian-beam wave large and small scale refractive index frequency cutoffs, respectively. In (108) and (109), we make the argument that $\exp\left(-\frac{\kappa^2}{\kappa_{x(gb)}^2}\right)$ and $\exp\left(-\frac{\kappa^2}{\kappa_{y(gb)}^2}\right)$ act as low-pass spatial filters, ensuring that under the integral[7]

$$\exp\left(-\frac{\Lambda L \kappa^2 \xi^2}{k}\right) \approx 1, \tag{110}$$

which is the geometric optics approximation. Under this assumption, the integrals (108) and (109) can be evaluated as (see Appendix D)

$$d_x(\rho, L) \approx 7.08 \sigma_1^2 \eta_{x(gb)}^{-5/6} \left[\frac{1}{\bar{\Theta}} {}_2F_2\left(-\tfrac{5}{6}, \tfrac{1}{2}; 1, \tfrac{3}{2}; -\tfrac{\rho^2 k \eta_{x(gb)}}{4L}\right) - \frac{\Theta}{\bar{\Theta}} {}_2F_2\left(-\tfrac{5}{6}, \tfrac{1}{2}; 1, \tfrac{3}{2}; -\tfrac{\rho^2 k \Theta^2 \eta_{x(gb)}}{4L}\right) - 1\right], \tag{111}$$

$$d_y(\rho, L) \approx 0.889\sigma_1^2\left[A\left(\frac{k\rho^2}{L}\right)^{5/6}\right] - 7.08\sigma_1^2\eta_{y(gb)}^{-5/6}\left[\frac{1}{\bar{\Theta}}{}_2F_2\left(-\tfrac{5}{6}, \tfrac{1}{2}; 1, \tfrac{3}{2}; -\tfrac{\rho^2 k\eta_{y(gb)}}{4L}\right)\right.$$
$$\left. -\frac{\Theta}{\bar{\Theta}}{}_2F_2\left(-\tfrac{5}{6}, \tfrac{1}{2}; 1, \tfrac{3}{2}; -\tfrac{\rho^2 k\Theta^2\eta_{y(gb)}}{4L}\right) - 1\right]. \tag{112}$$

The nondimensional Gaussian-beam wave frequency cutoff parameters, $\eta_{x(gb)}$ and $\eta_{y(gb)}$, are given by[7]

$$\eta_{x(gb)} = \frac{L\kappa_{x(gb)}^2}{k} = \left(\frac{1}{3} - \frac{1}{2}\bar{\Theta} + \frac{1}{5}\bar{\Theta}^2\right)\left(\frac{\sigma_1}{\sigma_B}\right)^{-12/7}\left(1 + 0.56\sigma_B^{12/5}\right)^{-1}, \tag{113}$$

$$\eta_{y(gb)} = \frac{L\kappa_{y(gb)}^2}{k} = 3\left(\frac{\sigma_1}{\sigma_B}\right)^{12/5} + 2.07\sigma_1^{12/5}. \tag{114}$$

The Rytov variance for a beam wave, σ_B^2, is given by[2,23]

$$\sigma_B^2 = 3.86\sigma_1^2\left\{0.4\left[(1+2\Theta)^2 + 4\Lambda^2\right]^{5/12}\cos\left[\frac{5}{6}\arctan\left(\frac{1+2\Theta}{2\Lambda}\right)\right] - \frac{11}{16}\Lambda^{5/6}\right\} \tag{115}$$

Finally, using the binomial approximation for the hypergeometric function, ${}_2F_2(a, b; c, d; -x)$, given by (97), we can write

$$d(\rho, L) = d_x(\rho, L) + d_y(\rho, L), \tag{116}$$

where

$$d_x(\rho, L) = 0.49\sigma_1^2 \eta_{x(gb)}^{1/6} \left(\frac{k\rho^2}{L}\right) \left[\frac{1}{\bar{\Theta}}\left(1 + 0.033\frac{k\rho^2\eta_{x(gb)}}{L}\right)^{-1/6} - \frac{\Theta^3}{\bar{\Theta}}\left(1 + 0.033\frac{k\rho^2\Theta^2\eta_{x(gb)}}{L}\right)^{-1/6}\right], \quad (117)$$

$$d_y(\rho, L) = 0.889\sigma_1^2\left[A\left(\frac{k\rho^2}{L}\right)^{5/6}\right] - 0.49\sigma_1^2\eta_{y(gb)}^{1/6}\left(\frac{k\rho^2}{L}\right)\left[\frac{1}{\bar{\Theta}}\left(1 + 0.033\frac{k\rho^2\eta_{y(gb)}}{L}\right)^{-1/6} - \frac{\Theta^3}{\bar{\Theta}}\left(1 + 0.033\frac{k\rho^2\Theta^2\eta_{y(gb)}}{L}\right)^{-1/6}\right]. \quad (118)$$

To find the radial component of the Gaussian-beam wave structure function, we substitute the effective Kolmogorov spectrum into (104) and evaluate. For the sake of clarity the evaluation is left to Appendix D. The resulting radial component is the sum of a large scale component, $\sigma_{r,x}^2$, and a small scale component, $\sigma_{r,y}^2$. Thus the radial component is given by[11]

$$\sigma_r^2(\rho, L) = \sigma_{r,x}^2(\rho, L) + \sigma_{r,y}^2(\rho, L), \quad (119)$$

where

$$\sigma_{r,x}^2(\rho, L) = 0.123\sigma_1^2\left(\frac{k\rho^2\Lambda^2}{L}\right)\eta_{x(gb)}^{1/6}\left(1 + 0.547\Lambda\eta_{x(gb)}\right)^{-1/6}, \quad (120)$$

$$\sigma_{r,y}^2(\rho, L) = 0.137\sigma_1^2\Lambda^{11/6}\left(\frac{k\rho^2}{L}\right) - 0.123\sigma_1^2\left(\frac{k\rho^2\Lambda^2}{L}\right)\eta_{y(gb)}^{1/6}\left(1 + 0.547\Lambda\eta_{y(gb)}\right)^{-1/6}. \quad (121)$$

Finally, the modified Rytov method model for the Gaussian-beam wave structure function is given by

$$D(\rho, L) = d_x(\rho, L) + d_y(\rho, L) + 4\left[\sigma_{r,x}^2(\rho, L) + \sigma_{r,y}^2(\rho, L)\right], \quad (122)$$

where $d_x(\rho, L)$, $d_y(\rho, L)$, $\sigma_{r,x}^2(\rho, L)$, and $\sigma_{r,y}^2(\rho, L)$ are given by (117), (118), (120), and (121), respectively.

6.5.3 Comparisons

For the Gaussian-beam wave, Andrews *et al.*[2,23] presented an expression for the wave structure function in the moderate to strong turbulence regimes that is based on effective beam parameters, given by

$$D(\rho, L) = 0.889\sigma_1^2\left[A_e\left(\frac{k\rho^2}{L}\right)^{5/6} + 0.618\Lambda_e^{11/6}\left(\frac{k\rho^2}{L}\right)\right] \quad l_0 \ll \rho \ll L_0, \quad (123)$$

where

$$A_e = \begin{cases} \dfrac{1 - \Theta_e^{8/3}}{1 - \Theta_e}, & \Theta \geq 0, \\ \dfrac{1 + |\Theta_e|^{8/3}}{1 - \Theta_e}, & \Theta < 0. \end{cases} \quad (124)$$

The *effective* beam parameters, Λ_e and Θ_e, are given by

$$\Lambda_e = \frac{\Lambda}{1 + 4q\Lambda/3}, \tag{125}$$

$$\Theta_e = \frac{\Theta - 2q\Lambda/3}{1 + 4q\Lambda/3}, \tag{126}$$

where $q = 1.22\left(\sigma_1^2\right)^{6/5}$ is a measure of the optical turbulence strength.

Let us now compare the modified Rytov method model for the Gaussian beam wave structure function, (122), to those given by the standard Rytov method, (105) and (107), and that given by Andrews *et al.*[2,23] using effective beam parameters, (123). The results in figure 8 are for $\Theta_0 = 1$ and $\Lambda_0 = 1$ which corresponds to a collimated Gaussian-beam wave. In the weak turbulence regime, (105), (122), and (123) yield nearly identical results. However, as the Rytov variance increases into the moderate to strong fluctuation regimes, both (122) and (123) begin to separate significantly from (105) and (107). These results are similar to those seen for the plane and spherical wave cases. Again, as a function of increasing turbulence strength for a fixed value of scalar separation distance, the traditional standard Rytov theory results, (105) and (107), predict a linear increase in the value of the wave structure function (on a log-log graph). However, the results based on the effective beam parameters and the modified Rytov method, (122), and (123), predict a non-linear behavior with a decreasing slope as Rytov variance increases. As in the case of plane and spherical waves, all three methods yield identical behavior when considered as a function of separation distance, ρ, for a fixed value of fluctuation strength, all the way out to the beam edge.

In the case of weak fluctuations, if we set $\Theta_0 = 1$ and let $\Lambda_0 \to 0$ or $\Lambda_0 \to \infty$ in (105), (122) and (123), the results should reduce to those for a plane and spherical wave, respectively. These results are displayed in figure 9 for $\sigma_1^2 = 0.1$, which is considered to be in the weak fluctuation regime. Indeed, we see the results approach the limiting cases. However, if we consider a similar graph in the moderate to strong turbulence regime, we find a large disagreement between the predicted results of the standard Rytov method, the modified Rytov method, and the effective beam parameters. In particular, we expect that in the moderate fluctuation regime there is a significant difference in the values predicted by the modified Rytov wave structure function model and that based on effective beam parameters. This result is expected because the wave structure function developed using the effective beam parameters is based on the assumption that the standard Rytov plane and spherical wave structure functions, the five-thirds power laws, are valid in all fluctuation regimes and tends to reduce to these results in the limiting cases of plane and spherical waves. However, the expressions presented here for plane and spherical waves based on the modified Rytov method do not agree with standard Rytov theory in the moderate to strong fluctuation regimes.

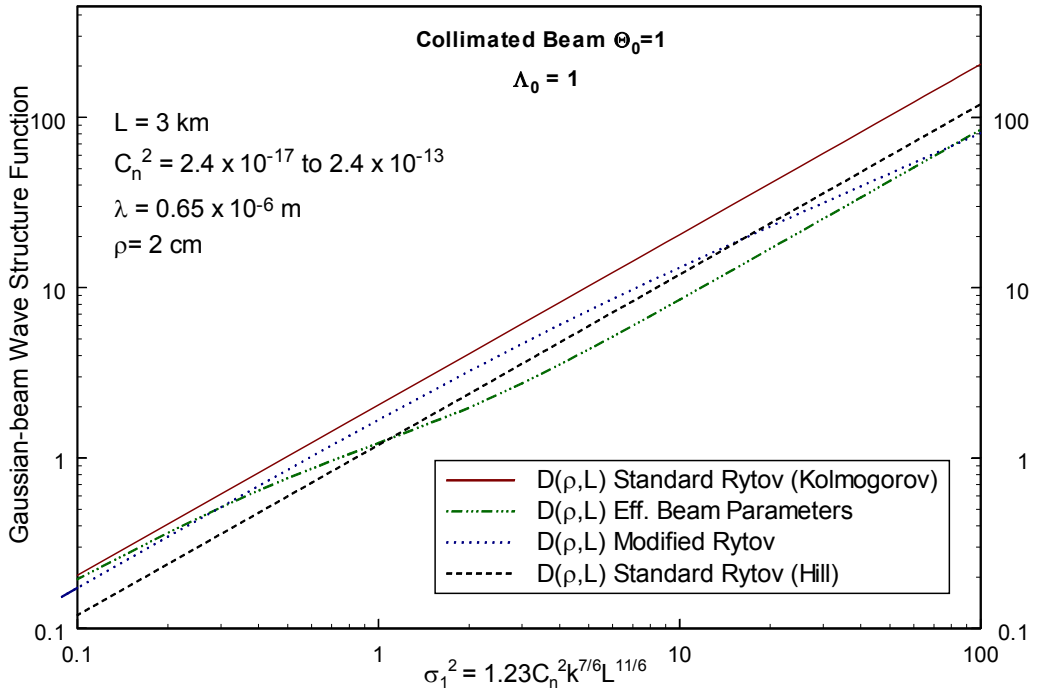

Figure 8 Gaussian-beam WSF as a function of increasing turbulence strength. The Kolmogorov curve represents equation (105), the Hill curve represents equation (107), the Eff. Beam Parameters curve represents equation (123), and the modified Rytov curve represents equation (122). For the parameters used, the free space beam diameter at the distance *L* from the transmitter is approximately 7 cm.

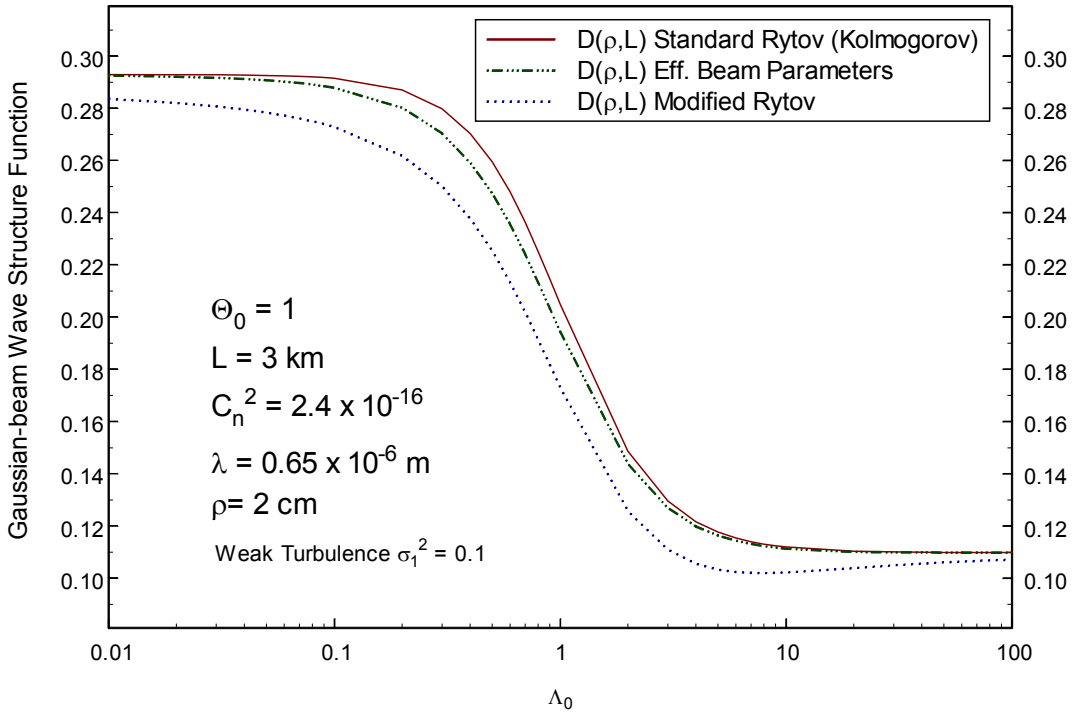

Figure 9 Gaussian-beam WSF as a function of the Fresnel ratio of the beam at the transmitter, Λ_0. The Kolmogorov curve represents equation (105), the Eff. Beam Parameters curve represents equation (123), and the modified Rytov curve represents equation (122). The resulting free space beam diameter at the distance L from the transmitter for the given parameters ranges from 7 cm to 48 cm. The limiting cases of $\Lambda_0 = 0$ and $\Lambda_0 = \infty$ correspond to a plane wave and a spherical wave, respectively.

6.6 Comparison to experimental data

As previously discussed, many authors have presented experimental results of the wave structure function as a function of separation distance, ρ, for a fixed value of fluctuation strength.[14−20] However, no information can be obtained from these works about the validity of the modified Rytov method models presented in this paper as compared to the traditional standard Rytov method models because the qualitative behavior as a function of separation distance is identical. Though the exact values predicted are quantitatively different in the moderate to strong turbulence regime, the numerical difference is too insignificant when considering experimental results. This is due to the fact that the measured values of experimental conditions such as C_n^2, l_0, and L_0 are too imprecise to conduct an exact comparison.

However, at least one author, Gurvich,[13] has presented wave structure function data as a function of increasing turbulence strength for a fixed value of scalar separation distance. In [13], fluctuations in the angle of incidence for a spherical wave were measured and used to compute the mean value of the image "center of gravity". The mean value of the square of the center of gravity of the image, $\langle \alpha_c^2 \rangle$, is given as[13]

$$\left\langle \alpha_c^2 \right\rangle = 0.97 \frac{D_s\,(2R)}{(2kR)^2}, \tag{127}$$

where D_s is the spherical wave structure function. For the experiment conducted in [13], $R = 6$ cm is the radius of the receiving aperture and $k = 2\pi/\lambda$ is the wave number with wavelength $\lambda = 0.55$ mm. The experiment was conducted over steppe terrain at a height of 2 m.[13] Thus, the outer scale will be taken to be $L_0 = 1$ m. No values for inner scale were provided, so typical

values are assumed. Taking the spherical wave structure function, D_s, to be that of the standard Rytov method, given by (91), we have

$$\left\langle \alpha_c^2 \right\rangle_1 = 1.06 C_n^2 L \, (2R)^{-1/3} \, . \tag{128}$$

In [13], the measured value of (127) is presented as a function of (128). This corresponds to the measured value of the spherical wave structure function as a function of increasing fluctuation strength for a fixed value of separation distance. The data presented in figure 10 is for $L = 1750\, m$ with varying values of the index of refraction structure parameter, C_n^2. The measured values of C_n^2 are not presented in [13], so reasonable values have been assumed for comparison. The open circles in figure 10 represent the measured data. It is clear that the data does not follow a straight line as turbulence strength increases. The standard Rytov theory results, (91) and (92), predict a straight line, whereas the expression developed using the modified Rytov method, (93), predicts a nonlinear behavior with decreasing slope as turbulence strength increases which is the same qualitative behavior observed in the experimental data. Note that the modified Rytov method model does not fit the measured results exactly from a quantitative perspective. This is most likely due to the fact that no inner or outer scale has been included.

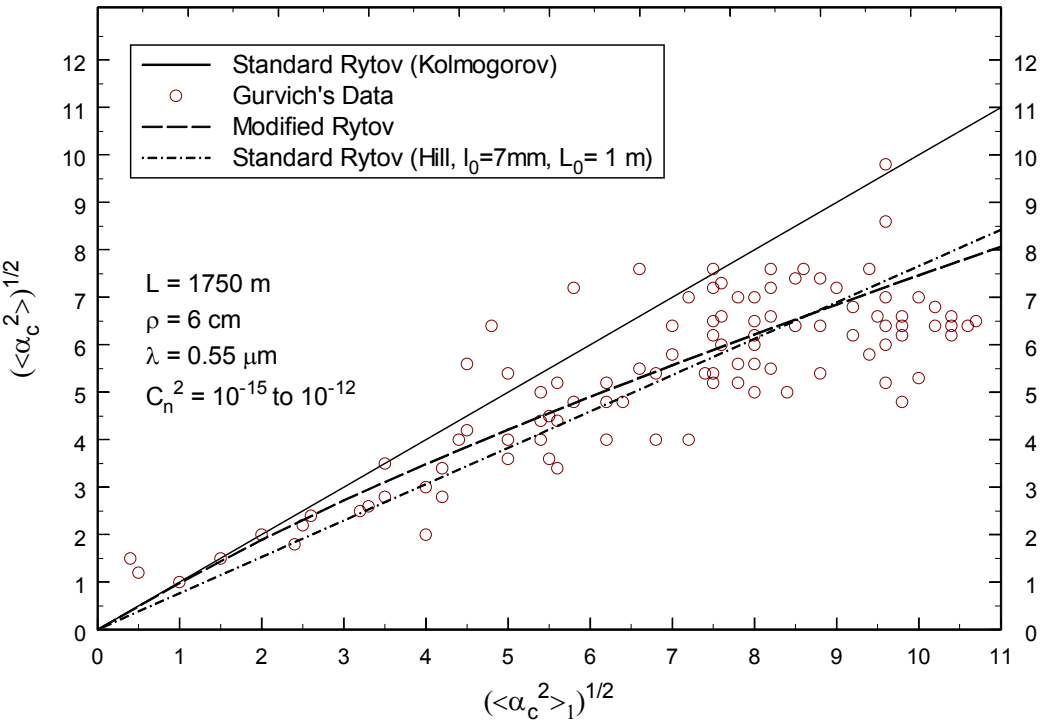

Figure 10 A comparison of the spherical wave structure function analytic results with experimental results of Gurvich. The mean value of the measured value of the image center of gravity, (127), is plotted as a function of (128). In each of the theoretical curves, the analytic expression for the wave structure function is substituted into (127). The Kolmogorov curve represents the use of equation (91), the Hill curve represents the use of equation (92), and the modified Rytov curve represents the use of equation (93).

Gurvich also presented the measured quantity[13]

$$\left(\frac{\langle \alpha_c^2 \rangle}{\langle \alpha_c^2 \rangle_1}\right)^{1/2}, \tag{129}$$

as a function of σ_1, where $\sigma_1^2 = 1.23 C_n^2 k^{7/6} L^{11/6}$ is the Rytov variance. The analytical and experimental results are presented in figure 11. The open circles represent the experimental data. The data points correspond to different values of the path length, L, and different index of refraction structure parameter values, C_n^2. When we substitute the wave structure functions, (91) and (92), developed using the standard Rytov method with the Kolmogorov spectrum and the Hill spectrum, respectively, into (129) the particular values of L and C_n^2 are irrelevant. This is due to the fact that the ratio of the two results does not change as a function of turbulence strength. Thus only one curve is given for the Hill spectrum. The exact value of this ratio does change for the Hill spectrum for different values of the inner scale, l_0, however the change is only minor. For the Kolmogorov spectrum, the ratio is one. However, for the spherical wave structure function derived using the modified Rytov method, (129) is explicitly dependent on the turbulence strength, so a curve has been presented for each value of the propagation path length. The important characteristic of figure 11 is that the data does not follow a straight line as predicted when the standard Rytov method wave structure functions are used in (129). Indeed, the data indicates a decrease in this ratio. This is the same qualitative behavior predicted when the modified Rytov method wave structure function is used in (129).

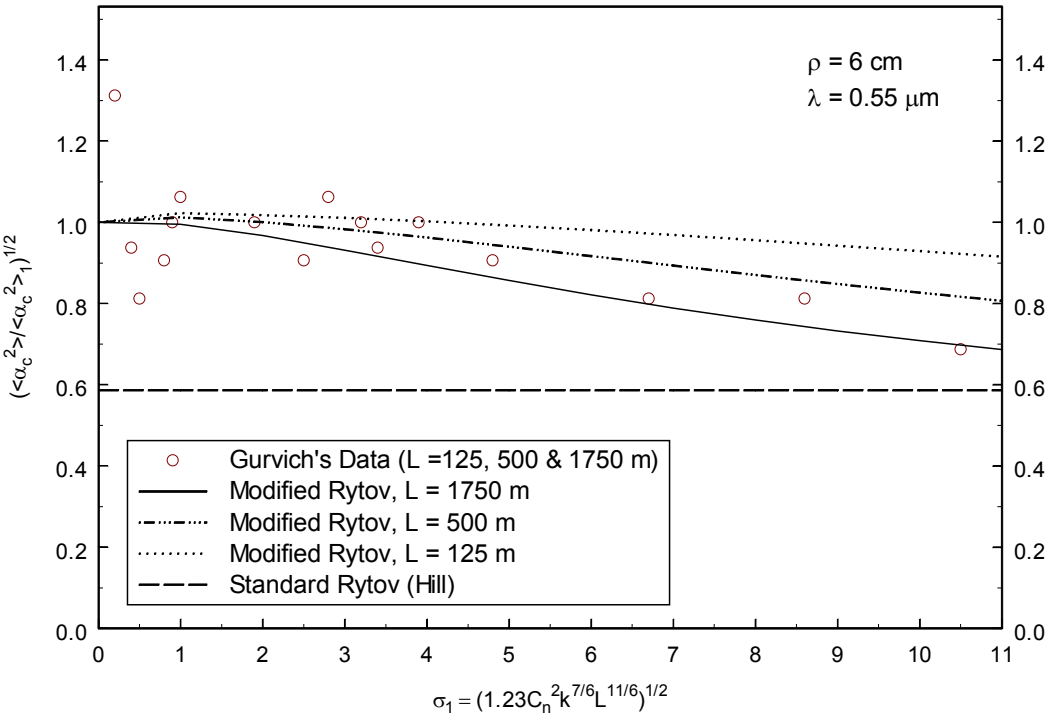

Figure 11 Equation (129), which is the ratio of the image center of gravity, (127), to that predicted using the Kolmogorov spherical wave structure function, (128), as a function of the square root of the Rytov variance. Curves are given using (92) and (93) in (127). For the Kolmogorov spectrum, the ratio is one.

7. HORIZONTAL PATH TEMPORAL FREQUENCY SPREAD AND SPECTRUM

7.1 Introduction

Random fluctuations are imparted onto the frequency of an optical signal propagating in the Earth's atmosphere as a result of the random fluctuations in phase and amplitude of the optical wave. These random frequency fluctuations result in a spreading of the frequency spectrum around the line centroid of the spectrum. Furthermore, as noted by several authors,[4,24,25] as the strength of optical turbulence increases there is also a random wandering of the line centroid of the frequency spectrum. Thus, to describe the width of the average frequency spectrum, one must account for not only the frequency spread due to atmospheric turbulence, but the average position of the line centroid as well.

As described by Ishimaru,[4] the average frequency spectrum, accounting for both the wandering of the line centroid and the atmospheric induced frequency spread, is given by the Fourier transform of the mutual coherence function, $\Gamma(\mathbf{r}_1,\mathbf{r}_2)$. The mutual coherence function of the random optical field is given by[2]

$$\Gamma_2(\mathbf{r}_1, \mathbf{r}_2, L) = \left\langle U(\mathbf{r}_1, L)\, U^*(\mathbf{r}_2, L) \right\rangle, \tag{130}$$

where $U(\mathbf{r}, L)$ is the random optical field, $\mathbf{r}_1$ and $\mathbf{r}_2$ are points in the receiver plane, L is the propagation path length, and $\langle x \rangle$ denotes the ensemble average of x. Ishimaru examined the temporal frequency spectrum for a plane wave. From that result, he obtained the angular temporal

frequency spread, ω_c, of the temporal frequency spectrum, *W(ω)*. Specifically, Ishimaru states that, for a plane wave, $\omega_c = V/\rho_{pl}$, where V is the wind velocity transverse to the propagation direction, or crosswind velocity, and ρ_{pl} is the plane wave coherence radius of the optical wave at the receiver. This expression can also be obtained via the following simple intuitive argument. Since the transverse coherence radius is ρ_{pl}, by applying Taylor's frozen flow hypothesis, the temporal coherence time, τ_c, is given by $\tau_c \approx \rho_{pl}/V$. Therefore the atmospheric induced frequency spread is approximately $\omega_c \approx 1/\tau_c \approx V/\rho_{pl}$.

In general, the coherence radius, ρ_0, of an optical wave is the e^{-1} point of the modulus of the complex degree of coherence function, *DOC*, given by[2]

$$\begin{aligned} DOC(\mathbf{r}_1, \mathbf{r}_2, L) &= \frac{|\Gamma_2(\mathbf{r}_1, \mathbf{r}_2, L)|}{[\Gamma_2(\mathbf{r}_1, \mathbf{r}_1, L)\,\Gamma_2(\mathbf{r}_2, \mathbf{r}_2, L)]^{1/2}} \\ &= \exp\left[-\frac{1}{2}D(\mathbf{r}_1, \mathbf{r}_2, L)\right] \end{aligned} \tag{131}$$

where $D(\mathbf{r}_1, \mathbf{r}_2, L)$ is the wave structure function discussed in the preceding chapter and $\Gamma_2(\mathbf{r}_1, \mathbf{r}_2, L)$ is the mutual coherence function. In the last chapter, the wave structure function was expressed in terms of the magnitude of the separation distance between the two observation points $\mathbf{r}_1$ and $\mathbf{r}_2$, that is $\rho = |\mathbf{r}_2 - \mathbf{r}_1|$. Thus, the e^{-1} point of the complex degree of coherence occurs when the wave structure function is equal to two. The value of ρ such that the wave structure function is equal to two is denoted as the coherence radius, ρ_0; i.e. $D(\rho_0) = 2$.

Note that Ishimaru[4] defines the angular frequency spread, ω_c, in units of rad/sec. We can express the frequency spread in *Hertz* through the relation $\sigma_f = \frac{\omega_c}{2\pi}$, where σ_f is used to denote

the frequency spread in *Hertz*. In this chapter, we compare the value of the plane wave frequency spread, σ_f, using the expression $\sigma_f = \frac{\omega_c}{2\pi} = \frac{V}{2\pi\rho_{pl}}$, for two different expressions for ρ_{pl}. The value of the coherence radius obtained using the plane wave structure function derived using the modified Rytov method is compared with that obtained using the standard five-thirds power law plane wave structure function found using the standard Rytov approximation. It is shown that in conditions of moderate to strong optical turbulence, the frequency spread, σ_f, given by the modified Rytov method is significantly less than that predicted using the five-thirds power law. Furthermore, via a direct analytic approach, independent of the temporal frequency spectrum, exact expressions are developed that predict the plane wave frequency spread. These expressions are then compared to the expression, $\sigma_f = \frac{V}{2\pi\rho_{pl}}$. Note that these expressions account for the frequency spread, σ_f, only, and not the wandering of the line centroid of the frequency spectrum. However the advantage of this approach is that the frequency spread can be described for spherical and Gaussian-beam waves without considering the mutual coherence function. Results for the spherical wave case are also considered and similar comparisons are presented.

7.2 Plane wave

To conduct our analysis, we will need expressions for the plane wave coherence radius, ρ_{pl}. Using the standard Rytov method and applying the Kolmogorov spectrum, the plane wave structure function is given by (79). Setting this equation equal to two and solving for ρ yields an analytic

expression for the plane wave coherence radius, ρ_{pl}, given by[2]

$$\rho_{pl} = \left(1.46 C_n^2 k^2 L\right)^{-3/5}, \qquad l_0 \ll \rho \ll L_0. \tag{132}$$

Additionally, we need to find the plane wave coherence radius as obtained from the plane wave structure function, (81), derived using the modified Rytov method. Unfortunately, the coherence radius obtained from this method cannot be expressed exactly in closed form; however, it can be computed numerically by setting (81) equal to two and solving for ρ. The modified Rytov method coherence radius results presented here were obtained numerically using a simple bisection method.

7.2.1 Coherence, frequency spread, and frequency spectrum analysis

In figure 12, we compare the plane wave coherence radius obtained via the standard Rytov approximation, (132), to that obtained using the modified Rytov approximation, which is obtained from (81), (86), and (87). It is clear that as turbulence strength increases the coherence radius decreases as would be expected. However, the results of the modified Rytov method indicate that the decrease is not as great as that predicted by the standard Rytov approximation.

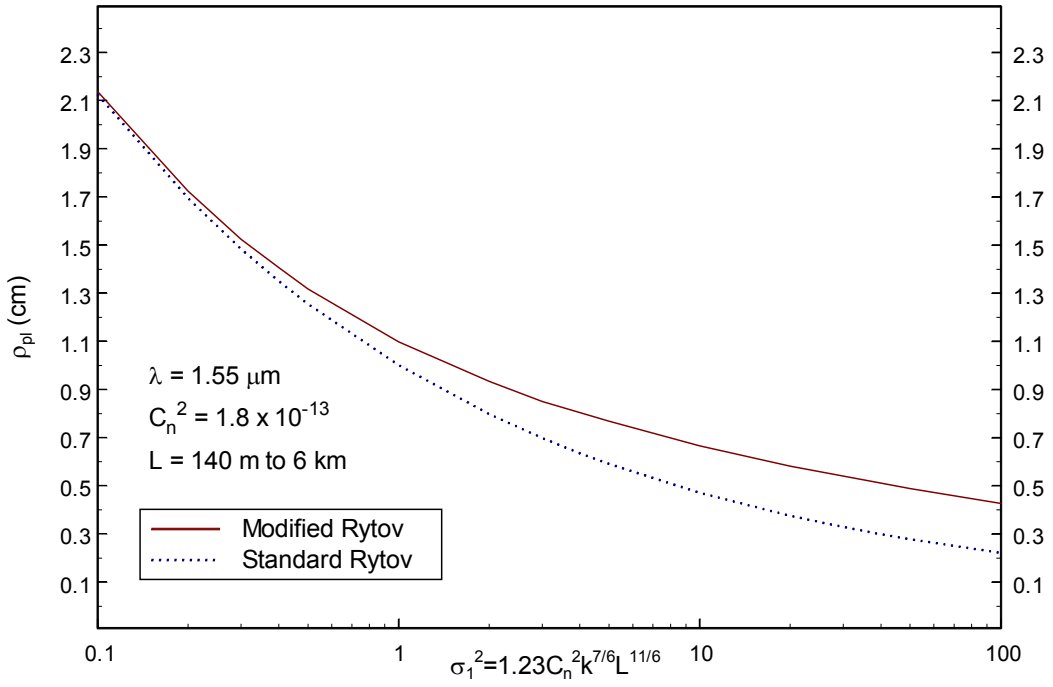

Figure 12 The plane wave coherence radius in cm as a function of increasing turbulence strength. The index of refraction structure parameter, C_n^2, is held constant, while the propagation path length, L, is allowed to vary. The standard Rytov curve is obtained from (132) and the modified Rytov curve is obtained by setting (81) equal to two and numerically solving for ρ.

As stated in the introduction, Ishimaru[4] argued that the atmospheric induced temporal frequency spread, σ_f, of the temporal frequency spectrum is given by

$$\sigma_f = \frac{\omega_c}{2\pi} = \frac{V}{2\pi\rho_{pl}}, \tag{133}$$

where V is the crosswind velocity and ρ_{pl} is the plane wave coherence radius. Figure 13 presents the plane wave atmospheric induced frequency spread where, in the standard Rytov approximation, ρ_{pl} is given by (132) and, in the modified Rytov approximation, ρ_{pl} is deduced from (81), (86), and (87). The propagation conditions in figure 13 are the same as those for figure 12. A moderate crosswind velocity of 10 km/hr has been assumed. We see in figure 13 that the results are identical in the weak turbulence regime. This is expected because the wave structure functions of the standard and modified Rytov methods are identical in weak turbulence. However, in the moderate to strong turbulence regime the predicted frequency spread given by the modified Rytov approximation is significantly less than that predicted by the standard Rytov approximation. This is a result of the fact that the modified Rytov approximation predicts a larger value for the coherence radius than the standard approximation in the moderate to strong turbulence regimes. Given the comparison of the two wave structure functions to the experimental data of Gurvich conducted in the preceding chapter, where it was shown that the modified Rytov results agreed well in all turbulence regimes, it is arguable that the frequency spread predicted by the modified Rytov method is more accurate.

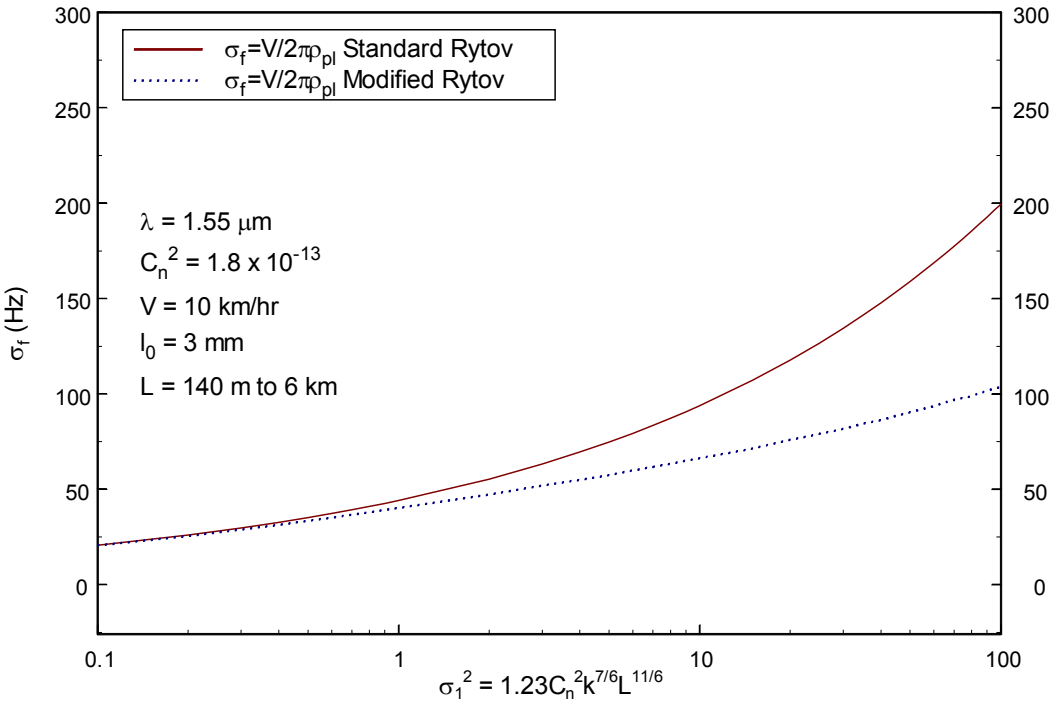

Figure 13 The plane wave frequency spread, (133), in *Hz* as a function of increasing turbulence strength. The index of refraction structure parameter, C_n^2, is held constant, while the propagation path length, L, is allowed to vary. The standard Rytov curve is obtained by using (132) to evaluate the coherence radius, while the modified Rytov curve is obtained by using (81) to determine the coherence radius.

As stated previously, (133) accounts for the atmospheric induced frequency spread around the frequency line centroid but does not account for the wandering of the line centroid. Ishimaru asserted that the average temporal frequency spectrum, accounting for both the frequency spread and the wandering of the line centroid, is found via the Fourier transform of the mutual coherence function. Ishimaru stated that the plane wave spatial mutual coherence function is given by[4]

$$\Gamma_2(\rho, L) = \exp\left[-\frac{1}{2} D_{pl}(\rho, L)\right], \tag{134}$$

where $D_{pl}(\rho, L)$ is the *spatial* plane wave structure function. Ishimaru's result for the temporal frequency spectrum is based on the assumption that the plane wave structure function obtained from the standard Rytov approximation is valid in all optical turbulence conditions. Thus, substituting (79) into (134), using Taylor's frozen flow hypothesis, $\rho = V\tau$, and taking the Fourier transform, Ishimaru gives the temporal frequency spectrum, $W(\omega)$ as[4]

$$\begin{aligned} W(\omega) &= 2\int \exp\left[-\frac{1}{2} D_{pl}(V\tau, L)\right] \exp(-i\omega\tau)\, d\tau \\ &= \frac{2}{\omega_c}\int \exp\left[-t^{5/3}\right] \exp\left(-i\frac{\omega}{\omega_c} t\right) dt, \end{aligned} \tag{135}$$

where $D_{pl}(V\tau, L)$ is the standard Rytov method *temporal* plane wave structure function given by

$$D_{pl}(V\tau, L) \approx 2.914 C_n^2 k^2 L (V\tau)^{5/3}, \tag{136}$$

and $\omega_c = 2\pi\sigma_f$ is obtained from (133) using the plane wave coherence radius given by (132).

We now compare this result to that obtained by substituting the plane wave structure function obtained from the modified Rytov method, (81), into (134). Applying Taylor's frozen flow hypothesis to (81), the modified Rytov method temporal plane wave structure function is given by[26]

$$D_{pl}\left(V\tau, L\right) = D_x\left(V\tau, L\right) + D_y\left(V\tau, L\right), \tag{137}$$

where

$$D_x\left(V\tau, L\right) = 1.47\sigma_1^2\left[\frac{k\left(V\tau\right)^2\eta_{x(pl)}^{1/6}}{L}\right]\left[1 + 0.058\frac{k\left(V\tau\right)^2\eta_{x(pl)}}{L}\right]^{-1/6}, \tag{138}$$

$$\begin{aligned} D_y\left(V\tau, L\right) &= 2.37\sigma_1^2\left[\frac{k\left(V\tau\right)^2}{L}\right]^{5/6} \\ &\quad -1.47\sigma_1^2\left[\frac{k\left(V\tau\right)^2\eta_{y(pl)}^{1/6}}{L}\right]\left[1 + 0.058\frac{k\left(V\tau\right)^2\eta_{y(pl)}}{L}\right]^{-1/6}. \end{aligned} \tag{139}$$

Now, substituting (137) into (134), the modified Rytov method plane wave temporal frequency spectrum is given by[26]

$$\begin{aligned} W\left(\omega\right) &= 2\int \exp\left\{-\frac{1}{2}\left[D_x\left(V\tau, L\right) + D_y\left(V\tau, L\right)\right]\right\}\exp\left(-i\omega\tau\right)d\tau \\ &= \frac{2}{\omega_c}\int \exp\left\{-\frac{1}{2}\left[D_x\left(t\rho_{pl}, L\right) + D_y\left(t\rho_{pl}, L\right)\right]\right\}\exp\left(-i\frac{\omega}{\omega_c}t\right)dt, \end{aligned} \tag{140}$$

where $\omega_c = 2\pi\sigma_f$ is obtained from (133) using the plane wave coherence radius obtained from modified Rytov method using (81), (86), and (87), and we have made the substitution $V\tau = t\rho_{pl}$ so that (140) is notationally consistent with (135).

The question that naturally arises is what impact does the use of the plane wave structure function given by modified Rytov method, (81), have on the average temporal frequency spectrum, that is how (135) compares to (140). In the weak turbulence regime, there is no difference between the two approaches because the plane wave structure function values predicted by standard Rytov method are equal to those predicted by the modified Rytov method as seen in figure 6 of the last chapter. However, if we consider the case of moderate to strong optical turbulence, we find that the predicted average temporal frequency spectrum is steeper and narrower when using the wave structure function obtained from the modified Rytov approximation as compared to that obtained using the standard Rytov approximation.

We consider the case of strong optical turbulence allowing $\sigma_1^2 = 100$ with the propagation parameters used in figures 12 and 13. In this case, from figure 13, we find that the atmospheric induced angular frequency spread obtained when using the standard Rytov approximation coherence radius is approximately 1253 rad/s, which we denote as ω_{c1}. Using the modified Rytov approximation coherence radius, the angular frequency spread under the same conditions is approximately 651 rad/s, which we denote as ω_{c2}.

In figure 14, we have plotted the average temporal frequency spectrum, $W(\omega)$, given by (135) and (140), in the case of strong optical turbulence, $\sigma_1^2 = 100$. $W(\omega)$ is plotted as function of ω/ω_{c1} in both cases so that the same values of ω are considered for both curves. We see that the average temporal frequency spectrum, (140), obtained when using the plane wave structure function derived from the modified Rytov approximation is indeed steeper and narrower than that predicted when using the standard Rytov approximation. The interpretation of these results is that

the broadening around the average position of the line centroid, that is the frequency spread of the frequency spectrum, is not as significant in strong turbulence as predicted by the standard Rytov approximation.

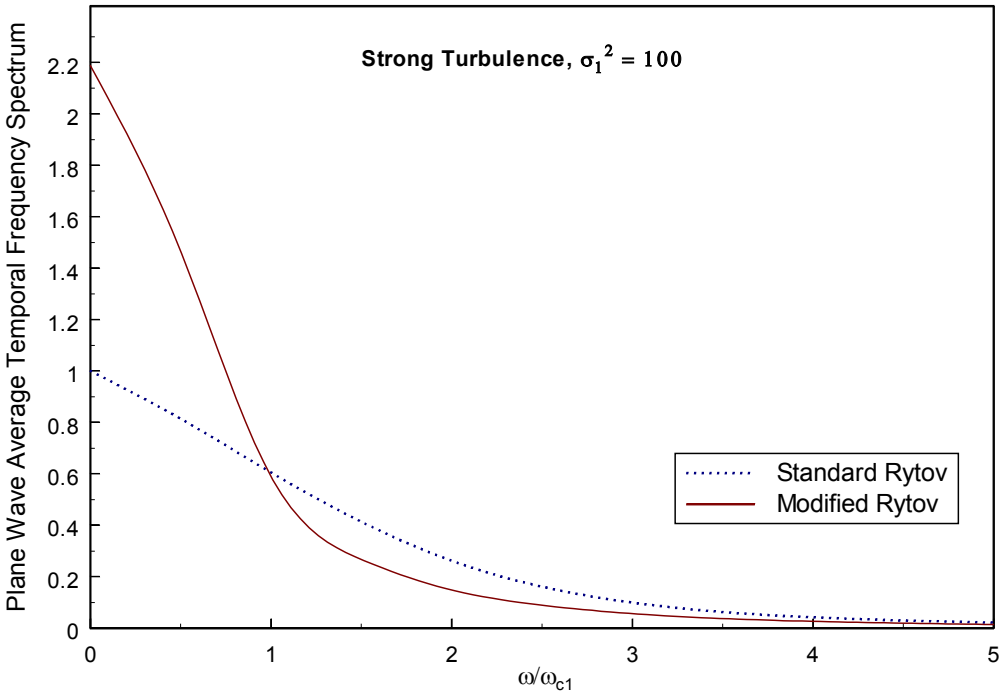

Figure 14 The plane wave average temporal frequency spectrum, (135) and (140), as a function of ω/ω_{c1} for strong optical turbulence, $\sigma_1^2 = 100$. The vertical axis is in arbitrary units.

7.2.2 *Analytic derivation of plane wave frequency spread*

Although (133) provides a simple expression governing the frequency spread, it is derived from an evaluation of the temporal frequency spectrum, which relies on knowledge of the mutual coherence function. While evaluating the mutual coherence function for a plane wave is relatively straightforward, doing so is significantly more difficult in the cases of spherical and Gaussian-beam waves. Here, we present a derivation for the frequency spread that is independent of an analysis of the mutual coherence function and compare the result to (133).

The characteristic equation for an electromagnetic signal is given by

$$v = \mathrm{Re}\left\{ A(t)\, e^{j\left[2\pi f_0 t + \phi(t)\right]} \right\}, \tag{141}$$

where $A(t)$ is the amplitude of the signal, f_0 is the carrier frequency, $\phi(t)$ is the phase shift associated with propagation, v is the voltage of the signal at the receiver, and $\mathrm{Re}(x)$ denotes the real part of x.

The instantaneous angular frequency, $\omega(t)$, of a signal is given by the derivative of the total phase of the signal. Therefore,

$$\omega(t) = \frac{d}{dt}\left[2\pi f_0 t + \phi(t)\right]. \tag{142}$$

In units of cycles per second (Hz), the frequency is therefore given by

$$f(t) = \frac{\omega(t)}{2\pi} = f_0 + \frac{d}{dt}\frac{\phi(t)}{2\pi}. \tag{143}$$

The phase shift associated with propagation, $\phi(t)$, can be separated into two components: a deterministic component, made up of all known sources of phase, and a non-deterministic component, made up of all random sources of phase. Hence,

$$f(t) = f_0 + \frac{d}{dt}\frac{\phi_d(t)}{2\pi} + \frac{d}{dt}\frac{\phi_s(t)}{2\pi}, \tag{144}$$

where we use ϕ_d to denote the deterministic component of phase and ϕ_s to denote the non-deterministic component of phase. The mean value of the frequency, therefore, is given by

$$\langle f \rangle = f_0 + \frac{\phi_d'(t)}{2\pi} + \frac{\langle \phi_s'(t) \rangle}{2\pi}, \tag{145}$$

where the prime indicates differentiation with respect to t. Thus, the frequency variance, σ_f^2, is given by

$$\begin{aligned} \sigma_f^2 &= \left\langle f(t)^2 \right\rangle - \langle f(t) \rangle^2 \\ &= \frac{\left\langle \phi_s'(t)^2 \right\rangle}{4\pi^2} - \frac{\left\langle \phi_s'(t) \right\rangle^2}{4\pi^2} \end{aligned} \tag{146}$$

which is in units Hz^2. It can be shown (see Appendix E) that the frequency variance, σ_f^2, is related to the *temporal phase covariance*, $B_s(\tau)$, by[26]

$$\sigma_f^2 = -\frac{B_s''(\tau)}{4\pi^2}\bigg|_{\tau=0}, \tag{147}$$

where the differentiation is with respect to τ.

The *spatial phase covariance* function, $B_s(\rho)$, of a plane wave is given by[2]

$$B_{s,pl}(\rho) = 2\pi^2 k^2 L \int_0^1 \int_0^\infty \kappa \Phi_n(\kappa) J_0(\kappa\rho) \left[1 + \cos\left(\frac{L\kappa^2\xi}{k}\right)\right] d\kappa d\xi. \tag{148}$$

From (148), we obtain the temporal phase covariance function by applying Taylor's frozen flow hypothesis. Taylor's frozen flow hypothesis dictates that the time scale for changes in the characteristics of a given eddy is much longer than that related to the transverse motion of eddies, i.e. the motion of the eddies in the direction perpendicular to the propagation path. Thus, Taylor's theory indicates that temporal fluctuations in the optical wave are directly related to the geometry of the wave and the wind speed perpendicular to the propagation path, V. This allows spatial statistics to be directly related to temporal statistics. Assuming the turbulent atmosphere is frozen, i.e. that the characteristics of individual eddies are not changing, then observation of the optical wave at two points separated by a distance ρ is equivalent to observing the wave at a single observation point for a time τ. The relation between τ and ρ is determined by the geometry of the wave. In the plane wave case, the wave front can be thought of as "flat" so that the relation is given by $\rho = V\tau$. Thus, making the substitution $\rho = V\tau$, the resulting plane wave temporal phase

covariance function is given by

$$B_{s,pl}\left(V\tau\right)=2\pi^{2}k^{2}L\int_{0}^{1}\int_{0}^{\infty}\kappa\Phi_{n}\left(\kappa\right)J_{0}\left(\kappa V\tau\right)\left[1+\cos\left(\frac{L\kappa^{2}\xi}{k}\right)\right]d\kappa d\xi. \tag{149}$$

Using the relation given by (147), the integral expression for the plane wave frequency variance is now

$$\sigma_{f,pl}^{2}=0.25k^{2}LV^{2}\int_{0}^{1}\int_{0}^{\infty}\kappa^{3}\Phi_{n}\left(\kappa\right)\left[1+\cos\left(\frac{L\kappa^{2}\xi}{k}\right)\right]d\kappa d\xi. \tag{150}$$

In this expression, it is necessary to include a finite inner scale of turbulence, l_0, for convergence. Unlike the case of the wave structure function no appropriate restrictions can be made after integration in order to eliminate the dependence on the inner scale. We first develop an expression for the plane wave frequency variance using the standard Rytov method. We, substitute into (150) an analytic approximation to the Hill spectrum

$$\Phi_{n}\left(\kappa\right)=0.033C_{n}^{2}\kappa^{-11/3}\exp\left(-\frac{\kappa^{2}}{\kappa_{l}^{2}}\right)\left[1+1.802\left(\frac{\kappa}{\kappa_{l}}\right)-0.254\left(\frac{\kappa}{\kappa_{l}}\right)^{\frac{7}{6}}\right], \tag{151}$$

that is identical to (27) except that an infinite outer scale has been assumed. Substituting (151) into (150) and evaluating yields the standard Rytov method frequency variance given by[26] (see

Appendix F)

$$\begin{aligned}\sigma^2_{f,pl,SR} &= 0.0258\sigma_1^2\left(\frac{k}{L}\right)V^2Q_l^{1/6} \\ &\times\left\{1+0.723_2F_1\left(\tfrac{1}{12},\tfrac{7}{12};\tfrac{3}{2};-Q_l^2\right)\right. \\ &\left.+0.317_2F_1\left(\tfrac{1}{3},\tfrac{5}{6};\tfrac{3}{2};-Q_l^2\right)-0.04_2F_1\left(\tfrac{3}{8},\tfrac{7}{8};\tfrac{3}{2};-Q_l^2\right)\right\}, \end{aligned} \tag{152}$$

where $Q_l = \frac{L\kappa_l^2}{k}$ and the $''SR''$ subscript denotes that this is for the standard Rytov method. The ${}_2F_1\left(a,b;c,x\right)$ hypergeometric functions are approximated by binomial functions as follows[2]

$${}_2F_1\left(\tfrac{1}{12},\tfrac{7}{12};\tfrac{3}{2};-x\right)\approx\left[1+0.28x\right]^{-1/12}, \tag{153}$$

$${}_2F_1\left(\tfrac{1}{3},\tfrac{5}{6};\tfrac{3}{2};-x\right)\approx\left[1+0.426x\right]^{-1/3}, \tag{154}$$

and

$${}_2F_1\left(\tfrac{3}{8},\tfrac{7}{8};\tfrac{3}{2};-x\right)\approx\left[1+0.4523x\right]^{-3/8}. \tag{155}$$

The approximations (153)-(155) have a maximum relative error on the order of 10% as x approaches infinity. Replacing the hypergeometric functions in (152) with these approximations, we obtain a simpler algebraic expression for the standard Rytov plane wave frequency variance

given by

$$\sigma^2_{f,pl,SR} \cong 0.0258\sigma_1^2\left(\frac{k}{L}\right)V^2Q_l^{1/6}\times\left\{1+0.723\left[1+0.28Q_l^2\right]^{-1/12}\right.$$
$$\left.+0.317\left[1+0.426Q_l^2\right]^{-1/3}-0.04\left[1+0.4523Q_l^2\right]^{-3/8}\right\}. \quad (156)$$

The plane wave frequency spread, σ_f, is the square root of the frequency variance, i.e.

$$\sigma_f=\sqrt{\sigma_f^2}. \quad (157)$$

Note that (156)-(157) describe only the frequency spread, σ_f, of the frequency spectrum, and do not account for the wandering position of the frequency spectrum line centroid.

In figure 15, we compare the frequency spread as predicted by (156)-(157) to that predicted by , $\sigma_f=\frac{V}{2\pi\rho_{pl}}$, (133), where the plane wave coherence radius is given by the standard Rytov approximation, (132). The figure indicates that both expressions have the same qualitative behavior as a function of turbulence strength and are of the same order numerically. This indicates that the expression derived here, (156)-(157), provides a good approximation of the frequency spread without any knowledge of the mutual coherence function.

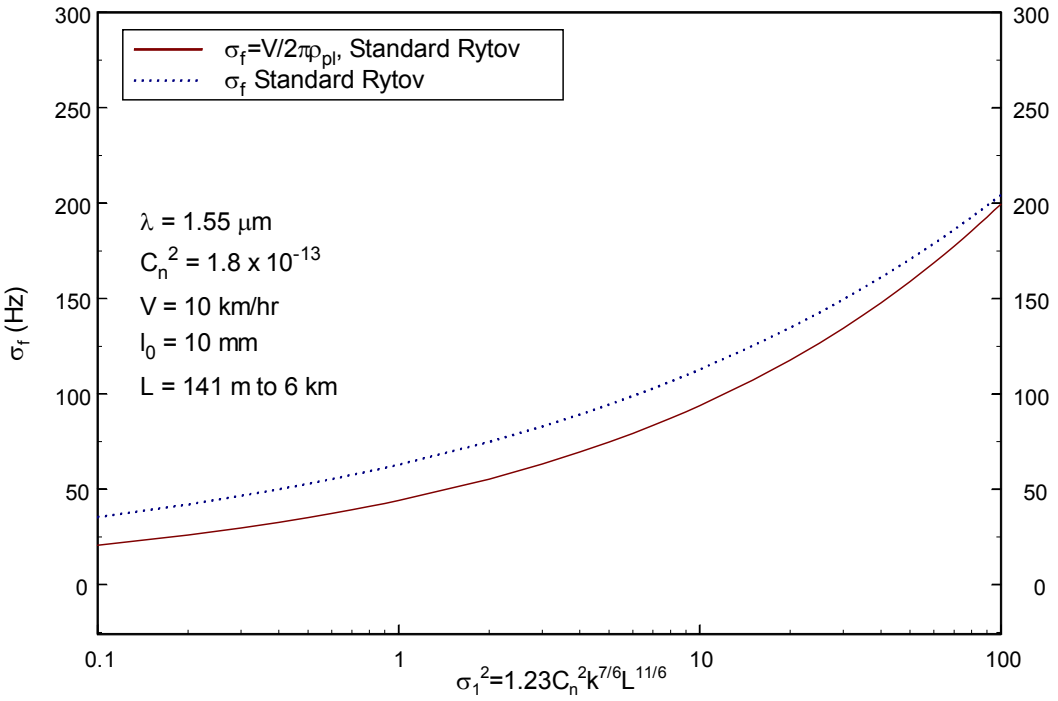

Figure 15 The plane wave frequency spread in *Hz* as a function of increasing turbulence strength. The solid line represents the frequency spread given by (132)-(133). The dashed curve is the frequency spread given by (156)-(157). The index of refraction structure parameter, C_n^2, is held constant, while the propagation path length, L, is allowed to vary.

We note that the frequency variance, (156), was developed using the standard Rytov approximation method and therefore is expected to be valid in weak turbulence conditions only. However, a similar expression can be developed that is believed to be valid in all turbulence conditions by applying the modified Rytov method. As stated earlier, it is necessary to include a finite inner scale. Thus, we allow

$$f\left(\kappa l_0\right) = \exp\left(-\frac{\kappa^2}{\kappa_l^2}\right)\left[1 + 1.802\left(\frac{\kappa}{\kappa_l}\right) - 0.254\left(\frac{\kappa}{\kappa_l}\right)^{\frac{7}{6}}\right] \tag{158}$$

and $g\left(\kappa L_0\right) = 1$ in the effective atmospheric spectrum, (67). Substituting (67) and (158) into (150) and using the approximations (153)-(155), the resulting plane wave frequency variance is given by[26]

$$\sigma_{f,pl,MR}^2 = \sigma_{f,x}^2 + \sigma_{f,y}^2 \tag{159}$$

where the *"MR"* subscript indicates that this is for the modified Rytov method. The large scale and small scale frequency variance components, $\sigma_{f,x}^2$ and $\sigma_{f,y}^2$, are given by (see Appendix F)

$$\begin{aligned}\sigma_{f,x}^2 \;\cong\; & 0.0258\sigma_1^2\left(\frac{k}{L}\right)V^2\alpha_x^{1/6} \times \left\{1 + 0.723\left[1 + 0.28\alpha_x^2\right]^{-1/12}\right. \\ & \left. +0.317\left[1 + 0.426\alpha_x^2\right]^{-1/3} - 0.04\left[1 + 0.4523\alpha_x^2\right]^{-3/8}\right\},\end{aligned} \tag{160}$$

$$\begin{aligned}\sigma_{f,y}^2 \;\cong\; & \sigma_{f,pl,SR}^2 - 0.0258\sigma_1^2\left(\frac{k}{L}\right)V^2\alpha_y^{1/6} \times \left\{1 + 0.723\left[1 + 0.28\alpha_y^2\right]^{-1/12}\right. \\ & \left. +0.317\left[1 + 0.426\alpha_y^2\right]^{-1/3} - 0.04\left[1 + 0.4523\alpha_y^2\right]^{-3/8}\right\},\end{aligned} \tag{161}$$

where

$$\alpha_x = \frac{\eta_{x(pl)Q_l}}{\eta_{x(pl)+Q_l}},\ \alpha_y = \frac{\eta_{y(pl)Q_l}}{\eta_{y(pl)+Q_l}}. \tag{162}$$

Expressions for the non-dimensional parameters $\eta_{x(pl)}$ and $\eta_{y(pl)}$, that include an inner scale dependency are given by Andrews *et al*[7] as

$$\eta_{x(pl)} = \frac{2.61}{1 + 0.45\sigma_1^2 Q_l^{1/6}}, \tag{163}$$

$$\eta_{y(pl)} = 3\left(\frac{\sigma_1}{\sigma_p}\right)^{12/5}\left(1 + 0.69\sigma_p^{12/5}\right), \tag{164}$$

where

$$\begin{aligned}\sigma_p^2 &= 3.86\sigma_1^2\left\{\left(1 + 1/Q_l^2\right)^{11/12}\left[\sin\left(\frac{11}{6}\tan^{-1}Q_l\right) + \frac{1.51}{\left(1+Q_l^2\right)^{1/4}}\sin\left(\frac{4}{3}\tan^{-1}Q_l\right)\right.\right.\\ &\left.\left. - \frac{0.27}{\left(1+Q_l^2\right)^{7/24}}\sin\left(\frac{5}{4}\tan^{-1}Q_l\right)\right] - 3.50Q_l^{-5/6}\right\}.\end{aligned} \tag{165}$$

In figure 16, the frequency spread, σ_f, obtained from (157) and (159), is compared to $\sigma_f = \frac{V}{2\pi\rho_{pl}}$, equation (133), as obtained from the temporal frequency spectrum analysis, where now the plane wave coherence radius is that obtained from the wave structure function derived using the modified Rytov approximation, given by (81). The two expressions have the same qualitative behavior and are of the same order numerically, indicating that the expression derived in (159), serves as a good approximation to the frequency spread of the frequency spectrum in all turbulence regimes including the moderate to strong turbulence regimes.

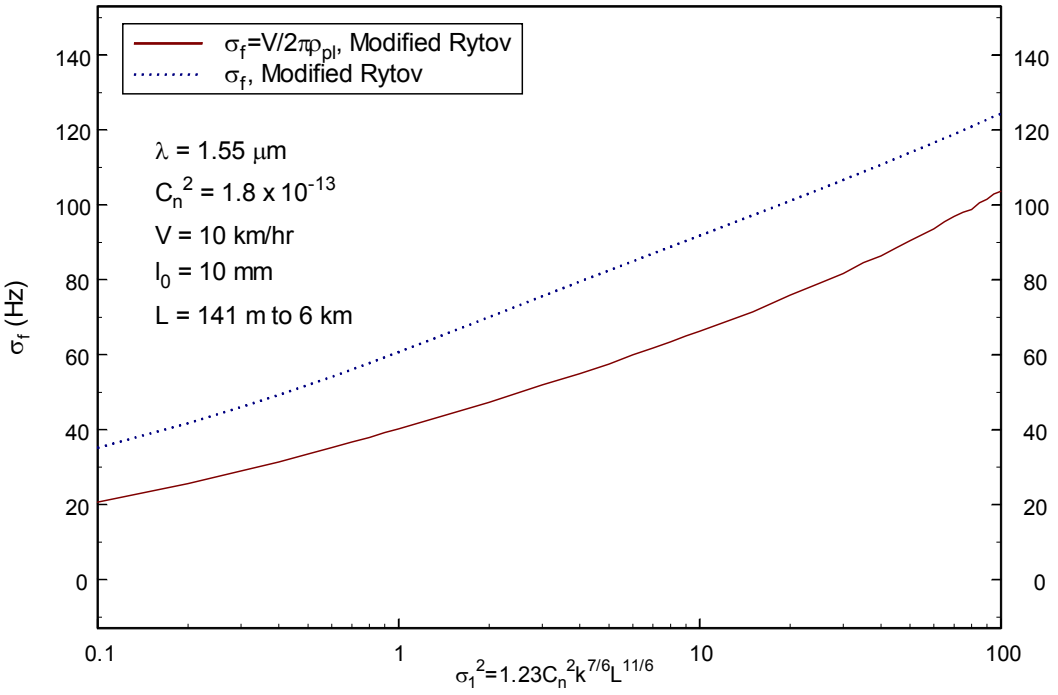

Figure 16 The plane wave frequency spread in *Hz* as a function of increasing turbulence strength. The solid line represents the frequency spread given by (81) and (133). The dashed curve is the frequency spread given by (157) and (159). The index of refraction structure parameter, C_n^2, is held constant, while the propagation path length, L, is allowed to vary.

7.3 Spherical wave

Here, we conduct a similar analysis for a spherical wave. We will need expressions for the spherical wave coherence radius, ρ_{sp}. Using the standard Rytov method and applying the Kolmogorov spectrum, the spherical wave structure function is given by (91). Setting this equation equal to two and solving for ρ yields an analytic expression for the spherical wave coherence radius, ρ_{sp}, given by[2]

$$\rho_{sp} = \left(0.55 C_n^2 k^2 L\right)^{-3/5}, \qquad l_0 \ll \rho \ll L_0. \tag{166}$$

As in the plane wave case, the coherence radius obtained from the modified Rytov method cannot be expressed exactly in closed form. However, it can be computed numerically, again using a bisection method, by setting (93) equal to two and solving for ρ.

7.3.1 Coherence, frequency spread, and frequency spectrum analysis

We now compare the spherical wave coherence radius derived from the standard Rytov approximation, (166), to that obtained from the modified Rytov approximation determined numerically from (93). The results as a function of increasing turbulence strength are presented in figure 17. The behavior is the same as that of the plane wave case and we see that the two results agree in the weak turbulence regime. However, in the moderate to strong turbulence regime the modified Rytov approximation method predicts larger values for the coherence radius

as compared to the standard Rytov approximation, consistent with the results observed in the plane wave analysis.

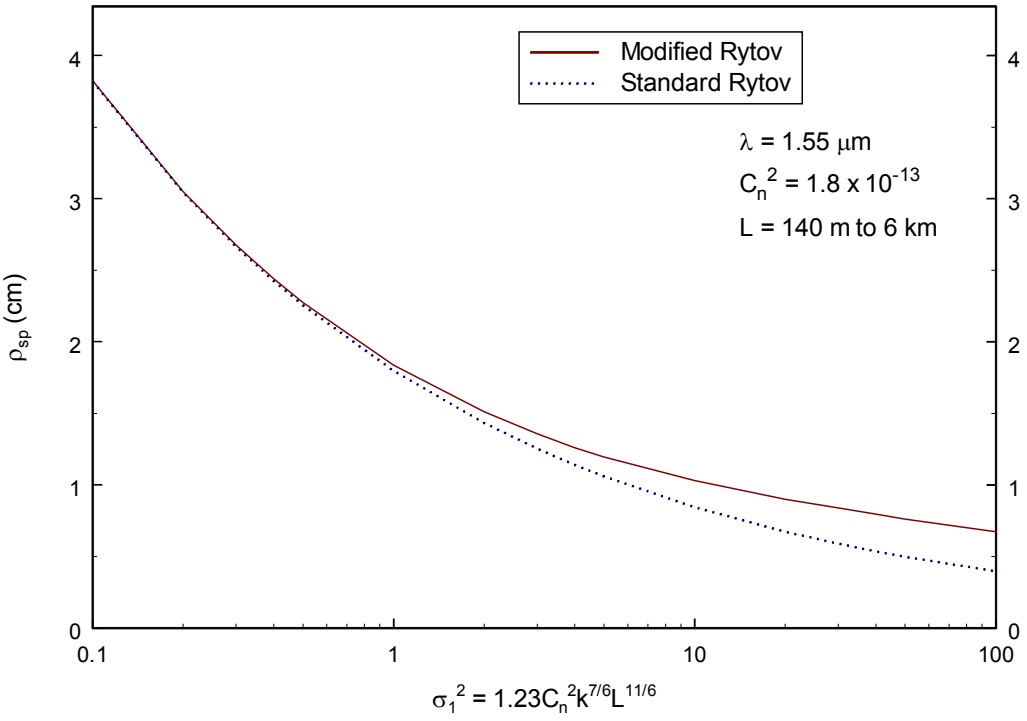

Figure 17 The spherical wave coherence radius in cm as a function of increasing turbulence strength. The index of refraction structure parameter, C_n^2, is held constant, while the propagation path length, L, is allowed to vary. The standard Rytov curve is obtained from (166) and the modified Rytov curve is obtained by setting (93) equal to two and numerically solving for ρ.

In the introduction, a very simple intuitive argument was given that led to an expression for the angular frequency spread, ω_c, of the frequency spectrum for a plane wave. The result for the angular frequency spread was also derived analytically by Ishimaru[4] and is given by $\omega_c = \frac{V}{\rho_{pl}}$. However, in the case of a spherical wave, the same intuitive argument does not apply because of the geometry associated with a spherical wave.

As noted by Belen'kiĭ and Mironov,[27] to correctly account for the spherical wave geometry when applying Taylor's frozen flow hypothesis, one must make the substitution $\rho = V\tau/\xi$ in the integral definition of the statistical quantity of interest. To see that this is indeed necessary, consider a turbulent eddy of size l at the point z along the propagation path of length L moving perpendicular to the propagation path with velocity V. Because the spherical wave front is expanding as it propagates, unlike the plane wave, the portion of the wave front disturbed by the eddy is also expanding. An observer at the distance $L - z$ from the turbulent eddy "sees" the eddy as being of size $l_{dist} = l\left(\frac{L}{z}\right)$ as can be determined from the relation between concentric spherical wave fronts. Thus, for the observer, the apparent velocity of the disturbance is $v_{dist} = V\left(\frac{L}{z}\right)$. Therefore the relation between spatial observation distance, ρ, and the equivalent observation time, τ, as discussed in plane wave case, is now $\rho = v_{dist}\tau = V\left(\frac{L}{z}\right)\tau$. In the substitution $\rho = V\tau/\xi$, $\xi = \frac{z}{L}$ is the normalized path length argument and is also the variable of integration. Note that in the case of the plane wave geometry, the substitution $\rho = V\tau$ is independent of the variable of integration; hence this substitution can be made after the integration is completed. However, in the case of a spherical wave, the substitution is explicitly dependent on the variable of integration, ξ, and therefore must be made prior to the completion of the integration. Thus, one cannot use

the same simple intuitive argument to derive an expression governing the frequency spread of a spherical wave as was used for the plane wave.

The frequency spread of a spherical wave can be determined from an examination of the temporal frequency spectrum, i.e. the Fourier transform of the mutual coherence function. However, as noted by Ishimaru,[4] the spherical wave mutual coherence function is statistically inhomogeneous because it depends explicitly on the location of the two points in the observation plane. However, if we consider the special case when the observation points are symmetrically located with respect to the optical axis, i.e. $\mathbf{r}_1 = -\mathbf{r}_2$, then the mutual coherence function is a function of the separation distance of the two points, ρ, as was the case for a plane wave. In this case, the spherical wave spatial mutual coherence function is given by[2,4]

$$\Gamma_2(\rho, L) = \exp\left[-\frac{1}{2} D_{sp}(\rho, L)\right], \tag{167}$$

where $D_{sp}(\rho, L)$ is the spatial spherical wave structure function whose integral definition is given by (90). We recall that the average spherical wave temporal frequency spectrum is given by the Fourier transform of the temporal mutual coherence function. Thus, we must first convert (167) from a spatial statistic to a temporal one in the manner suggested by Belen'kiĭ and Mironov[27] as discussed above. This means that in the integral definition of the spatial spherical wave structure function we must make the substitution $\rho = V\tau/\xi$, which yields

$$D(V\tau, L) = 8\pi^2 k^2 L \int_0^\infty \kappa \Phi_n(\kappa) [1 - J_0(\kappa V \tau)]\, d\kappa. \tag{168}$$

This is the exact result that one obtains for the temporal plane wave structure function. This indicates the temporal mutual coherence function for a spherical wave is identical to that of a plane wave when one considers points in the observation plane that are symmetrically located about the optical axis. Therefore, in turn, this suggests that the temporal frequency spectrum and the frequency spread of the spectrum are identical in the plane and spherical wave cases.

Although this may seem surprising, we show in the next section, that the spherical wave frequency spread can also be determined independently of the mutual coherence function as was done for the plane wave and that the plane and spherical wave results agree. Indeed, although we do not make the assumption that the observation points are symmetrically located about the optical axis in the derivation of the next section, we will see that the numerical values of the frequency spread derived in the manner given are nearly identical to the plane wave case.

7.3.2 Analytic derivation of spherical wave frequency spread

Here, we derive an expression for the spherical wave frequency variance independent of the mutual coherence function in the same manner as was done in the plane wave case. Recall that the frequency variance was related to the temporal phase covariance function through the relation given by (147). The spherical wave spatial phase covariance function is given by[2]

$$B_{s,sp}(\rho) = 2\pi^2 k^2 L \int_0^1 \int_0^\infty \kappa \Phi_n(\kappa) J_0(\kappa\xi\rho) \left\{1 + \cos\left[\frac{L\kappa^2\xi}{k}(1-\xi)\right]\right\} d\kappa d\xi. \qquad (169)$$

Applying Taylor's frozen flow hypothesis for a spherical wave, we make the substitution $\rho = V\tau/\xi$, so that the spherical wave temporal phase covariance function is given by

$$B_{s,sp}(V\tau) = 2\pi^2 k^2 L \int_0^1 \int_0^\infty \kappa \Phi_n(\kappa) J_0(\kappa V\tau) \left\{1 + \cos\left[\frac{L\kappa^2\xi}{k}(1-\xi)\right]\right\} d\kappa d\xi. \quad (170)$$

Now applying the relation given by (147), we find that the spherical wave frequency variance is given by[26]

$$\sigma^2_{f,sp} = 0.25 k^2 L V^2 \int_0^1 \int_0^\infty \kappa^3 \Phi_n(\kappa) \left\{1 + \cos\left[\frac{L\kappa^2\xi}{k}(1-\xi)\right]\right\} d\kappa d\xi. \quad (171)$$

Assuming an infinite outer scale, we substitute the analytic approximation to the Hill spectrum, (151), into equation (171) to obtain spherical wave frequency variance results based on the standard Rytov approximation. The resulting spherical wave frequency variance is given by[26] (see Appendix F)

$$\begin{aligned} \sigma^2_{f,sp,SR} &= 0.0258\sigma_1^2 \left(\frac{k}{L}\right) V^2 Q_l^{1/6} \times \left\{1 + 0.723\, {}_3F_2\left(\tfrac{1}{12}, \tfrac{7}{12}, 1; \tfrac{3}{4}, \tfrac{5}{4}; -\tfrac{Q_l^2}{16}\right)\right. \\ &\quad + 0.317\, {}_3F_2\left(\tfrac{1}{3}, \tfrac{5}{6}, 1; \tfrac{3}{4}, \tfrac{5}{4}; -\tfrac{Q_l^2}{16}\right) \\ &\quad \left. - 0.04\, {}_3F_2\left(\tfrac{3}{8}, \tfrac{7}{8}, 1; \tfrac{3}{4}, \tfrac{5}{4}; -\tfrac{Q_l^2}{16}\right)\right\}, \end{aligned} \quad (172)$$

where the *"SR"* subscript indicates that this is for the standard Rytov method and ${}_3F_2(x)$ is a generalized hypergeometric function. We note that because (172) is based on the standard Rytov approximation, it is believed to be valid only in weak optical turbulence. In figure 18 we compare

the results for the spherical wave frequency spread, σ_f, obtained when (172) is substituted into (157), to the plane wave frequency spread obtained by substituting (156) into (157). Additionally, we have plotted the plane wave frequency spread, (133), where the coherence radius is that given by (132), obtained from an analysis of the Fourier transform of the mutual coherence function. From the analysis conducted in last section where it was concluded that the plane and spherical wave frequency spectrums are identical for the case when $\mathbf{r}_1 = -\mathbf{r}_2$, we expect that all three results should be identical and indeed from figure 18, we see that is approximately the case. As in the case of a plane wave, this supports the conclusion that (172) serves as a good approximation to the frequency spread of the frequency spectrum with the advantage of avoiding an analysis of the mutual coherence function.

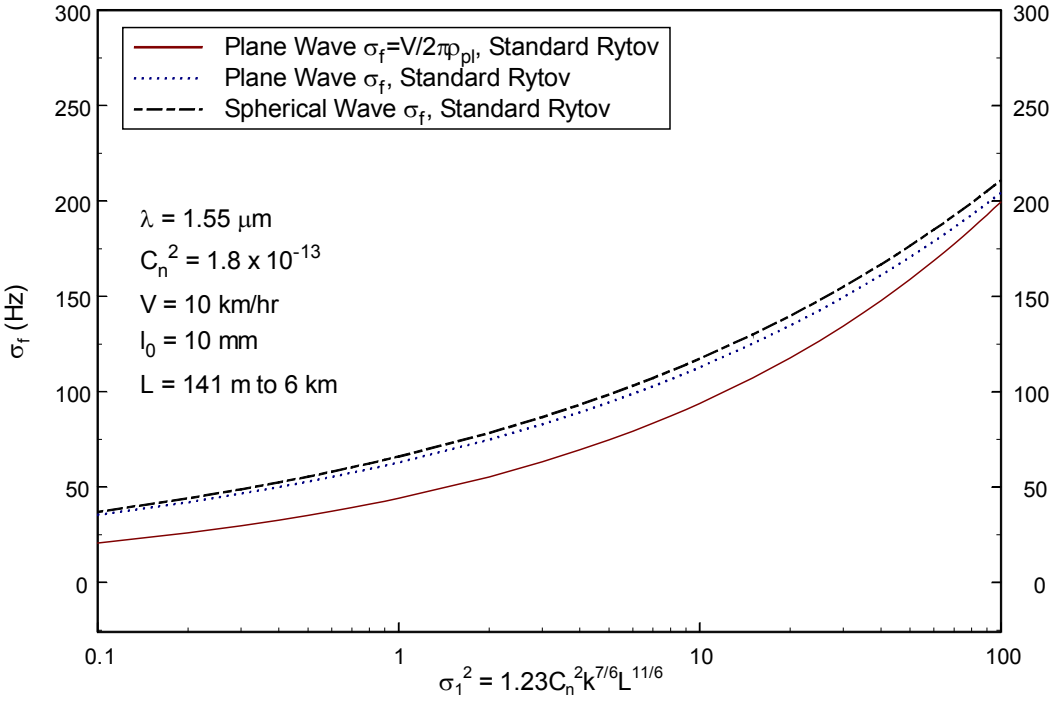

Figure 18 The plane and spherical wave frequency spread in *Hz* as a function of increasing turbulence strength. The solid line represents the frequency spread given by (132) and (133). The dotted curve is the frequency spread given by (156)-(157). The dashed curve is the spherical wave frequency spread given by (157) and (172). The index of refraction structure parameter, C_n^2, is held constant, while the propagation path length, L, is allowed to vary.

To derive an expression for the spherical wave frequency variance that is believed to be valid in all optical turbulence conditions we substitute the effective Hill spectrum, (67), where again $f(\kappa l_0)$ is given by (158) and $g(\kappa L_0) = 1$, into (171). The resulting expression for the spherical wave frequency variance is given by[26]

$$\sigma^2_{f,sp,MR} = \sigma^2_{f,x} + \sigma^2_{f,y}, \tag{173}$$

where the *"MR"* subscript indicates that this is for the modified Rytov method and (see Appendix F)

$$\begin{aligned}\sigma^2_{f,x} &= 0.0258\sigma_1^2 \left(\frac{k}{L}\right) V^2 \alpha_x^{1/6} \times \left\{1 + 0.723\ {}_3F_2\left(\tfrac{1}{12}, \tfrac{7}{12}, 1; \tfrac{3}{4}, \tfrac{5}{4}; -\tfrac{\alpha_x^2}{16}\right)\right. \\ &\left. +0.317\ {}_3F_2\left(\tfrac{1}{3}, \tfrac{5}{6}, 1; \tfrac{3}{4}, \tfrac{5}{4}; -\tfrac{\alpha_x^2}{16}\right) - 0.04\ {}_3F_2\left(\tfrac{3}{8}, \tfrac{7}{8}, 1; \tfrac{3}{4}, \tfrac{5}{4}; -\tfrac{\alpha_x^2}{16}\right)\right\}, \end{aligned} \tag{174}$$

$$\begin{aligned}\sigma^2_{f,y} &= \sigma^2_{f,sp,SR} - 0.0258\sigma_1^2 \left(\frac{k}{L}\right) V^2 \alpha_y^{1/6} \times \left\{1 + 0.723\ {}_3F_2\left(\tfrac{1}{12}, \tfrac{7}{12}, 1; \tfrac{3}{4}, \tfrac{5}{4}; -\tfrac{\alpha_y^2}{16}\right)\right. \\ &\left. +0.317\ {}_3F_2\left(\tfrac{1}{3}, \tfrac{5}{6}, 1; \tfrac{3}{4}, \tfrac{5}{4}; -\tfrac{\alpha_y^2}{16}\right) - 0.04\ {}_3F_2\left(\tfrac{3}{8}, \tfrac{7}{8}, 1; \tfrac{3}{4}, \tfrac{5}{4}; -\tfrac{\alpha_y^2}{16}\right)\right\}. \end{aligned} \tag{175}$$

The remaining parameters in (174) and (175) are given by[7]

$$\eta_{x(sp)} = \frac{8.56}{1 + 0.18\sigma_1^2 Q_l^{1/6}}, \qquad \eta_{y(sp)} = 9\left(\frac{0.4\sigma_1^2}{\sigma_s^2}\right)^{6/5} \left(1 + 0.69\sigma_s^{12/5}\right), \tag{176}$$

$$\alpha_x = \frac{\eta_{x(sp)Q_l}}{\eta_{x(sp)+Q_l}}, \ \alpha_y = \frac{\eta_{y(sp)Q_l}}{\eta_{y(sp)+Q_l}}, \tag{177}$$

where $\beta_0^2 = 0.4\sigma_1^2$ and

$$\sigma_s^2 = 3.86\sigma_1^2 \left\{ 0.4\left(1+9/Q_l^2\right)^{11/12} \left[\sin\left(\frac{11}{6}\tan^{-1}\frac{Q_l}{3}\right) + \frac{2.61}{\left(9+Q_l^2\right)^{1/4}} \sin\left(\frac{4}{3}\tan^{-1}\frac{Q_l}{3}\right) - \frac{0.52}{\left(9+Q_l^2\right)^{7/24}} \sin\left(\frac{5}{4}\tan^{-1}\frac{Q_l}{3}\right) \right] - 3.50 Q_l^{-5/6} \right\}. \quad (178)$$

When graphed as a function of increasing turbulence strength, the frequency spread obtained using (157) where σ_f^2 is the modified Rytov method frequency variance, (173), the results are similar to those presented in figure 18. Indeed, it is found that the modified Rytov method plane and spherical wave frequency spread are nearly identical. To avoid redundancy, the graph is intentionally not presented.

8. SLANT PATH TEMPORAL FREQUENCY SPREAD

8.1 Introduction

Many free space optical systems, such as ground to satellite communication systems, transmit an optical signal along a slant path. This situation is fundamentally different than horizontal path transmission because the atmospheric index of refraction structure parameter, C_n^2, is altitude dependent. Furthermore, the uplink case, in which transmission occurs from the ground to a receiver at some altitude H, yields different results than the downlink case, in which transmission occurs from a transmitter at an altitude H to the ground. In this chapter, the frequency spread results for horizontal paths of the last chapter are extended to slant paths. Both the uplink and downlink scenarios are considered. Integral expressions valid in conditions of weak irradiance fluctuations are developed using the standard Rytov method. Expressions believed valid under all conditions of irradiance fluctuations, i.e. all optical turbulence conditions, are derived using the modified Rytov method.

8.2 Hufnagel-Valley model

In the horizontal path work considered so far, the atmospheric index of refraction structure parameter, C_n^2, has been assumed to be constant along the propagation path. However, this parameter is altitude dependent. Thus, this dependence must be accounted for in slant path problems. The *Hufnagel-Valley* (H-V) model is commonly used to describe the altitude dependency of the refractive index structure parameter and is given by[2]

$$C_n^2(h) = 0.00594\left(\frac{v}{27}\right)^2\left(10^{-5}h\right)^{10}\exp\left(-\frac{h}{1000}\right) + 2.7\times10^{-16}\exp\left(-\frac{h}{1500}\right) + A\exp\left(-\frac{h}{100}\right), \quad (179)$$

where h is the altitude in meters (m), v is the rms windspeed (pseudowind) in meters per second (m/s), and A is the nominal value of $C_n^2(0)$ at the ground in $\mathrm{m}^{-2/3}$. The rms windspeed, v, is given by[2]

$$v = \left[\frac{1}{15\times10^3}\int_{5\times10^3}^{20\times10^3} V^2(h)\,dh\right]^{1/2}, \quad (180)$$

where $V(h)$ is often described by the *Bufton* wind model

$$V(h) = \omega_s h + v_g + 30\exp\left[-\left(\frac{h-9400}{4800}\right)^2\right]. \quad (181)$$

The quantity v_g is the ground wind speed and ω_s is the slew rate associated with the receiver (i.e. plane or satellite) moving with respect to an observer on the ground. In the work that follows, the H-V model will be substituted into the integral definitions of the plane and spherical wave frequency variance, σ_f^2, developed in the previous chapter, (150) and (171), to develop slant path temporal frequency spread results.

It is also necessary to address the differences between the uplink and donwlink scenarios. If we let h_0 be the transmitter height above the ground in meters, H be the receiver altitude in meters, and ζ be the zenith angle then the transmission path length, L, is given by

$$L = (H - h_0) \sec(\zeta). \tag{182}$$

In the horizontal path integral formulation the variable of integration, ξ, is a normalized distance, that is $\xi = \frac{z}{L}$, where z ranges from 0 to L, so that integration is over the path from the transmitter to the receiver. For the slant path scenario, integration is over the path from h_0 to H for the uplink scenario (i.e. transmission from the ground) and over the path from H to h_0 for the downlink scenario (i.e. transmission to the ground). Therefore, in order to maintain the integral formulation for the frequency variance of the transmitted wave, we integrate over the variable of integration, h, from h_0 to H for the uplink, where we set

$$\xi = 1 - \frac{h - h_0}{H - h} \tag{183}$$

and from H to h_0 for the downlink, where we set

$$\xi = \frac{h - h_0}{H - h} \tag{184}$$

in equations (150) and (171) for a transmitted plane wave and spherical wave, respectively.

8.3 Plane wave

Applying the standard Rytov method, slant path plane wave frequency variance expressions can be obtained by substituting the Hill spectral model, (151), and the H-V refractive index structure parameter model for C_n^2, (179), into (150). Completing the integration on κ yields the resulting integral expression for the plane wave frequency variance along a slant path[28]

$$\begin{aligned}\sigma^2_{f,pl,SR} &= 0.0317\kappa_l^{1/3}k^2V^2\sec(\zeta)\times\int_{h_0}^{H}C_n^2(h)\\ &\quad\times\left[1+0.723\,{}_2F_1\left(\tfrac{1}{12},\tfrac{7}{12};\tfrac{1}{2};-Q_l^2\xi^2\right)\right.\\ &\quad\left.+0.317\,{}_2F_1\left(\tfrac{1}{3},\tfrac{5}{6};\tfrac{1}{2};-Q_l^2\xi^2\right)-0.04\,{}_2F_1\left(\tfrac{3}{8},\tfrac{7}{8};\tfrac{1}{2};-Q_l^2\xi^2\right)dh\right],\end{aligned} \tag{185}$$

where the *"SR"* subscript indicates that this is from the standard Rytov method, ξ is given by (183) for the uplink case and by (184) for downlink the downlink case. As in the horizontal path case, the outer scale of turbulence is assumed to be infinite. As equation (185) was derived using the standard Rytov method, it is expected to be valid only in weak optical turbulence.

The modified Rytov method can be used to derive results that are expected to be valid in all turbulence conditions. Again assuming an infinite outer scale, the effective Hill spectral model, (67), with $f(\kappa l_0)$ given by (158) and $g(\kappa L_0) = 1$, and the H-V model are substituted into the integral definition of the plane wave frequency variance, (150). Completing the integration on κ, the slant path plane wave frequency variance is given by the sum of a large and small scale component[28]

$$\sigma^2_{f,pl,MR} = \sigma^2_{f,x} + \sigma^2_{f,y}. \tag{186}$$

where the *"MR"* subscript denotes that this is for the modified Rytov method. The large and small scale components are defined by

$$\begin{aligned}\sigma^2_{f,x} &= 0.0317\alpha_x^{1/6}k^2V^2\sec(\zeta)\times\int_{h_0}^{H} C_n^2(h)\times\Big[1+0.723\,{}_2F_1\left(\tfrac{1}{12},\tfrac{7}{12};\tfrac{1}{2};-\alpha_x^2\xi^2\right)\\ &\quad +0.317\,{}_2F_1\left(\tfrac{1}{3},\tfrac{5}{6};\tfrac{1}{2};-\alpha_x^2\xi^2\right)-0.04\,{}_2F_1\left(\tfrac{3}{8},\tfrac{7}{8};\tfrac{1}{2};-\alpha_x^2\xi^2\right)dh\Big],\end{aligned} \tag{187}$$

$$\begin{aligned}\sigma^2_{f,y} &= \sigma^2_{f,pl,SR} - 0.0317\alpha_y^{1/6}k^2V^2\sec(\zeta)\times\int_{h_0}^{H} C_n^2(h)\\ &\quad\times\Big[1+0.723\,{}_2F_1\left(\tfrac{1}{12},\tfrac{7}{12};\tfrac{1}{2};-\alpha_y^2\xi^2\right)\\ &\quad +0.317\,{}_2F_1\left(\tfrac{1}{3},\tfrac{5}{6};\tfrac{1}{2};-\alpha_y^2\xi^2\right)-0.04\,{}_2F_1\left(\tfrac{3}{8},\tfrac{7}{8};\tfrac{1}{2};-\alpha_y^2\xi^2\right)dh\Big].\end{aligned} \tag{188}$$

In (188), $\sigma^2_{f,pl,SR}$ is the standard Rytov method frequency variance along a slant path given by (185) and ξ is given by (183) for uplink paths and (184) for downlink paths. The parameters α_x and α_y are identical in form to those of the horizontal path case, however an altitude dependency is built into the nondimensional frequency cutoffs through the Rytov variance. The parameters are given by

$$\eta_{x(pl)} = \frac{L\kappa_x^2}{k},\ \alpha_x = \frac{\eta_{x(pl)Q_l}}{\eta_{x(pl)+Q_l}},\ \eta_{y(pl)} = \frac{L\kappa_y^2}{k},\ \alpha_y = \frac{\eta_{y(pl)Q_l}}{\eta_{y(pl)+Q_l}}, \tag{189}$$

where

$$\eta_x = \frac{2.61}{1 + 1.11\sigma_1^{12/5}}, \tag{190}$$

$$\eta_y = 3\left(1 + 0.69\sigma_1^{12/5}\right). \tag{191}$$

In (190) and (191) the Rytov variance, σ_1^2, is that for a plane wave along a slant path given by[2]

$$\sigma_1^2 = 2.25k^{7/6}\left(H - h_0\right)^{5/6}\sec\left(\zeta\right)\int_{h_0}^{H} C_n^2\left(h\right)\xi^{5/6}dh. \tag{192}$$

Figure 19 details results for the temporal frequency spread, σ_f, of a plane wave for both uplink and downlink paths for a fixed target altitude as a function of zenith angle, ζ. The software package *Maple* was used to numerically evaluate the remaining integrals in expressions (185), (187) and (188). For convenience, a nominal value of $v = 3\ m/s$ has been assumed. It is seen in figure 19 that for zenith angles less than about 50^o the temporal frequency spread is almost constant for both the uplink and donwlink scenarios and the standard and modified Rytov methods predict frequency spread values that are approximately equal. This is expected because for these angles the majority of the propagation path lies in the upper atmosphere where the value of C_n^2

decreases rapidly corresponding to weak turbulence conditions. However, the two methods predict different results, particularly for the uplink case, as the zenith angle increases beyond 50^o as the propagation path becomes nearly horizontal and strong turbulence conditions arise.

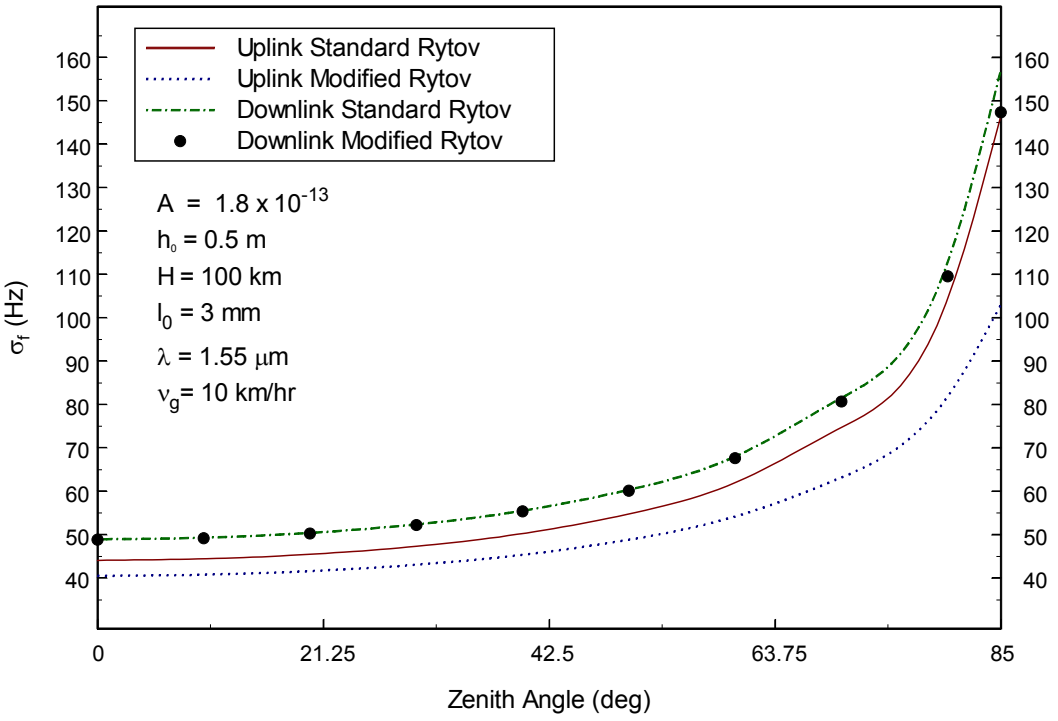

Figure 19 Plane wave slant path temporal frequency spread as a function of zenith angle, ζ. The uplink/downlink standard Rytov curves are given by (185). The uplink/downlink modified Rytov curves are given by (186).

In figure 20, the slant path plane wave frequency spread is plotted as a function of the target altitude, H, for a fixed zenith angle of $\zeta = 85^o$. This is effectively a plot of the frequency spread as a function of propagation path length and represents the worst case scenario for a communication system because the high zenith angle corresponds to a situation where the optical signal propagates a great distance through the Earth's atmosphere at low altitudes where degradation of the optical signal is most severe. Comparing figure 20 to figure 13 indicates that for large zenith angles, the results are nearly the same as for a horizontal path as is expected.

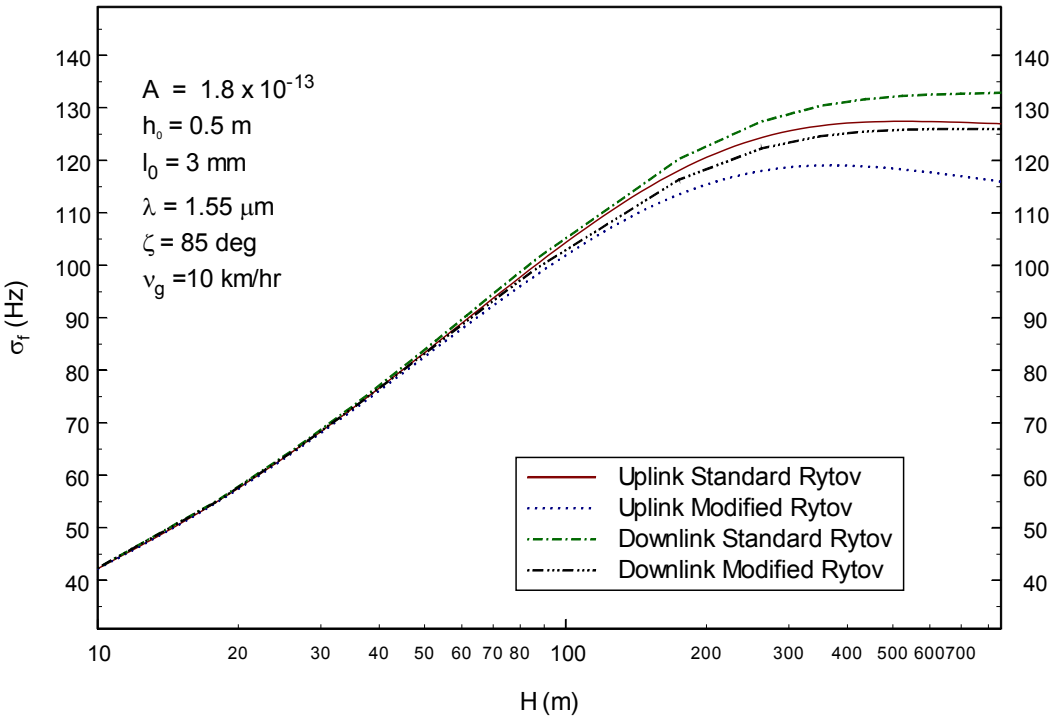

Figure 20 Plane wave slant path temporal frequency spread as a function of altitude, H. The uplink/downlink standard Rytov curves are given by (185). The uplink/downlink modified Rytov curves are given by (186).

8.4 Spherical wave

A similar analysis of the slant path frequency spread can be conducted for a transmitted spherical wave. The standard Rytov method is considered first. The Hill spectral model, (151), and the H-V refractive index structure parameter model for C_n^2, (179), are substituted into the integral definition of the spherical wave frequency variance, (171). Completing the integration on κ, the resulting integral expression for the slant path spherical wave frequency variance is[28]

$$\begin{aligned}\sigma^2_{f,sp,SR} &= 0.0317\kappa_l^{1/3}k^2V^2\sec(\zeta)\times\int_{h_0}^{H}C_n^2(h)\\ &\quad\times\Big[1+0.723\,{}_2F_1\left(\tfrac{1}{12},\tfrac{7}{12};\tfrac{1}{2};-Q_l^2\xi^2(1-\xi)^2\right)\\ &\quad+0.317\,{}_2F_1\left(\tfrac{1}{3},\tfrac{5}{6};\tfrac{1}{2};-Q_l^2\xi^2(1-\xi)^2\right)\\ &\quad-0.04\,{}_2F_1\left(\tfrac{3}{8},\tfrac{7}{8};\tfrac{1}{2};-Q_l^2\xi^2(1-\xi)^2\right)dh\Big],\end{aligned}\tag{193}$$

where either (183) or (184) can be used for ξ because this result is a function of $\xi^2(1-\xi)^2$ which will have an identical dependency on the integration parameter, h, regardless of which form of ξ is applied. This indicates that (193) will yield identical results for both uplink and downlink paths. Because it was derived using the standard Rytov method, equation (193) is expected to be valid in weak turbulence only.

Slant path spherical wave temporal frequency spread results using the modified Rytov method are developed in the same manner as in the plane wave case. The effective Hill spectral model, (67), with $f(\kappa l_0)$ given by (158) and $g(\kappa L_0)=1$, and the H-V model are substituted into

the integral definition of the spherical wave frequency variance, (171). Completing the integration on κ, the slant path spherical wave frequency variance is given by the sum of a large and small scale component[28]

$$\sigma^2_{f,sp,MR} = \sigma^2_{f,x} + \sigma^2_{f,y}, \tag{194}$$

where

$$\begin{aligned}
\sigma^2_{f,x} &= 0.0317\alpha_x^{1/6}k^2V^2\sec(\zeta) \times \int_{h_0}^{H} C_n^2(h) \\
&\times \left[1 + 0.723\ {}_2F_1\left(\tfrac{1}{12}, \tfrac{7}{12}; \tfrac{1}{2}; -\alpha_x^2\xi^2(1-\xi)^2\right)\right. \\
&\left. +0.317\ {}_2F_1\left(\tfrac{1}{3}, \tfrac{5}{6}; \tfrac{1}{2}; -\alpha_x^2\xi^2(1-\xi)^2\right) - 0.04\ {}_2F_1\left(\tfrac{3}{8}, \tfrac{7}{8}; \tfrac{1}{2}; -\alpha_x^2\xi^2(1-\xi)^2\right) dh\right],
\end{aligned} \tag{195}$$

$$\begin{aligned}
\sigma^2_{f,y} &= \sigma^2_{f,sp,SR} - 0.0317\alpha_y^{1/6}k^2V^2\sec(\zeta) \times \int_{h_0}^{H} C_n^2(h) \\
&\times \left[1 + 0.723\ {}_2F_1\left(\tfrac{1}{12}, \tfrac{7}{12}; \tfrac{1}{2}; -\alpha_y^2\xi^2(1-\xi)^2\right)\right. \\
&\left. +0.317\ {}_2F_1\left(\tfrac{1}{3}, \tfrac{5}{6}; \tfrac{1}{2}; -\alpha_y^2\xi^2(1-\xi)^2\right) - 0.04\ {}_2F_1\left(\tfrac{3}{8}, \tfrac{7}{8}; \tfrac{1}{2}; -\alpha_y^2\xi^2(1-\xi)^2\right) dh\right].
\end{aligned} \tag{196}$$

In (196), $\sigma^2_{f,sp,SR}$ is that along a slant path given by (193). The parameters α_x and α_y again incorporate an altitude dependency and are given by

$$\eta_{x(sp)} = \frac{L\kappa_x^2}{k},\ \alpha_x = \frac{\eta_{x(sp)Q_l}}{\eta_{x(sp)+Q_l}},\ \eta_{y(sp)} = \frac{L\kappa_y^2}{k},\ \alpha_y = \frac{\eta_{y(sp)Q_l}}{\eta_{y(sp)+Q_l}}, \tag{197}$$

where

$$\eta_x = \frac{8.56}{1 + 0.19\sigma_1^{12/5}}, \tag{198}$$

$$\eta_y = 9\left(1 + 0.23\sigma_1^{12/5}\right). \tag{199}$$

In (198) and (199), the Rytov variance, σ_1^2, is that along a slant path given by (192).

We now examine the slant path temporal frequency spread, σ_f, of a spherical wave for both uplink and downlink paths. Figure 21 presents the data for a fixed target altitude as a function of zenith angle, ζ. Again a nominal value of $v = 3\ m/s$ has been used. As previously noted the frequency variance given by the standard Rytov method, (193), yields identical results for uplink and downlink due to the functional dependency on ξ. However, the modified Rytov method model, (194), yields numerically different values for uplink and downlink because the the values of the nondimensional frequency cutoff parameters, η_x and η_y, are dependent on the slant path Rytov variance, (192), which has different values for uplink and downlink. It is seen in figure 21 that for zenith angles less than about 50^o the frequency spread is almost constant for both uplink and donwlink, as was the case for plane waves. Additionally the numerical values are approximately equal to the values obtained in the plane wave case. This is expected given the analysis of the

horizontal path frequency spread where it was also observed that the plane and spherical wave cases were approximately equal.

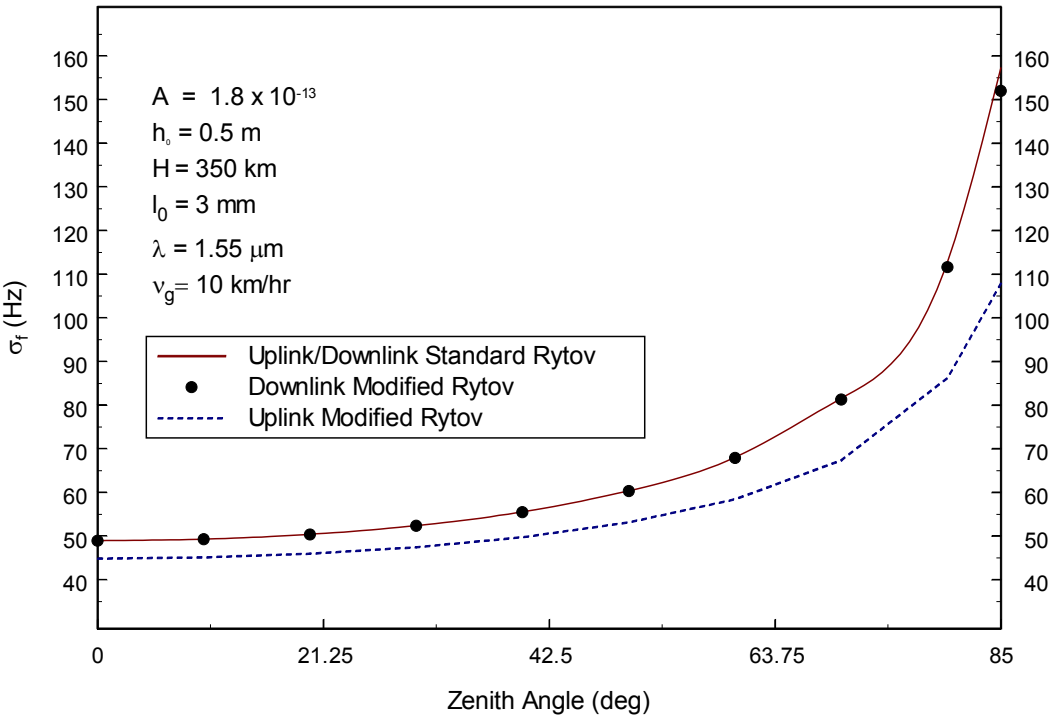

Figure 21 Spherical wave slant path temporal frequency spread as a function of zenith angle, ζ. The uplink/downlink standard Rytov curve is given by (193). The uplink/downlink modified Rytov curves are given by (194).

In figure 22, the slant path spherical wave frequency spread is plotted as a function of the target altitude for a fixed zenith angle of $\zeta = 85^o$ It is seen that the behavior of the results is the same as the plane wave case.

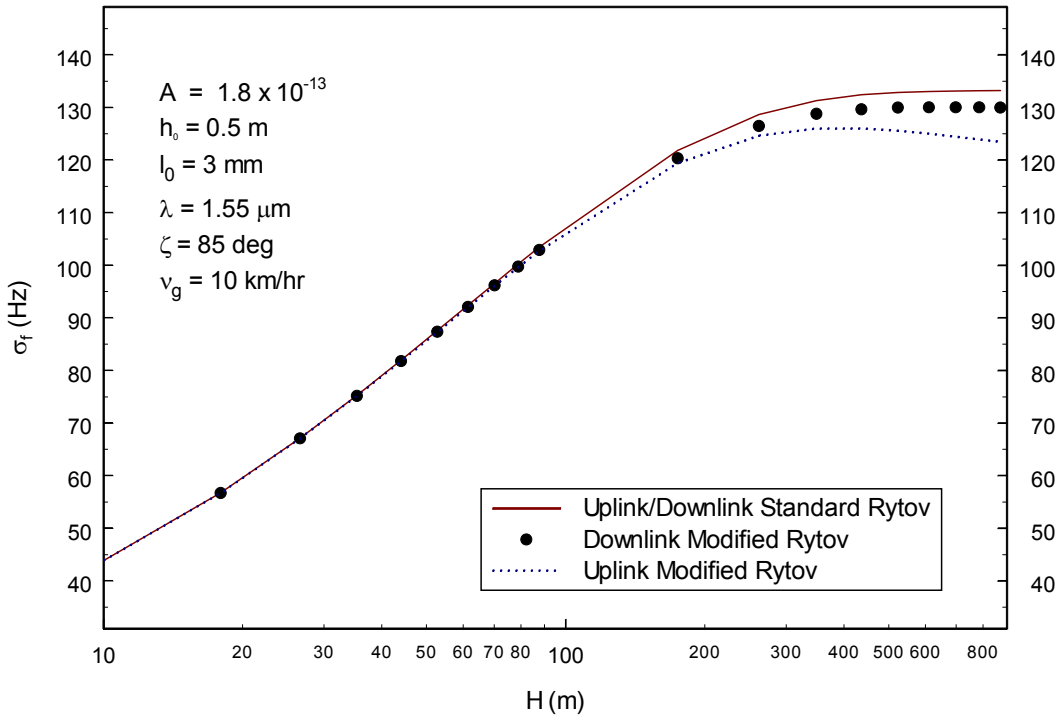

Figure 22 Spherical wave slant path temporal frequency spread as a function of altitude, H. The uplink/downlink standard Rytov curve is given by (193). The uplink/downlink modified Rytov curves are given by (194).

It should be noted that the decrease in the frequency spread observed in figures 20 and 22 at higher altitudes for the modified Rytov method expressions (186) and (194) is most likely non-physical. Rather, it is expected that the results should level off in the manner of the expressions for the horizontal path case, (159) and (173). The observed decrease is most likely a result of the fact that the nondimensional parameters, η_x and η_y, used in the slant path modeling do not include the effects of a finite inner scale. Parameters including a finite inner scale were used for the horizontal path development and no such decrease was noted. However, for a slant path, these parameters would require integral expressions for the scintillation index of a plane or spherical wave along a slant path using the Hill spectrum and we are not aware, at this time, of such expressions.

Finally, slant path spherical wave frequency spread values in *Hz* are provided for fixed path lengths in table 1. The standard Rytov method results are used, so that the values correspond to both uplink and downlink scenarios (spherical wave only). Table 1 represents the worst-case scenario for an optical communication system where the ground level index of refraction structure parameter is $A = C_n^2(0) = 10^{-12}$, corresponding to very strong atmospheric turbulence. The receiver altitude, H, is allowed to vary depending on ζ, $v_g = 10\ km/hr$, and $\lambda = 1.55\ \mu m$. The values in table 1 are derived from equation (193) for zenith angles, $\zeta < 90^o$. Values for horizontal paths, $\zeta = 90^o$, are derived from the horizontal path expression, (172).

Table 1 Spherical wave slant path temporal frequency spread (Hz).

Zenith Angle (deg)	*90*	*60*	*30*	*0*
Path Length (km)	Frequency Spread, σ_f			
1	241	136	105	99
10	724	137	107	100
100	N/A	140	108	101
1000	N/A	141	109	102

9. DOUBLE PASS WAVE STRUCTURE FUNCTION

9.1 Introduction

Recently, there has been increased interest in using laser radar, or lidar, systems to augment conventional microwave radar systems. Lidar systems offer certain advantages over their microwave counterparts, such as reduced size and power requirements and more secure channels. However, there are many challenges associated with the development and implementation of lidar systems due to the random fluctuations in phase and amplitude of the optical signal propagating through the Earth's atmosphere. As compared to one-way propagation systems, such as laser communications, these atmospheric effects are further complicated in a lidar system. In particular, the reflected wave often traverses a medium that is statistically correlated with the medium traversed by the incident wave. Additionally, the effects of reflection from a target must be considered. Thus, to effectively design a lidar system, it is useful to develop analytic models describing the atmospheric effects on the propagating signal that incorporate the target characteristics and the channel statistical correlation effects. Furthermore, any real world lidar system is likely to operate under conditions of moderate to strong irradiance fluctuations, that is moderate to strong optical turbulence. Thus, for any analytic model to be of practical value, it must accurately model the atmospheric turbulence induced effects in the moderate to strong optical turbulence regimes.

This chapter details the development of analytic wave structure function expressions for the horizontal double pass scenario for reflection from a smooth target, i.e. a plane mirror or a retroreflector. Expressions are given for point and finite size targets. It has been shown

previously[2] that in the Rytov approximation the horizontal double pass wave structure function reduces analytically to the one-way horizontal path *spherical* wave structure function for incident plane, spherical and Gaussian-beam waves for the point target case. However, in the finite target case the double pass wave structure function is dependent on the incident wave type. Hence, the finite target case is considered only for incident spherical waves. Comparisons are presented between the standard and modified Rytov approximation results. Further comparisons are presented between the coherence radius obtained from the wave structure functions and the strong turbulence asymptotic coherence radius results given by Banakh and Mironov.[29]

9.2 Integral definitions

In order to develop models describing the wave structure function associated with the double pass problem, it is necessary to incorporate the effects of reflection from a target and the statistical correlation effects associated with the double pass propagation of the optical wave. In the double pass problem, the reflected wave may or may not pass through a medium that is statistically correlated with the medium traversed by the incident wave. When the incident and reflected wave travel through statistically dependent atmospheric turbulence, enhanced backscatter effects may be observed. Thus, two cases must be considered. In the work that follows, the propagation channel is considered *bistatic* when the incident wave and reflected wave propagate through statistically independent atmospheric turbulence. The propagation channel is considered *monostatic* when the incident wave and reflected wave propagate through statistically dependent atmospheric turbulence. Additionally, it is useful to classify the target as a point, unbounded or

finite target. The target size is classified by its relation to the first Fresnel zone, $\sqrt{L/k}$, through the Fresnel-target ratio Ω_R given by

$$\Omega_R = \frac{2L}{kW_R^2} \tag{200}$$

where W_R is the reflector radius. The target is considered to be a point target when $\Omega_R \gg 1$, an unbounded target when $\Omega_R \ll 1$, and a finite target otherwise.

The statistical moments of the optical field encountered in the double pass problem after reflection from a smooth target can be derived from the spectral representations of the complex phase perturbations encountered in this scenario. This approach is well documented by Andrews and Phillips.[2] The spectral representations of the complex phase perturbations arising from propagation in the atmosphere are derived using ABCD ray matrices that incorporate the effects of reflection from a smooth target. Additionally, Andrews and Phillips[2] have used this ABCD ray matrix approach to account for the enhanced backscatter effects. Given the spectral representations of the complex phase perturbations, one can then develop expressions for various statistical quantities of the optical field by considering the appropriate ensemble averages.

In the special cases of a point target and an unbounded target, the integral definitions of the wave structure function can be greatly simplified. Andrews and Phillips showed that, applying the Rytov approximation method, the double pass wave structure function for a point target is defined by[2]

$$D_{point}(\rho, L) = 8\pi^2 k^2 L \int_0^1 \int_0^\infty \kappa \Phi_n(\kappa) \left[1 - J_0(\kappa\xi\rho)\right] d\kappa d\xi \tag{201}$$

This expression is valid for incident plane, spherical and Gaussian-beam waves in both monostatic and bistatic channels. We point out that (201) is equivalent to the one-way horizontal path spherical wave structure function, (90).

When the target is finite, the wave structure function is explicitly dependent on the position of the points in the observation plane. That is, if $\mathbf{r}_1$ and $\mathbf{r}_2$ are any two points in the observation plane, the wave structure function is a function of $\mathbf{r}_1$ and $\mathbf{r}_2$. However, in the special case when the observation points are symmetrically located about the optical axis, i.e. $\mathbf{r}_1 = -\mathbf{r}_2$, the wave structure function is dependent only on the separation distance of the two points, $\rho = |\mathbf{r}_2 - \mathbf{r}_1|$. It can be shown that, for observation points symmetrically located about the optical axis, applying the Rytov approximation, the finite target double pass wave structure function is defined by[2]

$$D_{finite}(\rho, 2L) = \Delta^i(\rho, L) + \Delta^R(\rho, L) \pm \mathrm{Re}\left[\Delta^{iR}(\rho, L)\right] \tag{202}$$

where L is the one-way distance from the transmitter to the target, i denotes the incident term, R denotes the reflected term, and iR denotes the correlation term arising in a monostatic channel. The upper plus sign in (202) is used for a plane mirror and the lower minus sign is used for a retroreflector. In the bistatic case, the correlation term, $\Delta^{iR}(\rho, L)$, in (202), is taken to be zero. When the incident wave is a spherical wave, the three terms appearing in (202) are defined by[2]

$$\begin{aligned}\Delta^i(\rho, L) &= 8\pi^2 k^2 L \int_0^1 \int_0^\infty \kappa \Phi_n(\kappa) \exp\left(-\frac{\Lambda_2 L \kappa^2 \xi^2}{k}\right) \\ &\quad \left[I_0(\Lambda_2 \kappa \xi \rho) - J_0(\Theta_2 \kappa \xi \rho)\right] d\kappa d\xi,\end{aligned} \tag{203}$$

$$\Delta^R(\rho, L) = 8\pi^2 k^2 L \int_0^1 \int_0^\infty \kappa \Phi_n(\kappa) \exp\left(-\frac{\Lambda_2 L \kappa^2 \xi^2}{k}\right) \times \left\{ I_0(\Lambda_2 \kappa \xi \rho) - J_0\left[\left(1 - \bar{\Theta}_2 \xi\right) \kappa \rho\right] \right\} d\kappa d\xi, \quad (204)$$

$$\Delta^{iR}(\rho, L) = 8\pi^2 k^2 L \int_0^1 \int_0^\infty \kappa \Phi_n(\kappa) \exp\left(-\frac{\Lambda_2 L \kappa^2 \xi^2}{k}\right) \left\{ J_0\left[(1 - \xi + 2j\Lambda_2 \xi)\frac{\kappa\rho}{2}\right] + J_0\left[(1 - \xi - 2j\Lambda_2 \xi)\frac{\kappa\rho}{2}\right] - 2J_0\left[(1 - \xi + 2\Theta_2 \xi)\frac{\kappa\rho}{2}\right] \right\} d\kappa d\xi, \quad (205)$$

where $j = \sqrt{-1}$ and $I_0(x)$ is the zeroth order modified Bessel function of the first kind. The nondimensional parameters Λ_2, Θ_2, and $\bar{\Theta}_2$ are beam parameters characterizing the reflected wave. Assuming the incident wave is a spherical wave, these beam parameters are defined by[2]

$$\Lambda_2 = \frac{\Omega_R}{4 + \Omega_R^2}, \ \Theta_2 = \frac{2}{4 + \Omega_R^2}, \ \bar{\Theta}_2 = 1 - \Theta_2. \quad (206)$$

9.3 Point target

In the special case when the target radius is much smaller than the first Fresnel zone size, that is, when $\Omega_R \gg 1$, the target can be treated as a point target. In this case, the double pass horizontal path wave structure function is given by (201). As previously stated, this is equivalent to the one-way horizontal path spherical wave structure function for a wave propagating over a path length of L. This expression is valid for an incident plane, spherical or Gaussian-beam wave for both a bistatic and monostatic channel.

We can derive an analytic expression for the wave structure function using the standard Rytov approximation by using the Tatarskii spectrum, (25). It is necessary to include a finite inner scale in the spectral model to allow for convergence of the integrals. However, the dependence of the wave structure function on the inner scale is removed after integration by assuming appropriate restrictions on ρ. In this work, we ignore the finite inner and outer scale effects as we are seeking only the basic behavior of the wave structure function. Substituting the Tatarskii spectrum, (25), into the integral definition of the point target wave structure function expression, (201), evaluating the integrals, and then removing the inner scale effects, the resulting expression is[2]

$$D_{point}^{SR}(\rho, 2L) = 1.093 C_n^2 k^2 L \rho^{5/3}, \qquad l_0 \ll \rho \ll L_0, \tag{207}$$

where L is the one-way distance from the transmitter to the target. This is the previously describe five-thirds power law expression for the one-way spherical wave structure function, (91). The "SR" superscript is used to denote that this expression is obtained from the standard Rytov approximation.

To obtain a wave structure function expression using the modified Rytov method, we allow $f(\kappa l_0) = \exp\left(-\frac{\kappa^2}{\kappa_m^2}\right)$ and $g(\kappa L_0) = 1$ in the effective atmospheric spectrum, (67). This is equivalent to using an effective Tatarskii spectrum. It was shown in the chapter on the one-way horizontal path wave structure function, that upon substitution of (67) into the integral definition of the wave structure function, (201), after evaluation of the integrals and allowing the inner scale

to go to zero, the resulting wave structure function expression is given by

$$D_{point}^{MR}(\rho, 2L) = D_x(\rho, L) + D_y(\rho, L), \qquad l_0 \ll \rho \ll L_0, \tag{208}$$

where the "*MR*" superscript denotes that this expression is for the modified Rytov method and D_x and D_y are approximately given by (98) and (99). The nondimensional parameters $\eta_{x(sp)}$ and $\eta_{y(sp)}$ incorporate the large and small scale frequency cutoffs for a spherical wave, $\kappa_{x(sp)}$ and $\kappa_{y(sp)}$, and are given by (100) and (101). The comparison of the double pass point target wave structure function expressions, (207) and (208), is equivalent to the comparison of the one-way horizontal path spherical wave structure functions given in figure 7.

9.4 Finite target

When the target radius is on the order of the first Fresnel zone, that is when Ω_R is close to one, then the full integral expression for the double pass wave structure function, (202), must be evaluated. Recall that the integral definition of the finite target double pass wave structure function given by (202) assumes that the incident, or transmitted, wave is spherical. We can obtain an analytic expression using the standard Rytov approximation for the finite target case in the same manner as for the point target case. As was the case for the one-way horizontal path Gaussian-beam wave structure function, it is mathematically sufficient in the double pass finite target case to use the Kolmogorov spectrum and still have convergence of the integrals. The reason for this is that the exponential function in equations (203)-(205) allows for convergence of the integrals. Substituting the Kolmogorov spectrum, (24), into the three equations (203)-(205)

defining the finite target double pass wave structure function and evaluating yields[2]

$$D_{finite}^{SR}(\rho, 2L) = 1.093 C_n^2 k^{7/6} L^{11/6} \left\{ \left[|\Theta_2|^{5/3} + a_2 \pm \left(\frac{1}{2}\right)^{5/3} (a_3 - a_4) \right] \left(\frac{k\rho^2}{L}\right)^{5/6} + 1.236 \Lambda_2^{11/6} \left(\frac{k\rho^2}{L}\right) \right\}, \tag{209}$$

where L is the one-way distance from the transmitter to the target, Θ_2 and Λ_2 are given by (206), and

$$a_2 = \begin{cases} \dfrac{1 - \Theta_2^{8/3}}{1 - \Theta_2}, & \Theta_2 \geq 0, \\ \dfrac{1 + |\Theta_2|^{8/3}}{1 - \Theta_2}, & \Theta_2 < 0, \end{cases} \tag{210}$$

$$a_3 = \begin{cases} \dfrac{1 - (2\Theta_2)^{8/3}}{1 - 2\Theta_2}, & \Theta_2 \geq 0, \\ \dfrac{1 + |2\Theta_2|^{8/3}}{1 - 2\Theta_2}, & \Theta_2 < 0, \end{cases} \tag{211}$$

$$a_4 = \frac{1}{1 + 4\Lambda_2^2} - \frac{(2\Lambda_2)^{8/3}}{\left(1 + 4\Lambda_2^2\right)^{1/2}} \cos\left[\tan^{-1}(2\Lambda_2) + \frac{4\pi}{3} \right]. \tag{212}$$

The wave structure function given by (209) is for the monostatic case. The upper plus sign is used for a plane mirror target and the lower minus sign is used for a retroreflector target. In the bistatic case, the terms a_3 and a_4 are both identically zero. Thus, we see that, in the bistatic case, the wave structure function for a plane mirror and retroreflector target are identical.

As in the case of a point target, we can develop expressions for the finite target wave structure function using the modified Rytov method by substituting the effective Kolmogorov spectrum,

(67), where we let $f(\kappa l_0) = 1$ and $g(\kappa L_0) = 1$, into each of the three integral equations defining the wave structure function, (203)-(205) and evaluating. For the sake of clarity, the evaluation of these integrals is presented in Appendix G. The resulting finite target wave structure function for the modified Rytov approximation is given by[30]

$$\begin{aligned} D_{finite}^{MR}(\rho, 2L) &= \Delta_x^i(\rho, L) + \Delta_y^i(\rho, L) + \Delta_x^R(\rho, L) + \Delta_y^R(\rho, L) \\ &\quad \pm \mathrm{Re}\left[\Delta_x^{iR}(\rho, L) + \Delta_y^{iR}(\rho, L)\right]. \end{aligned} \tag{213}$$

The terms in (213) are defined by[30]

$$\begin{aligned} \Delta_x^i(\rho, L) &= 0.49\sigma_1^2 \eta_{x(gb)}^{1/6} \left(\frac{k\rho^2}{L}\right) \left\{ \Lambda_2^2 \left[1 + 0.547\eta_{x(gb)}\Lambda_2\right]^{-1/6} \right. \\ &\quad \left. + \Theta_2^2 \left[1 + 0.033\left(\frac{\Theta_2^2 k\rho^2 \eta_{x(gb)}}{L}\right)\right]^{-1/6} \right\}, \end{aligned} \tag{214}$$

$$\begin{aligned} \Delta_y^i(\rho, L) &= 0.89\sigma_1^2 \left\{ |\Theta_2|^{5/3} \left(\frac{k\rho^2}{L}\right)^{5/6} + 0.622\Lambda_2^{11/6} \left(\frac{k\rho^2}{L}\right) \right\} \\ &\quad - 0.49\sigma_1^2 \eta_{y(gb)}^{1/6} \left(\frac{k\rho^2}{L}\right) \left\{ \Lambda_2^2 \left[1 + 0.547\eta_{y(gb)}\Lambda_2\right]^{-1/6} \right. \\ &\quad \left. + \Theta_2^2 \left[1 + 0.033\left(\frac{\Theta_2^2 k\rho^2 \eta_{y(gb)}}{L}\right)\right]^{-1/6} \right\}, \end{aligned} \tag{215}$$

$$\begin{aligned}\Delta_x^R(\rho,L) &= 0.49\sigma_1^2\eta_{x(gb)}^{1/6}\left(\frac{k\rho^2}{L}\right)\left\{\Lambda_2^2\left[1+0.547\eta_{x(gb)}\Lambda_2\right]^{-1/6}\right.\\ &\quad+\frac{1}{\bar{\Theta}_2}\left(1+0.033\frac{k\rho^2\eta_{x(gb)}}{L}\right)^{-1/6}\\ &\quad\left.-\frac{\Theta_2^3}{\bar{\Theta}_2}\left(1+0.033\frac{k\rho^2\Theta_2^2\eta_{x(gb)}}{L}\right)^{-1/6}\right\},\end{aligned} \tag{216}$$

$$\begin{aligned}\Delta_y^R(\rho,L) &= 0.89\sigma_1^2\left\{0.622\Lambda_2^{11/6}\left(\frac{k\rho^2}{L}\right)+a_2\left(\frac{k\rho^2}{L}\right)^{5/6}\right\}\\ &\quad-0.49\sigma_1^2\eta_{y(gb)}^{1/6}\left(\frac{k\rho^2}{L}\right)\left\{\Lambda_2^2\left[1+0.547\eta_{y(gb)}\Lambda_2\right]^{-1/6}\right.\\ &\quad+\frac{1}{\bar{\Theta}_2}\left(1+0.033\frac{k\rho^2\eta_{y(gb)}}{L}\right)^{-1/6}\\ &\quad\left.-\frac{\Theta_2^3}{\bar{\Theta}_2}\left(1+0.033\frac{k\rho^2\Theta_2^2\eta_{y(gb)}}{L}\right)^{-1/6}\right\},\end{aligned} \tag{217}$$

$$\begin{aligned}\mathrm{Re}\left[\Delta_x^{iR}(\rho,L)\right] &= 14.15\sigma_1^2\eta_{x(gb)}^{-5/6}\left[1+(c_1)\,{}_2F_2\left(-\tfrac{5}{6},\tfrac{1}{2};1,\tfrac{3}{2};-\tfrac{k\rho^2\eta_{x(gb)}}{16L}\right)\right.\\ &\quad-(c_2)\,{}_2F_2\left(-\tfrac{5}{6},\tfrac{1}{2};1,\tfrac{3}{2};\tfrac{k\rho^2\Lambda_2^2\eta_{x(gb)}}{4L}\right)\\ &\quad\left.-(c_3)\,{}_2F_2\left(-\tfrac{5}{6},\tfrac{1}{2};1,\tfrac{3}{2};-\tfrac{k\rho^2\Theta_2^2\eta_{x(gb)}}{4L}\right)\right],\end{aligned} \tag{218}$$

$$\begin{aligned}\mathrm{Re}\left[\Delta_y^{iR}(\rho,L)\right] &= 0.89\sigma_1^2\left(\frac{1}{2}\right)^{5/3}\left(\frac{k\rho^2}{L}\right)^{5/6}(a_3-a_4)\\ &\quad -14.15\sigma_1^2\eta_{y(gb)}^{-5/6}\left[1+(c_1)\,{}_2F_2\left(-\tfrac{5}{6},\tfrac{1}{2};1,\tfrac{3}{2};-\tfrac{k\rho^2\eta_{y(gb)}}{16L}\right)\right.\\ &\quad -(c_2)\,{}_2F_2\left(-\tfrac{5}{6},\tfrac{1}{2};1,\tfrac{3}{2};\tfrac{k\rho^2\Lambda_2^2\eta_{y(gb)}}{4L}\right)\\ &\quad \left.-(c_3)\,{}_2F_2\left(-\tfrac{5}{6},\tfrac{1}{2};1,\tfrac{3}{2};-\tfrac{k\rho^2\Theta_2^2\eta_{y(gb)}}{4L}\right)\right].\end{aligned} \tag{219}$$

The parameters a_2 through a_4 are given by (210)-(212), ${}_2F_2(x)$ is a generalized hypergeometric function and

$$c_1 = \frac{1}{1-2\Theta_2} - \frac{1}{1+4\Lambda_2^2}, \tag{220}$$

$$c_2 = \frac{4\Lambda_2^2}{1+4\Lambda_2^2}, \tag{221}$$

$$c_3 = \frac{1}{1-2\Theta_2}. \tag{222}$$

Finally, we address the use of the Gaussian-beam wave frequency cutoffs, $\kappa_{x(gb)}$ and $\kappa_{y(gb)}$, in (214)-(219). Unlike the point target case where the reflected wave is spherical, the reflected wave in the finite target case is like a Gaussian-beam wave, thus, it is necessary to use the Gaussian-beam frequency cutoffs. The nondimensional parameters $\eta_{x(gb)}$ and $\eta_{y(gb)}$ are of the same form as those used in the one-way horizontal path Gaussian-beam wave structure function and are given by

$$\eta_{x(gb)} = \frac{L\kappa_{x(gb)}^2}{k} = \left(\frac{1}{3}-\frac{1}{2}\bar{\Theta}_2+\frac{1}{5}\bar{\Theta}_2^2\right)^{-6/7}\left(\frac{\sigma_1^2}{\sigma_B^2}\right)^{-6/7}\left[1+0.56\left(\sigma_B^2\right)^{6/5}\right]^{-1}, \tag{223}$$

$$\eta_{y(gb)} = \frac{L\kappa_{y(gb)}^2}{k} = 3\left(\frac{\sigma_1^2}{\sigma_B^2}\right)^{6/5} + 2.07\left(\sigma_1^2\right)^{6/5}, \tag{224}$$

where

$$\sigma_B^2 = 3.86\sigma_1^2 \left\{ 0.4 \left[(1+2\Theta_2)^2 + 4\Lambda_2^2 \right]^{5/12} \cos\left[\frac{5}{6} \tan^{-1}\left(\frac{1+2\Theta_2}{2\Lambda_2} \right) \right] - \frac{11}{16}\Lambda_2^{5/6} \right\}. \quad (225)$$

We now compare the results of the two finite target wave structure function expressions, (209) and (213). In figure 23, the results are presented as a function of increasing turbulence strength for the bistatic scenario. The propagation path length, L, is held constant while the index of refraction structure parameter, C_n^2, is allowed to vary. Varying the Rytov variance, i.e. the turbulence strength, in this manner allows Ω_R to be held constant without changing the target radius. Recall, that in the bistatic scenario the wave structure function is the same for both a plane mirror and a retroreflector, so the curves presented in figure 23 are valid for both target types. The comparative behavior is the same as for that of the point target case. The standard and modified Rytov methods agree in the weak turbulence regime. However, in the moderate to strong turbulence regime, the modified Rytov method predicts values smaller than those of the standard Rytov method.

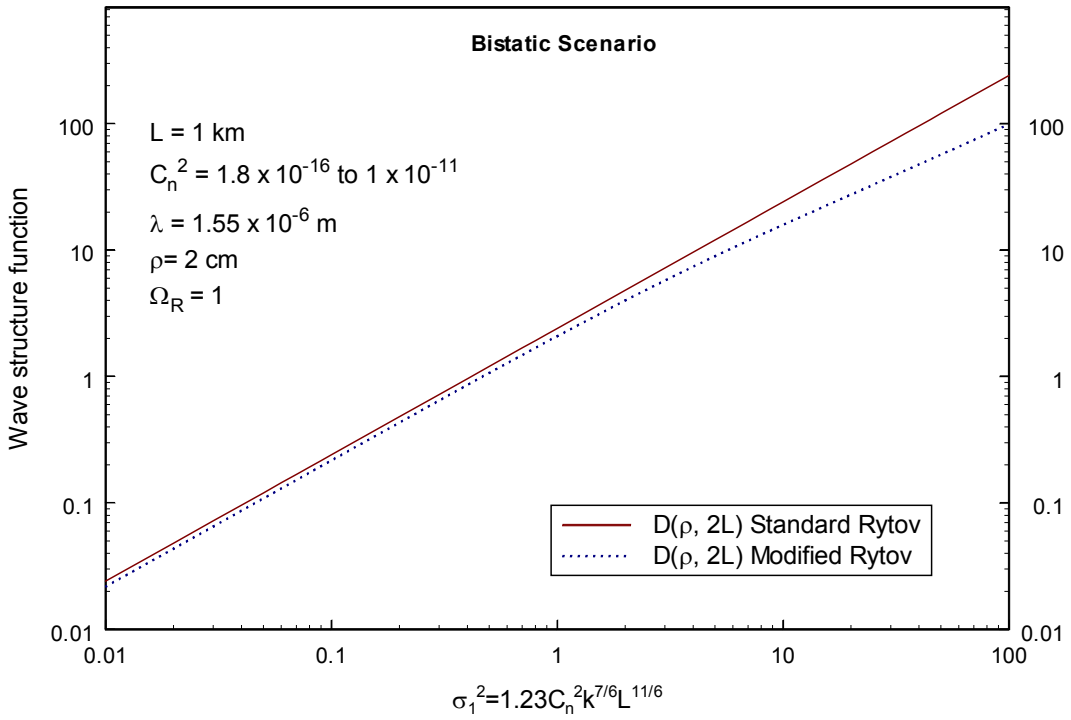

Figure 23 The finite target double pass wave structure function as a function of increasing turbulence strength for a bistatic scenario. The standard Rytov curve is given by (209). The modified Rytov curve is given by (213). The Rytov variance is increased by allowing C_n^2 to vary while L is held constant.

In figure 24, the wave structure function results are compared as a function of increasing turbulence for a monostatic scenario for both a plane mirror target and a retroreflector target. The qualitative behavior is the same as that observed in the bistatic scenario. We see that the retroreflector target produces wave structure function values that are less than the plane mirror target. This is a result of the effects of the statistical correlation term in the wave structure function. Essentially, there are two types of statistical correlations that arise in monostatic propagation channels as explained in detail by Andrews *et al.*[7] The two types of correlations can be explained by considering the optical wave in terms of ray optics. The first type of correlation arises from a "folded path" geometry in which the ray travels along the exact same path in both the incident and reflected directions. The second type of correlation arises when two rays travel along a "reciprocal path" geometry in which the rays do not travel along the exact same path in both directions but the reflected rays do travel back along each other's incident path. As stated in [7], the folded path geometry creates a negative correlation that causes a decrease in the mean irradiance, while the reciprocal path geometry creates a positive correlation that causes an increase in the mean irradiance. Andrews and Phillips[2] showed that the wave structure function is independent of the reciprocal path terms. Thus, no positive correlation exists for the wave structure function and it appears that the retroreflector case yields "less" folded paths than the plane mirror, resulting in an overall decrease in the wave structure function as compared to the plane mirror case.

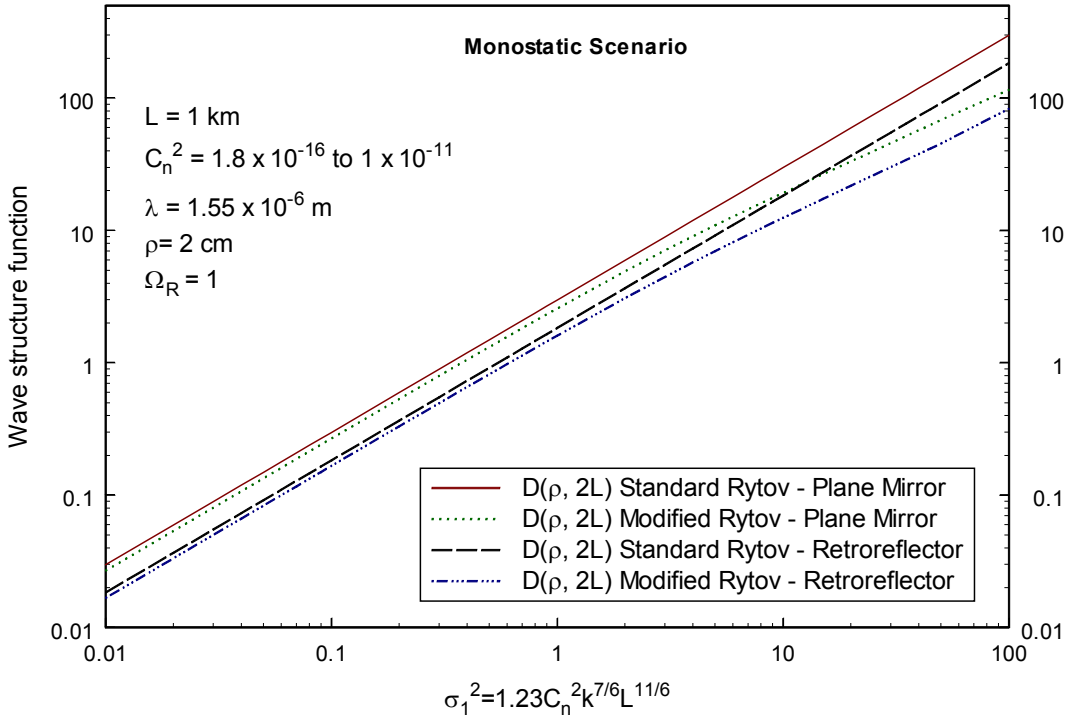

Figure 24 The finite target double pass wave structure function as a function of increasing turbulence strength for a monostatic scenario. The standard Rytov curves are given by (209). The modified Rytov curves are given by (213). The Rytov variance is increased by allowing C_n^2 to vary while L is held constant.

Finally, in figure 25, we compare the finite target wave structure function of the standard Rytov method to that of the modified Rytov method as a function of target radius, i.e. as a function of Ω_R, in the weak turbulence regime, $\sigma_1^2 = 0.1$. In the weak turbulence regime, we expect the two results to agree for all target sizes. This is important because it is believed that the standard Rytov method is valid in the weak turbulence regime. We see in figure 25 that there is very little numerical difference between the two methods in the weak turbulence regime and that their qualitative behavior is identical. Further, we see that as Ω_R increases the plane mirror and retroreflector curves approach the same limiting value. This result is expected because, for large values of Ω_R, the target is like a point target, where the value of the wave structure function is independent of the target type and the channel type. Although we have not presented specific expressions for an unbounded target, that is where Ω_R approaches zero, we can infer from figure 25 that, unlike the point target, an expression for the unbounded target case will depend on the target type as the plane mirror and retroreflector curves do not approach the same limiting value as Ω_R decreases.

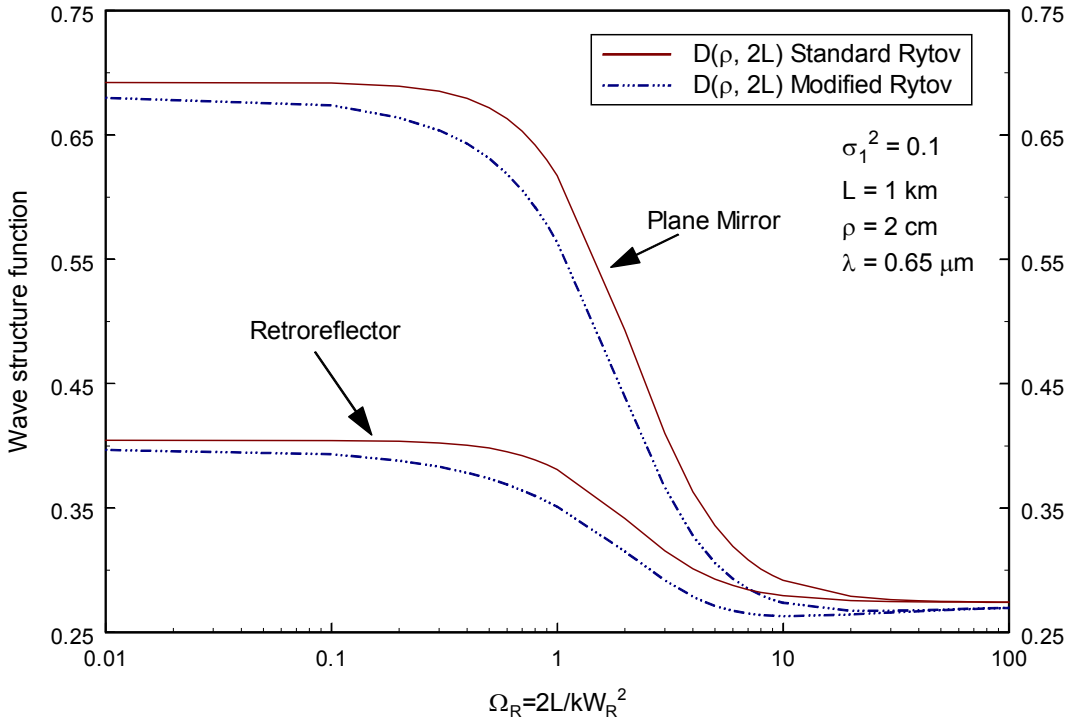

Figure 25 The finite target double pass wave structure function as a function of Ω_R for a monostatic scenario in weak turbulence, $\sigma_1^2 = 0.1$. The standard Rytov curves are given by (209). The modified Rytov curves are given by (213). The upper set of curves are for a plane mirror and the lower set of curves are for a retroreflector.

9.5 Double pass coherence radius

Recall from our earlier work that the spatial coherence radius, ρ_0, of an optical wave can be defined as the e^{-1} point of the complex degree of coherence function, (131), and that finding the coherence radius is equivalent to finding the value of ρ such that the wave structure function is equal to two, i.e. $D\left(\rho_0, L\right) = 2$. Banakh and Mironov[29] presented asymptotic results for the double pass coherence radius for an incident spherical wave in strong turbulence for several cases. Of relevance to this work is the special case where the observation points, $\mathbf{r}_1$ and $\mathbf{r}_2$, are symmetrically located about the optical axis, i.e. $\mathbf{r}_1 = -\mathbf{r}_2$. Banakh and Mironov[29] presented point target and infinite, i.e. unbounded, plane mirror results for this case. Here, we consider the coherence radius predicted by the double pass wave structure functions found for the standard and modified Rytov methods in these limiting cases and compare these results to those of Banakh and Mironov.[29] Specifically, for a spherical wave incident on a point target with observation points symmetrically located about the optical axis, Banakh and Mironov found that the coherence radius in the asymptotic limit of strong turbulence is given by[29]

$$\rho_0 = 1.6\rho_{pl}, \tag{226}$$

where ρ_{pl} is the coherence radius of a plane wave propagating along a path of length L given by

$$\rho_{pl} = \left(1.46C_n^2k^2L\right)^{-3/5}, \tag{227}$$

which is the result obtained from the standard Rytov approximation one-way plane wave structure function. They also found, for a spherical wave incident on an infinite plane mirror in a monostatic channel with observation points symmetrically located about the optical axis, that the coherence radius in the asymptotic limit of strong turbulence is given by[29]

$$\rho_0 = 2.46\rho_{pl}. \tag{228}$$

In figure 26, we compare the double pass coherence radius for a point target as obtained from the standard Rytov approximation wave structure function, (207), and that obtained from the modified Rytov approximation wave structure function, (208), to the asymptotic result, (226). While the coherence radius derived from the modified Rytov wave structure function, (208), cannot be expressed analytically it can be found numerically by setting the function equal to two and solving for ρ. The results presented in figure 26 were found using a standard bisection method. Figure 26 presents the value of the coherence radius as a function of increasing turbulence strength in the moderate to strong optical turbulence regimes. We note that the results in this figure are valid for a bistatic or monostatic channel as the point target wave structure function is independent of the channel type.

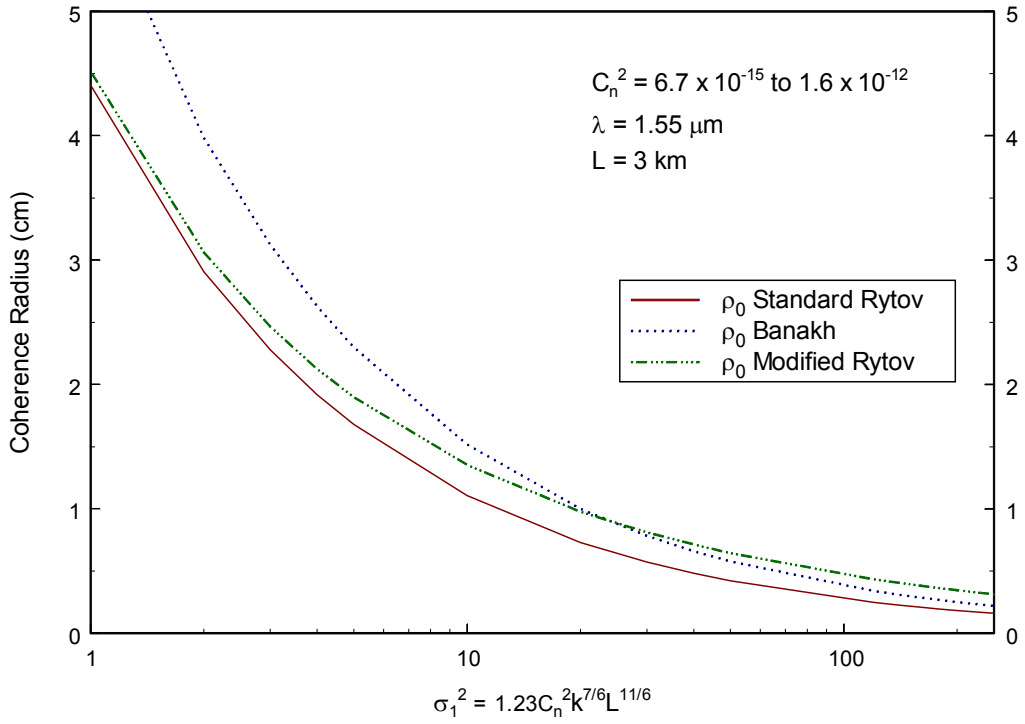

Figure 26 The double pass point target coherence radius (cm) as a function of increasing turbulence strength, σ_1^2, in the moderate to strong regime. The standard Rytov curve is obtained from (207), the modified Rytov curve is obtained from (208), and the Banakh curve is obtained from (226). The propagation path length, L, is held constant while C_n^2 is allowed to vary.

In figure 27, we compare the double pass coherence radius results for an unbounded target in a monostatic channel. We determine the coherence radius for an unbounded target as predicted by the standard Rytov method and the modified Rytov method by setting $\Omega_R = 0.01$ in (209) and (213), respectively, and solving for ρ. For both methods, these results are found numerically using a bisection method. The results are compared to the asymptotic result given by (228). We note that the results of figure 27 are valid only for a plane mirror target in a monostatic channel. As previously noted, unlike the point target case, the limiting case of an unbounded target is dependent on the channel and target type.

Although the results in figures 26 and 27 are not conclusive, it does appear that the coherence radii predicted by the modified Rytov method agree with Banakh and Mironov's[29] asymptotic results better than then the standard Rytov approximation. Particularly, in the strong turbulence regime, $\sigma_1^2 > 10$, where the asymptotic results are expected to be valid, we see in both figures that the modified Rytov results are nearly identical to the asymptotic results, while the standard Rytov results seem to underpredict the coherence radius values.

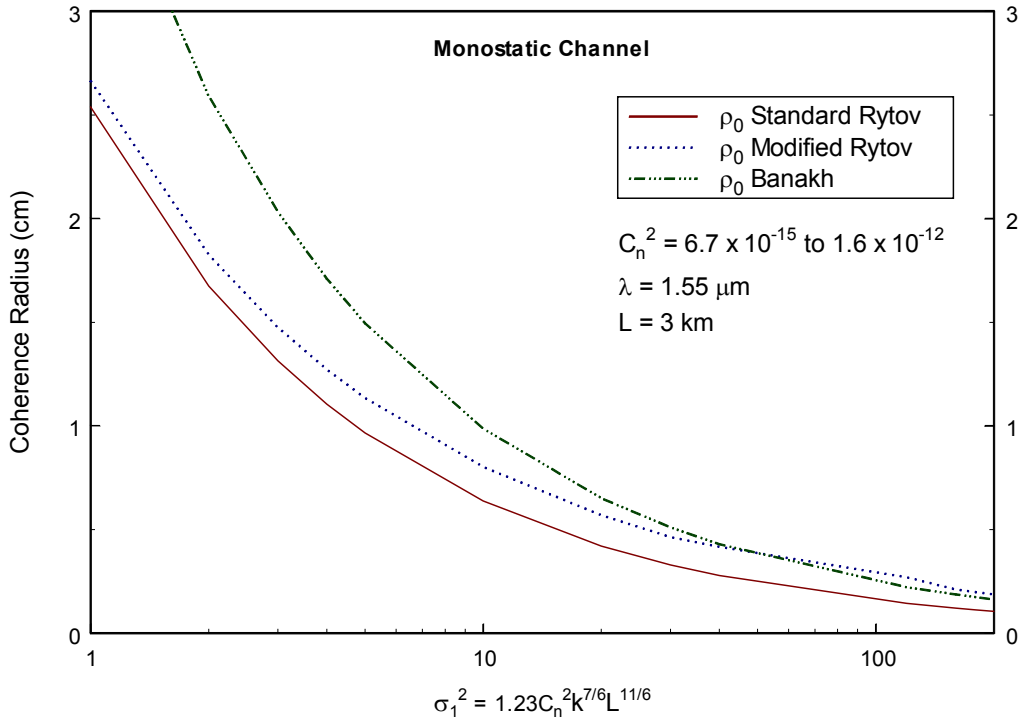

Figure 27 The monostatic channel double pass unbounded target coherence radius (cm) as a function of increasing turbulence strength, σ_1^2, in the moderate to strong regime. The standard Rytov curve is obtained from (209), the modified Rytov curve is obtained from (213), and the Banakh curve is obtained from (228). The propagation path length, L, is held constant while C_n^2 is allowed to vary.

10. DOUBLE PASS TEMPORAL FREQUENCY SPREAD

10.1 Introduction

As mentioned in the preceding chapter, laser radar, or lidar, systems are directly analogous to conventional microwave radar systems in the sense that their purpose is to determine target characteristics such as range and rate. Additionally, by analyzing micro-Doppler shifts in the received frequency of the echo wave, such systems can determine various target characteristics such as reflectivity and temperature. This information is particularly valuable for target identification. However, the random phase fluctuations caused by propagation in a turbulent atmosphere impart random frequency fluctuations on the optical signal. Thus, in order to use measurements of the micro-Doppler shift to determine target characteristics, it is first necessary to understand the impact of atmospheric induced frequency fluctuations on the optical signal. Furthermore, as most real world systems would operate in conditions of moderate to strong irradiance fluctuations, i.e. moderate to strong optical turbulence, it is necessary to model atmospheric frequency fluctuations in these conditions. In this chapter, the previously developed models for frequency variance along a one-way horizontal path are extended to double pass horizontal paths with reflection from a smooth target assuming a transmitted spherical wave. As in the case of the double pass wave structure function, it is necessary to consider both bistatic and monostatic channels. Point and finite size target expressions are developed using the standard and modified Rytov methods.

10.2 Integral definitions

Recall from the earlier chapter on the horizontal path temporal frequency spread, it was determined that the frequency variance, σ_f^2, is related to the temporal phase covariance function, $B_s(\tau)$, through the relation

$$\sigma_f^2 = -\frac{B_s''(\tau)}{4\pi^2}\bigg|_{\tau=0}. \tag{229}$$

Assuming that this same relation holds for the double pass frequency variance, it is necessary to determine expressions for the double pass temporal phase covariance function. This expression must include the effects of reflection of the optical wave from a target and the statistical correlation effects that arise when propagation occurs in a monostatic channel. An expression for the double pass spatial phase covariance function can be developed using ABCD ray matrices in the same manner as for the double pass wave structure function. Given the double pass spatial phase covariance function, Taylor's frozen flow hypothesis can be applied to yield the double pass temporal phase covariance function.

Recall that in the case of a spherical wave, Taylor's frozen flow hypothesis dictates that, prior to integration, we make the substitution $\rho = V\tau/\xi = V\tau\left(\frac{L}{z}\right)$, where V is the crosswind velocity. This substitution will be sufficient in the point target case where the reflected wave is spherical. However, recall that in the double pass wave structure function work, it was noted that reflection from a finite target results in a reflected wave that is like a Gaussian-beam wave. In this case, the geometry is no longer spherical. To arrive at an appropriate substitution in this case, consider the

horizontal path amplitude ratio

$$\gamma = 1 - \left(\bar{\Theta} + i\,\Lambda\right)\left(1 - \frac{z}{L}\right), \tag{230}$$

as presented in the horizontal path wave structure function development. Recall that the second order statistical moments, E_1, E_2, and E_3, given by equations (46)-(48), which have been used to define the various statistical quantities considered, all involve integration over γ. In their work on the Gaussian-beam wave temporal covariance of the irradiance fluctuations, Andrews and Phillips[2] suggest that the appropriate substitution for Taylor's frozen flow is given by replacing $\gamma\,\rho$ with $V\tau$ prior to integration. However, when this substitution is used in the integral definitions defining the double pass spatial phase covariance function, it is found that the resulting finite target temporal phase covariance function fails to reduce to the corresponding point target temporal phase covariance function when the limit of the target size approaching zero is considered. Furthermore, it is found that this substitution yields plane mirror and retroreflector frequency variance expressions that are identical in the monostatic case, contrary to the results obtained for the monostatic wave structure function. However, a substitution can be made that does allow the finite target expression to reduce to the point target case in the limit and results in differing expressions for the monostatic case.

Consider the substitution $\rho = V\tau/\gamma$ for one-way horizontal path propagation. In the case of a plane wave, $\Lambda = 0$, $\bar{\Theta} = 0$, and $\gamma = 1$, so that the substitution $\rho = V\tau/\gamma$ is equivalent to the previously discussed plane wave substitution, $\rho = V\tau$. In the case of a spherical wave,

$\Lambda = 0$, $\bar{\Theta} = 1$, and $\gamma = \frac{z}{L} = \xi$, so that the substitution $\rho = V\tau/\gamma$ is equivalent to the previously discussed spherical wave substitution, $\rho = V\tau/\xi$. Given these results, the substitution, $\rho = V\tau/\gamma_2$, where γ_2 is the path amplitude ratio of the reflected wave in the double pass problem, was attempted. It was found that the resulting finite target temporal phase covariance function reduces to the corresponding point target temporal phase covariance function in the limit. This substitution also yields monostatic frequency spread behavior that is consistent with the double pass wave structure function results. Specifically, when considered as a function of target size, the observed monostatic frequency spread for a plane mirror and retroreflector differ for finite targets but approach the same limit for a point target. Additionally, the monostatic and plane mirror frequency spread do not approach the same limit in the case of an unbounded target. This behavior is completely consistent with the monostatic wave structure function behavior presented in figure 25. Thus, in the work that follows the substitution $\rho = V\tau/\gamma_2$ has been used.

Using the double pass finite target spatial phase covariance function presented in [2] and applying Taylor's frozen flow hypothesis in the manner discussed above, it can be shown (see Appendix H) that the double pass temporal phase covariance function after reflection from a smooth target is given by[31]

$$B_s\left(V\tau/\gamma_2, 2L\right) = \frac{1}{2}\,\mathrm{Re}\left[\alpha_1 + \alpha_2 + \alpha_3 + \alpha_4\right], \tag{231}$$

where $\mathrm{Re}\,(x)$ denotes the real part of x and a_1 through a_4 are defined below. Note that the expressions for a_1 through a_4 assume an incident spherical wave and that the observation points

are symmetrically located about the optical axis and are valid only for that case. For both a plane mirror and a retroreflector, α_1 and α_2 are given by[31]

$$\begin{aligned}\alpha_1 &= 4\pi^2 k^2 L \int_0^1 \int_0^\infty \kappa \Phi_n(\kappa) J_0\left[\frac{\Theta_2(1-\xi)}{\gamma_2}\kappa V\tau\right] \exp\left[-\frac{L\kappa^2\Lambda_2}{k}(1-\xi)^2\right] d\kappa d\xi \\ &\quad + 4\pi^2 k^2 L \int_0^1 \int_0^\infty \kappa \Phi_n(\kappa) J_0\left[\frac{(\Theta_2 - j\Lambda_2)(1-\xi)}{\gamma_2}\kappa V\tau\right] \\ &\quad \times \exp\left[-\frac{jL\kappa^2}{k}(1-\xi)\left(\Theta_2 + \bar{\Theta}_2\xi\right)\right] \exp\left[-\frac{L\kappa^2\Lambda_2}{k}(1-\xi)^2\right] d\kappa d\xi, \end{aligned} \tag{232}$$

$$\begin{aligned}\alpha_2 &= 4\pi^2 k^2 L \int_0^1 \int_0^\infty \kappa \Phi_n(\kappa) J_0\left[\frac{\left(\Theta_2 + \bar{\Theta}_2\xi\right)}{\gamma_2}\kappa V\tau\right] \exp\left[-\frac{L\kappa^2\Lambda_2}{k}(1-\xi)^2\right] d\kappa d\xi \\ &\quad + 4\pi^2 k^2 L \int_0^1 \int_0^\infty \kappa \Phi_n(\kappa) J_0\left\{\frac{\left[\xi + (\Theta_2 - j\Lambda_2)(1-\xi)\right]}{\gamma_2}\kappa V\tau\right\} \\ &\quad \times \exp\left[-\frac{jL\kappa^2}{k}(1-\xi)\left(\Theta_2 + \bar{\Theta}_2\xi\right)\right] \exp\left[-\frac{L\kappa^2\Lambda_2}{k}(1-\xi)^2\right] d\kappa d\xi, \end{aligned} \tag{233}$$

where V is the crosswind velocity, $j = \sqrt{-1}$, the beam parameters (Λ_2, Θ_2, and $\bar{\Theta}_2$) are given by (206), and for an incident spherical wave

$$\gamma_2 = 1 - \left(\bar{\Theta}_2 + j\Lambda_2\right)(1-\xi). \tag{234}$$

In the case of a bistatic propagation channel $\alpha_3 = \alpha_4 = 0$ for both a plane mirror and a retroreflector target. However, in the case of a monostatic propagation channel, for reflection from

a plane mirror, we have[31]

$$\alpha_3 = 8\pi^2 k^2 L \int_0^1 \int_0^\infty \kappa \Phi_n(\kappa) J_0 \left\{ \frac{[\xi + 2\Theta_2 (1-\xi)]}{\gamma_2} \frac{\kappa V \tau}{2} \right\} \times \exp\left[-\frac{L\kappa^2 \Lambda_2}{k} (1-\xi)^2 \right] d\kappa d\xi, \quad (235)$$

$$\alpha_4 = 8\pi^2 k^2 L \int_0^1 \int_0^\infty \kappa \Phi_n(\kappa) J_0 \left\{ \frac{\left[\xi + 2(\Theta_2 - j\Lambda_2)(1-\xi)\right]}{\gamma_2} \frac{\kappa V \tau}{2} \right\} \times \exp\left[-\frac{jL\kappa^2}{k} (1-\xi)\left(\Theta_2 + \bar{\Theta}_2 \xi\right) \right] \exp\left[-\frac{L\kappa^2 \Lambda_2}{k} (1-\xi)^2 \right] d\kappa d\xi. \quad (236)$$

In the case of a monostatic propagation channel, for reflection from a retroreflector, we have

$$\begin{aligned} \alpha_3 = {} & 4\pi^2 k^2 L \int_0^1 \int_0^\infty \kappa \Phi_n(\kappa) J_0 \left\{ -\frac{\left[\xi + 2j\Lambda_2 (1-\xi)\right]}{\gamma_2} \frac{\kappa V \tau}{2} \right\} \\ & \times \exp\left[-\frac{L\kappa^2 \Lambda_2}{k} (1-\xi)^2 \right] d\kappa d\xi \\ & + 4\pi^2 k^2 L \int_0^1 \int_0^\infty \kappa \Phi_n(\kappa) J_0 \left\{ \frac{\left[\xi - 2j\Lambda_2 (1-\xi)\right]}{\gamma_2} \frac{\kappa V \tau}{2} \right\} \\ & \times \exp\left[-\frac{L\kappa^2 \Lambda_2}{k} (1-\xi)^2 \right] d\kappa d\xi, \end{aligned} \quad (237)$$

$$\alpha_4 = 8\pi^2 k^2 L \int_0^1 \int_0^\infty \kappa \Phi_n(\kappa) J_0 \left\{ \frac{\xi \kappa V \tau}{2\gamma_2} \right\} \exp\left[-\frac{L\kappa^2 \Lambda_2}{k} (1-\xi)^2 \right] \times \exp\left[-\frac{jL\kappa^2}{k} (1-\xi)\left(\Theta_2 + \bar{\Theta}_2 \xi\right) \right] d\kappa d\xi. \quad (238)$$

10.3 Point target

When the target radius, W_R, is much less than the Fresnel zone, $\sqrt{L/k}$, Ω_R approaches infinity so that Λ_2 and Θ_2 both approach zero. In this case, the system behaves as if reflection occurs from a point target and the resulting frequency variance expressions are significantly simplified. We note, however, that is a very restrictive case. Indeed, for propagation at $\lambda = 1.55\ \mu m$ where the distance from the transmitter to the target is 500 m, the Fresnel zone is approximately 1 cm. Even when the distance to the target is 2 km, the Fresnel zone is just over 2 cm. However, it is instructive to consider reflection from a point target as a special case.

If we assume a point target with a bistatic propagation channel, we find, after simplifying α_1 and α_2 and substituting the resulting temporal phase covariance function into (229), that the atmospheric induced frequency variance obtained for reflection from either a plane mirror or a retroreflector is given by

$$\sigma_f^2 = 0.25k^2LV^2 \int_0^1 \int_0^\infty \kappa^3 \Phi_n(\kappa) \left\{1 + \cos\left[\frac{L\kappa^2\xi}{k}(1-\xi)\right]\right\} d\kappa d\xi, \tag{239}$$

which is equivalent to (171), the spherical wave frequency variance observed for one-way propagation. Note, that (239) is independent of the incident wave type, that is, it holds for an incident plane, spherical or Gaussian-beam wave. This is physically intuitive since reflection from a point target should result in an echo wave that is spherical and is consistent with the double pass point target wave structure function.

In the case where propagation occurs in a monostatic channel for reflection from a point target, the spherical wave atmospheric induced frequency variance is given by

$$\sigma_f^2 = 0.375k^2LV^2\int_0^1\int_0^\infty \kappa^3\Phi_n(\kappa)\left\{1+\cos\left[\frac{L\kappa^2\xi}{k}(1-\xi)\right]\right\}d\kappa d\xi, \tag{240}$$

which is exactly $\frac{3}{2}$ times (239). Thus the standard Rytov method double pass point target frequency variance is described by (172) in the bistatic case and $\frac{3}{2}$ times (172) in the monostatic case. The modified Rytov method double pass point target frequency variance is described by (173) in the bistatic case and $\frac{3}{2}$ times (173) in the monostatic case.

10.4 Finite target

When the target radius, W_R, is of the same order as the first Fresnel zone the system must be characterized as reflection occurring from a finite target and no simplifications can be made on α_1 through α_4. Thus, in order to determine the frequency variance in the case of a finite target it is necessary to evaluate expressions (232), (233), and (235)-(238) without simplification. However, we do not evaluate these expressions directly. Noting that the frequency variance is given by (229), we first differentiate the integral expressions for α_1 through α_4 with respect to τ and evaluate the resulting expressions at $\tau = 0$, which yields an integral expression for the frequency variance[31]

$$\sigma_f^2 = -\frac{1}{8\pi^2}\left[\beta_1+\beta_2+\beta_3+\beta_4\right] \tag{241}$$

where the terms β_1 through β_4 will be defined below. For clarity, the derivation of these expressions is presented in Appendix H and Appendix I. Note that in the case of a bistatic channel, $\beta_3 = \beta_4 = 0$.

We can now apply the standard Rytov method to derive an integral expression for the finite target frequency variance. Using the analytic approximation of the Hill spectrum, (151), where an infinite outer scale is assumed, and letting

$$A = \left(\frac{k\kappa_l^2}{\kappa_l^2 L \Lambda_2 (1-\xi)^2 + k} \right)^{1/2}, \tag{242}$$

we find that for both a plane mirror and a retroreflector[31] (see Appendix H and Appendix I)

$$\begin{aligned}
\beta_1 \;=\;& 2\pi^2 k^2 L V^2 \Theta_2^2 \int_0^1 \frac{I_1}{D^2} (1-\xi)^2 \\
& \times \left[\left(\Lambda_2^2 - \bar{\Theta}_2 \right) \xi^2 - 2 \left(\Theta_2 \bar{\Theta}_2 + \Lambda_2^2 \right) \xi + \Lambda_2^2 - \Theta_2^2 \right] d\xi \\
& + 2\pi^2 k^2 L V^2 \int_0^1 \frac{I_2}{D^2} (1-\xi)^2 \left\{ \left[\Lambda_2^2 - \left(\Lambda_2^2 - \Theta_2 \bar{\Theta}_2 \right)^2 \right] \xi^2 \right. \\
& \left. + \left[2\Lambda_2^2 \left(2\Theta_2^2 - \Theta_2 + \Lambda_2^2 \right) - 2\Theta_2^3 \bar{\Theta}_2 \right] \xi - \left(\Lambda_2^2 + \Theta_2^2 \right)^2 \right\} d\xi \\
& + 4\pi^2 k^2 L V^2 \Lambda_2 \int_0^1 \frac{I_3}{D^2} (1-\xi)^2 \left[\left(\Theta_2 \bar{\Theta}_2 - \Lambda_2^2 \right) \xi^2 + \left(\Lambda_2^2 + \Theta_2^2 \right) \xi \right] d\xi,
\end{aligned} \tag{243}$$

$$\begin{aligned}
\beta_2 \;=\;& 2\pi^2 k^2 L V^2 \int_0^1 \frac{I_1}{D^2} \left(\bar{\Theta}_2 \xi + \Theta_2 \right)^2 \\
& \times \left[\left(\Lambda_2 + \bar{\Theta}_2 \right) \xi - \Lambda_2 + \Theta_2 \right] \left[\left(\Lambda_2 - \bar{\Theta}_2 \right) \xi - \Lambda_2 - \Theta_2 \right] d\xi \\
& - 2\pi^2 k^2 L V^2 \int_0^1 I_2 d\xi,
\end{aligned} \tag{244}$$

where $I_1 = I_a(A)$, $I_2 = I_b(A)$, and $I_3 = I_c(A)$ are defined below, and

$$D = \left(\bar{\Theta}_2^2 + \Lambda_2^2\right)\xi^2 + 2\left(\Theta_2\bar{\Theta}_2 - \Lambda_2^2\right)\xi + \Lambda_2^2 + \Theta_2^2. \tag{245}$$

In the case of a monostatic channel for reflection from a plane mirror, we have (see Appendix H and Appendix I)

$$\begin{aligned}\beta_3 &= -\pi^2 k^2 L V^2 \int_0^1 \frac{I_1}{D^2}\left[2\Theta_2 + (1-2\Theta_2)\xi\right]^2 \\ &\quad \times \left[\Lambda_2 - \Theta_2 - \left(\Lambda_2 + \bar{\Theta}_2\right)\xi\right]\left[\left(\Lambda_2 - \bar{\Theta}_2\right)\xi - \Lambda_2 - \Theta_2\right] d\xi,\end{aligned} \tag{246}$$

$$\begin{aligned}\beta_4 &= -\pi^2 k^2 L V^2 \int_0^1 \frac{I_2}{D^2} \\ &\quad \times \left\{\left[2\Lambda_2^2 + \Lambda_2 + 2\Theta_2^2 - 3\Theta_2 + 1\right]\xi^2\right. \\ &\quad \left. + \left[3\Theta_2 - \Lambda_2 - 4\left(\Lambda_2^2 + \Theta_2^2\right)\right]\xi + 2\left(\Lambda_2^2 + \Theta_2^2\right)\right\} \\ &\quad \times \left\{\left[2\left(\Lambda_2^2 + \Theta_2^2\right) - 3\Theta_2 - \Lambda_2 + 1\right]\xi^2\right. \\ &\quad \left.\left[3\Theta_2 + \Lambda_2 - 4\left(\Lambda_2^2 + \Theta_2^2\right)\right]\xi + 2\left(\Lambda_2^2 + \Theta_2^2\right)\right\} d\xi \\ &\quad -2\pi^2 k^2 L V^2 \Lambda_2 \int_0^1 \frac{I_3}{D^2}(1-\xi)\xi \\ &\quad \times \left\{\left[2\left(\Theta_2\bar{\Theta}_2 - \Lambda_2^2\right) - \bar{\Theta}_2\right]\xi^2\right. \\ &\quad \left. + \left[4\left(\Lambda_2^2 - \Theta_2\bar{\Theta}_2\right) + \Theta_2\right]\xi - 2\left(\Lambda_2^2 + \Theta_2^2\right)\right\} d\xi.\end{aligned} \tag{247}$$

For the monostatic case, when reflection occurs from a retroreflector, we have (see Appendix H and Appendix I)

$$\begin{aligned}
\beta_3 &= 0.5\pi^2 k^2 L V^2 \int_0^1 \frac{I_1}{D^2} \left\{ \left[4\Lambda_2^2 \left(\Theta_2^2 - 4\Theta_2 - \Lambda_2^2 + \frac{13}{4} \right) - \bar{\Theta}_2^2 \right] \xi^4 \right. \\
&\quad + \left[16\Lambda_2^2 \left(\Lambda_2^2 - \Theta_2^2 + 3\Theta_2 - \frac{13}{8} \right) - 2\Theta_2 \bar{\Theta}_2 \right] \xi^3 \\
&\quad + \left[24\Lambda_2^2 \left(\Theta_2^2 - 2\Theta_2 - \Lambda_2^2 + \frac{24}{13} \right) - \Theta_2^2 \right] \xi^2 \\
&\quad \left. + 16\Lambda_2^2 \left(\Theta_2 \bar{\Theta}_2 + \Lambda_2^2 \right) \xi - 4\Lambda_2^2 \left(\Lambda_2^2 - \Theta_2^2 \right) \right\} d\xi \\
&\quad - 0.5\pi^2 k^2 L V^2 \int_0^1 \frac{I_1}{D^2} \left\{ \left[\bar{\Theta}_2 + 4\Lambda_2^2 \left(\Lambda_2^2 - \Theta_2^2 + \frac{3}{4} \right) \right] \xi^4 \right. \\
&\quad + \left[16\Lambda_2^2 \left(\Theta_2^2 - \Lambda_2^2 - \frac{3}{8} \right) + 2\Theta_2 \bar{\Theta}_2 \right] \xi^3 \\
&\quad + \left[24\Lambda_2^2 \left(\Lambda_2^2 - \Theta_2^2 \right) + \Theta_2^2 + 3\Lambda_2^2 \right] \xi^2 \\
&\quad \left. + 16\Lambda_2^2 \left(\Theta_2^2 - \Lambda_2^2 \right) \xi + 4\Lambda_2^2 \left(\Lambda_2^2 - \Theta_2^2 \right) \right\} d\xi, \qquad (248)
\end{aligned}$$

$$\begin{aligned}
\beta_4 &= \pi^2 k^2 L V^2 \int_0^1 \frac{I_2}{D^2} \xi^2 \left[\left(\Lambda_2^2 - \bar{\Theta}_2^2 \right) \xi^2 \right. \\
&\quad \left. - 2 \left(\Lambda_2^2 + \Theta_2 \bar{\Theta}_2 \right) \xi + \Lambda_2^2 - \Theta_2^2 \right] d\xi \\
&\quad + 2\pi^2 k^2 L V^2 \Lambda_2 \int_0^1 \frac{I_3}{D^2} \xi^2 \left[\bar{\Theta}_2 \xi^2 - (1 - 2\Theta_2) \xi - \Theta_2 \right] d\xi. \qquad (249)
\end{aligned}$$

The functions $I_1 = I_a(A)$, $I_2 = I_b(A)$, and $I_3 = I_c(A)$ are defined by (see Appendix I)

$$I_a(\mathcal{A}) = 0.092 C_n^2 \mathcal{A}^{1/3} \left[1 + 0.44 \frac{\mathcal{A}}{\kappa_l} - 0.056 \left(\frac{\mathcal{A}}{\kappa_l} \right)^{7/6} \right], \qquad (250)$$

$$
\begin{aligned}
I_b(\mathcal{A}) &= 0.092 C_n^2 \mathcal{A}^{1/3} \Big[{}_2F_1\left(\tfrac{1}{12}, \tfrac{7}{12}; \tfrac{1}{2}; -B^2\mathcal{A}^4\right) \\
&\quad + 0.44 \left(\frac{\mathcal{A}}{\kappa_l}\right) {}_2F_1\left(\tfrac{1}{3}, \tfrac{5}{6}; \tfrac{1}{2}; -B^2\mathcal{A}^4\right) \\
&\quad - 0.056 \left(\frac{\mathcal{A}}{\kappa_l}\right)^{7/6} {}_2F_1\left(\tfrac{3}{8}, \tfrac{7}{8}; \tfrac{1}{2}; -B^2\mathcal{A}^4\right) \Big],
\end{aligned} \tag{251}
$$

$$
\begin{aligned}
I_c(\mathcal{A}) &= 0.015 C_n^2 B \mathcal{A}^{7/3} \Big[{}_2F_1\left(\tfrac{7}{12}, \tfrac{13}{12}; \tfrac{3}{2}; -B^2\mathcal{A}^4\right) \\
&\quad + 1.75 \left(\frac{\mathcal{A}}{\kappa_l}\right) {}_2F_1\left(\tfrac{5}{6}, \tfrac{4}{3}; \tfrac{3}{2}; -B^2\mathcal{A}^4\right) \\
&\quad - 0.25 \left(\frac{\mathcal{A}}{\kappa_l}\right)^{7/6} {}_2F_1\left(\tfrac{7}{8}, \tfrac{11}{8}; \tfrac{3}{2}; -B^2\mathcal{A}^4\right) \Big],
\end{aligned} \tag{252}
$$

where $\kappa_l = \frac{3.3}{l_0}$ and

$$
B = \frac{L}{k}(1-\xi)\left(\Theta_2 + \bar{\Theta}_2 \xi\right). \tag{253}
$$

Expressions for the frequency variance can now be obtained using the modified Rytov method by applying the effective hill spectrum, (67), where $f(\kappa l_0)$ is given by (158), so that an infinite outer scale is assumed, and $g(\kappa L_0) = 1$. Applying this method yields an expression for the frequency variance that is the sum of a large and small scale component

$$
\sigma_f^2 = \sigma_{f,x}^2 + \sigma_{f,y}^2, \tag{254}
$$

where

$$
\sigma_{f,x}^2 = -\frac{1}{8\pi^2}\left[\beta_{x,1} + \beta_{x,2} + \beta_{x,3} + \beta_{x,4}\right], \tag{255}
$$

$$\sigma_{f,y}^2 = -\frac{1}{8\pi^2}\left[\beta_{y,1} + \beta_{y,2} + \beta_{y,3} + \beta_{y,4}\right] \tag{256}$$

The terms $\beta_{x,n}$ for $n = 1,\ 2,\ 3,\ 4$ are defined as follows. Let

$$A_{xl} = \left(\frac{k\kappa_{xl}^2}{\kappa_{xl}^2 L\Lambda_2 (1-\xi)^2 + k}\right)^{1/2}, \tag{257}$$

where

$$\kappa_{xl}^2 = \frac{\kappa_l^2 \kappa_{x(gb)}^2}{\kappa_{x(gb)}^2 + \kappa_l^2} \tag{258}$$

where $\kappa_{x(gb)}^2$ is defined by (223). Now the terms $\beta_{x,n}$ are exactly the same as the β_n terms in the standard Rytov method except that now $I_1 = I_a(A_{xl})$, $I_2 = I_b(A_{xl})$, and $I_3 = I_c(A_{xl})$. Similarly, the terms $\beta_{y,n}$ for $n = 1,\ 2,\ 3,\ 4$ can be defined by letting

$$A_{yl} = \left(\frac{k\kappa_{yl}^2}{\kappa_{yl}^2 L\Lambda_2 (1-\xi)^2 + k}\right)^{1/2}, \tag{259}$$

where

$$\kappa_{yl}^2 = \frac{\kappa_l^2 \kappa_{y(gb)}^2}{\kappa_{y(gb)}^2 + \kappa_l^2}, \tag{260}$$

where $\kappa_{y(gb)}^2$ is defined by (224). Again the terms $\beta_{y,n}$ are exactly the same as those in the standard Rytov method except that now $I_1 = I_a(A) - I_a\left(A_{yl}\right)$, $I_2 = I_b(A) - I_b\left(A_{yl}\right)$, and $I_3 = I_c(A) - I_c\left(A_{yl}\right)$. Note, in a bistatic channel the terms $\beta_{x,3}$, $\beta_{x,4}$, $\beta_{y,3}$, and $\beta_{y,4}$ are taken to be zero.

10.5 Comparisons

In this section we compare the frequency spread results predicted by the modified and standard Rytov methods. In the figures presented the data was obtained by numerically integrating the remaining integrals in the β terms defining the frequency variance using *Maple*.

In figure 28 the finite target frequency spread, σ_f, is given as a function of increasing turbulence strength for $\Omega_R = 1$ in a bistatic channel. Recall, that in the bistatic channel the frequency variance is identical for plane mirror and retroreflector targets, thus the curves in figure 28 are representative of both cases. The qualitative behavior is identical to the horizontal path case in the sense that in the weak turbulence regime the two methods predict similar values. However, in the moderate to strong turbulence regime the modified Rytov method predicts frequency spread values that are less than those predicted by the standard Rytov method.

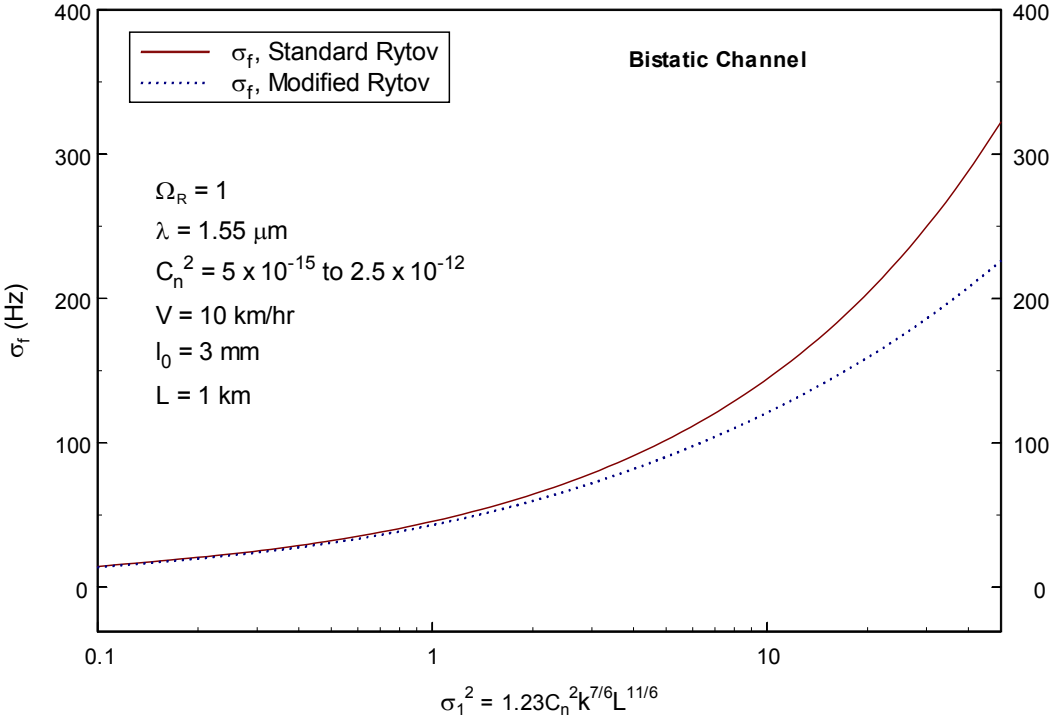

Figure 28 The finite target double pass frequency spread, σ_f, in a bistatic propagation channel as a function of increasing turbulence strength. The value of L is held constant while C_n^2 is allowed to vary.

In figure 29 the double pass frequency spread, σ_f, is presented as a function of increasing turbulence strength for $\Omega_R = 1$ in a monostatic channel. Recall that in the monostatic channel the β_3 and β_4 terms are different for a plane mirror and a retroreflector, hence curves for both cases are presented. Notice that the frequency spread for the plane mirror is greater than that of the retroreflector. This is consistent with the argument regarding the two types of statistical correlation paths discussed in the presentation of the double pass wave structure function (see figure 24). Note that the frequency variance is also independent of the reciprocal path terms.

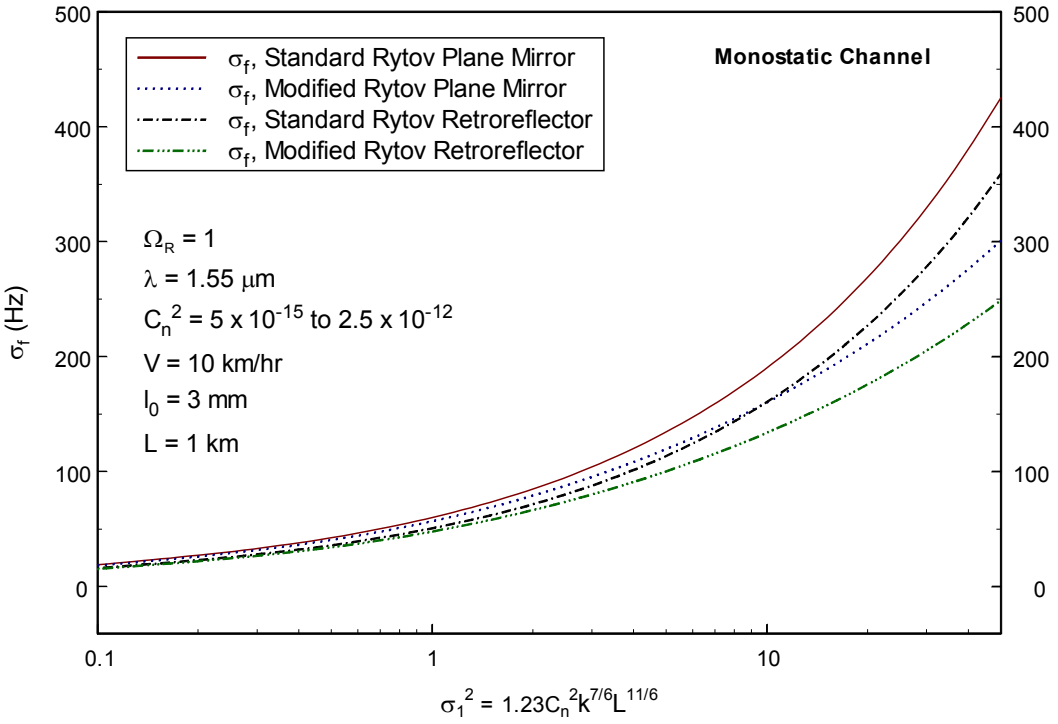

Figure 29 The finite target double pass frequency spread, σ_f, in a monostatic propagation channel as a function of increasing turbulence strength. The value of L is held constant while C_n^2 is allowed to vary.

Figures 30 and 31 present the frequency spread, σ_f, as a function of the target ratio parameter, Ω_R, for the bistatic, monostatic plane mirror, and monostatic retroreflector cases. The figures are for the weak turbulence regime, $\sigma_1^2 = 0.1$. Comparing the two figures we see that in the weak turbulence regime, the standard and modified Rytov methods predict identical frequency spread results for all target sizes. This is significant because it is expected that the standard Rytov method is valid in this regime. Notice that for the monostatic case as Ω_R increases the plane mirror and retroreflector curves approach the same limiting value. This result is expected because for these large values of Ω_R the target is like a point target. Recall that it was found that the monostatic point target frequency variance expression, (240), is independent of the target type, i.e. plane mirror or retroreflector. Also notice that as Ω_R decreases, the monostatic plane mirror and retroreflector curves do not approach the same limiting value. This indicates that an expression for the unbounded target frequency variance will be dependent on the target type. We see that these results are completely consistent with the double pass wave structure function results by comparing the frequency spread behavior presented in figures 30 and 31 to the double pass wave structure function behavior as a function of Ω_R presented in figure 25.

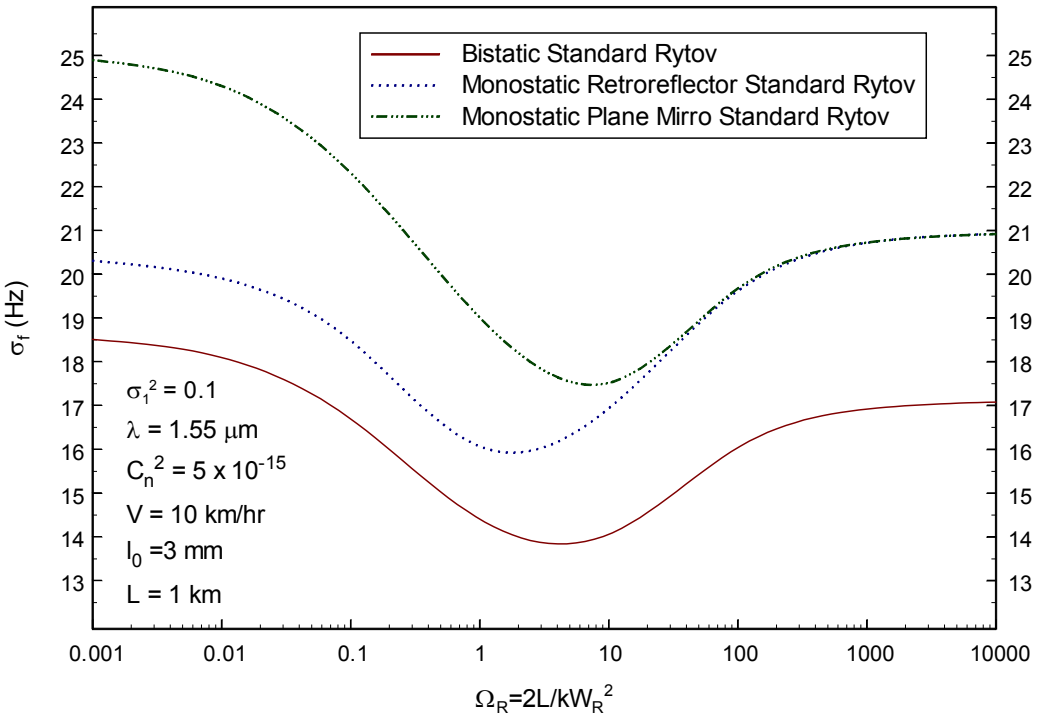

Figure 30 The double pass frequency spread as a function of the target ratio parameter, Ω_R. All curves are for the standard Rytov method.

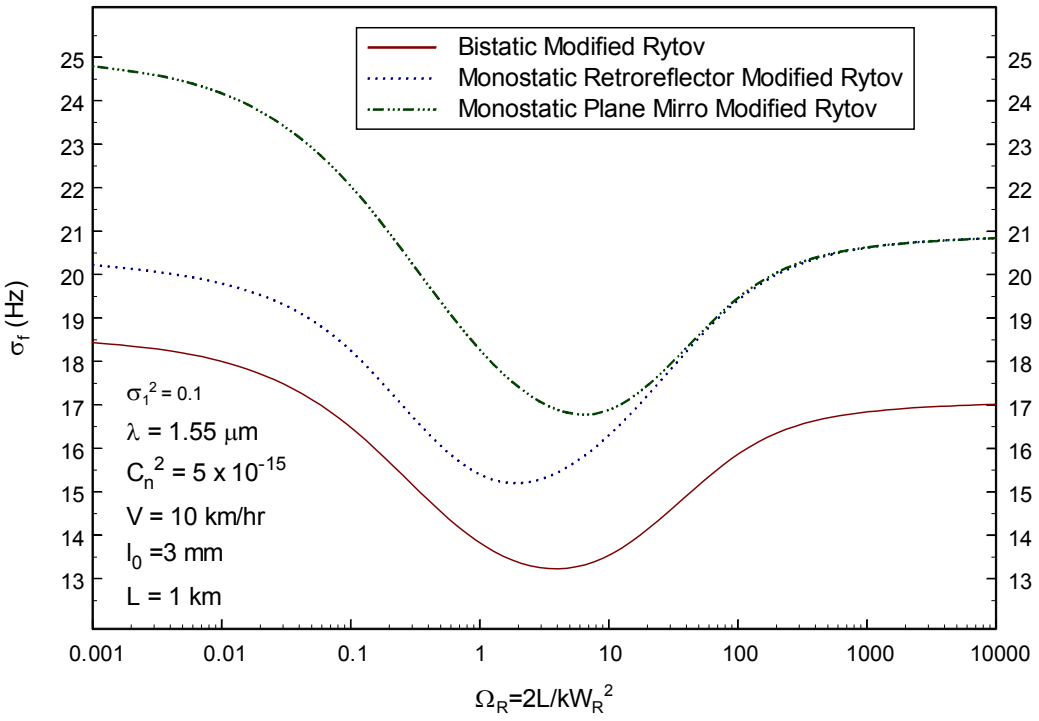

Figure 31 The double pass frequency spread as a function of the target ratio parameter, Ω_R. All curves are for the modified Rytov method.

11. DISCUSSION

11.1 Research accomplished

The wave structure function and the temporal frequency spread of an optical wave propagating in the Earth's atmosphere were the main focus of this research. The modified Rytov method was used to develop wave structure function results for a horizontal path for plane, spherical, and Gaussian-beam waves. Comparisons were presented between these new wave structure function results, the standard Rytov method results, and Gurvich's[13] experimental results. It was shown that the expressions derived using the modified Rytov method agree with the standard Rytov method results in the weak turbulence regime, but predict lesser wave structure function values in the moderate to strong turbulence regime. Furthermore, it was seen that the new results presented here predict the same qualitative behavior as the experimental data in all turbulence regimes and that the standard Rytov method expressions fail to agree with the data in the moderate to strong turbulence regimes. Double pass wave structure function results were also developed using the modified Rytov method. Recall, that the coherence radius can be obtained from the wave structure function. It was shown in the double pass scenario that the coherence radius found from the modified Rytov method seems to agree better with the strong turbulence asymptotic results of Banakh and Mironov.[29] While these comparisons are not conclusive, they do lend confidence to the results obtained here using the modified Rytov method.

Additionally, analytic expressions for the temporal frequency spread were derived for plane, spherical and Gaussian-beam waves in the horizontal path case and spherical waves incident on a smooth target in the double pass case. Both the standard and modified Rytov methods were

used. In general, it was found that in the moderate to strong turbulence regime, the modified Rytov method predicted less spreading than the standard Rytov method. In the horizontal path case, it was shown that these expressions have the same qualitative behavior and nearly identical quantitative predictions of the frequency spread results found from an analysis of the temporal frequency spectrum as presented by Ishimaru.[4]

11.2 Signifincance

The importance of the modified Rytov method wave structure function results beyond their apparently correct modeling of the wave structure function in all turbulence regimes is that they indicate that the modified Rytov method can be applied to phase fluctuation related statistics as well as amplitude fluctuation related statistics. Recall that the modified Rytov method was originally developed by Andrews *et al.*[6–8] in an effort to model the scintillation index in all turbulence regimes. The scintillation index is a statistical quantity that is dominated by amplitude fluctuations. It was not known whether the same method could be used to model statistical quantities that are dominated by phase fluctuations. Given the results obtained here for the wave structure function and their favorable comparisons to experimental and asymptotic results, it appears that this method can indeed be applied to phase fluctuation related statistics.

Thus, this method was also used to derive results for the temporal frequency spread of the temporal frequency spectrum, which is a phase fluctuation related statistic. It has been shown previously that the temporal frequency spread can be obtained from the temporal frequency spectrum. The significant advantage of the derivation presented here is that it can more easily

be applied in the spherical and Gaussian-beam wave cases for horizontal paths and the double pass case than the analysis of the temporal frequency spectrum. This is because analyzing the temporal frequency spectrum directly requires knowledge of the mutual coherence function, which is difficult to obtain for the cases mentioned.

11.3 Future work

All of the results presented here have direct use in applications. In particular, the results seem to provide valid estimates in the moderate to strong turbulence regimes. It is in these regimes that most real world systems of practical value are likely to operate. However, much future work still remains. Though comparisons to experimental and asymptotic results have been presented, they are limited. Thus, in order to validate, and, if necessary, modify these results, further comparisons to experimental data are required, particularly in the moderate to strong turbulence regimes. Assuming these comparisons prove favorable, certain extensions of the results would be useful for application to real world systems. In particular, for the double pass wave structure function and the double pass frequency variance, it is necessary to incorporate a target "roughness" model. In this work, results were presented for smooth targets only. However, this is a limited case and many real world targets will not satisfy the conditions of a smooth target. Additionally, the work presented here in the double pass case only considered an incident spherical wave. As one of the main advantages to be gained from using a lidar system as compared to a conventional microwave radar system is security of the channel, which comes from the narrow beam size, it would be advantageous to further these results by considering a transmitted Gaussian-beam wave.

APPENDIX A. MAGNITUDE BARS IN SECOND ORDER MOMENTS

The || notation appearing in the Bessel functions, $J_0(x)$, used in the formulation of the moments $E_2(\mathbf{r}_1, \mathbf{r}_2)$ and $E_3(\mathbf{r}_1, \mathbf{r}_2)$, equations (47) and (48) respectively, is not the standard mathematical vector magnitude notation. Consider the Bessel function $J_0(|\alpha\mathbf{r} + \beta\mathbf{p}|)$, where α and β are some scalar quantities and $\mathbf{r}$ and $\mathbf{p}$ are some vector quantities. As used in in the development of the second order moments, $E_2(\mathbf{r}_1, \mathbf{r}_2)$ and $E_3(\mathbf{r}_1, \mathbf{r}_2)$, the operator || refers only to the vectors $\mathbf{r}$ and $\mathbf{p}$ and does not act on the scalar quantities α and β. Hence for real scalars α and β we have the following

$$|\alpha\mathbf{p}| = \alpha\,|\mathbf{p}|\,, \tag{A1}$$

$$|i\alpha\mathbf{p}| = i\alpha\,|\mathbf{p}|\,, \tag{A2}$$

where $i = \sqrt{-1}$.

Note that this notation only appears in the Bessel function, $J_0(x)$, which is an even function, i.e. $J_0(x) = J_0(-x)$. Hence there is no inconsistency if a vector, $\mathbf{p}$, has a negative common factor. That is, if

$$\mathbf{p} = -\gamma\,\mathbf{b}, \tag{A3}$$

where, $\gamma < 0$, is a real scalar such that

$$|\mathbf{p}| = p = |\gamma\,|\,b = -\gamma\,b, \tag{A4}$$

where

$$b = |\mathbf{b}|\,, \tag{A5}$$

then, because $J_0(x)$ is an even function, we have

$$J_0(|\mathbf{p}|) = J_0(p) = J_0(-\gamma b) = J_0(\gamma b) = J_0(|\gamma \mathbf{b}|). \tag{A6}$$

Additionally, we have the relation

$$J_0(|-i\mathbf{p}|) = J_0(-ip) = I_0(-ip) = I_0(ip), \tag{A7}$$

where it is noted that $I_0(x)$ is also an even function, so again there is no inconsistency in the $||$ notation.

Generally, we consider only the real part of the integral quantities $E_2(\mathbf{r}_1, \mathbf{r}_2)$ and $E_3(\mathbf{r}_1, \mathbf{r}_2)$. In the case where the argument of the Bessel function in $E_2(\mathbf{r}_1, \mathbf{r}_2)$ and $E_3(\mathbf{r}_1, \mathbf{r}_2)$ is the sum of two vectors, say $\mathbf{p}$ and $\mathbf{r}$ and we are considering the real part only, we use the following relation[22]

$$\begin{aligned} \mathrm{Re}[J(|\mathbf{Q}|)] &= J_0(\alpha|\mathbf{x}|) I_0(\beta|\mathbf{y}|) + 2\sum_{n=1}^{\infty} (-1)^n J_{2n}(\alpha|\mathbf{x}|) I_{2n}(\beta|\mathbf{y}|) \cos(2n\psi) \\ &\approx J_0(\alpha|\mathbf{x}|) I_0(\beta|\mathbf{y}|) \end{aligned} \tag{A8}$$

where $\mathbf{Q} = \alpha\mathbf{x} + \beta\mathbf{y}$, α and β are real scalars, and ψ is the angle between the vectors $\mathbf{x}$ and $\mathbf{y}$.

APPENDIX B. HORIZONTAL PATH PLANE WSF

For the derivations presented in the appendices, it will be useful to divide the effective atmospheric spectrum, (67), into a large scale component given by

$$\Phi_{n,x}(\kappa) = 0.033 C_n^2 \kappa^{-11/3} f(\kappa l_0)\, g(\kappa L_0) \exp\left(-\frac{\kappa^2}{\kappa_x^2}\right) \tag{B1}$$

and a small scale component given by

$$\Phi_{n,y}(\kappa) = 0.033 C_n^2 \kappa^{-11/3} f(\kappa l_0)\, g(\kappa L_0) \left\{1 - \exp\left[-\frac{\kappa^2}{\kappa_y^2}\right]\right\} \tag{B2}$$

To develop a horizontal path plane wave structure function using the modified Rytov method, we substitute the large and small scale components of the effective atmospheric spectrum, where we let $f(\kappa l_0) = \exp\left(-\frac{\kappa^2}{\kappa_m^2}\right)$ and $g(\kappa L_0) = \kappa^{11/3}\left(\kappa^2 + \kappa_0^2\right)^{-11/6}$, into the plane wave structure function integral definition given by (78) and evaluate. Substituting the large scale portion, (B1), into the integral definition, (78), we have the large scale portion of the plane wave structure function

$$D_x(\rho, L) \approx 2.606 k^2 L C_n^2 \int_0^\infty \kappa^{-8/3} \left[1 - J_0(\kappa\rho)\right] \exp\left(-\frac{\kappa^2}{\kappa_{xm}^2}\right) d\kappa, \tag{B3}$$

where $\kappa_m = 5.92/l_0$ and

$$\kappa_{xm}^2 = \frac{\kappa_m^2 \kappa_{x(pl)}^2}{\kappa_{x(pl)}^2 + \kappa_m^2}. \tag{B4}$$

The refractive index spatial frequency cutoff, $\kappa_{x(pl)}$, is defined by (B14). Notice that for the large scale portion of the wave structure function the outer scale is not required for convergence of the

integral, so here the limit as the outer scale goes to infinity has already been considered. To calculate the integral in (B3), it is necessary to replace the Bessel function, $J_0(x)$, by it's series representation[22]

$$1 - J_0(\kappa\rho) = -\sum_{l=1}^{\infty} \frac{\left(-\kappa^2\rho^2/4\right)^l}{(l!)^2}. \tag{B5}$$

in equation (B3), which yields

$$D_x(\rho, L) \approx -2.606k^2LC_n^2 \sum_{l=1}^{\infty} \frac{\left(-\rho^2/4\right)^l}{(l!)^2} \int_0^{\infty} \kappa^{2l-8/3} \exp\left(-\frac{\kappa^2}{\kappa_{xm}^2}\right) d\kappa. \tag{B6}$$

The integral in (B6) can be evaluated as[22]

$$\int_0^{\infty} \kappa^{2l-8/3} \exp\left(-\frac{\kappa^2}{\kappa_{xm}^2}\right) d\kappa = \frac{1}{2}\kappa_{xm}^{2l-5/3}\Gamma\left(l - \frac{5}{6}\right) \tag{B7}$$

where $\Gamma(x)$ is the Gamma function. Note that this integral requires that the exponent on κ be greater than negative one. This condition is satisfied as $l \geq 1$ so that $2l - 8/3 \geq -2/3$. Thus, we now have

$$D_x(\rho, L) \approx -1.303k^2LC_n^2\kappa_{xm}^{-5/3} \sum_{l=1}^{\infty} \frac{\left(-\rho^2\kappa_{xm}^2/4\right)^l}{(l!)^2}\Gamma\left(l - \frac{5}{6}\right) \tag{B8}$$

Note the following *Pochhammer* relations[22]

$$\Gamma\left(l - \frac{5}{6}\right) = \left(-\frac{5}{6}\right)_l \Gamma\left(-\frac{5}{6}\right) \approx -6.68\left(-\frac{5}{6}\right)_l, \tag{B9}$$

$$(1)_l = l!, \tag{B10}$$

where $(a)_l = \Gamma(a+l)/\Gamma(a)$. Using these relations, the large scale component of the wave structure function is now given by

$$D_x(\rho, L) \approx 8.7k^2 L C_n^2 \kappa_{xm}^{-5/3} \left[{}_1F_1\left(-\tfrac{5}{6}; 1; -\tfrac{\rho^2 \kappa_{xm}^2}{4}\right) - 1 \right]. \tag{B11}$$

Now taking the limit as the inner scale goes to zero, so that $\kappa_{xm}^2 \to \kappa_x^2$, and making the approximation

$${}_1F_1\left(-\tfrac{5}{6}; 1; -x\right) - 1 \approx \frac{5x}{6}(1 + 0.232x)^{-1/6}, \tag{B12}$$

we obtain

$$D_x(\rho, L) = 1.47\sigma_1^2 \left(\frac{k\rho^2 \eta_{x(pl)}^{1/6}}{L}\right)\left(1 + 0.058\frac{k\rho^2 \eta_{x(pl)}}{L}\right)^{-1/6}, \tag{B13}$$

where

$$\eta_{x(pl)} = \frac{L\kappa_{x(pl)}^2}{k} = \frac{2.61}{1 + 1.11\left(\sigma_1^2\right)^{6/5}} \tag{B14}$$

Now substituting the small scale portion, (B2), into (78) we have the small scale portion of the plane wave structure function

$$\begin{aligned} D_y(\rho, L) \approx\ & 2.606k^2 L C_n^2 \int_0^\infty [1 - J_0(\kappa\rho)] \frac{\kappa}{\left(\kappa^2 + \kappa_0^2\right)^{-11/6}} \\ & \times \left\{ \exp\left(-\frac{\kappa^2}{\kappa_m^2}\right) - \exp\left(-\frac{\kappa^2}{\kappa_{ym}^2}\right) \right\} d\kappa, \end{aligned} \tag{B15}$$

where

$$\kappa_{ym}^2 = \frac{\kappa_m^2 \kappa_{y(pl)}^2}{\kappa_{y(pl)}^2 + \kappa_m^2}. \tag{B16}$$

The refractive index spatial frequency cutoff, $\kappa_{y(pl)}$, is defined by (B22). We can express $D_y(\rho, L)$ as the sum of the two integrals

$$I_1 = 2.606k^2LC_n^2\int_0^\infty [1 - J_0(\kappa\rho)]\frac{\kappa}{\left(\kappa^2+\kappa_0^2\right)^{11/6}}\exp\left(-\frac{\kappa^2}{\kappa_m^2}\right)d\kappa, \tag{B17}$$

$$I_2 = -2.606k^2LC_n^2\int_0^\infty [1 - J_0(\kappa\rho)]\frac{\kappa}{\left(\kappa^2+\kappa_0^2\right)^{11/6}}\exp\left(-\frac{\kappa^2}{\kappa_{ym}^2}\right)d\kappa. \tag{B18}$$

The integral I_1 is the standard Rytov plane wave structure function using the von Kármán spectrum, (26), and it's solution is presented by Andrews and Phillips.[2] It is in this integral that both the inner and outer scales are required for convergence. However, as shown in [2], after completion of the integration the dependency on the inner and outer scale can be removed by applying the restriction $l_0 \ll \rho \ll L_0$. This yields

$$I_1 \approx 2.37\sigma_1^2\left(\frac{k\rho^2}{L}\right)^{5/6}, \qquad l_0 \ll \rho \ll L_0 \tag{B19}$$

The outer scale is not necessary for convergence of the integral I_2. So, letting the outer scale approach infinity, the integral I_2 reduces to

$$I_2 = -2.606k^2LC_n^2\int_0^\infty \kappa^{-8/3}[1 - J_0(\kappa\rho)]\exp\left(-\frac{\kappa^2}{\kappa_{ym}^2}\right)d\kappa, \tag{B20}$$

which is of the exact same form as (B3) and can therefore be evaluated in the same manner. Thus, the small scale component of the plane wave structure function is given by

$$D_y(\rho, L) = 2.37\sigma_1^2 \left(\frac{k\rho^2}{L}\right)^{5/6} - 1.47\sigma_1^2 \left(\frac{k\rho^2 \eta_{y(pl)}^{1/6}}{L}\right)\left(1 + 0.058\frac{k\rho^2 \eta_{y(pl)}}{L}\right)^{-1/6}, \quad \text{(B21)}$$

where

$$\eta_{y(pl)} = \frac{L\kappa_{y(pl)}^2}{k} = 3\left[1 + 0.69\left(\sigma_1^2\right)^{6/5}\right]. \quad \text{(B22)}$$

The plane wave structure function is now the sum of the large and small scale components, i.e. $D(\rho, L) = D_x(\rho, L) + D_y(\rho, L)$.

APPENDIX C. HORIZONTAL PATH SPHERICAL WSF

To develop a horizontal path spherical wave structure function using the modified Rytov method, we follow the same method as presented in Appendix B. We substitute the large and small scale components of the effective atmospheric spectrum, where we let $f(\kappa l_0) = \exp\left(-\frac{\kappa^2}{\kappa_m^2}\right)$ and $g(\kappa L_0) = \kappa^{11/3}\left(\kappa^2+\kappa_0^2\right)^{-11/6}$, into the spherical wave structure function integral definition given by (90) and evaluate. Substituting the large scale portion of the effective atmospheric spectrum, (B1), into the integral definition, (90), we have the large scale portion of the spherical wave structure function

$$D_x(\rho, L) \approx 2.606k^2LC_n^2\int_0^1\int_0^\infty \kappa^{-8/3}\left[1-J_0(\kappa\xi\rho)\right]\exp\left(-\frac{\kappa^2}{\kappa_{xm}^2}\right)d\kappa d\xi, \tag{C1}$$

where κ_{xm}^2 is given by

$$\kappa_{xm}^2 = \frac{\kappa_m^2\kappa_{x(sp)}^2}{\kappa_{x(sp)}^2+\kappa_m^2}. \tag{C2}$$

The refractive index spatial frequency cutoff, $\kappa_{x(sp)}$, is defined by (C12). As in the plane wave case, the outer scale is not required for convergence of the integral in the large scale portion of the wave structure function . Following the calculations in Appendix B, the Bessel function, $J_0(x)$, in (C1) is replaced by it's series representation[22]

$$1-J_0(\kappa\rho) = -\sum_{l=1}^{\infty}\frac{\left(-\kappa^2\xi^2\rho^2/4\right)^l}{(l!)^2}. \tag{C3}$$

Using (C3) in (C2), we now have

$$D_x(\rho, L) \approx -2.606k^2LC_n^2 \sum_{l=1}^{\infty} \frac{\left(-\rho^2/4\right)^l}{(l!)^2} \int_0^1 \xi^{2l} d\xi \times \int_0^{\infty} \kappa^{2l-8/3} \exp\left(-\frac{\kappa^2}{\kappa_{xm}^2}\right) d\kappa \tag{C4}$$

The first integral in (C4) is evaluated as

$$\int_0^1 \xi^{2l} d\xi = \frac{1}{2l+1} \tag{C5}$$

Noting the Pochhammer relations[22]

$$(2l)! = 2^{2l} \left(\tfrac{1}{2}\right)_l l!, \tag{C6}$$

$$(2l+1)! = 2^{2l} \left(\tfrac{3}{2}\right)_l l!, \tag{C7}$$

(C5) can be expressed as

$$\frac{1}{2l+1} = \frac{\left(\frac{1}{2}\right)_l}{\left(\frac{3}{2}\right)_l}. \tag{C8}$$

The second integral in (C4) is identical to the integral (B7) of the plane wave case and it's solution has already been presented. Thus, the large scale portion of the spherical wave structure function is now given by

$$D_x(\rho, L) = 8.7C_n^2k^2L\kappa_{xm}^{-5/3} \left[{}_2F_2\left(-\tfrac{5}{6}, \tfrac{1}{2}; 1, \tfrac{3}{2}; -\tfrac{\rho^2\kappa_{xm}^2}{4}\right) - 1\right]. \tag{C9}$$

Now taking the limit as the inner scale goes to zero, so that $\kappa_{xm}^2 \rightarrow \kappa_x^2$, and making the approximation

$$ {}_2F_2\left(-\tfrac{5}{6}, \tfrac{1}{2}; 1, \tfrac{3}{2}; -x\right) - 1 \approx \frac{5x}{18}\left(1 + 0.132x\right)^{-1/6}, \tag{C10} $$

we obtain

$$ D_x\left(\rho, L\right) = 0.49\sigma_1^2 \left(\frac{k\rho^2 \eta_{x(sp)}^{1/6}}{L}\right)\left(1 + 0.033\frac{k\rho^2\eta_{x(sp)}}{L}\right)^{-1/6}, \tag{C11} $$

where

$$ \eta_{x(sp)} = \frac{L\kappa_{x(sp)}^2}{k} = \frac{8.56}{1 + 0.19\left(\sigma_1^2\right)^{6/5}}. \tag{C12} $$

Now substituting the small scale portion, (B2), into (90) we have the small scale portion of the spherical wave structure function

$$ \begin{aligned} D_y\left(\rho, L\right) \approx\ & 2.606k^2 L C_n^2 \int_0^\infty \left[1 - J_0\left(\kappa\xi\rho\right)\right] \frac{\kappa}{\left(\kappa^2 + \kappa_0^2\right)^{-11/6}} \\ & \times \left\{\exp\left(-\frac{\kappa^2}{\kappa_m^2}\right) - \exp\left(-\frac{\kappa^2}{\kappa_{ym}^2}\right)\right\} d\kappa, \end{aligned} \tag{C13} $$

where

$$ \kappa_{ym}^2 = \frac{\kappa_m^2 \kappa_{y(sp)}^2}{\kappa_{y(sp)}^2 + \kappa_m^2}. \tag{C14} $$

The refractive index spatial frequency cutoff, $\kappa_{y(sp)}$, is defined by (C20). We can express $D_y\left(\rho, L\right)$ as the sum of the two integrals

$$ I_1 = 2.606k^2 L C_n^2 \int_0^\infty \left[1 - J_0\left(\kappa\xi\rho\right)\right] \frac{\kappa}{\left(\kappa^2 + \kappa_0^2\right)^{11/6}} \exp\left(-\frac{\kappa^2}{\kappa_m^2}\right) d\kappa, \tag{C15} $$

$$I_2 = -2.606k^2 L C_n^2 \int_0^\infty \left[1 - J_0\left(\kappa\xi\rho\right)\right] \frac{\kappa}{\left(\kappa^2 + \kappa_0^2\right)^{11/6}} \exp\left(-\frac{\kappa^2}{\kappa_{ym}^2}\right) d\kappa. \tag{C16}$$

The integral I_1 is the standard Rytov spherical wave structure function using the von Kármán spectrum, (26), and it's solution is presented by Andrews and Phillips.[2] In this integral, both the inner and outer scales are required for convergence. However, as in the plane wave case, after completion of the integration the dependency on the inner and outer scale can be removed by applying the restriction $l_0 \ll \rho \ll L_0$. This yields

$$I_1 \approx 0.89\sigma_1^2 \left(\frac{k\rho^2}{L}\right)^{5/6}, \qquad l_0 \ll \rho \ll L_0 \tag{C17}$$

The outer scale is not necessary for convergence of the integral I_2. So, letting the outer scale approach infinity, the integral I_2 reduces to

$$I_2 = -2.606k^2 L C_n^2 \int_0^\infty \kappa^{-8/3} \left[1 - J_0\left(\kappa\xi\rho\right)\right] \exp\left(-\frac{\kappa^2}{\kappa_{ym}^2}\right) d\kappa, \tag{C18}$$

which is of the exact same form as (C1) and can therefore be evaluated in the same manner. Thus, the small scale component of the spherical wave structure function is given by

$$D_y\left(\rho, L\right) = 0.89\sigma_1^2 \left(\frac{k\rho^2}{L}\right)^{5/6} - 0.49\sigma_1^2 \left(\frac{k\rho^2 \eta_{y(sp)}^{1/6}}{L}\right)\left(1 + 0.033\frac{k\rho^2 \eta_{y(sp)}}{L}\right)^{-1/6}, \tag{C19}$$

where

$$\eta_{y(sp)} = \frac{L\kappa_{y(sp)}^2}{k} = 9\left[1 + 0.23\left(\sigma_1^2\right)^{6/5}\right]. \tag{C20}$$

The spherical wave structure function is now the sum of the large and small scale components, i.e.

$D(\rho, L) = D_x(\rho, L) + D_y(\rho, L)$.

APPENDIX D. HORIZONTAL PATH GAUSSIAN-BEAM WSF

When $\mathbf{r}_1 = -\mathbf{r}_2$, the Gaussian-beam wave structure function, $D(\rho)$, is given by[2]

$$D(\rho, L) = d(\rho, L) + 4\sigma_r^2(\rho, L), \tag{D1}$$

where $d(\rho, L)$ describes the on axis, or longitudinal, component and $\sigma_r^2(\rho, L)$ describes the transverse, or radial, component and are given by

$$d(\rho, L) = 8\pi^2 k^2 L \int_0^1 \int_0^\infty \kappa \Phi_n(\kappa) \exp\left(-\frac{\Lambda L \kappa^2 \xi^2}{k}\right) \left\{1 - J_0\left[\left(1 - \bar{\Theta}\xi\right)\rho\kappa\right]\right\} d\kappa d\xi, \tag{D2}$$

$$\sigma_r^2(\rho, L) = 2\pi^2 k^2 L \int_0^1 \int_0^\infty \kappa \Phi_n(\kappa) \exp\left(-\frac{\Lambda L \kappa^2 \xi^2}{k}\right) \left[I_0(\Lambda \rho \xi \kappa) - 1\right] d\kappa d\xi. \tag{D3}$$

We apply the modified Rytov method to develop Gaussian-beam wave structure function results by substituting the effective atmospheric spectrum, (67), into each of the integrals (D2) and (D3). Note, in the Gaussian beam case, the exponential functions appearing in (D2) and (D3) allow for the convergence of the integrals without the inclusion of a finite inner or outer scale. Thus, we set $f(\kappa l_0) = g(\kappa L_0) = 1$. Substituting the large scale portion of the effective spectrum, (B1), into the longitudinal component, (D2), we obtain

$$\begin{aligned} d_x(\rho, L) &= 2.606 C_n^2 k^2 L \int_0^1 \int_0^\infty \kappa^{-8/3} \exp\left(-\frac{\kappa^2}{\kappa_{x(gb)}^2}\right) \exp\left(-\frac{\Lambda L \kappa^2 \xi^2}{k}\right) \\ &\quad \times \left\{1 - J_0\left[\left(1 - \bar{\Theta}\xi\right)\rho k\right]\right\} d\kappa d\xi. \end{aligned} \tag{D4}$$

In (D4), we make the argument that $\exp\left(-\frac{\kappa^2}{\kappa_{x(gb)}^2}\right)$ acts as a low-pass spatial filter, ensuring that under the integral[7]

$$\exp\left(-\frac{\Lambda L\kappa^2\xi^2}{k}\right) \approx 1, \tag{D5}$$

so that the integral (D4) is approximately given by

$$\begin{aligned} d_x(\rho, L) &= 2.606C_n^2k^2L\int_0^1\int_0^\infty \kappa^{-8/3}\exp\left(-\frac{\kappa^2}{\kappa_{x(gb)}^2}\right) \\ &\quad\times\left\{1 - J_0\left[\left(1-\bar{\Theta}\xi\right)\rho k\right]\right\}d\kappa d\xi \end{aligned} \tag{D6}$$

Letting $\eta = \frac{L\kappa^2}{k}$ and $\eta_{x(gb)} = \frac{L\kappa_{x(gb)}^2}{k}$, the integral (D6) becomes

$$\begin{aligned} d_x(\rho, L) &= 1.303C_n^2k^{7/6}L^{11/6}\int_0^1\int_0^\infty \eta^{-11/6}\exp\left(-\frac{\eta}{\eta_{x(gb)}}\right) \\ &\quad\times\left\{1 - J_0\left[\left(1-\bar{\Theta}\xi\right)\sqrt{\frac{k\eta\rho^2}{L}}\right]\right\}d\eta d\xi. \end{aligned} \tag{D7}$$

Now, expressing the Bessel function, $J_0(x)$, in its series form

$$1 - J_0\left[\left(1-\bar{\Theta}\xi\right)\sqrt{\frac{k\eta\rho^2}{L}}\right] = -\sum_{l=1}^{\infty}\frac{\left(1-\bar{\Theta}\xi\right)^{2l}}{(l!)^2}\left(-\frac{k\eta\rho^2}{4L}\right)^l \tag{D8}$$

the large scale longitudinal component becomes

$$\begin{aligned} d_x(\rho, L) &\approx -1.06\sigma_1^2 \sum_{l=1}^{\infty} \frac{\left(-\frac{k\rho^2}{4L}\right)^l}{(l!)^2} \int_0^1 \left(1-\bar{\Theta}\xi\right)^{2l} d\xi \\ &\quad \times \int_0^{\infty} \eta^{l-11/6} \exp\left(-\frac{\eta}{\eta_{x(gb)}}\right) d\eta. \end{aligned} \tag{D9}$$

We can evaluate the two integrals in (D9) as

$$\begin{aligned} &\int_0^{\infty} \eta^{l-11/6} \exp\left(-\frac{\eta}{\eta_{x(gb)}}\right) d\eta \\ &= n_{x(gb)}^{l-5/6} \Gamma\left(l-\frac{5}{6}\right) \\ &= n_{x(gb)}^{l-5/6} \left(-\frac{5}{6}\right)_l \Gamma\left(-\frac{5}{6}\right) \\ &\approx -6.68 n_{x(gb)}^{l-5/6} \left(-\frac{5}{6}\right)_l, \end{aligned} \tag{D10}$$

$$\int_0^1 \left(1-\bar{\Theta}\xi\right)^{2l} d\xi = \left(\frac{1}{\bar{\Theta}}\right)\left(\frac{1}{2l+1} - \frac{\Theta^{2l+1}}{2l+1}\right). \tag{D11}$$

Substituting (D10) and (D11) into (D9) yields

$$\begin{aligned} d_x(\rho, L) &\approx 7.08\sigma_1^2 \eta_{x(gb)}^{-5/6} \left[\frac{1}{\bar{\Theta}} {}_2F_2\left(-\tfrac{5}{6}, \tfrac{1}{2}; 1, \tfrac{3}{2}; -\tfrac{\rho^2 k \eta_{x(gb)}}{4L}\right)\right. \\ &\quad \left. -\frac{\Theta}{\bar{\Theta}} {}_2F_2\left(-\tfrac{5}{6}, \tfrac{1}{2}; 1, \tfrac{3}{2}; -\tfrac{\rho^2 k \Theta^2 \eta_{x(gb)}}{4L}\right) - 1\right]. \end{aligned} \tag{D12}$$

Finally, applying the approximation for the hypergeometric function given by (C10), the large scale longitudinal component is given by

$$d_x(\rho, L) = 0.49\sigma_1^2 \eta_{x(gb)}^{1/6} \left(\frac{k\rho^2}{L}\right) \left[\frac{1}{\bar{\Theta}} \left(1 + 0.033 \frac{k\rho^2 \eta_{x(gb)}}{L}\right)^{-1/6} - \frac{\Theta^3}{\bar{\Theta}} \left(1 + 0.033 \frac{k\rho^2 \Theta^2 \eta_{x(gb)}}{L}\right)^{-1/6}\right], \quad \text{(D13)}$$

where $\eta_{x(gb)}$ is defined by (113).

Now, substituting the small scale portion of the effective atmospheric spectrum, (B2), into (D2), yields the small scale longitudinal component

$$\begin{aligned} d_y(\rho, L) = {} & 2.606 C_n^2 k^2 L \int_0^1 \int_0^\infty \kappa^{-8/3} \exp\left(-\frac{\Lambda L \kappa^2 \xi^2}{k}\right) \\ & \times \left\{1 - J_0\left[\left(1 - \bar{\Theta}\xi\right)\rho k\right]\right\} d\kappa d\xi \\ & - 2.606 C_n^2 k^2 L \int_0^1 \int_0^\infty \kappa^{-8/3} \exp\left(-\frac{\Lambda L \kappa^2 \xi^2}{k}\right) \exp\left(-\frac{\kappa^2}{\kappa_{y(gb)}^2}\right) \\ & \times \left\{1 - J_0\left[\left(1 - \bar{\Theta}\xi\right)\rho k\right]\right\} d\kappa d\xi \end{aligned} \quad \text{(D14)}$$

The first integral in (D14) is equivalent to standard Rytov method longitudinal component using the Kolmogorov spectrum and it's solution is presented by Andrews and Phillips.[2] The second integral is of the exact same form as the large scale component, (D4), and can be evaluated in the same manner. Note that we argue that $\exp\left(-\frac{\kappa^2}{\kappa_{y(gb)}^2}\right)$ also acts as a low-pass spatial filter so that the approximation given by (D5) is used in the small scale case as well. In the same manner

as the large scale component, this yields the small scale longitudinal component

$$d_y(\rho, L) = 0.889\sigma_1^2\left[A\left(\frac{k\rho^2}{L}\right)^{5/6}\right] - 0.49\sigma_1^2\eta_{y(gb)}^{1/6}\left(\frac{k\rho^2}{L}\right)\left[\frac{1}{\bar{\Theta}}\left(1+0.033\frac{k\rho^2\eta_{y(gb)}}{L}\right)^{-1/6} - \frac{\Theta^3}{\bar{\Theta}}\left(1+0.033\frac{k\rho^2\Theta^2\eta_{y(gb)}}{L}\right)^{-1/6}\right] \tag{D15}$$

where A is given by (106) and $\eta_{y(gb)}$ is given by (114). The longitudinal component is now the sum of the large and small scale components, i.e. $d(\rho, L) = d_x(\rho, L) + d_y(\rho, L)$.

To evaluate the radial component, we substitute the effective atmospheric spectrum into (D3) where again we let $f(\kappa l_0) = g(\kappa L_0) = 1$. Substituting the large scale component of the effective spectrum into (D3) yields

$$\sigma_{r,x}^2(\rho, L) = 0.65C_n^2k^2L\int_0^1\int_0^\infty \kappa^{-8/3}\exp\left(-\frac{\kappa^2}{\alpha_x^2}\right)\{I_0(\Lambda\rho\xi\kappa) - 1\}\,d\kappa d\xi, \tag{D16}$$

where

$$\alpha_x^2 = \frac{k\kappa_x^2}{k + \kappa_x^2\Lambda L\xi^2}. \tag{D17}$$

Notice, in the radial component we do not use the approximation given by (D5). Using this approximation in the radial component produces large errors that were not observed in the longitudinal component. Expressing the modified Bessel function, $I_0(x)$ in (D16) by its series

representation[22] and completing the remaining integration, we obtain

$$\sigma_{r,x}^2(\rho, L) = \frac{0.65 C_n^2 k^2 L \kappa_x^{-5/3}}{4} \times \sum_{l=1}^{\infty} \frac{\left(0.25\Lambda^2\rho^2\kappa_x^2\right)^l}{(l!)^2} \frac{\Gamma\left(l-\frac{5}{6}\right)}{\left(l+\frac{1}{2}\right)} {}_2F_1\left(l-\tfrac{5}{6}, l+\tfrac{1}{2}; l+\tfrac{3}{2}; -\tfrac{\kappa_x^2\Lambda L}{k}\right). \quad \text{(D18)}$$

It can be shown numerically that for the range of parameters under consideration, the series in (D18) is dominated by the first term. Hence, approximating (D18) by its first term, the large scale portion of the radial component of the Gaussian-beam wave structure function is given by

$$\sigma_{r,x}^2(\rho, L) \approx 0.123\sigma_1^2 \left(\frac{k}{L}\right) \Lambda^2\rho^2\eta_x^{1/6} {}_2F_1\left(\tfrac{1}{6}, \tfrac{3}{2}; \tfrac{5}{2}; -\eta_x^2\Lambda\right). \quad \text{(D19)}$$

Finally, making the approximation

$${}_2F_1\left(\tfrac{1}{6}, \tfrac{3}{2}; \tfrac{5}{2}; -x\right) \approx [1 + 0.547x]^{-1/6}, \quad \text{(D20)}$$

we have

$$\sigma_{r,x}^2(\rho, L) \approx 0.123\sigma_1^2 \left(\frac{k\rho^2\Lambda^2}{L}\right) \eta_{x(gb)}^{1/6} \left(1 + 0.547\Lambda\eta_{x(gb)}\right)^{-1/6}. \quad \text{(D21)}$$

Substituting the small scale component of the effective spectrum into the radial component, (D3), yields

$$\begin{aligned}\sigma_{r,y}^2(\rho,L) &= 0.65C_n^2k^2L\int_0^1\int_0^\infty \kappa^{-8/3}\exp\left(-\frac{\Lambda L\kappa^2\xi^2}{k}\right)\{I_0(\Lambda\rho\xi\kappa)-1\}\,d\kappa d\xi \\ &\quad -0.65C_n^2k^2L\int_0^1\int_0^\infty \kappa^{-8/3}\exp\left(-\frac{\kappa^2}{\alpha_y^2}\right)\{I_0(\Lambda\rho\xi\kappa)-1\}\,d\kappa d\xi, \qquad \text{(D22)}\end{aligned}$$

where

$$\alpha_y^2 = \frac{k\kappa_x^2}{k+\kappa_x^2\Lambda L\xi^2}. \qquad \text{(D23)}$$

The first integral in (D22) is the standard Rytov equation for the radial component and its solution is presented by Andrews and Phillips.[2] The second integral in (D22) is of the same form as (D16) and is evaluated in the exact same manner. Thus, the small scale portion of the radial component is given by

$$\begin{aligned}\sigma_{r,y}^2(\rho,L) &= 0.137\sigma_1^2\Lambda^{11/6}\left(\frac{k\rho^2}{L}\right) \\ &\quad -0.123\sigma_1^2\left(\frac{k\rho^2\Lambda^2}{L}\right)\eta_{y(gb)}^{1/6}\left(1+0.547\Lambda\eta_{y(gb)}\right)^{-1/6}. \qquad \text{(D24)}\end{aligned}$$

The radial component is now the sum of the large and small scale components, i.e. $\sigma_r^2(\rho,L) = \sigma_{r,x}^2(\rho,L)+\sigma_{r,y}^2(\rho,L)$.

APPENDIX E. FREQUENCY VARIANCE DEFINITION

In this appendix, the relation between the phase covariance function and the frequency variance is derived. To do so, it is necessary to relate the derivative of a random process, namely $\phi_s'(t)$, to the process itself, namely $\phi_s(t)$. We assume that $\phi_s(t)$ is a linear random process, that is[32]

$$\left\langle L\left[\phi_s(t)\right]\right\rangle = L\left[\left\langle\phi_s(t)\right\rangle\right], \tag{E1}$$

where $\left\langle\phi_s(t)\right\rangle$ is the ensemble average or mean value of $\phi_s(t)$ and L is an operator. In this case, let L be the differentiation operator, so that

$$\left\langle L\left[\phi_s(t)\right]\right\rangle = L\left[\left\langle\phi_s(t)\right\rangle\right] = \left\langle\phi_s(t)\right\rangle'. \tag{E2}$$

Let ϕ_1 and ϕ_2 denote the random variables taken from $\phi_s(t)$ at times t_1 and t_2, respectively. Let $R_{s,s}(t_1,t_2)$ be the correlation function of $\phi_s(t)$, and let L_1 and L_2 denote the differentiation operators with respect to t_1 and t_2, respectively. Then,[32]

$$R_{s',s}(t_1,t_2) = L_1\left[R_{s,s}(t_1,t_2)\right] = \frac{\partial}{\partial t_1}R_{s,s}(t_1,t_2), \tag{E3}$$

$$R_{s,s'}(t_1,t_2) = L_2\left[R_{s,s}(t_1,t_2)\right] = \frac{\partial}{\partial t_2}R_{s,s}(t_1,t_2), \tag{E4}$$

so

$$R_{s',s'}(t_1,t_2) = L_1L_2\left[R_{s,s}(t_1,t_2)\right] = \frac{\partial^2}{\partial t_1\partial t_2}R_{s,s}(t_1,t_2). \tag{E5}$$

Note that (E5) provides a relation between the *phase correlation function*, $R_{s,s}(t_1, t_2)$, and the *frequency correlation function*, $R_{s',s'}(t_1, t_2)$ Further assume that $\phi_s(t)$ is wide sense stationary (wss) with constant mean, m. Hence,

$$\langle \phi_s'(t) \rangle = \langle \phi_s(t) \rangle' = 0 \tag{E6}$$

Furthermore, letting $\tau = t_1 - t_2$, we have $R_{s,s}(t_1, t_2) = R_{s,s}(\tau)$ and

$$\frac{\partial}{\partial t_1} R_{s,s}(t_1 - t_2) = \frac{\partial}{\partial \tau} R_{s,s}(\tau), \tag{E7}$$

$$\frac{\partial}{\partial t_2} R_{s,s}(t_1 - t_2) = -\frac{\partial}{\partial \tau} R_{s,s}(\tau), \tag{E8}$$

so

$$R_{s',s'}(\tau) = \frac{\partial^2}{\partial t_1 \partial t_2} R_{s,s}(t_1 - t_2) = -\frac{\partial^2}{\partial \tau^2} R_{s,s}(\tau) = -R_{s,s}''(\tau). \tag{E9}$$

Additionally, the covariance function $B_{s,s}(\tau)$ of $\phi_s(t)$ is given by

$$B_{s,s}(\tau) = R_{s,s}(\tau) - m^2, \tag{E10}$$

where m was assumed to be constant, so

$$B_{s,s}''(\tau) = \frac{d^2}{d\tau^2} B_{s,s}(\tau) = \frac{d^2}{d\tau^2} \left[R_{s,s}(\tau) - m^2 \right] = R_{s,s}''(\tau). \tag{E11}$$

In general, the variance, σ_x^2, of a random variable, x, is obtained by setting $\tau = 0$ in its corresponding covariance function, $B_x(\tau)$. Hence from this definition, we obtain the frequency variance by

$$\begin{aligned}
\sigma_f^2 &= \sigma_{s',s'}^2 = B_{s',s'}(0) \\
&= R_{s',s'}(0) - \left\langle \phi_s'(t) \right\rangle^2 \\
&= R_{s',s'}(0) \\
&= -R_{s,s}''(\tau)\big|_{\tau=0}. \\
&= -B_{s,s}''(\tau)\big|_{\tau=0}
\end{aligned} \tag{E12}$$

Converting from *radians*^{2} to *Hertz*^{2}, we have

$$\sigma_f^2 = -\frac{B_s''(\tau)}{4\pi^2}\bigg|_{\tau=0}, \tag{E13}$$

where we rewrite $B_{s,s}$ as B_s for simplicity.

APPENDIX F. PLANE AND SPHERICAL WAVE FREQUENCY VARIANCE

In order to develop expressions for the frequency variance, σ_f^2, we note the relation given previously

$$\sigma_f^2 = -\frac{B_s''(\tau)}{4\pi^2}\bigg|_{\tau=0}, \tag{F1}$$

where $B_s(\tau)$ is the temporal phase covariance function and the differentiation is with respect to τ. The plane wave temporal phase covariance function is given by[2]

$$B_{s,pl}(V\tau) = 2\pi^2 k^2 L \int_0^1 \int_0^\infty \kappa \Phi_n(\kappa) J_0(\kappa V\tau) \left[1 + \cos\left(\frac{L\kappa^2\xi}{k}\right)\right] d\kappa d\xi. \tag{F2}$$

Thus, to apply the relation given by (F1), we first differentiate this expression with respect to τ and take the limit as τ goes to zero. Thus, noting that

$$\lim_{\tau \longrightarrow 0} \frac{d^2}{d\tau^2} J_0(\kappa V\tau) = -\frac{\kappa^2 V^2}{2}, \tag{F3}$$

we find that the plane wave frequency variance is given by

$$\sigma_{f,pl}^2 = 0.25 k^2 L V^2 \int_0^1 \int_0^\infty \kappa^3 \Phi_n(\kappa) \left[1 + \cos\left(\frac{L\kappa^2\xi}{k}\right)\right] d\kappa d\xi. \tag{F4}$$

Using the standard Rytov method, the Hill spectrum given by (151) is substituted into (F4) yielding

$$\sigma_{f,pl}^2 = 0.00825 C_n^2 k^2 L V^2 \left[I_1 + 1.802 I_2 - 0.254 I_3\right], \tag{F5}$$

where I_1, I_2, and I_3 are integral quantities that are evaluated below. The first integral, I_1, is given by

$$I_1 = \int_0^1 \int_0^\infty \kappa^{-2/3} \exp\left(-\frac{\kappa^2}{\kappa_l^2}\right)\left[1 + \cos\left(\frac{L\kappa^2\xi}{k}\right)\right] d\kappa d\xi, \tag{F6}$$

which we treat as the sum of two integrals, I_a and I_b. The first integral is evaluated by letting $t^2 = \kappa^2/\kappa_l^2$, which yields

$$\begin{aligned} I_a &= \int_0^\infty \kappa^{-2/3} \exp\left(-\frac{\kappa^2}{\kappa_l^2}\right) d\kappa \\ &= \kappa_l^{1/3} \int_0^\infty t^{-2/3} \exp\left(-t^2\right) dt \\ &= \left(\frac{1}{2}\right)\Gamma\left(\frac{1}{6}\right)\kappa_l^{1/3} \\ &\approx 2.78\kappa_l^{1/3}. \end{aligned} \tag{F7}$$

The second integral is given by

$$I_b = \int_0^1 \int_0^\infty \kappa^{-2/3} \exp\left(-\frac{\kappa^2}{\kappa_l^2}\right) \cos\left(\frac{L\kappa^2\xi}{k}\right) d\kappa d\xi \tag{F8}$$

Expressing the cosine function in it's series representation, we now have

$$I_b = \sum_{n=0}^{\infty} \frac{\left(-L^2/k^2\right)^n}{(2n)!} \int_0^1 \xi^{2n} d\xi \int_0^\infty \kappa^{4n-2/3} \exp\left(-\frac{\kappa^2}{\kappa_l^2}\right) d\kappa. \tag{F9}$$

Now letting $t^2 = \kappa^2/\kappa_l^2$ and completing the integration on ξ we have

$$\begin{aligned} I_b &= \sum_{n=0}^{\infty} \frac{\left(-L^2/k^2\right)^n}{(2n)!} \frac{1}{(2n+1)} \kappa_l^{4n+1/3} \int_0^{\infty} t^{4n-2/3} \exp\left(-t^2\right) d\kappa \\ &= \frac{\kappa_l^{1/3}}{2} \sum_{n=0}^{\infty} \frac{\left(-L^2\kappa_l^4/k^2\right)^n}{(2n+1)!} \Gamma\left(2n+\frac{1}{6}\right) \end{aligned} \tag{F10}$$

Using the Pochhammer relations

$$\begin{aligned} \Gamma\left(2n+\frac{1}{6}\right) &= \left(\frac{1}{6}\right)_{2n} \Gamma\left(\frac{1}{6}\right) \\ &= 2^{2n} \left(\frac{1}{12}\right)_n \left(\frac{7}{12}\right)_n \Gamma\left(\frac{1}{6}\right), \end{aligned} \tag{F11}$$

$$\frac{1}{(2n+1)!} = \frac{1}{2^{2n}\,(3/2)_n\, n!}, \tag{F12}$$

we have

$$I_b = \Gamma\left(\frac{1}{6}\right) \frac{\kappa_l^{1/3}}{2} {}_2F_1\left(\tfrac{1}{12}, \tfrac{7}{12}; \tfrac{3}{2}; -Q_l^2\right), \tag{F13}$$

where $Q_l = L\kappa_l^2/k$. Making the approximation

$${}_2F_1\left(\tfrac{1}{12}, \tfrac{7}{12}; \tfrac{3}{2}; -x\right) \approx \left[1 + 0.28x\right]^{-1/12}, \tag{F14}$$

we obtain

$$I_1 \approx \Gamma\left(\frac{1}{6}\right) \frac{\kappa_l^{1/3}}{2} \left\{1 + \left[1 + 0.28\,Q_l^2\right]^{-1/12}\right\}. \tag{F15}$$

The second integral, I_2, is given by

$$I_2 = \int_0^1 \int_0^\infty \frac{\kappa^{1/3}}{\kappa_l} \exp\left(-\frac{\kappa^2}{\kappa_l^2}\right)\left[1 + \cos\left(\frac{L\kappa^2\xi}{k}\right)\right] d\kappa d\xi. \tag{F16}$$

This integral is evaluated in the same manner as I_1. Considering I_2 as the sum of the two integrals I_c and I_d, we have

$$\begin{aligned} I_c &= \frac{1}{\kappa_l}\int_0^\infty \kappa^{1/3} \exp\left(\frac{\kappa^2}{\kappa_l^2}\right) d\kappa \\ &= \Gamma\left(\frac{2}{3}\right)\frac{\kappa_l^{1/3}}{2}, \end{aligned} \tag{F17}$$

$$\begin{aligned} I_d &= \int_0^1 \int_0^\infty \frac{\kappa^{1/3}}{\kappa_l} \exp\left(-\frac{\kappa^2}{\kappa_l^2}\right)\cos\left(\frac{L\kappa^2\xi}{k}\right) d\kappa d\xi \\ &= \frac{1}{\kappa_l}\sum_{n=0}^\infty \frac{\left(-L^2/k^2\right)^n}{(2n)!}\int_0^1 \xi^{2n} d\xi \int_0^\infty \kappa^{4n+1/3} \exp\left(-\frac{\kappa^2}{\kappa_l^2}\right) d\kappa \\ &= \frac{\kappa_l^{1/3}}{2}\sum_{n=0}^\infty \frac{\left(-L^2\kappa_l^4/k^2\right)^n}{(2n+1)!}\Gamma\left(2n+\frac{2}{3}\right). \end{aligned} \tag{F18}$$

Noting the Pochhammer relations given by (F12) and

$$\begin{aligned} \Gamma\left(2n+\frac{2}{3}\right) &= \Gamma\left(\frac{2}{3}\right)\left(\frac{2}{3}\right)_{2n} \\ &\quad 2^{2n}\Gamma\left(\frac{2}{3}\right)\left(\frac{1}{3}\right)_n\left(\frac{5}{6}\right)_n, \end{aligned} \tag{F19}$$

we have

$$I_d = \Gamma\left(\frac{2}{3}\right)\frac{\kappa_l^{1/3}}{2}{}_2F_1\left(\tfrac{1}{3},\tfrac{5}{6};\tfrac{3}{2};-Q_l^2\right). \tag{F20}$$

Making the approximation

$${}_2F_1\left(\tfrac{1}{3},\tfrac{5}{6};\tfrac{3}{2};-x\right) \approx [1+0.426x]^{-1/3}, \tag{F21}$$

we have

$$I_2 \approx \Gamma\left(\frac{2}{3}\right)\frac{\kappa_l^{1/3}}{2}\left\{1+\left[1+0.426Q_l^2\right]^{-1/3}\right\}. \tag{F22}$$

The third integral, I_3, is given by

$$I_3 = \int_0^1\int_0^\infty \frac{\kappa^{1/2}}{\kappa_l^{7/6}}\exp\left(-\frac{\kappa^2}{\kappa_l^2}\right)\left[1+\cos\left(\frac{L\kappa^2\xi}{k}\right)\right]d\kappa d\xi, \tag{F23}$$

and is also evaluated in the same manner as I_1 and I_2. Considering I_3 as the sum of the two integrals I_e and I_f, we have

$$\begin{aligned} I_e &= \kappa_l^{-7/6}\int_0^\infty \kappa^{1/2}\exp\left(\frac{\kappa^2}{\kappa_l^2}\right)d\kappa \\ &= \Gamma\left(\frac{3}{4}\right)\frac{\kappa_l^{1/3}}{2}, \end{aligned} \tag{F24}$$

$$
\begin{aligned}
I_f &= \kappa_l^{-7/6} \int_0^1 \int_0^\infty \kappa^{1/2} \exp\left(-\frac{\kappa^2}{\kappa_l^2}\right) \cos\left(\frac{L\kappa^2\xi}{k}\right) d\kappa d\xi \\
&= \kappa_l^{-7/6} \sum_{n=0}^{\infty} \frac{\left(-L^2/k^2\right)^n}{(2n)!} \int_0^1 \xi^{2n} d\xi \int_0^\infty \kappa^{4n+1/2} \exp\left(-\frac{\kappa^2}{\kappa_l^2}\right) d\kappa \\
&= \frac{\kappa_l^{1/3}}{2} \sum_{n=0}^{\infty} \frac{\left(-L^2\kappa_l^4/k^2\right)^n}{(2n+1)!} \Gamma\left(2n+\frac{3}{4}\right). \qquad \text{(F25)}
\end{aligned}
$$

Noting the Pochhammer relations given by (F12) and

$$
\Gamma\left(2n+\frac{3}{4}\right) = 2^{2n}\Gamma\left(\frac{3}{4}\right)\left(\frac{3}{8}\right)_n\left(\frac{7}{8}\right)_n, \qquad \text{(F26)}
$$

we have

$$
I_f = \Gamma\left(\frac{3}{4}\right)\frac{\kappa_l^{1/3}}{2}{}_2F_1\left(\tfrac{3}{8},\tfrac{7}{8};\tfrac{3}{2};-Q_l^2\right). \qquad \text{(F27)}
$$

Making the approximation

$$
{}_2F_1\left(\tfrac{3}{8},\tfrac{7}{8};\tfrac{3}{2};-x\right) \approx \left[1+0.4523x\right]^{-3/8}, \qquad \text{(F28)}
$$

we have

$$
I_3 \approx \Gamma\left(\frac{3}{4}\right)\frac{\kappa_l^{1/3}}{2}\left\{1+\left[1+0.4523Q_l^2\right]^{-3/8}\right\}. \qquad \text{(F29)}
$$

Finally, substituting (F15), (F22), and (F29) for I_1, I_2, and I_3, respectively, into (F5) and simplifying, we obtain the standard Rytov method plane wave frequency variance

$$\begin{aligned}\sigma^2_{f,pl,SR} \cong\ & 0.0258\sigma_1^2\left(\frac{k}{L}\right)V^2 Q_l^{1/6}\times\left\{1+0.723\left[1+0.28Q_l^2\right]^{-1/12}\right.\\ & \left.+0.317\left[1+0.426Q_l^2\right]^{-1/3}-0.04\left[1+0.4523Q_l^2\right]^{-3/8}\right\}. \end{aligned} \tag{F30}$$

To obtain an expression for the plane wave frequency variance using the modified Rytov method, we substitute the effective atmospheric spectrum (67) into (F4). As in Appendix B, we consider the effective spectrum as the sum of a large scale component, $\Phi_{n,x}(\kappa)$, given by (B1) and a small scale component, $\Phi_{n,y}(\kappa)$, given by (B2). Thus letting $g(\kappa L_0)=1$,

$$f(\kappa l_0)=\exp\left(-\frac{\kappa^2}{\kappa_l^2}\right)\left[1+1.802\left(\frac{\kappa}{\kappa_l}\right)-0.254\left(\frac{\kappa}{\kappa_l}\right)^{\frac{7}{6}}\right], \tag{F31}$$

and substituting the large scale portion of the effective spectrum into (F4) yields

$$\sigma^2_{f,x}=0.00825C_n^2k^2LV^2\left[I_1+1.802I_2-0.254I_3\right]. \tag{F32}$$

The three integrals, I_1 through I_3, in (F32), are defined by

$$I_1=\int_0^1\int_0^\infty \kappa^{-2/3}\exp\left(-\frac{\kappa^2}{\kappa_{xl}^2}\right)\left[1+\cos\left(\frac{L\kappa^2\xi}{k}\right)\right]d\kappa d\xi, \tag{F33}$$

$$I_2=\int_0^1\int_0^\infty \frac{\kappa^{1/3}}{\kappa_l}\exp\left(-\frac{\kappa^2}{\kappa_{xl}^2}\right)\left[1+\cos\left(\frac{L\kappa^2\xi}{k}\right)\right]d\kappa d\xi, \tag{F34}$$

$$I_3 = \int_0^1 \int_0^\infty \frac{\kappa^{1/2}}{\kappa_l^{7/6}} \exp\left(-\frac{\kappa^2}{\kappa_{xl}^2}\right)\left[1 + \cos\left(\frac{L\kappa^2\xi}{k}\right)\right] d\kappa d\xi, \tag{F35}$$

where

$$\kappa_{xl}^2 = \frac{\kappa_x^2 \kappa_l^2}{\kappa_x^2 + \kappa_l^2}. \tag{F36}$$

These integrals are identical in form to those in the standard Rytov derivation and are evaluated in the exact same manner. Their evaluation yields the equation given by (160). In the same manner, substituting the small scale portion of the effective spectrum, (B2), into (F4), yields

$$\sigma_{f,y}^2 = \sigma_{f,pl,SR}^2 - 0.00825 C_n^2 k^2 L V^2 \left[I_1 + 1.802 I_2 - 0.254 I_3\right], \tag{F37}$$

where $\sigma_{f,pl,SR}^2$ is given by (F30) and

$$I_1 = \int_0^1 \int_0^\infty \kappa^{-2/3} \exp\left(-\frac{\kappa^2}{\kappa_{yl}^2}\right)\left[1 + \cos\left(\frac{L\kappa^2\xi}{k}\right)\right] d\kappa d\xi, \tag{F38}$$

$$I_2 = \int_0^1 \int_0^\infty \frac{\kappa^{1/3}}{\kappa_l} \exp\left(-\frac{\kappa^2}{\kappa_{yl}^2}\right)\left[1 + \cos\left(\frac{L\kappa^2\xi}{k}\right)\right] d\kappa d\xi, \tag{F39}$$

$$I_3 = \int_0^1 \int_0^\infty \frac{\kappa^{1/2}}{\kappa_l^{7/6}} \exp\left(-\frac{\kappa^2}{\kappa_{yl}^2}\right)\left[1 + \cos\left(\frac{L\kappa^2\xi}{k}\right)\right] d\kappa d\xi, \tag{F40}$$

where

$$\kappa_{yl}^2 = \frac{\kappa_y^2 \kappa_l^2}{\kappa_y^2 + \kappa_l^2}. \tag{F41}$$

These integrals are also of the same form as those in the standard Rytov derivation and can be evaluated in the same manner to yield (161). Finally, the modified Rytov method plane wave frequency variance is the sum of $\sigma^2_{f,x}$ and $\sigma^2_{f,y}$.

The spherical wave temporal phase covariance function is given by[2]

$$B_{s,sp}(V\tau) = 2\pi^2 k^2 L \int_0^1 \int_0^\infty \kappa \Phi_n(\kappa) J_0(\kappa V\tau) \left\{1 + \cos\left[\frac{L\kappa^2\xi}{k}(1-\xi)\right]\right\} d\kappa d\xi. \quad \text{(F42)}$$

We can develop the spherical wave frequency variance by applying the relation given by (F1), and (F3) to obtain

$$\sigma^2_{f,sp} = 0.25 k^2 L V^2 \int_0^1 \int_0^\infty \kappa^3 \Phi_n(\kappa) \left\{1 + \cos\left[\frac{L\kappa^2\xi}{k}(1-\xi)\right]\right\} d\kappa d\xi. \quad \text{(F43)}$$

Note that this integral definition is nearly identical to that of the plane wave frequency variance, (F4), with the only difference being the argument of the cosine function. This fact will greatly simplify the spherical wave calculations. Using the standard Rytov method, the Hill spectrum given by (151) is substituted into (F43) yielding

$$\sigma^2_{f,sp} = 0.00825 C_n^2 k^2 L V^2 \left[I_1 + 1.802 I_2 - 0.254 I_3\right], \quad \text{(F44)}$$

where I_1, I_2, and I_3 are each integral quantities that are evaluated below. The first integral, I_1, is given by

$$I_1 = \int_0^1 \int_0^\infty \kappa^{-2/3} \exp\left(-\frac{\kappa^2}{\kappa_l^2}\right) \left\{1 + \cos\left[\frac{L\kappa^2\xi}{k}(1-\xi)\right]\right\} d\kappa d\xi. \quad \text{(F45)}$$

As in the plane wave case, this integral can be treated as the sum of two integrals, I_a and I_b. The first integral, I_a, is identical to (F7) and the second integral, I_b, is

$$\begin{aligned} I_b &= \int_0^1 \int_0^\infty \kappa^{-2/3} \exp\left(-\frac{\kappa^2}{\kappa_l^2}\right) \cos\left[\frac{L\kappa^2\xi}{k}(1-\xi)\right] d\kappa d\xi \\ &= \sum_{n=0}^{\infty} \frac{\left(-L^2/k^2\right)^n}{(2n)!} \int_0^1 \xi^{2n} (1-\xi)^{2n} d\xi \int_0^\infty \kappa^{4n-2/3} \exp\left(-\frac{\kappa^2}{\kappa_l^2}\right) d\kappa. \end{aligned} \tag{F46}$$

Noting that

$$\begin{aligned} \int_0^1 \xi^{2n} (1-\xi)^{2n} d\xi &= B(2n+1, 2n+1) \\ &= \frac{\Gamma(2n+1)\,\Gamma(2n+1)}{\Gamma(4n+2)}, \end{aligned} \tag{F47}$$

where $B(x, y)$ is the Beta function, we have

$$I_b = \frac{\kappa_l^{1/3}}{2} \sum_{n=0}^{\infty} \left(-\frac{L^2\kappa_l^4}{k^2}\right)^n \Gamma\left(2n+\frac{1}{6}\right) \frac{\Gamma(2n+1)}{\Gamma(4n+2)}. \tag{F48}$$

Using the Pochhammer relations (F11) and

$$\frac{\Gamma(2n+1)}{\Gamma(4n+2)} = \left(\frac{1}{16^n}\right) \frac{1}{2^{2n}(3/4)_n (5/4)_n}, \tag{F49}$$

we have

$$I_b = \Gamma\left(\frac{1}{6}\right) \frac{\kappa_l^{1/3}}{2} {}_3F_2\left(\tfrac{1}{12}, \tfrac{7}{12}, 1; \tfrac{3}{4}, \tfrac{5}{4} - \tfrac{Q_l^2}{16}\right). \tag{F50}$$

Thus

$$I_1 = \Gamma\left(\frac{1}{6}\right)\frac{\kappa_l^{1/3}}{2}\left\{1 + {}_3F_2\left(\tfrac{1}{12}, \tfrac{7}{12}, 1; \tfrac{3}{4}, \tfrac{5}{4} - \tfrac{Q_l^2}{16}\right)\right\}. \tag{F51}$$

The second integral, I_2, is given by

$$I_2 = \int_0^1 \int_0^\infty \frac{\kappa^{1/3}}{\kappa_l} \exp\left(-\frac{\kappa^2}{\kappa_l^2}\right)\left\{1 + \cos\left[\frac{L\kappa^2\xi}{k}(1-\xi)\right]\right\} d\kappa d\xi. \tag{F52}$$

We treat this integral as the sum of the two integrals I_c, which is identical to (F17), and I_d, given by

$$\begin{aligned} I_d &= \int_0^1 \int_0^\infty \frac{\kappa^{1/3}}{\kappa_l} \exp\left(-\frac{\kappa^2}{\kappa_l^2}\right)\cos\left[\frac{L\kappa^2\xi}{k}(1-\xi)\right] d\kappa d\xi \\ &= \frac{1}{\kappa_l}\sum_{n=0}^{\infty}\frac{\left(-L^2/k^2\right)^n}{(2n)!}\int_0^1 \xi^{2n}(1-\xi)^{2n}\, d\xi \int_0^\infty \kappa^{4n+1/3}\exp\left(-\frac{\kappa^2}{\kappa_l^2}\right) d\kappa \\ &= \frac{\kappa_l^{1/3}}{2}\sum_{n=0}^{\infty}\left(-\frac{L^2\kappa_l^4}{k^2}\right)\Gamma\left(2n+\frac{2}{3}\right)\frac{\Gamma(2n+1)}{\Gamma(4n+2)} \\ &= \Gamma\left(\frac{2}{3}\right)\frac{\kappa_l^{1/3}}{2}{}_3F_2\left(\tfrac{1}{3}, \tfrac{5}{6}, 1; \tfrac{3}{4}, \tfrac{5}{4} - \tfrac{Q_l^2}{16}\right), \end{aligned} \tag{F53}$$

where we have used the relations (F19) and (F49). Thus we have

$$I_2 = \Gamma\left(\frac{2}{3}\right)\frac{\kappa_l^{1/3}}{2}\left\{1 + {}_3F_2\left(\tfrac{1}{3}, \tfrac{5}{6}, 1; \tfrac{3}{4}, \tfrac{5}{4} - \tfrac{Q_l^2}{16}\right)\right\} \tag{F54}$$

The third integral, I_3 is given by

$$I_3 = \int_0^1 \int_0^\infty \frac{\kappa^{1/2}}{\kappa_l^{7/6}} \exp\left(-\frac{\kappa^2}{\kappa_l^2}\right) \left\{1 + \cos\left[\frac{L\kappa^2\xi}{k}(1-\xi)\right]\right\} d\kappa d\xi. \tag{F55}$$

This integral is also treated as the sum of the two integrals I_e, which is identical to (F24), and I_f, given by

$$\begin{aligned} I_f &= \kappa_l^{-7/6} \int_0^1 \int_0^\infty \exp\left(-\frac{\kappa^2}{\kappa_l^2}\right) \left\{1 + \cos\left[\frac{L\kappa^2\xi}{k}(1-\xi)\right]\right\} d\kappa d\xi \\ &= \kappa_l^{-7/6} \sum_{n=0}^{\infty} \frac{\left(-L^2/k^2\right)^n}{(2n)!} \int_0^1 \xi^{2n} (1-\xi)^{2n} d\xi \int_0^\infty \kappa^{4n+1/2} \exp\left(-\frac{\kappa^2}{\kappa_l^2}\right) d\kappa \\ &= \frac{\kappa_l^{1/3}}{2} \sum_{n=0}^{\infty} \left(-\frac{L^2\kappa_l^4}{k^2}\right) \Gamma\left(2n + \frac{3}{4}\right) \frac{\Gamma(2n+1)}{\Gamma(4n+2)} \\ &= \Gamma\left(\frac{3}{4}\right) \frac{\kappa_l^{1/3}}{2} {}_3F_2\left(\tfrac{3}{8}, \tfrac{7}{8}, 1; \tfrac{3}{4}, \tfrac{5}{4} - \tfrac{Q_l^2}{16}\right). \end{aligned} \tag{F56}$$

Thus we have

$$I_3 = \Gamma\left(\frac{3}{4}\right) \frac{\kappa_l^{1/3}}{2} \left\{1 + {}_3F_2\left(\tfrac{3}{8}, \tfrac{7}{8}, 1; \tfrac{3}{4}, \tfrac{5}{4} - \tfrac{Q_l^2}{16}\right)\right\} \tag{F57}$$

Finally, substituting (F51), (F54), and (F57) for I_1, I_2, and I_3 respectively into (F44) and simplifying, we obtain the standard Rytov method spherical wave frequency variance

$$\begin{aligned} \sigma^2_{f,sp,SR} &= 0.0258\sigma_1^2 \left(\frac{k}{L}\right) V^2 Q_l^{1/6} \times \left\{1 + 0.723\ {}_3F_2\left(\tfrac{1}{12}, \tfrac{7}{12}, 1; \tfrac{3}{4}, \tfrac{5}{4}; -\tfrac{Q_l^2}{16}\right)\right. \\ &\quad + 0.317\ {}_3F_2\left(\tfrac{1}{3}, \tfrac{5}{6}, 1; \tfrac{3}{4}, \tfrac{5}{4}; -\tfrac{Q_l^2}{16}\right) \\ &\quad \left. - 0.04\ {}_3F_2\left(\tfrac{3}{8}, \tfrac{7}{8}, 1; \tfrac{3}{4}, \tfrac{5}{4}; -\tfrac{Q_l^2}{16}\right)\right\}. \end{aligned} \tag{F58}$$

To develop expressions for the spherical wave frequency variance using the modified Rytov method, the large and small scale components of the effective spectrum, (B1) and (B2), are substituted into (F43) where again $g(\kappa L_0) = 1$ and $f(\kappa l_0)$ is given by (F31). The resulting integrals are identical in form to those of the standard Rytov method spherical wave formulation, (F45), (F52), and (F55). They are evaluated in the same manner by combining the exponential functions $\exp\left(-\frac{\kappa^2}{\kappa_l^2}\right)$ and $\exp\left(-\frac{\kappa^2}{\kappa_x^2}\right)$ using the term κ_{xl} in the large scale calculation, and by combining the exponential functions $\exp\left(-\frac{\kappa^2}{\kappa_l^2}\right)$ and $\exp\left(-\frac{\kappa^2}{\kappa_y^2}\right)$ using the term κ_{yl} in the small scale calculation, as was done in the modified Rytov method plane wave frequency variance calculations. These calculations yield the modified Rytov method spherical wave frequency variance given by (173)-(175).

APPENDIX G. MODIFIED RYTOV FINITE TARGET WSF

Here we present the derivation of equations (214)-(219). To facilitate the derivation, we shall divide the effective Kolmogorov atmospheric spectrum, (67), into a large scale portion given by

$$\Phi_n(\kappa) = 0.033 C_n^2 \kappa^{-11/3} \exp\left[-\frac{\kappa^2}{\kappa_x^2}\right], \tag{G1}$$

and a small scale portion given by

$$\Phi_n(\kappa) = 0.033 C_n^2 \kappa^{-11/3} \left(1 - \exp\left[-\frac{\kappa^2}{\kappa_y^2}\right]\right), \tag{G2}$$

where we have let $f(\kappa l_0) = g(\kappa L_0) = 1$.

Upon substituting the large scale portion, (G1), into (203) we have

$$\begin{aligned} \Delta_x^i(\rho, L) &\approx 2.6 k^2 L C_n^2 \int_0^1 \int_0^\infty \kappa^{-8/3} \exp\left(-\frac{\kappa^2}{a_x^2}\right) \\ &\quad \times \left[I_0(\Lambda_2 \kappa \xi \rho) - 1 + 1 - J_0(\Theta_2 \kappa \xi \rho)\right] d\kappa d\xi, \end{aligned} \tag{G3}$$

where

$$\alpha_x^2 = \frac{k \kappa_x^2}{k + \kappa_x^2 \Lambda_2 L \xi^2}, \tag{G4}$$

Now consider the integral

$$I_1 = 2.6 k^2 L C_n^2 \int_0^1 \int_0^\infty \kappa^{-8/3} \exp\left(-\frac{\kappa^2}{a_x^2}\right) \left[I_0(\Lambda_2 \kappa \xi \rho) - 1\right] d\kappa d\xi. \tag{G5}$$

Notice that this integral is of the exact same form as (D16). Expressing the Bessel function in (G5) by it's series representation and completing the integration we obtain

$$\begin{aligned} I_1 &= 2.6k^2LC_n^2\left(\frac{\kappa_x^{-5/3}}{4}\right) \\ &\quad\times\sum_{l=1}^{\infty}\frac{\left(\Lambda_2^2\rho^2\kappa_x^2\right)^l}{4\left(l!\right)^2}\frac{\Gamma\left(l-\frac{5}{6}\right)}{\left(l+\frac{1}{2}\right)}\left[{}_2F_1\left(l-\tfrac{5}{6},l+\tfrac{1}{2};l+\tfrac{3}{2};-\tfrac{\kappa_x^2\Lambda_2L}{k}\right)\right], \end{aligned} \tag{G6}$$

where $\Gamma(x)$ is the Gamma function and ${}_2F_1(x)$ is the hypergeometric function. It can be shown numerically that, for the range of parameters under consideration, the series in (G6) is dominated by the first term. Hence, we make the approximation

$$I_1 \approx 0.49\sigma_1^2\left(\frac{k}{L}\right)\Lambda_2^2\rho^2\eta_x^{1/6}\left[{}_2F_1\left(\tfrac{1}{6},\tfrac{3}{2};\tfrac{5}{2};-\eta_x^2\Lambda_2\right)\right], \tag{G7}$$

where $\eta_x = \frac{L\kappa_x^2}{k}$. Using the approximation for the hypergeometric function given by (D20), I_1 can be approximated as

$$I_1 \approx 0.49\sigma_1^2\left(\frac{k}{L}\right)\Lambda_2^2\rho^2\eta_x^{1/6}\left(1+0.547\eta_x\Lambda_2\right)^{-1/6} \tag{G8}$$

We now consider the integral

$$\begin{aligned} I_2 &= 2.6k^2LC_n^2\int_0^1\int_0^\infty \kappa^{-8/3}\exp\left(-\frac{\kappa^2}{\kappa_x^2}\right)\exp\left(-\frac{\Lambda_2L\kappa^2\xi^2}{k}\right) \\ &\quad\times\left[1-J_0\left(\Theta_2\kappa\xi\rho\right)\right]d\kappa d\xi. \end{aligned} \tag{G9}$$

Unlike the integral (G5) which makes up the radial component of the incident wave, (G9) makes up the longitudinal component. In this case we argue that the filter function $\exp\left(-\kappa^2/\kappa_x^2\right)$ acts as a low-pass spatial filter and use the approximation given by (D5). Making this approximation and expressing the Bessel function in its series representation, we have

$$I_2 \approx 2.6k^2 L C_n^2 \sum_{l=1}^{\infty} \left(-\frac{\Theta_2^2 \rho^2}{4}\right)^l \frac{1}{(l!)^2} \int_0^1 \xi^{2l} d\xi \int_0^{\infty} \kappa^{-8/3+2l} \exp\left(-\frac{\kappa^2}{\kappa_x^2}\right) d\kappa. \tag{G10}$$

Evaluation of the remaining integrals yields

$$I_2 \approx 7.07\sigma_1^2 \eta_x^{-5/6} \left[{}_2F_2\left(-\tfrac{5}{6}, \tfrac{1}{2}; 1, \tfrac{3}{2}; -\frac{\Theta_2^2 \rho^2 k \eta_x}{4L}\right) - 1 \right]. \tag{G11}$$

Using the approximation for the hypergeometric function given by (C10), I_2 is given by

$$I_2 \approx 0.49\sigma_1^2 \eta_x^{1/6} \left(\frac{\rho^2 \Theta_2^2 k}{L}\right) \left[1 + 0.033\left(\frac{\Theta_2^2 \rho^2 k \eta_x}{L}\right)\right]^{-1/6}. \tag{G12}$$

Thus, $\Delta_x^i(\rho, L)$ is now given by the sum of (G8) and (G12).

Substitution of the small scale portion of the effective Kolmogorov spectrum, (G2), into (203) yields

$$\begin{aligned}\Delta_y^i(\rho, L) &= 8\pi^2 k^2 L \int_0^1 \int_0^\infty \kappa^{-8/3} \exp\left(-\frac{\Lambda_2 L \kappa^2 \xi^2}{k}\right) \\ &\quad \times \left[I_0(\Lambda_2 \kappa \xi \rho) - 1 + 1 - J_0(\Theta_2 \kappa \xi \rho)\right] d\kappa d\xi \\ &\quad -8\pi^2 k^2 L \int_0^1 \int_0^\infty \kappa^{-8/3} \exp\left(-\frac{\kappa^2}{\alpha_y^2}\right) \\ &\quad \times \left[I_0(\Lambda_2 \kappa \xi \rho) - 1 + 1 - J_0(\Theta_2 \kappa \xi \rho)\right] d\kappa d\xi, \end{aligned} \tag{G13}$$

where

$$\alpha_y^2 = \frac{k \kappa_y^2}{k + \kappa_y^2 \Lambda_2 L \xi^2} \tag{G14}$$

The first double integral in (G13), is precisely that obtained for $\Delta^i(\rho, L)$ in the standard Rytov method and the solution is presented by Andrews and Phillips.[2] The second double integral is evaluated in the exact same manner as for the evaluation of (G3).

Upon substituting the large scale portion, (G1), into (204) we have

$$\begin{aligned}\Delta_x^R(\rho, L) &= 2.6 k^2 L \int_0^1 \int_0^\infty \kappa^{-8/3} \exp\left(-\frac{\kappa^2}{\kappa_x^2}\right) \exp\left(-\frac{\Lambda_2 L \kappa^2 \xi^2}{k}\right) \\ &\quad \times \left\{I_0(\Lambda_2 \kappa \xi \rho) - 1 + 1 - J_0\left[\left(1 - \bar{\Theta}_2 \xi\right) \kappa \rho\right]\right\} d\kappa d\xi, \end{aligned} \tag{G15}$$

which can be expressed as the sum of two integrals, the first of which is identical to (G5), and the second of which is given by

$$\begin{aligned} I_3 &= 2.6k^2LC_n^2\int_0^1\int_0^\infty \kappa^{-8/3}\exp\left(-\frac{\kappa^2}{\kappa_x^2}\right)\exp\left(-\frac{\Lambda_2 L\kappa^2\xi^2}{k}\right) \\ &\quad\times\left\{1-J_0\left[\left(1-\bar{\Theta}_2\xi\right)\kappa\rho\right]\right\}d\kappa d\xi. \end{aligned} \tag{G16}$$

This integral is identical to (G9) except for the argument in the Bessel function. Thus it can be evaluated in the same manner. We again write the Bessel function using its series definition, use the approximation given by (D5), and evaluate the remaining integrals, yielding

$$\begin{aligned} I_3 &\approx 0.49\sigma_1^2\eta_x^{1/6}\left(\frac{k\rho^2}{L}\right)\left[\frac{1}{\bar{\Theta}_2}\left(1+0.033\frac{k\rho^2\eta_x}{L}\right)^{-1/6}\right. \\ &\quad\left.-\frac{\Theta_2^3}{\bar{\Theta}_2}\left(1+0.033\frac{k\rho^2\Theta_2^2\eta_x}{L}\right)^{-1/6}\right], \end{aligned} \tag{G17}$$

where we have also made use of the approximation given by (C10) for the resulting hypergeometric functions.

Substitution of the small scale portion of the effective Kolmogorov spectrum, (G2), into (204) yields

$$\begin{aligned}\Delta_y^R(\rho,L) &= 8\pi^2k^2L\int_0^1\int_0^\infty \kappa^{-8/3}\exp\left(-\frac{\Lambda_2 L\kappa^2\xi^2}{k}\right)\\ &\times\left\{I_0\left(\Lambda_2\kappa\xi\rho\right)-1+1-J_0\left[\left(1-\bar{\Theta}_2\xi\right)\kappa\rho\right]\right\}d\kappa d\xi\\ &-8\pi^2k^2L\int_0^1\int_0^\infty \kappa^{-8/3}\exp\left[-\frac{\kappa^2}{\kappa_y^2}\right]\exp\left(-\frac{\Lambda_2 L\kappa^2\xi^2}{k}\right)\\ &\times\left\{I_0\left(\Lambda_2\kappa\xi\rho\right)-1+1-J_0\left[\left(1-\bar{\Theta}_2\xi\right)\kappa\rho\right]\right\}d\kappa d\xi. \qquad \text{(G18)}\end{aligned}$$

The first integral in (G18) is identical to that obtained for $\Delta^R(\rho,L)$ in the standard Rytov method and the solution is presented by Andrews and Phillips.[2] The second integral is evaluated in the exact same manner as for the evaluation of (G15).

Finally, upon substituting the large scale portion, (G1), into (205) we have

$$\begin{aligned}\mathrm{Re}\left[\Delta_x^{iR}(\rho,L)\right] &= \mathrm{Re}\left[2.6k^2L\int_0^1\int_0^\infty \kappa^{-8/3}\exp\left(-\frac{\kappa^2}{\kappa_x^2}\right)\exp\left(-\frac{\Lambda_2 L\kappa^2\xi^2}{k}\right)\right.\\ &\left\{\left(J_0\left[\left(1-\xi+2j\Lambda_2\xi\right)\frac{\kappa\rho}{2}\right]-1\right)\right.\\ &+\left(J_0\left[\left(1-\xi-2j\Lambda_2\xi\right)\frac{\kappa\rho}{2}\right]-1\right)\\ &\left.\left.-2\left(J_0\left[\left(1-\xi+2\Theta_2\xi\right)\frac{\kappa\rho}{2}\right]-1\right)\right\}d\kappa d\xi\right], \qquad \text{(G19)}\end{aligned}$$

which can be expressed as the sum of three integrals, that is

$$\Delta_x^{iR}(\rho,L) = I_4 + I_5 - 2I_6, \qquad \text{(G20)}$$

where

$$I_4 = -2.6k^2L\int_0^1\int_0^\infty \kappa^{-8/3}\exp\left(-\frac{\kappa^2}{\kappa_x^2}\right)\exp\left(-\frac{\Lambda_2 L\kappa^2\xi^2}{k}\right) \times\left(1-J_0\left[(1-\xi+2j\Lambda_2\xi)\frac{\kappa\rho}{2}\right]\right)d\kappa d\xi, \quad \text{(G21)}$$

$$I_5 = -2.6k^2L\int_0^1\int_0^\infty \kappa^{-8/3}\exp\left(-\frac{\kappa^2}{\kappa_x^2}\right)\exp\left(-\frac{\Lambda_2 L\kappa^2\xi^2}{k}\right) \times\left(1-J_0\left[(1-\xi-2j\Lambda_2\xi)\frac{\kappa\rho}{2}\right]\right)d\kappa d\xi, \quad \text{(G22)}$$

$$I_6 = -2.6k^2L\int_0^1\int_0^\infty \kappa^{-8/3}\exp\left(-\frac{\kappa^2}{\kappa_x^2}\right)\exp\left(-\frac{\Lambda_2 L\kappa^2\xi^2}{k}\right) \times\left(1-J_0\left[(1-\xi+2\Theta_2\xi)\frac{\kappa\rho}{2}\right]\right)d\kappa d\xi. \quad \text{(G23)}$$

Each of the integrals (G21)-(G23) is of the same form as (G9) and can therefore be evaluated in the same manner. In each integral the Bessel function is replaced by its series representation and the approximation given by (D5) is used. Evaluating the integrals and taking the real part yields equation (218). We note that the use of the binomial approximation given by (C10) for the hypergeometric functions in (218) results in large errors because the argument of the second hypergeometric function in that expression is positive. Thus, we have left the hypergeometric functions in the final result. The small scale correlation term, $\Delta_y^{iR}(\rho, L)$ is evaluated in the same manner.

APPENDIX H. DOUBLE PASS FREQUENCY VARIANCE DEFINITION

Here we present the derivation of the terms α_1 through α_4 given by equations (232), (233), and (235)-(238) that were used in the double pass finite target frequency variance. Assuming that the double pass frequency variance is related to the double pass temporal phase covariance function by the relation given in (229), it is necessary to first derive the double pass temporal phase covariance function.

Andrews and Phillips[2] showed that in the double pass case with reflection from a smooth target, the Rytov approximation for the optical field can be expressed in the form

$$U(\mathbf{r}, 2L) = U_0(\mathbf{r}, 2L) \exp[\Psi_1(\mathbf{r}, 2L) + \Psi_2(\mathbf{r}, 2L)] + \ldots, \tag{H1}$$

where $U_0(\mathbf{r}, 2L)$ is the optical field at the receiver in the absence of turbulence and $\Psi_1(\mathbf{r}, 2L)$ and $\Psi_2(\mathbf{r}, 2L)$ are the first and second order complex phase perturbations that include the effects of reflection from a smooth target and the statistical correlation terms that arise in a monostatic channel. Recalling that the statistical correlations can arise from a folded path geometry and a reciprocal path geometry, it is necessary to express the complex phase perturbation, Ψ_1, as the sum[2]

$$\begin{aligned} \Psi_1(\mathbf{r}, 2L) &= \Psi_a(\mathbf{r}, 2L) + \Psi_b(\mathbf{r}, 2L) \\ &= \Psi_a^i(\pm\mathbf{r}, L) + \Psi_a^R(\pm\mathbf{r}, L) + \Psi_b^{i*}(0, L) + \Psi_b^R(\mathbf{r}, L), \end{aligned} \tag{H2}$$

where $\Psi_a(\mathbf{r}, 2L)$ is the first order complex phase perturbation associated with folded path integrals and $\Psi_b(\mathbf{r}, 2L)$ is associated with reciprocal paths. The superscripts i and R refer to incident and reflected waves and the asterisk * denotes the complex conjugate. The upper plus sign is used for a plane mirror target and the lower minus sign is used for a retroreflector target.

The spatial phase covariance function, B_S, can be expressed in terms of ensemble averages of the complex phase perturbations by[2]

$$\begin{aligned} B_S(\mathbf{r}_1, \mathbf{r}_2, 2L) &= \frac{1}{2}\mathrm{Re}\left[\left\langle \Psi_a^i(\mathbf{r}_1)\,\Psi_a^{i*}(\mathbf{r}_2)\right\rangle - \left\langle \Psi_a^i(\mathbf{r}_1)\,\Psi_a^i(\mathbf{r}_2)\right\rangle\right] \\ &\quad + \frac{1}{2}\mathrm{Re}\left[\left\langle \Psi_a^R(\mathbf{r}_1)\,\Psi_a^{R*}(\mathbf{r}_2)\right\rangle - \left\langle \Psi_a^R(\mathbf{r}_1)\,\Psi_a^R(\mathbf{r}_2)\right\rangle\right] \\ &\quad + \frac{1}{2}\mathrm{Re}\left[\left\langle \Psi_a^i(\mathbf{r}_1)\,\Psi_a^{R*}(\mathbf{r}_2)\right\rangle + \left\langle \Psi_a^R(\mathbf{r}_1)\,\Psi_a^{i*}(\mathbf{r}_2)\right\rangle\right] \\ &\quad - \frac{1}{2}\mathrm{Re}\left[\left\langle \Psi_a^i(\mathbf{r}_1)\,\Psi_a^R(\mathbf{r}_2)\right\rangle + \left\langle \Psi_a^R(\mathbf{r}_1)\,\Psi_a^i(\mathbf{r}_2)\right\rangle\right]. \end{aligned} \tag{H3}$$

The ensemble averages in (H3) are given by Andrews and Phillips.[2] In terms of the vectors $\mathbf{r} = (\mathbf{r}_1 + \mathbf{r}_2)/2$ and $\mathbf{p} = \mathbf{r}_2 - \mathbf{r}_1$ and their magnitudes $r = |\mathbf{r}|$ and $\rho = |\mathbf{p}|$, they are given by

$$\begin{aligned} \alpha_1 &= \left\langle \Psi_a^i(\mathbf{r}_1)\,\Psi_a^{i*}(\mathbf{r}_2)\right\rangle - \left\langle \Psi_a^i(\mathbf{r}_1)\,\Psi_a^i(\mathbf{r}_2)\right\rangle \\ &= 4\pi^2 k^2 L \int_0^1 \int_0^\infty \kappa \Phi_n(\kappa) J_0\left[\left|\gamma_a^i\left(\mathbf{r} + \frac{\mathbf{p}}{2}\right) - \gamma_a^{i*}\left(\mathbf{r} - \frac{\mathbf{p}}{2}\right)\right| \kappa\right] \\ &\quad \times \exp\left\{-\frac{j\kappa^2}{2k}\left[\gamma_a^i B_a^i(\xi) - \gamma_a^{i*} B_a^{i*}(\xi)\right]\right\} d\kappa d\xi \\ &\quad + 4\pi^2 k^2 L \int_0^1 \int_0^\infty \kappa \Phi_n(\kappa) J_0\left(\gamma_a^i \kappa \rho\right) \\ &\quad \times \exp\left[-\frac{j\kappa^2}{k}\gamma_a^i B_a^i(\xi)\right] d\kappa d\xi, \end{aligned} \tag{H4}$$

$$
\begin{aligned}
\alpha_2 &= \left\langle \Psi_a^R(\mathbf{r}_1)\,\Psi_a^{R*}(\mathbf{r}_2)\right\rangle - \left\langle \Psi_a^R(\mathbf{r}_1)\,\Psi_a^{R}(\mathbf{r}_2)\right\rangle \\
&= 4\pi^2 k^2 L \int_0^1\int_0^\infty \kappa\Phi_n(\kappa)\,J_0\left[\left|\gamma_a^R\left(\mathbf{r}+\frac{\mathbf{p}}{2}\right)-\gamma_a^{R*}\left(\mathbf{r}-\frac{\mathbf{p}}{2}\right)\right|\kappa\right] \\
&\quad\times\exp\left\{-\frac{j\kappa^2}{2k}\left[\gamma_a^R B_a^R(\xi)-\gamma_a^{R*}B_a^{R*}(\xi)\right]\right\}d\kappa d\xi \\
&\quad+4\pi^2 k^2 L\int_0^1\int_0^\infty \kappa\Phi_n(\kappa)\,J_0\left(\gamma_a^R\kappa\rho\right) \\
&\quad\times\exp\left[-\frac{j\kappa^2}{k}\gamma_a^R B_a^R(\xi)\right]d\kappa d\xi,
\end{aligned}
\tag{H5}
$$

$$
\begin{aligned}
\alpha_3 &= \left\langle \Psi_a^i(\mathbf{r}_1)\,\Psi_a^{R*}(\mathbf{r}_2)\right\rangle + \left\langle \Psi_a^R(\mathbf{r}_1)\,\Psi_a^{i*}(\mathbf{r}_2)\right\rangle \\
&= 4\pi^2 k^2 L \int_0^1\int_0^\infty \kappa\Phi_n(\kappa)\,J_0\left[\left|\gamma_a^i\left(\mathbf{r}+\frac{\mathbf{p}}{2}\right)\mp\gamma_a^{R*}\left(\mathbf{r}-\frac{\mathbf{p}}{2}\right)\right|\kappa\right] \\
&\quad\times\exp\left\{-\frac{j\kappa^2}{2k}\left[\gamma_a^i B_a^i(\xi)-\gamma_a^{R*}B_a^{R*}(\xi)\right]\right\}d\kappa d\xi \\
&\quad+4\pi^2 k^2 L\int_0^1\int_0^\infty \kappa\Phi_n(\kappa)\,J_0\left[\left|\gamma_a^R\left(\mathbf{r}+\frac{\mathbf{p}}{2}\right)\mp\gamma_a^{i*}\left(\mathbf{r}-\frac{\mathbf{p}}{2}\right)\right|\kappa\right] \\
&\quad\times\exp\left\{\frac{j\kappa^2}{2k}\left[\gamma_a^{i*} B_a^{i*}(\xi)-\gamma_a^R B_a^R(\xi)\right]\right\}d\kappa d\xi,
\end{aligned}
\tag{H6}
$$

$$
\begin{aligned}
\alpha_4 &= -\left\langle \Psi_a^i(\mathbf{r}_1)\,\Psi_a^{R}(\mathbf{r}_2)\right\rangle - \left\langle \Psi_a^R(\mathbf{r}_1)\,\Psi_a^{i}(\mathbf{r}_2)\right\rangle \\
&= 4\pi^2 k^2 L \int_0^1\int_0^\infty \kappa\Phi_n(\kappa)\,J_0\left[\left|\gamma_a^i\left(\mathbf{r}+\frac{\mathbf{p}}{2}\right)\mp\gamma_a^{R}\left(\mathbf{r}-\frac{\mathbf{p}}{2}\right)\right|\kappa\right] \\
&\quad\times\exp\left\{-\frac{j\kappa^2}{2k}\left[\gamma_a^i B_a^i(\xi)+\gamma_a^{R}B_a^{R}(\xi)\right]\right\}d\kappa d\xi \\
&\quad+4\pi^2 k^2 L\int_0^1\int_0^\infty \kappa\Phi_n(\kappa)\,J_0\left[\left|\gamma_a^R\left(\mathbf{r}+\frac{\mathbf{p}}{2}\right)\mp\gamma_a^{i}\left(\mathbf{r}-\frac{\mathbf{p}}{2}\right)\right|\kappa\right] \\
&\quad\times\exp\left\{-\frac{j\kappa^2}{2k}\left[\gamma_a^i B_a^i(\xi)+\gamma_a^R B_a^R(\xi)\right]\right\}d\kappa d\xi,
\end{aligned}
\tag{H7}
$$

where $j = \sqrt{-1}$. Note that in the bistatic case, α_3 and α_4 are zero. In the case of an incident spherical wave, we have the following[2]

$$\gamma_a^i = (\Theta_2 - j\Lambda_2)(1-\xi), \tag{H8}$$

$$\gamma_a^R = \xi + \gamma_a^i, \tag{H9}$$

$$B_a^i = L(1+\xi+j\xi\Omega_R), \tag{H10}$$

$$B_a^R = L(1-\xi). \tag{H11}$$

Noting that the use of the magnitude bars, $||$, in α_1 through α_4 is the same as presented in Appendix A and applying the approximation given by (A8), we have

$$\begin{aligned}
\alpha_1 \;=\; & 4\pi^2 k^2 L \int_0^1 \int_0^\infty \kappa \Phi_n(\kappa) J_0\left[\left(\gamma_a^i - \gamma_a^{i*}\right) r\kappa\right] J_0\left[\left(\gamma_a^i + \gamma_a^{i*}\right)\frac{\rho\kappa}{2}\right] \\
& \times \exp\left\{-\frac{j\kappa^2}{2k}\left[\gamma_a^i B_a^i(\xi) - \gamma_a^{i*} B_a^{i*}(\xi)\right]\right\} d\kappa d\xi \\
& + 4\pi^2 k^2 L \int_0^1 \int_0^\infty \kappa \Phi_n(\kappa) J_0\left(\gamma_a^i \kappa\rho\right) \\
& \times \exp\left[-\frac{j\kappa^2}{k}\gamma_a^i B_a^i(\xi)\right] d\kappa d\xi,
\end{aligned} \tag{H12}$$

$$
\begin{aligned}
\alpha_2 &= 4\pi^2 k^2 L \int_0^1 \int_0^\infty \kappa \Phi_n(\kappa) J_0\left[\left(\gamma_a^R - \gamma_a^{R*}\right) r\kappa\right] J_0\left[\left(\gamma_a^R + \gamma_a^{R*}\right)\frac{\rho\kappa}{2}\right] \\
&\quad \times \exp\left\{-\frac{j\kappa^2}{2k}\left[\gamma_a^R B_a^R(\xi) - \gamma_a^{R*} B_a^{R*}(\xi)\right]\right\} d\kappa d\xi \\
&\quad + 4\pi^2 k^2 L \int_0^1 \int_0^\infty \kappa \Phi_n(\kappa) J_0\left(\gamma_a^R \kappa \rho\right) \\
&\quad \times \exp\left[-\frac{j\kappa^2}{k}\gamma_a^R B_a^R(\xi)\right] d\kappa d\xi, \qquad \text{(H13)}
\end{aligned}
$$

$$
\begin{aligned}
\alpha_3 &= 4\pi^2 k^2 L \int_0^1 \int_0^\infty \kappa \Phi_n(\kappa) J_0\left[\left(\gamma_a^i \mp \gamma_a^{R*}\right) r\kappa\right] J_0\left[\left(\gamma_a^i \pm \gamma_a^{R*}\right)\frac{\rho\kappa}{2}\right] \\
&\quad \times \exp\left\{-\frac{j\kappa^2}{2k}\left[\gamma_a^i B_a^i(\xi) - \gamma_a^{R*} B_a^{R*}(\xi)\right]\right\} d\kappa d\xi \\
&\quad + 4\pi^2 k^2 L \int_0^1 \int_0^\infty \kappa \Phi_n(\kappa) J_0\left[\left(\gamma_a^R \mp \gamma_a^{i*}\right) r\kappa\right] J_0\left[\left(\gamma_a^R \pm \gamma_a^{i*}\right)\frac{\rho\kappa}{2}\right] \\
&\quad \times \exp\left\{\frac{j\kappa^2}{2k}\left[\gamma_a^{i*} B_a^{i*}(\xi) - \gamma_a^R B_a^R(\xi)\right]\right\} d\kappa d\xi, \qquad \text{(H14)}
\end{aligned}
$$

$$
\begin{aligned}
\alpha_4 &= 4\pi^2 k^2 L \int_0^1 \int_0^\infty \kappa \Phi_n(\kappa) J_0\left[\left(\gamma_a^i \mp \gamma_a^R\right) r\kappa\right] J_0\left[\left(\gamma_a^i \pm \gamma_a^R\right)\frac{\rho\kappa}{2}\right] \\
&\quad \times \exp\left\{-\frac{j\kappa^2}{2k}\left[\gamma_a^i B_a^i(\xi) + \gamma_a^R B_a^R(\xi)\right]\right\} d\kappa d\xi \\
&\quad + 4\pi^2 k^2 L \int_0^1 \int_0^\infty \kappa \Phi_n(\kappa) J_0\left[\left(\gamma_a^R \mp \gamma_a^i\right) r\kappa\right] J_0\left[\left(\gamma_a^R \pm \gamma_a^i\right)\frac{\rho\kappa}{2}\right] \\
&\quad \times \exp\left\{-\frac{j\kappa^2}{2k}\left[\gamma_a^i B_a^i(\xi) + \gamma_a^R B_a^R(\xi)\right]\right\} d\kappa d\xi, \qquad \text{(H15)}
\end{aligned}
$$

where we note that the upper signs, i.e. $\mp$ and $\pm$, are associated with reflection from a plane mirror and the lower signs are associated with a retroreflector. Now note that α_1 through α_4 are statistically inhomogeneous in that they depend explicitly on the location of the two observation

points, $\mathbf{r}_1$ and $\mathbf{r}_2$. Thus, we consider the case when the observation points are symmetrically located about the optical axis, i.e. $\mathbf{r}_1 = -\mathbf{r}_2$, so that $r = 0$. Making this assumption, noting that $J_0(0) = 1$, substituting the parameters (H8)-(H11) where we are assuming an incident spherical wave, and applying Taylor's frozen flow hypothesis by making the substitution $\rho = V\tau/\gamma_2$, where γ_2 is given by (234), we find that the temporal phase covariance function for a finite target with an incident spherical wave is given by

$$B_S(V\tau, 2L) = \frac{1}{2}\,\mathrm{Re}\left[\alpha_1 + \alpha_2 + \alpha_3 + \alpha_4\right], \tag{H16}$$

where α_1 and α_2 are given by (232) and (233), respectively for both a plane mirror and a retroreflector. For a plane mirror, α_3 and α_4 are given by (235) and (236), respectively. For a retroreflector, α_3 and α_4 are given by (237) and (238), respectively. Again, in the bistatic case, α_3 and α_4 are zero.

Using the relation given by (229), we can obtain an expression for the double pass finite target frequency variance by taking the second derivative with respect to τ of each of the terms α_1 through α_4 and evaluating at $\tau = 0$. Completing these two operations and simplifying yields

$$\sigma_f^2 = -\frac{1}{8\pi^2}\left[\beta_1 + \beta_2 + \beta_3 + \beta_4\right], \tag{H17}$$

where in the bistatic case β_3 and β_4 are both zero. For both a plane mirror and a retroreflector

$$
\begin{aligned}
\beta_1 &= \mathrm{Re}\left[\frac{d^2}{d\tau^2}\alpha_1\bigg|_{\tau=0}\right] \\
&= 2\pi^2 k^2 L V^2 \Theta_2^2 \int_0^1 \int_0^\infty \kappa^3 \Phi_n(\kappa) \exp\left[-\frac{L\kappa^2\Lambda_2}{k}(1-\xi)^2\right] \frac{(1-\xi)^2}{D^2} \\
&\times \left[\left(\Lambda_2^2 - \bar{\Theta}_2\right)\xi^2 - 2\left(\Theta_2\bar{\Theta}_2 + \Lambda_2^2\right)\xi + \Lambda_2^2 - \Theta_2^2\right] d\kappa d\xi \\
&+ 2\pi^2 k^2 L V^2 \int_0^1 \int_0^\infty \kappa^3 \Phi_n(\kappa) \exp\left[-\frac{L\kappa^2\Lambda_2}{k}(1-\xi)^2\right] \\
&\times \cos\left[\frac{L\kappa^2}{k}(1-\xi)\left(\Theta_2 + \bar{\Theta}_2\xi\right)\right] \frac{(1-\xi)^2}{D^2} \\
&\times \left\{\left[\Lambda_2^2 - \left(\Lambda_2^2 - \Theta_2\bar{\Theta}_2\right)^2\right]\xi^2 \right. \\
&\left. + \left[2\Lambda_2^2\left(2\Theta_2^2 - \Theta_2 + \Lambda_2^2\right) - 2\Theta_2^3\bar{\Theta}_2\right]\xi - \left(\Lambda_2^2 + \Theta_2^2\right)^2\right\} d\kappa d\xi \\
&+ 4\pi^2 k^2 L V^2 \Lambda_2 \int_0^1 \int_0^\infty \kappa^3 \Phi_n(\kappa) \exp\left[-\frac{L\kappa^2\Lambda_2}{k}(1-\xi)^2\right] \\
&\times \sin\left[\frac{L\kappa^2}{k}(1-\xi)\left(\Theta_2 + \bar{\Theta}_2\xi\right)\right] \frac{(1-\xi)^2}{D^2} \\
&\times \left[\left(\Theta_2\bar{\Theta}_2 - \Lambda_2^2\right)\xi^2 + \left(\Lambda_2^2 + \Theta_2^2\right)\xi\right] d\kappa d\xi,
\end{aligned}
\tag{H18}
$$

$$
\begin{aligned}
\beta_2 &= \mathrm{Re}\left[\frac{d^2}{d\tau^2}\alpha_2\bigg|_{\tau=0}\right] \\
&= 2\pi^2 k^2 L V^2 \int_0^1 \int_0^\infty \kappa^3 \Phi_n(\kappa) \exp\left[-\frac{L\kappa^2\Lambda_2}{k}(1-\xi)^2\right] \frac{\left(\bar{\Theta}_2\xi + \Theta_2\right)^2}{D^2} \\
&\times \left[\left(\Lambda_2 + \bar{\Theta}_2\right)\xi - \Lambda_2 + \Theta_2\right]\left[\left(\Lambda_2 - \bar{\Theta}_2\right)\xi - \Lambda_2 - \Theta_2\right] d\kappa d\xi \\
&- 2\pi^2 k^2 L V^2 \int_0^1 \int_0^\infty \kappa^3 \Phi_n(\kappa) \exp\left[-\frac{L\kappa^2\Lambda_2}{k}(1-\xi)^2\right] \\
&\times \cos\left[\frac{L\kappa^2}{k}(1-\xi)\left(\Theta_2 + \bar{\Theta}_2\xi\right)\right] d\kappa d\xi.
\end{aligned}
\tag{H19}
$$

In the case of reflection from a plane mirror, we have

$$\begin{aligned}
\beta_3 &= \mathrm{Re}\left[\frac{d^2}{d\tau^2}\alpha_3\bigg|_{\tau=0}\right] \\
&= -\pi^2 k^2 L V^2 \int_0^1 \int_0^\infty \kappa^3 \Phi_n(\kappa) \exp\left[-\frac{L\kappa^2\Lambda_2}{k}(1-\xi)^2\right] \frac{\left[2\Theta_2 + (1-2\Theta_2)\xi\right]^2}{D^2} \\
&\quad \times \left[\Lambda_2 - \Theta_2 - \left(\Lambda_2 + \bar{\Theta}_2\right)\xi\right]\left[\left(\Lambda_2 - \bar{\Theta}_2\right)\xi - \Lambda_2 - \Theta_2\right] d\kappa d\xi, \qquad \text{(H20)}
\end{aligned}$$

$$\begin{aligned}
\beta_4 &= \mathrm{Re}\left[\frac{d^2}{d\tau^2}\alpha 4\bigg|_{\tau=0}\right] \\
&= -\pi^2 k^2 L V^2 \int_0^1 \int_0^\infty \kappa^3 \Phi_n(\kappa) \exp\left[-\frac{L\kappa^2\Lambda_2}{k}(1-\xi)^2\right] \frac{1}{D^2} \\
&\quad \times \left\{\left[2\Lambda_2^2 + \Lambda_2 + 2\Theta_2^2 - 3\Theta_2 + 1\right]\xi^2\right. \\
&\quad \left. + \left[3\Theta_2 - \Lambda_2 - 4\left(\Lambda_2^2 + \Theta_2^2\right)\right]\xi + 2\left(\Lambda_2^2 + \Theta_2^2\right)\right\} \\
&\quad \times \left\{\left[2\left(\Lambda_2^2 + \Theta_2^2\right) - 3\Theta_2 - \Lambda_2 + 1\right]\xi^2\right. \\
&\quad \left[3\Theta_2 + \Lambda_2 - 4\left(\Lambda_2^2 + \Theta_2^2\right)\right]\xi + 2\left(\Lambda_2^2 + \Theta_2^2\right)\Big\}\, d\kappa d\xi \\
&\quad -2\pi^2 k^2 L V^2 \Lambda_2 \int_0^1 \int_0^\infty \kappa^3 \Phi_n(\kappa) \exp\left[-\frac{L\kappa^2\Lambda_2}{k}(1-\xi)^2\right] \\
&\quad \times \frac{\xi}{D^2}(1-\xi)\sin\left[\frac{L\kappa^2}{k}(1-\xi)\left(\Theta_2 + \bar{\Theta}_2\xi\right)\right] \\
&\quad \times \left\{\left[2\left(\Theta_2\bar{\Theta}_2 - \Lambda_2^2\right) - \bar{\Theta}_2\right]\xi^2\right. \\
&\quad \left. + \left[4\left(\Lambda_2^2 - \Theta_2\bar{\Theta}_2\right) + \Theta_2\right]\xi - 2\left(\Lambda_2^2 + \Theta_2^2\right)\right\} d\kappa d\xi. \qquad \text{(H21)}
\end{aligned}$$

In the case of reflection from a retroreflector, we have

$$\begin{aligned}
\beta_3 &= 0.5\pi^2 k^2 L V^2 \int_0^1 \int_0^\infty \kappa^3 \Phi_n(\kappa) \exp\left[-\frac{L\kappa^2\Lambda_2}{k}(1-\xi)^2\right] \frac{1}{D^2} \\
&\quad \times \left\{ \left[4\Lambda_2^2 \left(\Theta_2^2 - 4\Theta_2 - \Lambda_2^2 + \frac{13}{4} \right) - \bar{\Theta}_2^2 \right] \xi^4 \right. \\
&\quad + \left[16\Lambda_2^2 \left(\Lambda_2^2 - \Theta_2^2 + 3\Theta_2 - \frac{13}{8} \right) - 2\Theta_2\bar{\Theta}_2 \right] \xi^3 \\
&\quad + \left[24\Lambda_2^2 \left(\Theta_2^2 - 2\Theta_2 - \Lambda_2^2 + \frac{24}{13} \right) - \Theta_2^2 \right] \xi^2 \\
&\quad \left. + 16\Lambda_2^2 \left(\Theta_2\bar{\Theta}_2 + \Lambda_2^2 \right) \xi - 4\Lambda_2^2 \left(\Lambda_2^2 - \Theta_2^2 \right) \right\} d\kappa d\xi \\
&\quad - 0.5\pi^2 k^2 L V^2 \int_0^1 \int_0^\infty \kappa^3 \Phi_n(\kappa) \exp\left[-\frac{L\kappa^2\Lambda_2}{k}(1-\xi)^2\right] \frac{1}{D^2} \\
&\quad \times \left\{ \left[\bar{\Theta}_2 + 4\Lambda_2^2 \left(\Lambda_2^2 - \Theta_2^2 + \frac{3}{4} \right) \right] \xi^4 \right. \\
&\quad + \left[16\Lambda_2^2 \left(\Theta_2^2 - \Lambda_2^2 - \frac{3}{8} \right) + 2\Theta_2\bar{\Theta}_2 \right] \xi^3 \\
&\quad + \left[24\Lambda_2^2 \left(\Lambda_2^2 - \Theta_2^2 \right) + \Theta_2^2 + 3\Lambda_2^2 \right] \xi^2 \\
&\quad \left. + 16\Lambda_2^2 \left(\Theta_2^2 - \Lambda_2^2 \right) \xi + 4\Lambda_2^2 \left(\Lambda_2^2 - \Theta_2^2 \right) \right\} d\kappa d\xi, \qquad \text{(H22)}
\end{aligned}$$

$$\begin{aligned}
\beta_4 &= \pi^2 k^2 L V^2 \int_0^1 \int_0^\infty \kappa^3 \Phi_n(\kappa) \exp\left[-\frac{L\kappa^2\Lambda_2}{k}(1-\xi)^2\right] \frac{\xi^2}{D^2} \\
&\quad \times \cos\left[\frac{L\kappa^2}{k}(1-\xi)\left(\Theta_2 + \bar{\Theta}_2\xi\right) \right] \\
&\quad \times \left[\left(\Lambda_2^2 - \bar{\Theta}_2^2 \right) \xi^2 - 2\left(\Lambda_2^2 + \Theta_2\bar{\Theta}_2 \right) \xi + \Lambda_2^2 - \Theta_2^2 \right] d\kappa d\xi \\
&\quad + 2\pi^2 k^2 L V^2 \Lambda_2 \int_0^1 \int_0^\infty \kappa^3 \Phi_n(\kappa) \exp\left[-\frac{L\kappa^2\Lambda_2}{k}(1-\xi)^2\right] \frac{\xi^2}{D^2} \\
&\quad \times \sin\left[\frac{L\kappa^2}{k}(1-\xi)\left(\Theta_2 + \bar{\Theta}_2\xi\right) \right] \left[\bar{\Theta}_2\xi^2 - (1-2\Theta_2)\xi - \Theta_2 \right] d\kappa d\xi. \qquad \text{(H23)}
\end{aligned}$$

APPENDIX I. FINITE TARGET FREQUENCY VARIANCE

Here we derive the expression for the finite target double pass frequency variance as given by equation (241) and (254). Recall that these expressions assume an incident spherical wave. In the previous appendix, it was determined that the finite target double pass frequency variance is given by

$$\sigma_f^2 = -\frac{1}{8\pi^2}\left[\beta_1 + \beta_2 + \beta_3 + \beta_4\right], \tag{I1}$$

where the terms β_1 through β_4 are defined by the integral equations (H18)-(H23). In each of these integral equations we will complete only the integration on the spatial frequency, κ. The remaining integration on the path length argument, ξ, is conducted numerically. Considering the the integral equations (H18)-(H23), we notice that only part of the expressions are dependent on κ. Thus, we see that the terms β_1 through β_4 can be expressed as functions of the following three integrals on κ

$$I_1 = \int_0^\infty \kappa^3 \Phi_n(\kappa) \exp\left[-\frac{L\kappa^2\Lambda_2}{k}(1-\xi)^2\right] d\kappa, \tag{I2}$$

$$I_2 = \int_0^\infty \kappa^3 \Phi_n(\kappa) \exp\left[-\frac{L\kappa^2\Lambda_2}{k}(1-\xi)^2\right] \cos\left[\frac{L\kappa^2}{k}(1-\xi)\left(\Theta_2 + \bar{\Theta}_2\xi\right)\right] d\kappa, \tag{I3}$$

$$I_3 = \int_0^\infty \kappa^3 \Phi_n(\kappa) \exp\left[-\frac{L\kappa^2\Lambda_2}{k}(1-\xi)^2\right] \sin\left[\frac{L\kappa^2}{k}(1-\xi)\left(\Theta_2 + \bar{\Theta}_2\xi\right)\right] d\kappa. \tag{I4}$$

We develop an expression for the double pass finite target frequency variance using the standard Rytov method by evaluating the expressions (I2)-(I4) using the Hill spectrum, (151) and then expressing β_1 through β_4 in terms of these results. Thus, substituting the Hill spectrum into (I2) yields

$$I_1 = I_{a1} + I_{b1} + I_{c1}, \tag{I5}$$

where

$$\begin{aligned} I_{a1} &= 0.033C_n^2 \int_0^\infty \kappa^{-2/3} \exp\left(-\frac{\kappa^2}{A^2}\right) d\kappa \\ &= 0.0165C_n^2 A^{1/3} \Gamma\left(\frac{1}{6}\right) \end{aligned} \tag{I6}$$

$$\begin{aligned} I_{b1} &= (1.802)\,(0.033)\,C_n^2 \int_0^\infty \frac{\kappa^{1/3}}{\kappa_l} \exp\left(-\frac{\kappa^2}{A^2}\right) d\kappa \\ &\approx 0.0297C_n^2 A^{4/3} \kappa_l^{-1} \Gamma\left(\frac{2}{3}\right), \end{aligned} \tag{I7}$$

$$\begin{aligned} I_{c1} &= (0.254)\,(0.033)\,C_n^2 \int_0^\infty \frac{\kappa^{1/2}}{\kappa_l^{7/6}} \exp\left(-\frac{\kappa^2}{A^2}\right) d\kappa \\ &\approx 0.0042C_n^2 A^{3/2} \kappa_l^{-7/6} \Gamma\left(\frac{3}{4}\right), \end{aligned} \tag{I8}$$

$$A^2 = \frac{k\kappa_l^2}{\kappa_l^2 L \Lambda_2 (1-\xi)^2 + k}. \tag{I9}$$

Combining these results and evaluating the Gamma functions yields

$$I_1 = 0.092C_n^2 A^{1/3} \left[1 + 0.44\frac{A}{\kappa_l} - 0.056\left(\frac{A}{\kappa_l}\right)^{7/6}\right]. \tag{I10}$$

Substituting the Hill spectrum into (I3) yields

$$I_2 = 0.033C_n^2 \left[I_{a2} + \frac{1.802}{\kappa_l} I_{b2} - \frac{0.254}{\kappa_l^{7/6}} I_{c2}\right], \tag{I11}$$

where

$$I_{a2} = \int_0^\infty \kappa^{-2/3} \exp\left(-\frac{\kappa^2}{A^2}\right) \cos\left(B\kappa^2\right) d\kappa, \tag{I12}$$

$$I_{b2} = \int_0^\infty \kappa^{1/3} \exp\left(-\frac{\kappa^2}{A^2}\right) \cos\left(B\kappa^2\right) d\kappa, \tag{I13}$$

$$I_{c2} = \int_0^\infty \kappa^{1/2} \exp\left(-\frac{\kappa^2}{A^2}\right) \cos\left(B\kappa^2\right) d\kappa, \tag{I14}$$

$$B = \frac{L}{k}(1-\xi)\left(\Theta_2 + \bar{\Theta}_2\xi\right). \tag{I15}$$

Each of the integrals I_{a2}, I_{b2}, and I_{c2} can be evaluated by expressing the cosine function in its series representation, interchanging the order of integration and summation, and evaluating. Utilizing the Pochhammer relations given by (F11) we have

$$\begin{aligned} I_{a2} &= \sum_{n=0}^{\infty} \frac{\left(-B^2\right)^n}{(2n)!} \int_0^\infty \kappa^{4n-2/3} \exp\left(-\frac{\kappa^2}{A^2}\right) d\kappa \\ &= \frac{A^{1/3}}{2} \sum_{n=0}^{\infty} \frac{\left(-B^2A^4\right)^n}{(2n)!} \Gamma\left(2n+\frac{1}{6}\right) \\ &= \frac{A^{1/3}}{2} \Gamma\left(\frac{1}{6}\right) {}_2F_1\left(\tfrac{1}{12}, \tfrac{7}{12}; \tfrac{1}{2}; -B^2A^4\right), \end{aligned} \tag{I16}$$

where we note the Pochhammer relation $(2n)! = 2^{2n}\,(1/2)_n\,n!$. Utilizing the Pochhammer relation given by (F19) we have

$$\begin{aligned} I_{b2} &= \sum_{n=0}^{\infty} \frac{\left(-B^2\right)^n}{(2n)!} \int_0^{\infty} \kappa^{4n+1/3} \exp\left(-\frac{\kappa^2}{A^2}\right) d\kappa \\ &= \frac{A^{4/3}}{2} \sum_{n=0}^{\infty} \frac{\left(-B^2A^4\right)^n}{(2n)!} \Gamma\left(2n+\frac{2}{3}\right) \\ &= \frac{A^{4/3}}{2} \Gamma\left(\frac{2}{3}\right) {}_2F_1\left(\tfrac{1}{3}, \tfrac{5}{6}; \tfrac{1}{2}; -B^2A^4\right). \end{aligned} \tag{I17}$$

Utilizing the Pochhammer relation given by (F26) we have

$$\begin{aligned} I_{c2} &= \sum_{n=0}^{\infty} \frac{\left(-B^2\right)^n}{(2n)!} \int_0^{\infty} \kappa^{4n+1/2} \exp\left(-\frac{\kappa^2}{A^2}\right) d\kappa \\ &= \frac{A^{3/2}}{2} \sum_{n=0}^{\infty} \frac{\left(-B^2A^4\right)^n}{(2n)!} \Gamma\left(2n+\frac{3}{4}\right) \\ &= \frac{A^{3/2}}{2} \Gamma\left(\frac{3}{4}\right) {}_2F_1\left(\tfrac{3}{8}, \tfrac{7}{8}; \tfrac{1}{2}; -B^2A^4\right). \end{aligned} \tag{I18}$$

Combining these results and evaluating the Gamma functions yields

$$\begin{aligned} I_2 &= 0.092 C_n^2 A^{1/3} \left[{}_2F_1\left(\tfrac{1}{12}, \tfrac{7}{12}; \tfrac{1}{2}; -B^2A^4\right) \right. \\ &\quad +0.44 \left(\frac{A}{\kappa_l}\right) {}_2F_1\left(\tfrac{1}{3}, \tfrac{5}{6}; \tfrac{1}{2}; -B^2A^4\right) \\ &\quad \left. -0.056 \left(\frac{A}{\kappa_l}\right)^{7/6} {}_2F_1\left(\tfrac{3}{8}, \tfrac{7}{8}; \tfrac{1}{2}; -B^2A^4\right) \right]. \end{aligned} \tag{I19}$$

Substituting the Hill spectrum into (I4) yields

$$I_3 = 0.033 C_n^2 \left[I_{a3} + \frac{1.802}{\kappa_l} I_{b3} - \frac{0.254}{\kappa_l^{7/6}} I_{c3} \right], \tag{I20}$$

where

$$I_{a3} = \int_0^\infty \kappa^{-2/3} \exp\left(-\frac{\kappa^2}{A^2}\right) \sin\left(B\kappa^2\right) d\kappa, \tag{I21}$$

$$I_{b3} = \int_0^\infty \kappa^{1/3} \exp\left(-\frac{\kappa^2}{A^2}\right) \sin\left(B\kappa^2\right) d\kappa, \tag{I22}$$

$$I_{c3} = \int_0^\infty \kappa^{1/2} \exp\left(-\frac{\kappa^2}{A^2}\right) \sin\left(B\kappa^2\right) d\kappa. \tag{I23}$$

Each of the integrals I_{a3}, I_{b3}, and I_{c3} can be evaluated by expressing the cosine function in its series representation, interchanging the order of integration and summation, and evaluating. For I_{a3}, we have

$$\begin{aligned} I_{a3} &= B \sum_{n=0}^{\infty} \frac{\left(-B^2\right)^n}{(2n+1)!} \int_0^\infty \kappa^{4n+4/3} \exp\left(-\frac{\kappa^2}{A^2}\right) d\kappa \\ &= \frac{B A^{7/3}}{2} \sum_{n=0}^{\infty} \frac{\left(-B^2 A^4\right)^n}{(2n+1)!} \Gamma\left(2n + \frac{7}{6}\right) \\ &= \frac{B A^{7/3}}{2} \Gamma\left(\frac{7}{6}\right) {}_2F_1\left(\tfrac{7}{12}, \tfrac{13}{12}; \tfrac{3}{2}; -B^2 A^4\right), \end{aligned} \tag{I24}$$

where we note the Pochhammer relations $(2n+1)! = 2^{2n}\,(3/2)_n\,n!$ and

$$\begin{aligned}\Gamma\left(2n+\frac{7}{6}\right) &= \Gamma\left(\frac{7}{6}\right)\left(\frac{7}{6}\right)_{2n} \\ &= 2^{2n}\Gamma\left(\frac{7}{6}\right)\left(\frac{7}{12}\right)_n\left(\frac{13}{12}\right)_n . \end{aligned} \tag{I25}$$

For I_{b3}, we have

$$\begin{aligned} I_{b3} &= B\sum_{n=0}^{\infty}\frac{\left(-B^2\right)^n}{(2n+1)!}\int_0^{\infty}\kappa^{4n+7/3}\exp\left(-\frac{\kappa^2}{A^2}\right)d\kappa \\ &= \frac{BA^{10/3}}{2}\sum_{n=0}^{\infty}\frac{\left(-B^2A^4\right)^n}{(2n+1)!}\Gamma\left(2n+\frac{5}{3}\right) \\ &= \frac{BA^{10/3}}{2}\Gamma\left(\frac{5}{3}\right){}_2F_1\left(\tfrac{5}{6},\tfrac{4}{3};\tfrac{3}{2};-B^2A^4\right), \end{aligned} \tag{I26}$$

where we note the Pochhammer relation

$$\begin{aligned}\Gamma\left(2n+\frac{5}{3}\right) &= \Gamma\left(\frac{5}{3}\right)\left(\frac{5}{3}\right)_{2n} \\ &= 2^{2n}\Gamma\left(\frac{5}{3}\right)\left(\frac{5}{6}\right)_n\left(\frac{4}{3}\right)_n . \end{aligned} \tag{I27}$$

For I_{c3}, we have

$$\begin{aligned} I_{c3} &= B\sum_{n=0}^{\infty}\frac{\left(-B^2\right)^n}{(2n+1)!}\int_0^{\infty}\kappa^{4n+5/2}\exp\left(-\frac{\kappa^2}{A^2}\right)d\kappa \\ &= \frac{BA^{7/2}}{2}\sum_{n=0}^{\infty}\frac{\left(-B^2A^4\right)^n}{(2n+1)!}\Gamma\left(2n+\frac{7}{4}\right) \\ &= \frac{BA^{7/2}}{2}\Gamma\left(\frac{7}{4}\right){}_2F_1\left(\tfrac{7}{8},\tfrac{11}{8};\tfrac{3}{2};-B^2A^4\right), \end{aligned} \tag{I28}$$

where we note the Pochhammer relation

$$\begin{aligned} \Gamma\left(2n+\frac{7}{4}\right) &= \Gamma\left(\frac{7}{4}\right)\left(\frac{7}{4}\right)_{2n} \\ &= 2^{2n}\Gamma\left(\frac{7}{4}\right)\left(\frac{7}{8}\right)_n\left(\frac{11}{8}\right)_n. \end{aligned} \tag{I29}$$

Combining these results and evaluating the Gamma functions yields

$$\begin{aligned} I_3 &= 0.015C_n^2BA^{7/3}\left[{}_2F_1\left(\tfrac{7}{12},\tfrac{13}{12};\tfrac{3}{2};-B^2A^4\right)\right. \\ &\quad +1.75\left(\frac{A}{\kappa_l}\right){}_2F_1\left(\tfrac{5}{6},\tfrac{4}{3};\tfrac{3}{2};-B^2A^4\right) \\ &\quad \left.-0.25\left(\frac{A}{\kappa_l}\right)^{7/6}{}_2F_1\left(\tfrac{7}{8},\tfrac{11}{8};\tfrac{3}{2};-B^2A^4\right)\right]. \end{aligned} \tag{I30}$$

The expressions for I_1 through I_3 can now be substituted into the terms β_1 through β_4 as done in equations (243), (244), and (246)-(249).

To develop expressions for the frequency variance using the modified Rytov method, we substitute the large and small scale components of the effective atmospheric spectrum, (B1) and

(B2) respectively, where $f(\kappa l_0)$ is given by (F31) and $g(\kappa L_0) = 1$ into the equations for I_1 through I_3 given by (I2)-(I4). When the large scale component, (B1), is substituted the results for I_1 through I_3 are identical to the standard Rytov method except that A is replaced by A_{xl} given by (257). When the small scale component is substituted the result is the difference between the standard Rytov method expression and an identical expression where A is replaced by A_{yl} given by (259).

LIST OF REFERENCES

1. Acampora, Anthony, “Last Mile by Laser”, *Scientific American*, 48-53, July 2002.
2. L. C. Andrews and R. L. Phillips, *Laser Beam Propagation through Random Media*, SPIE Engineering Press, 1998.
3. L. C. Andrews, "An analytical model for the refractive index power spectrum and its applications to optical scintillation in the atmosphere," *J. Mod.Opt*. **39**, 1849-1853 (1992).
4. A. Ishimaru, *Wave Propagation and Scattering in Random Media*, IEEE Press, Piscataway, 1997.
5. V.I. Tatarskii, *Wave Propagation in a Turbulent Medium*, McGraw-Hill, New York, 1961, trans. By R.A. Silverman.
6. L. C. Andrews, R. L. Phillips, C. Y. Hopen, and M. A. Al-Habash, "Theory of optical scintillation," *J. Opt. Soc Am A* **16**, 1417-1429, 1999.
7. L. C. Andrews, R. L. Phillips, and C. Y. Hopen, *Laser Beam Scintillation with Applications*, SPIE Engineering Press, Bellingham, 2001.
8. L. C. Andrews, M. A. Al-Habash, C. Y. Hopen, and R. L. Phillips, "Theory of optical scintillation: Gaussian-beam wave model", *Waves in Random Media* **11**, 271-91, 2001.
9. A. Consortini, F. Cochetti, J.H. Churnside, and R.J. Hill, *J. Opt. Soc. Am A* **10**, 2354-2362, 1993.
10. S. M. Flatte and J. S. Gerber, "Irradiance variance behavior by numerical simulation for plane wave and spherical wave optical propagation through strong turbulence", *J. Opt. Soc. Am. A* **17**, 1092-97, 2000.
11. C. Y. Young, A. J. Masino, F. E. Thomas, and C. J. Subich, "The wave structure function in weak to strong fluctuations: an analytic model based on heuristic theory", *Waves in Random Media* **14**, 75-95, 2004.
12. J.W. Strohbehn, “Line of Sight Wave Propagation Through the Turbulent Atmosphere,” *Proc. of IEEE* **56**, 1301-1318, 1968.
13. A. S. Gurvich and M. A. Kallistratova, “Experimental study of the fluctuations in angle of incidence of a light beam under conditions of strong intensity fluctuations”, *Radiophys. Quantum Electron*. **11**, 66-71, 1968.
14. G.M.B. Bouricius and S.F. Clifford, “Experimental study of atmospherically induced phase fluctuations in an optical signal,” *J. Opt. Soc Am*. **60**, 1484-1489, 1970.
15. W.A. Coles and R.G. Frehlich, “Simultaneous measurements of angular scattering and intensity scintillation in the atmosphere”, *J. Opt. Soc Am.* **8**, 1042-1048, 1981.

16. G.K. Born, R. Bogenberger, K.D. Erben, F. Frank, F. Mohr, and G. Sepp, “Phase-front distortion of laser radiation in a turbulent atmosphere”, *Appl. Opt.* **14**, 2857-2863, 1975.

17. V.P. Lukin and V.V. Pokasov, “Optical wave phase fluctuations”, *Appl. Opt.* **20**, 121-135, 1981.

18. V.P. Lukin, “Optical measurements of the outer scale of the atmospheric turbulence”, *Proc. SPIE* **1968**, 327-336, 1993.

19. M. Bertolotti, M. Carnevale, L. Muzii, and D. Sette, “Interferometric Study of Phase Fluctuations of a Laser Beam Through the Turbulent Atmosphere”, *Appl. Opt.* **7**, 2246-2251, 1968.

20. S. F. Clifford, G. M. B. Bouricius, G.R. Ochs, and M. H. Ackley, “Phase variations in Atmospheric Optical Propagation,” *JOSA* **61**, 1279-1284, 1971.

21. C. Y. Young, A. J. Masino, and F. E. Thomas, "Phase fluctuations in moderate to strong turbulence", *Proc. SPIE* **4976**, 141-8, 2003.

22. L. C. Andrews, *Special Functions of Mathematics for Engineers*, SPIE Engineering Press, Bellingham, 1998.

23. J. C. Ricklin, W. B. Miller, and L. C. Andrews, “Effective beam parameters and the turbulent beam waist for initially convergent Gaussian beams,” *Appl. Opt*. **34**, 7059-7065, 1995

24. V. I. Shishov, “Frequency fluctuations of a wave propagating in a moving, randomly inhomogeneous medium”, *Radiophys. Quantum Electron.* **19**, 1056-1059, 1976.

25. R. Woo, F. C. Yang, and A. Ishimaru, “Structure of density fluctuations near the sun deduced from Pioneer-6 spectral broadening measurements”, *The Astrophysical Journal* **210**, 593-602, 1976.

26. A. J. Masino, C. Y. Young, C. J. Subich, "Atmospheric induced frequency spread in optical waves", *Opt. Eng.* submitted (2004).

27. M. S. Belen’kiĭ and V. L. Mironov, “Coherence of the field of a laser beam in a turbulent atmosphere”, *Sov. J. Quan. Elec.* **10**, 595-597, 1980.

28. C. Y. Young, A. J. Masino, and C. J. Subich, "Frequency fluctuations along slant paths", *Proc. SPIE* **5338**, 2004.

29. V. A. Banakh and V. L. Mironov, *LIDAR in a Turbulent Atmosphere*, Artech House, 1987.

30. A. J. Masino and C. Y. Young, "Double pass wave structure function in weak to strong optical turbulence", *Waves in Random Media* submitted (2004).

31. A. J. Masino, C. J. Subich, F. E. Thomas, and C. Y. Young, "Atmospheric induced frequency fluctuations in LIDAR", *Proc. SPIE* **5413**, 2004.

32. A. Papoulis, *Probability, Random Variables, and Stochastic Processes*, McGraw-Hill, 1991.